Epoxidized Natural Rubber
in Vibration and Noise Control Applications

By:

Mahmud Iskandar Seth A Rahim

A thesis submitted in partial fulfilment of the requirements for the
degree of
Doctor of Philosophy

The University of Sheffield
Faculty of Engineering
Department of Mechanical Engineering

April 2019

Abstract

The rise of the synthetic rubber and the fall in natural rubber prices are all motivations for the natural rubber industry to produce new specialty grades of natural rubber such as Epoxidized Natural Rubber (ENR). The optimal way to ensure the successfully of this ENR depends on the operational conditions and the potential applications. ENR is specialty grade chemically modified natural rubber and it is produced by epoxidation of natural rubber at the latex stage. There are two commercial grades available for ENR which have different epoxidation levels: 25 mol% and 50 mol%. These are referred as ENR-25 and ENR-50 respectively. ENR has been developed mainly to be used in the tyre industry, but its actual ability to control vibration and noise is poorly understood. Therefore, the aim of the research is to develop a method to design Epoxidized Natural Rubber (ENR) that can be used in vibration and noise control applications.

In this study, dynamic properties of solid natural rubber with 0, 25 and 50 mol% epoxidation levels were firstly identified over a range of temperatures and frequencies, and a master curve for their dynamic properties was generated based on the time-temperature superposition principle. The natural rubber foams were then produced from the solid natural rubber formulations containing blowing agents using a two-roll mill mixer and a compression moulding. The foams were characterised physically with respect to their density, porosity and airflow resistivity. Dynamic properties of the foams were analysed over a range of temperatures and frequencies. The microstructure properties of the foams were scanned using Micro Computer Tomography (Micro-CT) scanner, and the mean pore size was generated based on the micrographs obtained, while the acoustic properties of the foams were measured using a two-microphone impedance tube to determine its sound absorption coefficient efficiency.

This research provides new data on the physical, dynamic, microstructure and acoustical properties of natural rubber foam with different epoxidation levels. In addition, the modelling work was carried out to understand the relationship between the key non-acoustical parameters of natural rubber foam properties and its acoustic absorption performance. These observations are of a high value to help design natural rubber foams for noise control applications.

Acknowledgements

Publications

Journal Publications

1. M. I. Seth A Rahim, K. V. Horoshenkov, J. Rongong, H. Ahmadi and J. Picken. Epoxidized natural rubber for vibro-acoustic isolation, *Polymer Testing*, **67**: 92-98, 2018.

2. P. Bonfiglio, F. Pompoli, K. V. Horoshenkov, M. I. Seth A Rahim, L. Jaouen, J. Rodenas, F-X. Becot, E. Gourdon, D. Jaeger, V. Kursch, M. Tarello, N. B. Roozen, C. Glorieux, F. Ferrian, P. Leroy, F. B. Vangosa, N. Dauchez, F. Foucart, L. Lei, K. Carillo, O. Doutres, F. Sgard, R. Panneton, K. Verdiere, C. Bertolini, R. Bar, J-P. Groby, A. Geslain, N. Poulain, L. Rouleau, A. Guinault, H. Ahmadi, C. Forge. How reproducible are methods to measure the dynamic viscoelastic properties of poroelastic media? *Journal of Sound and Vibration*, **428**: 26-43, 2018.

3. P. Bonfiglio, F. Pompoli, K. V. Horoshenkov, M. I. Seth A Rahim. A simplified transfer matrix approach for the determination of the complex modulus of viscoelastic materials, *Polymer Testing*, **53**:180-187, 2016.

Conference Publications

1. M. I. Seth A Rahim, K. V. Horoshenkov, J. Rongong, H. Ahmadi and J. Picken. Dynamic properties of epoxidized natural rubber, *The 24th International Congress on Sound and Vibration (ICSV24)*, London, 23-27 July 2017.

2. M. I. Seth A Rahim and P. Bonfiglio. Relationship between the temperature and frequency dependence of the damping properties of natural rubber with different epoxidation level, *Acoustics 2016*, Warwickshire, 5-6 September 2016.

Contents

List of Figures

xi

List of Tables

Nomenclature

Greek Symbols

α	Sound absorption coefficient
α_∞	Tortuosity
γ	Specific heat ratio
δ	Phase angle
η_0	Dynamic density of the equivalent fluid
ρ	Density
ρ_0	Air equilibrium density
ρ_b	Dynamic density of the equivalent fluid
ρ_x	Density of the rubber foam
ρ_y	Density of the solid rubber
σ or σ_x	Airflow resistivity
σ_s	Standard deviation in the pore size
σ'_x	Thermal flow resistivity
κ	Thermal conductivity of the equivalent fluid
$\tan \delta$ or η	Loss factor
ϕ	Porosity
τ	Relaxation time
ω	Angular frequency
ω_n	Normalised frequency
ω_t	Thermal frequency
ω_v	Viscous frequency

Roman Symbols

A	area
a_T	Horizontal shift coefficient
b_T	Vertical shift coefficient
C_1 or C_2	Viscoelastic coefficient
C_b	Compressibility of the equivalent fluid
C_p	Heat capacity
c_0	Sound speed in air
d	Hard-backed porous material of thickness
ER	Expansion ratio
E	Young's modulus
E^*	Complex modulus
E' or G'	Storage modulus
E'' or G''	Loss modulus
$F(x)$	Minimisation analysis
$\tilde{F}_p$	Viscosity correction function
f	Frequency
G	Shear modulus
G_0	Low-frequency storage modulus
G_∞	High-frequency storage modulus
h	Water level in the U-tube manometer
i	Imaginary part
k_0	Wavenumber
k_c	Sound wavenumber
L_p	Diameter of the foam sample
L_t	Diameter of the two-microphone impedance tube
N	Number of pores per unit volume
N_{Pr}	Prandtl number
ΔP	Change of pressure

P_0	Atmospheric pressure
P_I	Incident wave
P_R	Reflected wave
q_v	Volumetric airflow rate
S	Cross-sectional area of the U-tube manometer
s	Pore size
$\bar{s}$	Mean pore size
T	Temperature
T_0, T_s or T_{ref}	Reference temperature
T_g	Glass transition temperature
t	Thickness
t_{s2}	Scorch time
t_{95}	Time to 95% cure
ΔV_a	Reduction of air volume in the chamber
V_a	Air-filled volume in porous material
V_c	Volume of chamber
V_s	Total volume of porous material
v	Sound velocity
x_r	Multiplication factor
z_s	Surface impedance
z_c	Characteristic impedance

Abbreviations

AB	Ammonium Bicarbonate
ADC	Azodicarbonamide
BSH	Benzene sulphonylhydrazide
CBS	Benzothiazyl-2-cyclohexyl-sulfenamide
CTAn	Computer Tomography Analysis
DMA	Dynamic Mechanical Analyser
DNPT	N, N'-dinitrosopenta-methylenetetramine
DPNR	Deproteinized Natural Rubber
ENR	Epoxidized Natural Rubber
EPDM	Ethylene Propylene Diene Monomer Rubber
GNI	Gross National Income
^{1}H NMR	Proton Nuclear Magnetic Resonance
IIR	Isobutylene Isoprene Rubber
MDR	Moving Die Rheometer
MH	Maximum torque
ML	Minimum torque
MV	Mooney Viscosity
NBR	Nitrile Rubber
NKEA	National Key Economic Area
phr	Parts per hundred or rubber
PVI	Prevulcanisation Inhibitor
SB	Sodium Bicarbonate
SMR-CV	Standard Malaysian Rubber Constant-Viscosity
TARRC	Tun Abdul Razak Research Centre
USD	United States Dollar
WLF	Williams-Landel-Ferry

Samples

R0, R25, R50	Vulcanised rubber, the numbers stand for the epoxidation level of the rubber: 0, 25 and 50 mol%
DRF-8, DRF-20	Dry rubber foam with no mastication of raw rubber, the numbers stand for the amount of sodium bicarbonate in phr
F0, F25, F50	Dry rubber foam with mastication of raw rubber, the numbers stand for the epoxidation level of the rubber: 0, 25 and 50 mol%
R0-Raw	0 mol% vulcanised rubber with no activators and accelerators
R0-Activator	0 mol% vulcanised rubber with activators only
R0-Accelerator	0 mol% vulcanised rubber with accelerators only
F50 CS	50 mol% dry rubber foam with addition of calcium stearate
F50 AB	50 mol% dry rubber foam with addition of ammonium bicarbonate
F50 PO	50 mol% dry rubber foam with addition of process oil
F0 20:0, F25 20:0, F50 20:0	Dry rubber foam with 20 phr of sodium bicarbonate and no ammonium bicarbonate
F0 15:5, F25 15:5, F50 15:5	Dry rubber foam with 15 phr of sodium bicarbonate and 5 phr of ammonium bicarbonate
F0 10:10, F25 10:10, F50 10:10	Dry rubber foam with 10 phr of sodium bicarbonate and 10 phr of ammonium bicarbonate
LF0, LF25, LF50	Latex foam, the numbers stand for the epoxidation level of the rubber: 0, 25 and 50 mol%
RRF	Reconstituted rubber foam
PUF	Polyurethane foam

Chapter 1

Introduction

1.1 The fall in natural rubber prices

Natural rubber is facing serious threat from synthetic rubber. The fall of petroleum prices contributes to the high usage of synthetic rubber which is extracted from petroleum-based resources because it is a cheaper material and process. This scenario drives down the demand for natural rubber and causes the price of natural rubber to fall. Moreover, a slow recovery of the world economy has also made an impact on the downward trend in the price of natural rubber. As an example, the price of natural rubber such as Standard Malaysian Rubber Constant-Viscosity (SMR-CV) has declined drastically from USD 5.30/kg in the early of 2011 to USD 1.82/kg in the mid of 2018 [1] as illustrated in Figure 1.1. The low production of natural rubber is also making negative effect on the monthly income of the rubber tappers so that working as a rubber tapper is not a popular job anymore especially for the younger generation. Therefore, this situation will inevitably cause the manpower shortage in the longer term.
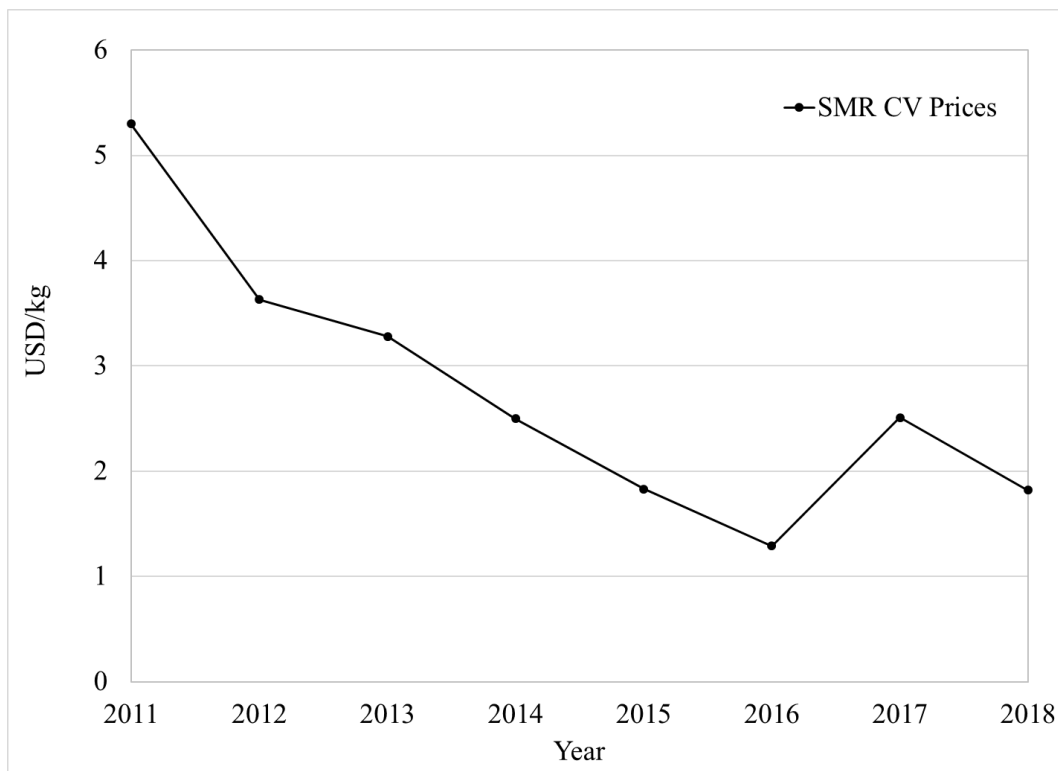
Figure 1.1: SMR-CV prices from 2011 to 2018 [1].

1

These issues have brought attention to the natural rubber industry which is now obliged to take serious steps by introducing new specialty grades of natural rubber that has greater market potential through innovation to compete or replace the synthetic rubber. One of the natural rubbers considered in this process is Epoxidized Natural Rubber (ENR).

ENR is a chemically modified natural rubber produced by epoxidation of natural rubber at the latex stage. The modification of natural rubber to ENR is to extend the benefits of natural rubber in a wide range of high-tech applications as well as to improve the properties of natural rubber. ENR is primarily designed to be used for the production of environmentally-friendly tyres or green tyres. These tyres can provide low rolling resistance, high wet grip and low heat buildup so that the fuel consumption can be reduced [2].

In response to the above, the Malaysian government has set up support for the natural rubber industry by selecting ENR as one of the key economic growth engines in Malaysia that is known as National Key Economic Area (NKEA). NKEA is a driven economic program that offers government funding and policy support. This program attracts Prime Minister's personal attention to the problem. The government believes this NKEA has significant impact on the Gross National Income (GNI) contribution to the economic growth in Malaysia. The commercialisation of ENR is expected to contribute to an incremental GNI up to USD 330 million by 2020 [3]. This commercialisation can facilitate the rubber tappers to increase their income by encouraging the production of natural rubber and increase export demand for ENR. Moreover, research on ENR and its potential applications other than in the tyre production is likely to provide an advantage in realising the vision of the Malaysian government to make natural rubber as a major commodity contributor to its GNI.

Currently, numerous studies are concentrating on the physical and dynamic properties of binary blends between ENR and other polymers, or also the implementation of new fillers in ENR matrix. However, there is a relatively small amount of published work on physical, dynamic and acoustic properties of materials based on ENR alone as the main matrix. Moreover, the effect of the epoxidation level on these properties of ENR has not been fully investigated.

There is also no research related on the acoustical properties of ENR foams, however, a few studies have been reported on these properties for natural rubber foams. For example, Najib *et al.* [4] studied the acoustic and dynamic properties of natural rubber foam at different foaming temperatures of 140°C, 150°C and 160°C. They observed that an effective sound absorption can be achieved at lowest foaming temperature with a maximum sound absorption coefficient of 0.94 at 1552 Hz. Another recent study, Vahidifar *et al.* [5] investigated the acoustic performance of natural rubber foam with variable carbon black (reinforcing filler) content using one-step foam processing. The results exhibited that a sound absorption decreases with increasing carbon black content with a maximum sound absorption coefficient reduced slightly from 0.4 to 0.25 at 5500 Hz. One problem with these studies is that none of them actually describe the link between key parameters of rubber foam microstructure and intrinsic acoustical properties which control our ability to design rubber foam intelligently as a generic noise control material.

1.2 Aim and objectives

Natural rubber is found routinely in vibration isolation elements. However, it struggles to compete against polymeric foams to solve the noise problem efficiently. Therefore, polymeric foams are in great demand in commercial noise control applications and dominate this market.

Figure 1.2 shows the research flow of ENR in vibration and noise control applications, and how this research can contribute to the knowledge in these applications. The performance of an elastomeric vibro-acoustic system is governed by the dynamic and acoustic properties of the material under service conditions. Based on the research status of ENR, most of the research were investigating dynamic properties of solid natural rubber and/or ENR, and very few studies were exploring the dynamic and acoustic properties of natural rubber foam. To the best of our knowledge no research on vibro-acoustic properties of ENR foams has been reported, either ENR as a single matrix or the effect of different epoxidation levels on those properties.
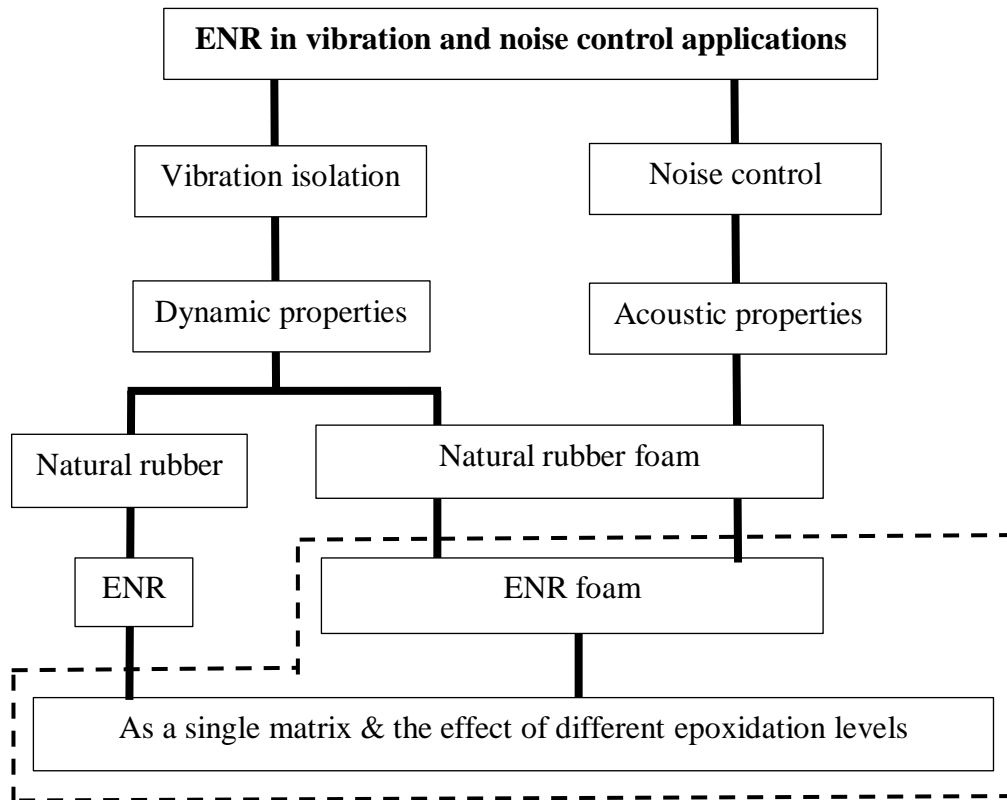
Figure 1.2: Research flow of the knowledge contribution.

Therefore, the aim of this research is to develop a method to design ENR and natural rubber that can be used in vibration and noise control applications. Specifically, there are several key objectives to achieve the above aim of this research:

a. To identify dynamical properties of solid ENR and solid natural rubber.

b. To develop a new manufacturing process of ENR foams and natural rubber foams.

c. To characterise the ENR and natural rubber foams in terms of their physical, dynamical, microstructural and acoustical properties, and to compare their behaviour with that of commercially available vibration and noise control foams.

d. To model the in-situ acoustic absorption behaviour of ENR foams and natural rubber foams.

1.3 Thesis structure

The thesis is organised as follows. Chapter 2 presents a literature review that can be related to a method to develop natural rubber and epoxidized natural rubber (ENR) as acoustic materials. A description of natural rubber and ENR is reviewed. The dynamic mechanical

properties of viscoelastic material, manufacturing process of natural rubber foam and porous material in vibro-acoustic applications are studied. The methodology chapter is not presented as one chapter in this thesis. The methodology of the experimental works and manufacturing processes involved in this research are included in the results and discussion chapters: Chapter 3, 4 and 5. In Chapter 3, the dynamical properties of solid ENR and natural rubber over a range of temperatures and frequencies are presented. A master curve for their dynamic properties is generated based on the time-temperature superposition principle. The 5-parameter fractional derivative Pritz model [6] is also applied to the experimented master curve. In Chapter 4, a new manufacturing process of natural rubber foams and ENR foams including formulations, mixing process and curing procedures is explained. In Chapter 5, the physical, dynamic, microstructure and acoustic properties of ENR and natural rubber foams manufactured in this research are studied, and their results are compared with that of commercially available foams. Then, the acoustic absorption of the foams is modelled, and the results are discussed. Chapter 6 provides the research conclusions and recommendations for future work.

Chapter 2

Literature Review

2.1 Introduction

The purpose of this chapter is to provide a background that can be related to a method to develop natural rubber and epoxidized natural rubber (ENR) as acoustic materials so that these rubbers can be used in vibration and noise control applications. The chapter begins with a description of natural rubber and ENR. An overview of dynamic mechanical properties of viscoelastic materials is studied, this includes the parameters used to measure the dynamic mechanical properties, methods to characterise the dynamic mechanical properties and the effect of temperature and frequency on the mechanical behavior of viscoelastic materials. Next, the production process of natural rubber foam is reviewed. A comparative study on the manufacturing process of natural rubber foam produced from latex and dry rubber is presented. The research status of natural rubber foam and ENR foam produced from dry rubber is also investigated. Finally, the use of porous material in vibro-acoustic applications is reviewed. The mechanisms of sound attenuation using porous material is presented and characterisation methods for porous material are discussed. The modelling of sound absorption of porous material is also explored to understand how to predict the acoustic behaviour of porous material.

2.2 Natural rubber

Natural rubber is a polymer that is categorised as a viscoelastic material. It is produced from a milky white liquid called latex. A common commercial source of natural rubber latex is from rubber tree known as Hevea Brasiliensis (Figure 2.1). Latex is also can be produced from certain plants such as Dandelion flower, Palaquium Gutta tree and Guayule flower.

Natural rubber is typically being obtained through three processing steps: field latex; coagulated latex; and value-added specialty rubber [7]. Each processing step is different from one another as they have different raw materials, manufacturing processes and applications as shown in Table 2.1.

Figure 2.1: The latex exudes from the rubber tree (Hevea Brasiliensis) [8].

Table 2.1
Natural rubber processing [7].

Processing step	Field latex	Coagulated latex	Value-added specialty rubber
Raw material	Latex concentrate	Block rubbers of SMR CV 60[1] or SMR 10.	Epoxidized natural rubber (ENR) or deproteinized natural rubber (DPNR)
Manufacturing process	Latex products	Dry rubber products	Niche dry rubber products
Applications	Gloves, balloons, latex foams.	Tyres, hoses, seals.	Green tyres, engine mountings, adhesives.

[1]Standard Malaysia Rubber Constant Viscosity 60

Natural rubber is chemically known as polyisoprene [9] and its polymer structure is shown in Figure 2.2. The uniqueness of natural rubber lies in its physical properties, great deformation capacity and very high strength that made them as a top material to be used in engineering applications [7]. It also has outstanding low temperature flexibility with a glass transition temperature (T_g) of the natural rubber is approximately -72°C [9].
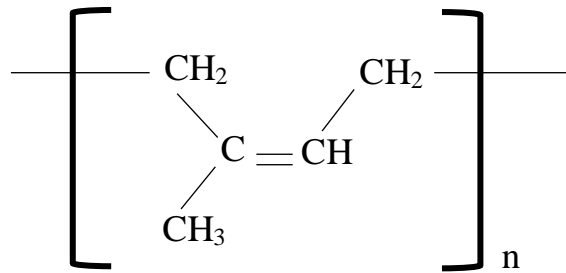
Figure 2.2: Chemical structure of natural rubber (polyisoprene) [10].

In its natural state, however, natural rubber has limiting properties. It is greatly affected by temperature, low resistance to oils, and low resistance to air (oxygen and ozone) in the atmosphere [7]. In order to overcome these weaknesses of natural rubber, many of rubber manufacturers have developed synthetic rubbers, so that they can be used in a wider range of applications. The main synthetic rubbers such as isobutylene isoprene rubber (IIR) or butyl rubber, nitrile rubber (NBR), and ethylene propylene diene monomer rubber (EPDM) are derived from petroleum-based resources. Each of these rubbers has its own advantages over natural rubber. IIR has low gas permeability and high resistance to abrasion. NBR has high resistance to oils and typically used for oil seals, gaskets and washing machine parts, while EPDM is normally used in automotive parts and electrical insulation because of its high resistance to heat and weather [11].

2.3 Epoxidized natural rubber

A chemically modified natural rubber, Epoxidized Natural Rubber (ENR) is produced by epoxidation of natural rubber with peracetic acid at the latex stage. Epoxidation is a stereospecific process, which is also related to the replacements on the double bond of the polymer backbone [12]. In the case of natural rubber, a known percentage of its double bonds are reacted to form epoxide groups. Figure 2.3 shows the reaction of natural rubber in latex stage with peracetic acid solution. In this reaction, epoxide groups can be observed distributed randomly along the natural rubber backbone.
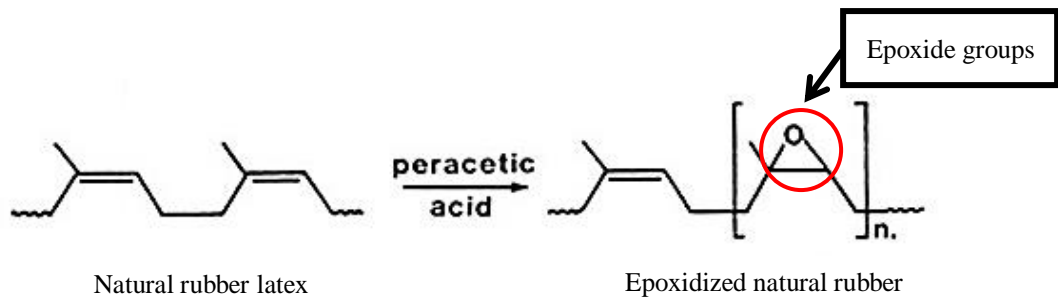
Figure 2.3: The formation of epoxide groups [12].

As the epoxide groups are introduced, ENR shows a higher glass transition temperature (T_g) as compared to natural rubber by approximately 1°C for every mol% epoxidation [13]. This result was also observed in previous research [12] which demonstrates that the T_g of ENR measured by differential scanning calorimetry increases linearly with the increasing epoxidation levels as shown in Figure 2.4. This will strongly affect the dynamic mechanical properties of ENR [14].
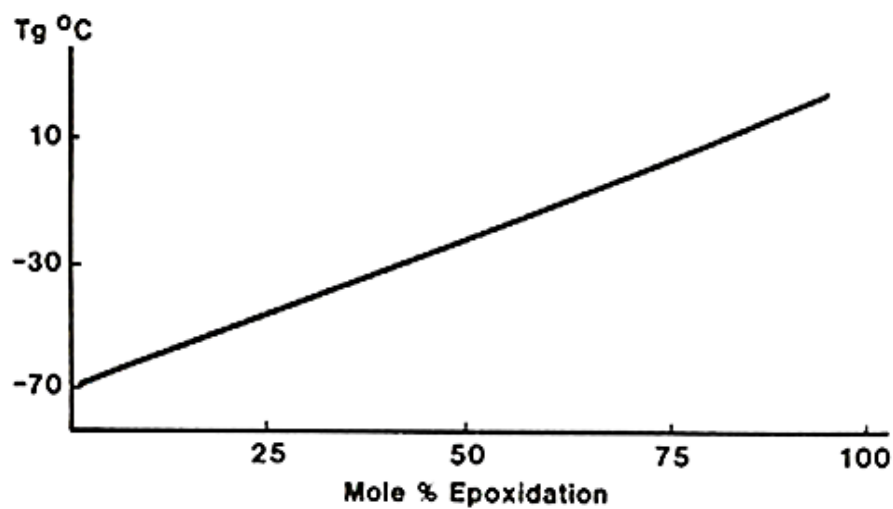
Figure 2.4: The effect of epoxidation level of natural rubber on the glass transition temperature, T_g [12].

ENR also provides a lower swelling characteristic as it has more polar group which influences reduction in swelling behaviour (Figure 2.5). The investigation reported in ref. [15] stated that ENR consists of polar group can contributes to three-dimensional network. The network restricts swelling because of a small amount of open chains and gaps between

rubber molecules. In addition, ENR provides good resistance to oils and non-polar solvents, low gas permeability, high damping at room temperature and great wet grip performance. These properties result from the high polarity of epoxide groups, which are randomly distributed along the natural rubber backbone [16, 17]. Moreover, some of these advantages are equivalent to the physical properties of other synthetic rubbers with oil resistance similar to NBR and gas permeability similar to IIR. The comparison of those physical properties for natural rubber, ENR and synthetic rubbers are shown in Table 2.2.
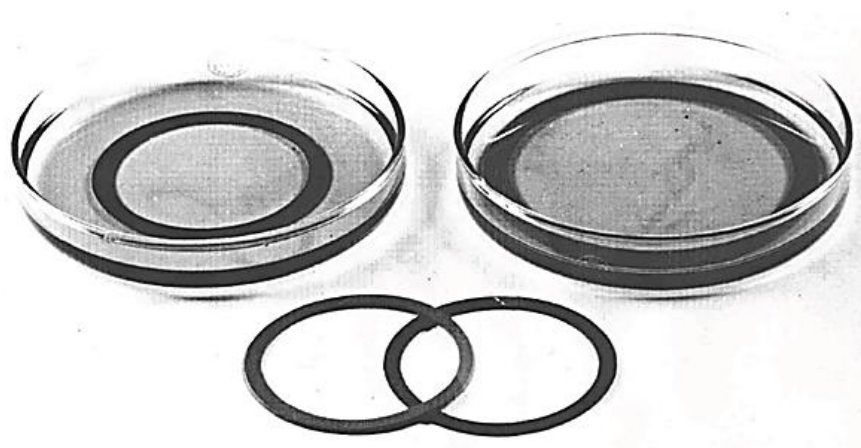
Figure 2.5: Swelling behaviour between ENR O-ring (left) and natural rubber O-ring (right) after soaking for four days at 23°C [18].

Table 2.2
The physical properties of natural rubber, ENR and synthetic rubbers [19].

Physical properties	Natural rubber	ENR-25[1]	ENR-50[2]	NBR	IIR
Oil resistance: volume increase in polymer[3] (%)	15	1.2	0.1	0.2	-
Relative gas permeability[4]	100	25	7	-	6

[1]Epoxidized natural rubber with 25 mol% epoxidation level.
[2]Epoxidized natural rubber with 50 mol% epoxidation level.
[3]After soaking for four days at 23°C.
[4]Natural rubber is taken as the reference and other polymers are rated accordingly.

10

There are two commercial grades of ENR which have different epoxidation levels: 25 mol%; and 50 mol% [14]. These are referred as ENR-25 and ENR-50, respectively. Rubber with any level of epoxidation can be developed under the right reaction conditions, which are mainly controlled by the peracetic acid concentration and epoxidation temperature [12]. However, a high level of epoxidation can lead to a reaction where the epoxide ring is opened, resulting in a non-homogenous product. In this process some of the epoxide groups experience ring opening reactions, which then proceeded with the formation of furan groups along the rubber backbone as shown in Figure 2.6. Therefore, at high concentrations and high temperatures, the level of furan groups in the natural rubber predominates [20], whereas at low concentrations and moderate temperatures, ENR is produced as a sole product [12].
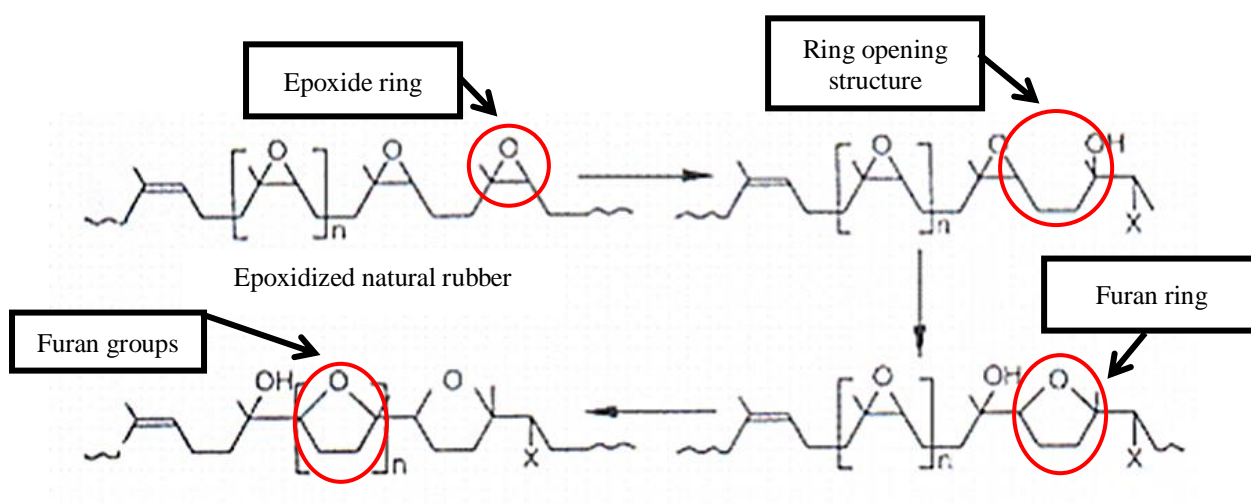
Figure 2.6: The formation of furan groups [12].

ENR experiences strain crystallisation contributing to the high strength properties. However, the degree of crystallinity decreases with the increasing epoxidation levels. Other properties such as oil resistance, damping and gas permeability also change linearly with the epoxidation levels. The investigation reported in ref. [12] on the reaction of natural rubber latex with 100 mol% peracetic acid produced a white amorphous powder that is known as 'furanised natural rubber'. The properties of furanised natural rubber are similar to polystyrene. It has no elastic properties of rubber [20] as shown in Figure 2.7, and it can be moulded using an injection molding machine [12].
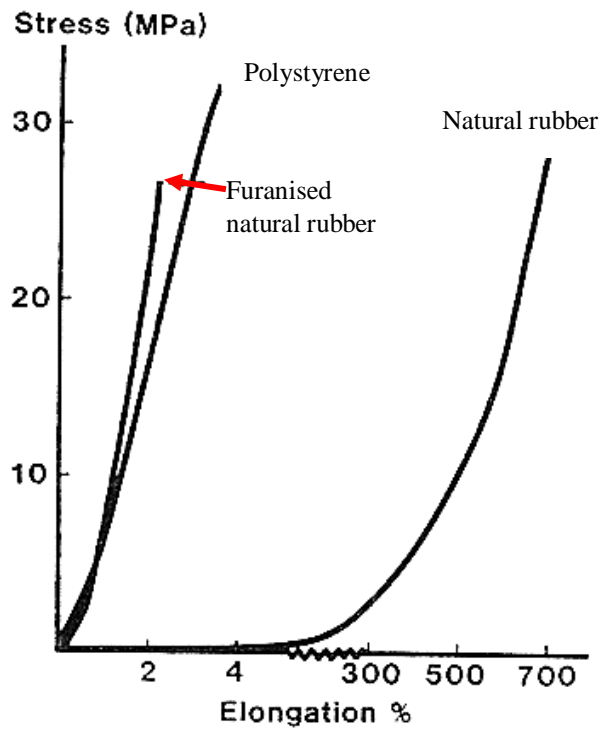
Figure 2.7: A stress-elongation properties comparison between furanised natural rubber, polystyrene and natural rubber [12].

2.3.1 Applications of epoxidized natural rubber

The advantages of ENR over natural rubber and some of its properties similar to other synthetic rubbers, suggest that this material can be used in a wide range of applications. ENR has been studied extensively by the tyre industry [21], and tyre applications are also the largest market for ENR [22]. For example, ENR-25 tyre compounds indicate low rolling resistance and excellent wet traction, hence contributing to the high performance that can accommodate for fuel efficiency and safety requirements for modern passenger vehicles [14]. ENR-50 has been used in tyre inner liners and tubes to replace butyl rubbers [22].

ENR is recognized as a commercial rubber and marketed as Ekoprena (Figure 2.8) [23]. Its implementation in the market are expected to increase rapidly and the applications of usage for ENR are listed in Table 2.3. However, there are many other specialised applications where ENR has not yet been evaluated extensively. ENR is produced from large-scale manufacturing in Malaysia and is currently discovering potential applications such as high damping mountings, squash balls, acoustic damping and cellular rubber [24].

12

Figure 2.8: EKOPRENA, a commercial name of epoxidized natural rubber [23].

Table 2.3
ENR applications [19].

Feature	Application	Recommended ENR grade
Oil resistance	Hoses, seals, blow-out preventors	ENR-50
	Milking inflation, connectors and tubes	ENR-25 and ENR-50
Gas permeability	Bladders, inner tubes and tyre liners	ENR-50[1]
Wet traction and rolling resistance	Tyre treads for passenger vehicles, motorcycles, racing cars and forklift trucks	ENR-25

[1]Preferably in blends with natural rubber.

2.3.2 Research status of epoxidized natural rubber

Numerous studies have concentrated on the physical and dynamic characteristics of ENR with the usage of a new filler such as rice husk ash [25], lignin [26], highly dispersible silica [27] and ionic liquid [28]. The synergistic study on the binary blends between ENR and other polymers have also been reported such as ENR/styrene butadiene rubber [29], ENR/asphalt [30], ENR/thermoplastic polyurethane [31, 32] and ENR/natural rubber [33, 34]. Several studies on ENR blends using different mixing approaches have also been conducted. For example, Rooj *et al.* [35], developed a mixing technology based on an in-line electron induced reactive processing technique. Wang *et al.* [36] introduced wet masterbatch technique instead of using the traditional dry mixing method.

There is a relatively small amount of published work on physical, dynamic and acoustic properties of materials based on ENR alone as the main matrix. Moreover, the effect of the epoxidation level on these properties of ENR has not been fully investigated. One particular study on ENR alone was reported by Lu and Li [37]. They implemented an alternative approach to produce ENR with effective damping in a broad temperature and frequency range. It was shown that the application of a different curing agent, phenolic resin, in the ENR matrix helps to achieve an effective damping with the loss factor of tan δ > 0.3 in the temperature range from -48°C to 100°C and in the frequency range from 10^{-5} to 10^{9} Hz. However, the research they conducted focused only on a single epoxidation level. The earlier work reported by Ahmadi *et al.* [38] in particular addressed the effect of different epoxidation levels on the dynamical properties of ENR matrix. The authors presented a more interesting finding for the shear modulus and loss factor of 0, 25 and 50 mol% epoxidation levels. The master curves obtained were found to be similar in shape as shown in Figure 2.9.
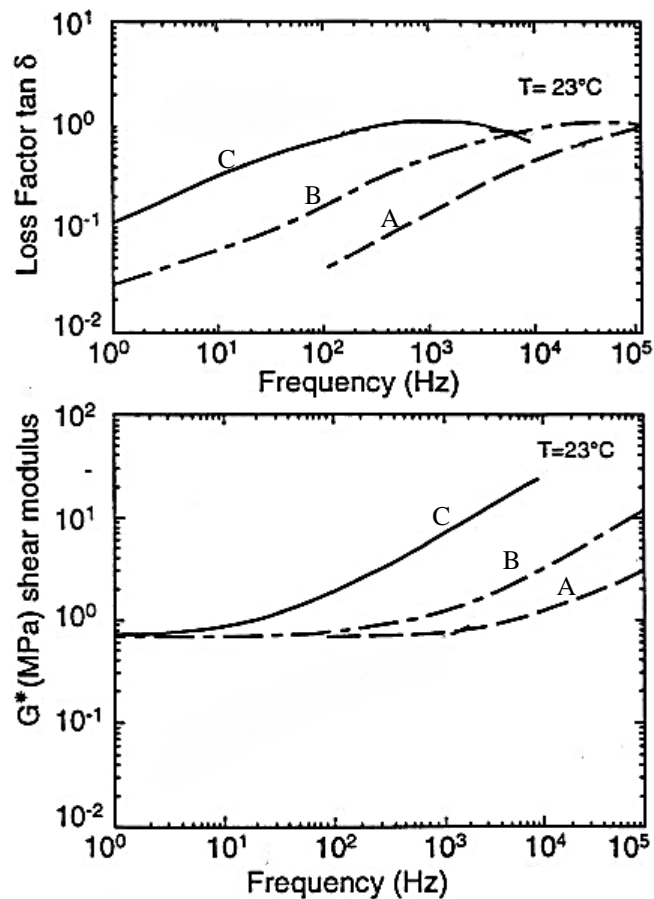
Figure 2.9: Master curves for dynamic properties of natural rubber (A), ENR-25 (B) and ENR-50 (C) [38].

14

2.4 Dynamic mechanical properties of viscoelastic material

Viscoelastic materials such as rubber are used extensively for vibro-acoustic isolation. These materials display both viscous and elastic behaviour at different temperatures and frequencies. The dynamic mechanical properties such as dynamic modulus and damping of these materials are dependent on the temperature and frequency. Therefore, it is necessary to test rubber compounds used in vibration and noise control applications in a range of environmental conditions and frequencies.

2.4.1 Dynamic modulus and damping

The stiffness represents the elastic nature of materials while the damping represents their viscous nature. These two properties are described by the complex modulus [39]. Any dynamic moduli such as Young's modulus (E) or shear modulus (G) can be defined as a complex modulus. For example, the complex modulus, E^*, can be expressed as:

$$E^* = E' + iE'', \tag{2.1}$$

where E' is the storage modulus and E'' is the loss modulus. These parameters are illustrated schematically in Figure 2.10. A ball is thrown down on a floor and it bounce back in the same distance to E'. This is a measure of the energy stored during the impact of the ball with the floor, while E'' is representing the energy lost as heat during the impact of the ball with the floor as the ball becomes warmer on bouncing.
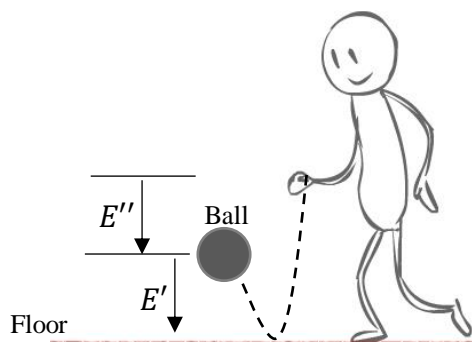
Figure 2.10: A difference between the storage modulus, E' and the loss modulus, E''.

The loss factor (η) is the ratio of the loss modulus to the storage modulus, and it can be expressed as:

$$\eta = \frac{E''}{E'} = \tan\delta . \qquad (2.2)$$

Another term of the loss factor is tan delta ($\tan\delta$), where δ is a phase angle between sinusoidal stress (σ) and strain (ε) as shown in Figure 2.11. The stress and the strain of a viscoelastic material are out of phase by some phase angle [40]. This is caused by the viscous and elastic nature of the material, where a part of the energy stored during the loading is recovered during the unloading phase, and the remaining energy is dissipated in the form of heat. In contrast, the stress and the strain of an elastic material are moving in phase because all the energy stored during the loading is fully recovered when unloaded. The two parameters, $\tan\delta$ and E'' are useful in determine the damping value. The damping value increases with the increasing of these parameters at a given temperature and frequency [41].
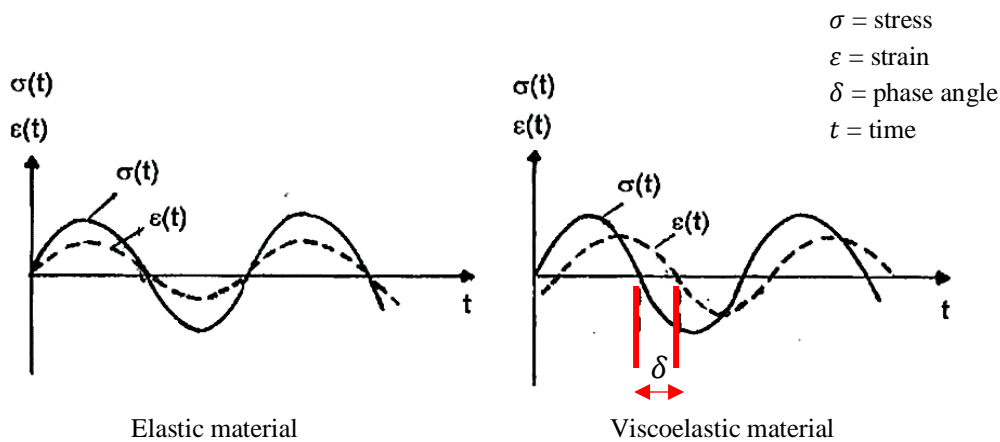
Figure 2.11: A comparison of sinusoidal stress and strain between elastic material and viscoelastic material [40].

Dynamic Mechanical Analysis (DMA) is a method used to determine the dynamic mechanical properties of a material as a function of temperature, frequency, stress, time or a combination of these parameters. The tested material or sample is deformed in a cyclic mode and it reacts to the selected temperature, frequency, stress and other parameters. DMA operates by applying oscillatory force to the sample and it provides information on the

stiffness and damping behaviour of the sample. Specifically, a sinusoidal force is applied to the sample with a controlled stress or a controlled strain. Then the sample will deform at a certain limit based on its stiffness. The measurement of stiffness and damping are determined by DMA as dynamic modulus and tan δ. As a sinusoidal force is applied, the dynamic modulus can be expressed as an in-phase component (storage modulus) and an out of phase component (loss modulus) as shown in Figure 2.12 [42].
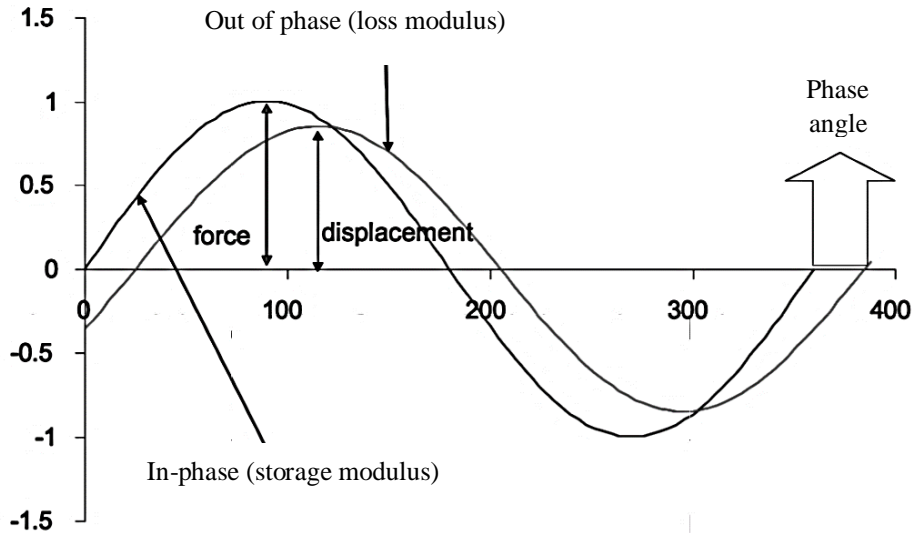
Figure 2.12: The relationship of sinusoidal stress and strain which resulting to phase angle [42].

2.4.2 Glass transition temperature

Glass transition temperature is a fundamental theory of polymeric materials that needs to be determined. Principally, the polymer becomes more viscous as temperature decreases. As the temperature is reduced further, the polymer becomes rubbery and then finally it reaches a glassy state at which the polymer is frozen and hardened. By definition, the glass transition temperature, T_g, is the temperature at which the polymer changes from rubber to glass. There are important changes in material properties of a polymer at the glass transition temperature. For example, the modulus of the polymer is drastically increased when its temperature is reduced below T_g [43].

One of the techniques to determine the T_g is to apply the concept of free volume. The free volume is an empty space in a polymer sample which is not occupied with the polymer molecules. At a high temperature, the free volume is large. The molecular motion in this

condition is relatively easy as more unoccupied volume provides enough space for the molecules to move freely and to change its structure easily, thereby resulting in a low modulus material. As the temperature is reduced, the free volume becomes lesser until there is no space for polymer molecules to move due to volumetric shrinkage. This condition contributing to a high modulus material. The temperature at this condition is close to T_g [43]. The schematic of stated condition is shown in Figure 2.13. The free volume is shown as a shaded area.
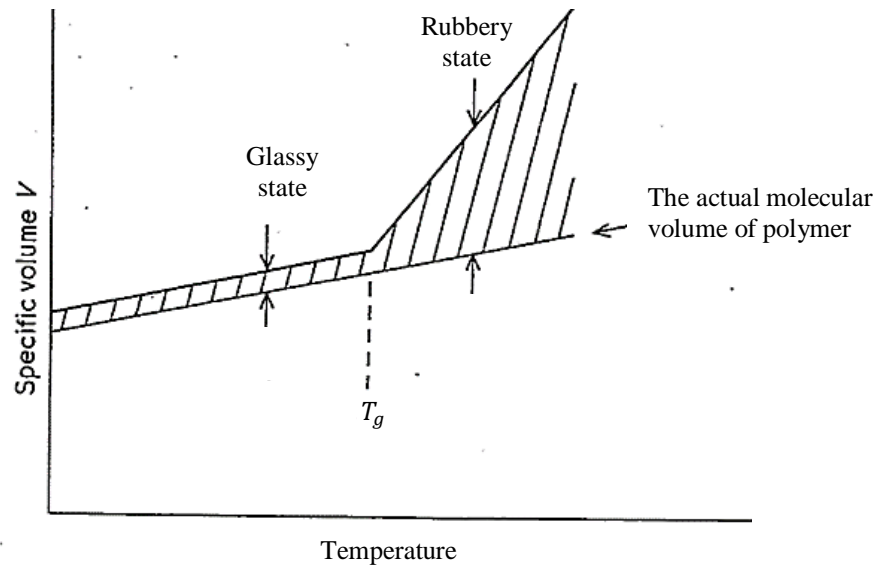
Figure 2.13: The specific volume of a polymer sample as a function of temperature [43].

Alternatively, T_g can also be defined through a thermal method by using Differential Scanning Calorimetry (DSC). This method applies the heat flow on a polymer sample which is undergoes a phase transition. The amount of heat flow is basically depending on heat capacity of the polymer through these two processes, exothermic (heat energy out) or endothermic (heat energy in) [44]. For example, a polymer at a glassy state will undergoes endothermic process to transform to a rubbery state. Therefore, more heat is needed to raise the polymer temperature as shown in Figure 2.14. At this physical transformation, a change in slope can be observed and this situation corresponds to T_g .
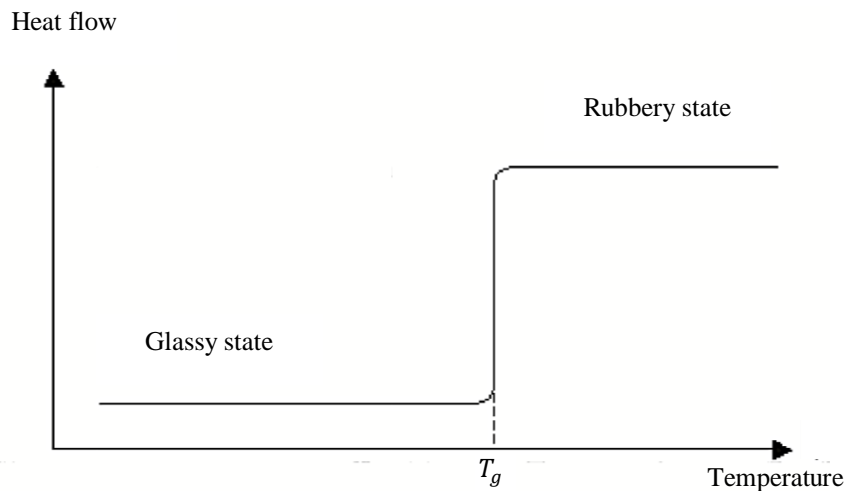
Figure 2.14: The heat flow of a polymeric material as a function of temperature [44].

In terms of mechanical method, the Dynamic Mechanical Analysis is an instrument that can estimate the T_g. According to this method, the T_g is temperature at the start of the transition in the dynamic properties of the tested material. However, this method can actually obtain the transition in T_g, as the T_g measurement is dependent on the frequency at which the dynamic properties are measured as shown in Figure 2.15.

There are several factors that can influence the T_g of natural rubber. One of these factors is the material structure. A *cis* isomers structure of natural rubber suggests that there is no influence on the T_g even with the existence of non-rubbers in raw natural rubber. However, there might be a very small changes in T_g if the natural rubber is replaced with synthetic polyisoprene due to the presence of *trans* isomers [9]. It is also found that the physical properties of the molecules such as molecular weight and crosslinking can affect the T_g. The value of the T_g increases with the increasing molecular weight, while crosslinking reduces the free volume and restricts the molecular motion of the polymer, hence increase the T_g value [43]. The molecular weight values of natural rubber are more than 100,000. In the case of polyisoprenes, the T_g can remain the same if the molecular weight is below than 5000. Therefore, this factor might also influence the T_g of natural rubber. Finally, the curing or vulcanisation of natural rubber can also increase the T_g value up to 3°C as a result of crosslinking between the curing agent (sulfur) and the rubber chain molecules during the curing process [9].

19

The value of the T_g for a natural rubber is an important parameter in vibration and noise control applications as it can be used to predict the temperature range in which the rubber can be applied efficiently as a good damping material.
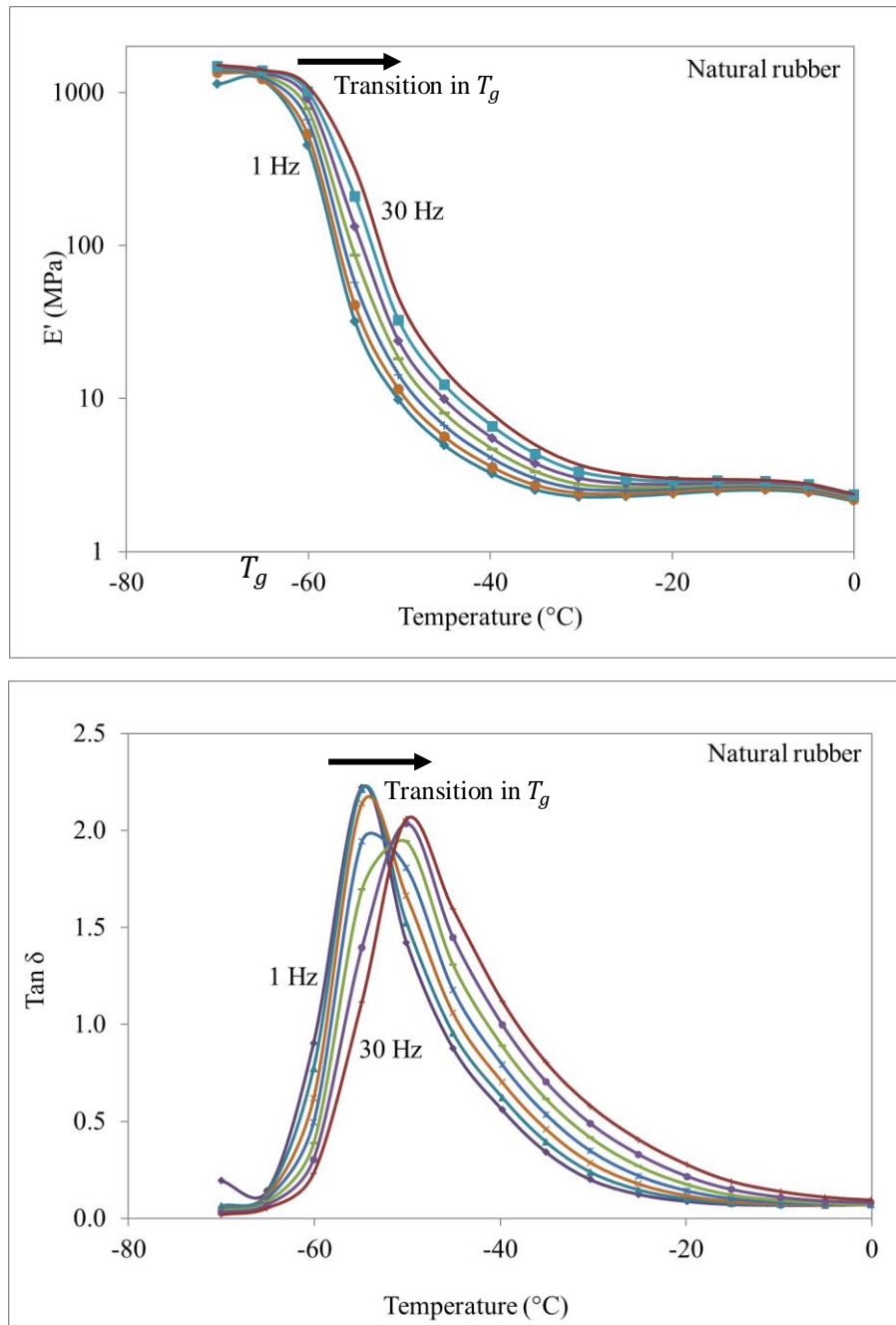
Figure 2.15: T_g transition in the storage modulus and loss factor for the natural rubber as a function of temperature at 1 Hz to 30 Hz [45].

2.4.3 Effect of temperature and frequency

In the case of temperature dependence, the rubber material behaviour is categorised into three regions, a glassy region, a transition region, and a rubbery region as shown in Figure 2.16 [46]. In the glassy region, the molecular movement of the material is restricted, resulting in the high value of the dynamic modulus whereas the loss factor is in the low value. As the temperature increases, molecule segments within the material move more and more. In this transition region, the dynamic modulus decreases drastically and the loss factor achieving its maximum value. Finally, in the rubbery region, the molecules are free to move. At this point, the dynamic modulus reaching its lowest value and the loss factor is back to the low value [46].
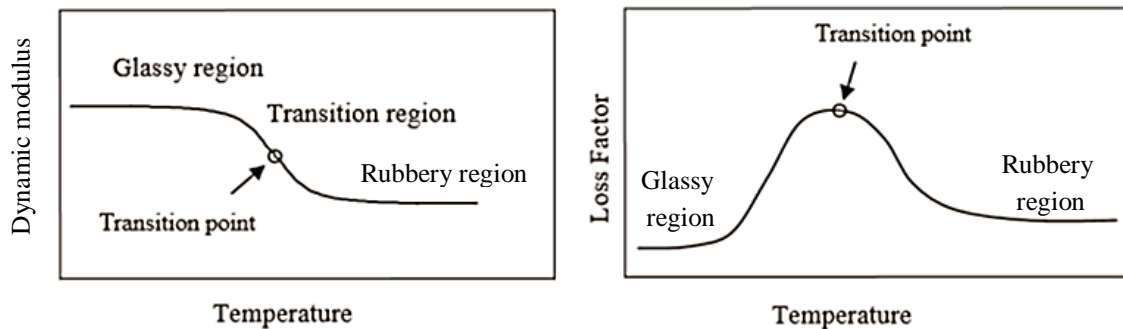
Figure 2.16: Temperature dependence of dynamic mechanical properties of rubber material at constant frequency [46].

A similar frequency dependence of the dynamic properties of rubber is shown in Figure 2.17. This example is for unfilled rubber for an extended frequency range at room temperature. Generally, the dynamic modulus increases with the increased frequency. The most dominant dependence on the frequency is in the transition region. The loss factor changes rapidly in the rubbery region. The loss factor reaches its peak in the transition region and decreases in the glassy region.

Referring to Figure 2.16 and 2.17, the effect of increasing temperature on the dynamic modulus is similar to that of decreasing frequency and vice versa. This relationship can provide the foundation for the time-temperature superposition principle [47].

21
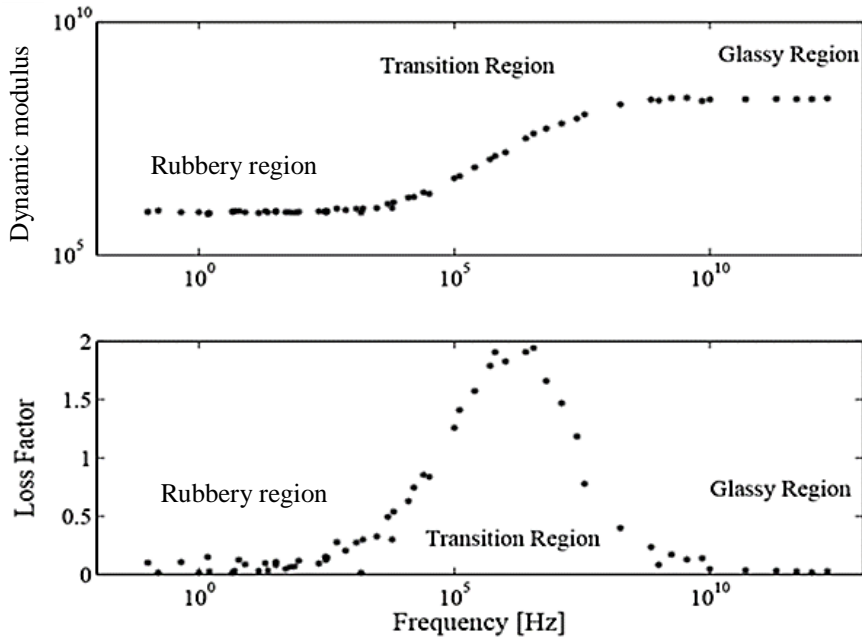
Figure 2.17: Frequency dependence of dynamic mechanical properties of rubber material at room temperature [46].

2.4.4 The time-temperature superposition principle

In practice, the dynamic mechanical properties of the rubber materials can be tested in a limited frequency range. However, it is possible to infer the dynamic mechanical properties of rubber over a wider frequency range using the time-temperature superposition principle. The advantage of this principle is that measurements at different temperatures can be used to predict the dynamic behaviour of the materials beyond the frequency range of the DMA machine [48].

Unfilled and unblended rubbers are single phase polymers with a single T_g [48], and these rubbers are known as thermorheologically simple materials [49]. The dynamic mechanical properties of these materials, at different temperatures can be shifted horizontally and vertically to obtain the master curves of dynamic modulus or loss factor in a wider frequency range for a given reference temperature [50]. Generally, the time-temperature superposition principle described by Rouleau *et al.* [50] is shown in Figure 2.18.
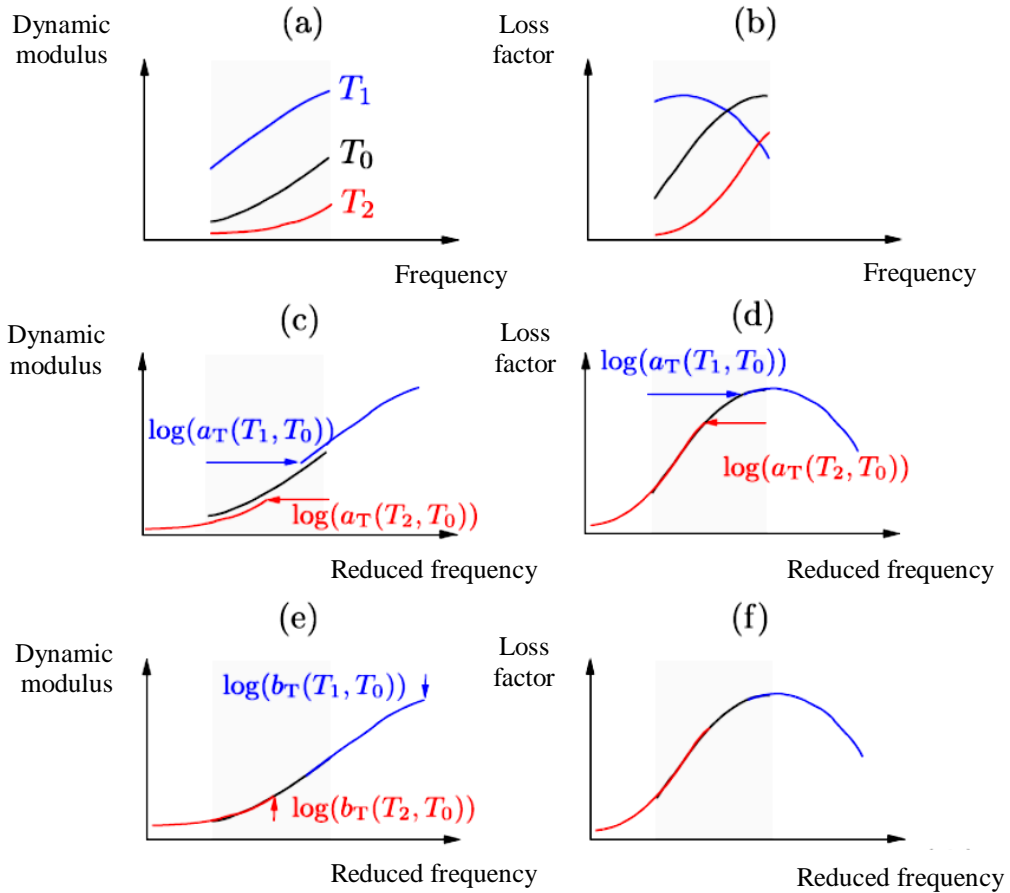
Figure 2.18: Time-temperature superposition principle [50].

Figure 2.18 (a) and (b) show the isothermal curves of the dynamic modulus and loss factor as a function of frequency measured at different temperatures, T_1, T_0 and T_2. These figures present data sets of complex moduli measured at a limited number of temperatures and over a very limited frequency range. Figure 2.18 (c) and (d) illustrate the method of horizontal shifting which is achieved using the shift coefficient, a_T. This enables us to express the dynamic modulus and loss factor as a function of a wider frequency range that is known as reduced frequency and at a reference temperature, T_0. In this process the isothermal curves are shifted either to the left or to the right along the frequency axis until they overlapped with the next curve. Figure 2.18 (e) and (f) demonstrate the method of vertical shifting using the coefficient b_T. The isothermal curves are shifted up or down along the complex modulus axis until they overlap with the next curve taken at a different temperature. Finally, a single master curve is obtained through this process so that the dynamic modulus or the loss factor can be determined as a function of the reduced frequency. The application of the time-temperature superposition principle on natural rubber and ENR will be discussed in detail in section 3.3.3.

2.5 Manufacturing process of natural rubber foam

It was earlier mentioned that a general way to produce natural rubber foams is through the use of natural rubber latex in liquid form or a dry natural rubber in solid form. A comparative study on the methods of manufacture between latex foam and dry rubber foam are presented in the following section.

2.5.1 Latex foam

Latex foam was invented in 1929 and now it serves a range of commercial applications. It has undergone many modifications and improvements to meet the demands of consumers [51]. Latex foam can be moulded in different shapes, sizes and also degrees of softness. The degree of softness can be varied from the softness of a bed pillow through the firmness of public transport seating. There are two major manufacturing processes to produce latex foam: Dunlop process; and Talalay process.

2.5.1.1 Dunlop Process

The Dunlop process was invented by Dunlop company in 1929 [52]. This process involves beating of air into compounded latex and adding a coagulating agent to gel or coagulate latex compounds. The production of latex foam can be achieved either with a batch process using a Hobart mixer with a wire cage mixing blade (Figure 2.19) or with a continuous foaming process using an Oakes mixer (Figure 2.20) [53].
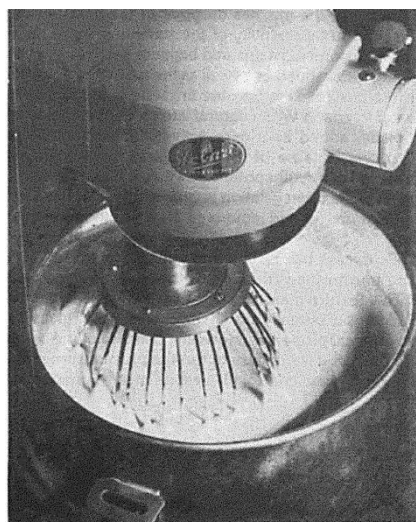
Figure 2.19: A Hobart mixer used to produce latex foam [52].
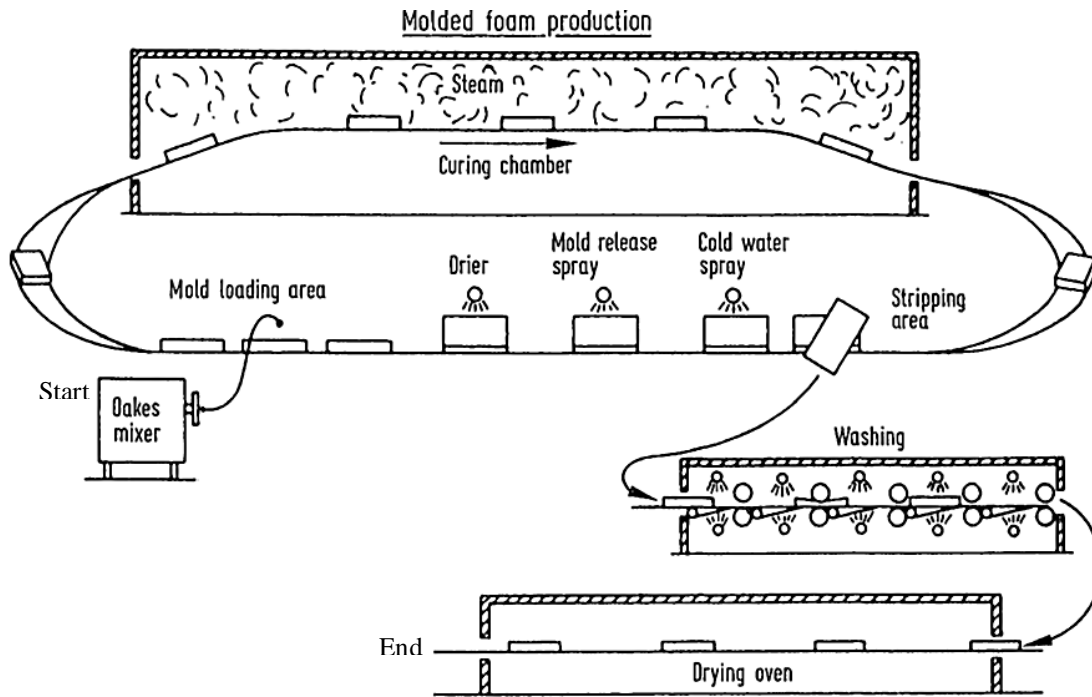
Figure 2.20: Production of latex foam using an Oakes mixer in the continuous foaming process [53].

Principally, the production of latex foam can be described into three stages: foaming, coagulating and curing. Foaming of the latex is achieved by mixing the latex mixture which contains soap solution with a mixing blade. The strong mixing action causes the air to be thoroughly mixed to provide a uniform foam. By controlling the amount of soap present in the latex compound, foams of various of density may be produced. The foam is then deposited into a series of moulds (Figure 2.21(a)). The mould lid is then closed. Coagulating or solidification of the foam inside the mould now occurs with the reaction of zinc oxide and coagulating agent (sodium silicofluoride). These chemicals were added immediately after the bubbling stage. As this reaction continues, the pH of the latex compound falls, and the destabilized rubber particles coalesce and form a gel. As pH of the latex compound decreases, the unconnected air bubbles break to form interconnecting pore structure in the coagulated foam. The mould is then pass through a steam chamber at $100°C$ for 25 minutes. The vulcanizing or curing process is taken place to convert the coagulated latex compounds inside the mould into latex foam. The mould from the steam chamber is then opened and cured latex foam is removed. This process is known as a stripping process (Figure 2.21(b)). Then, the latex foam is thoroughly washed to remove all the processing chemicals and dried to remove all moisture [51, 53].
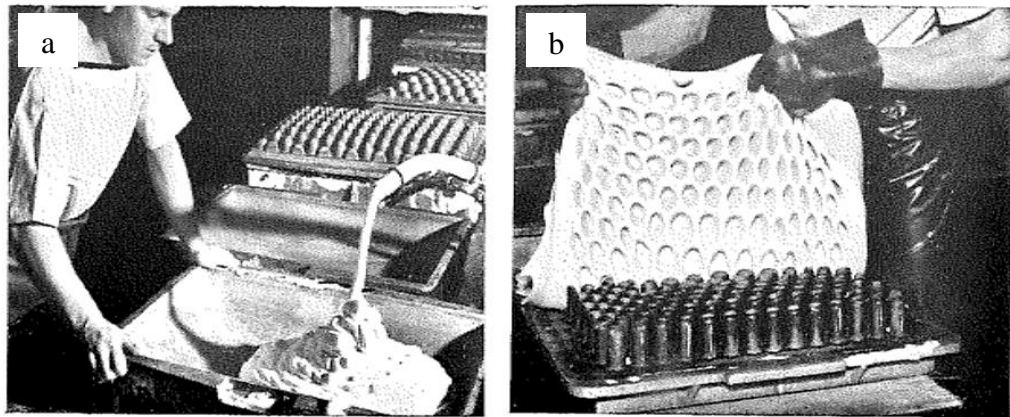
Figure 2.21: (a) Filling moulds; (b) Stripping a latex foam from the mould after vulcanisation [51].

Over the years, most of the large-scale latex foam manufacturers have been using the continuous foaming process because the mechanism of this process is relatively simple. The mixing process using an Oakes mixer has an internal coagulating system and it does not involve the transmission of heat and other external factors that can influence the coagulation directly. However, it is not always successful due to the complexity of the coagulating process. It needs good process control and well-experienced operators [52].

2.5.1.2 Talalay Process

The Talalay process, also known as the freeze process is the only commercial alternative to the Dunlop process. The Talalay process has similar procedure as the Dunlop process, with the exception that it has no coagulating agent [53]. The process starts with the foaming stage where the latex mixture is converting into foam with the action of a mixing blade. The foam is deposited in a closed mould. The air is extracted using vacuum to expand and distribute evenly the foam throughout the mould. The foam is then rapidly frozen to freeze its structure in place by circulating a coolant, glycol-water mixture at -30°C through passages in the mould. Then carbon dioxide gas is introduced in the mould to break the vacuum to concurrently permeate and to 'coagulate' the foam. The glycol-water mixture in the temperature range of 21°C to 27°C is then circulated through passages in the mould to thaw the foam. Glycol mixture is circulated again at 110°C to initiate the curing process. On completion of the curing process, this glycol-water mixture is circulated for the last time through the mould passages to cool the foam. The complete cycle of the whole process takes about 30 minutes. The mould is then opened and the foam is removed from the mould (Figure 2.22). The foam is thoroughly washed and dried as in way similar to the Dunlop process [52, 53].

The production of the latex foam using the Talalay process is relatively simple. However, the complexity of the mould can contribute to high expenditure and high maintenance costs. The process is typically used for the production of large samples of latex foams with regular shape such as pillows and mattresses and it is less suitable for the production of small and irregular shaped latex foam specimens [52]. The advantages and disadvantages between the Dunlop process and the Talalay process is given in Table 2.4.
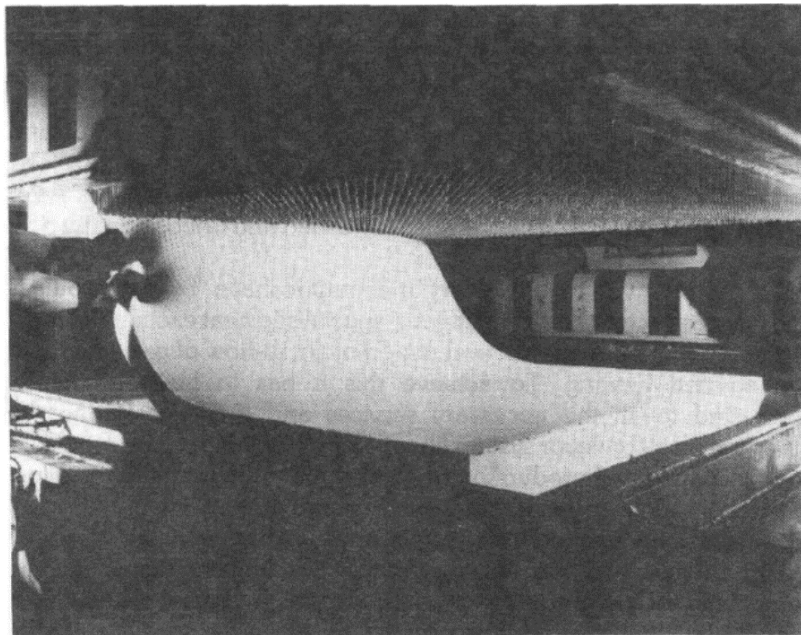
Figure 2.22: Removing the latex foam of a Talalay process from the mould after vulcanisation [52].

Table 2.4
Summary of latex foam processes [52].

	Dunlop process	Talalay process
Advantages	• Versatility. • Can produce moulded items of any shape and thickness.	• Easily automated. • No mould scrap. • Good foam stability at ambient temperatures.
Disadvantages	• Close process controls essential. • Foam stability very limited at ambient temperature. • Significant mould scrap.	• Relatively inflexible. • High capital outlay.

2.5.1.3 Natural latex and synthetic latex

All latex foam productions methods have been developed using natural latex until late 1950's [52]. Then, the demand for synthetic latex increased drastically. One of the factors is that synthetic latex is cheaper than natural latex. This factor has naturally encouraged latex foam manufacturers to consider using synthetic latex. At the beginning of 1960's synthetic latex manufactures made major improvements to synthetic latex which made them more practical to be used. Finally, the introduction of the Talalay process to the latex foam industry contributed to a high demand for synthetic latex. It is easier to use synthetic latex in this process as it can be cooled quickly before stripping. It reduces the possibility of tearing problem. However, the latex foam manufacturer is still using 0-20% and 30-50% of natural latex in synthetic latex compound in the Talalay and Dunlop processes, respectively. The natural latex compound is required to improve the tear strength of synthetic latex foam. The tear strength of the foam is important during the stripping process after cure and the low tear strength of the foam can cause major problems in the latex foam manufacturing process. The comparison of the characteristics of natural latex foams and synthetic latex foams is in Table 2.5.

Table 2.5
Comparison of natural latex and synthetic latex in foam manufacturing process [52].

	Natural latex	Synthetic latex
Stability of mixes	Fair-adequate	Very good
Coagulation	Easy	Difficult
Coagulate strength	Excellent	Fair
Tear strength	High	Poor
Mould shrinkage	High	Medium-low
Product tensile properties	Good	Fair

2.5.2 Dry rubber foam

The production of dry rubber foam can be produced either from natural rubber or synthetic rubber such as ethylene propylene diene monomer rubber (EPDM) and nitrile rubber (NBR).

However, as for natural rubber, the most typical method to manufacture foams is through the application of natural rubber latex [54]. Dry rubber foams can be categorized as open pore foam or closed-pore foam [53]. Open pore foam is similar to that of latex foam. They have an interconnecting pore structure, while closed-pore foam has no interconnecting between the pores completely as shown in Figure 2.23.
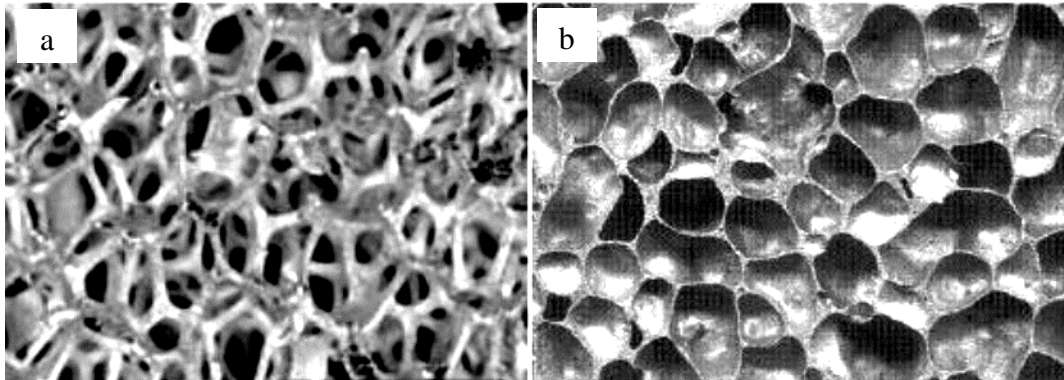
Figure 2.23: A comparison between (a) open pore foam and (b) closed-pore foam [55].

2.5.2.1 Open pore foam

Open pore foam can be produced in sheets, moulded strips and special shapes. The ingredients to produce open pore foam consist of inorganic blowing agents that produce gas. A most common blowing agent used by foam manufacturers is a carbon dioxide blowing agent known as sodium bicarbonate. Sodium bicarbonates or sodium carbonates are one of the alkali metals. However, all carbonates in this category require higher temperatures for their thermal decomposition than the bicarbonates. The decomposition pressures of the carbonates of alkali metals do not exceed 9 kPa to 12 kPa even at temperature of 1200°C, while the decomposition pressure of bicarbonates of alkali metals can reach 104 kPa at temperatures below than 200°C. Therefore, sodium bicarbonate seems to be the only material of interest in the production of polymeric foams. The thermal decomposition of sodium bicarbonate into carbon dioxide gas begins at 145°C to 150°C and it decomposed completely in 30 minutes. The foaming activity of this blowing agent system is relatively low, and the gas formation proceeds smoothly. Therefore, there is no risk of gas escaping immediately from the mould during the curing process. It is also relatively stable during transportation and prolonged storage [53]. Moreover, sodium bicarbonate is non-toxic, odourless and non-discolouring. Apart from sodium bicarbonate, a most typically used are ammonium carbonate and ammonium bicarbonate. These materials decompose into carbon

dioxide gas with a little ammonia gas upon heating process, and combination of both gases can create the synergistic effect in the blowing agent system [56]. The thermal decomposition of ammonia carbonate $((NH_4)_2CO_3)$ and ammonia bicarbonate (NH_4HCO_3) begins at 30°C and 60°C, respectively. Both blowing agents release the ammonia gas and the carbon dioxide gas as shown in the Equations 2.3 and 2.4 [53].

$$(NH_4)_2CO_3 \leftrightarrow 2\,NH_3 + CO_2 + H_2O \qquad\qquad (2.3)$$

$$NH_4HCO_3 \leftrightarrow NH_3 + CO_2 + H_2O \qquad\qquad (2.4)$$
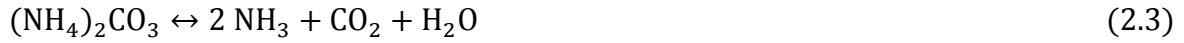
During the mixing process, a blowing agent is mixed together with raw rubber and other ingredients. Then, the blowing agent is dispersed to generate a medium of micro-spots which are stable at normal rubber processing temperatures. In the curing process, the temperature of the rubber is raised and these micro-spots of blowing agents are decomposed to release a gas which expands the soft rubber in the micro-spot area to produce a pore [56]. In order to prevent the pore structure from collapsing, the rubber compounds must allow the blown rubber to set up immediately prior to the vulcanisation or crosslinking process [53].

2.5.2.2 Closed-pore foam

Closed-pore foam can be manufactured into three methods: moulded at low pressure; moulded at high pressure; and continuously extruded at ambient pressure. These manufacturing methods use the same kind of organic blowing agents that decompose into nitrogen. Nitrogen has relatively lower solubility than carbon dioxide, and this property allows the production of closed-pore foam [53]. Table 2.6 shows major chemical types of organic blowing agents used to produce closed-pore foam. Among these organic blowing agents, BSH blowing agents are very active as they have lowest decomposition temperature. Therefore, they are normally used with other blowing agents as they have an advantages in reducing the cure rate [53].

Manufacturing processes to produce low-pressure moulded closed-pore foam are similar to those used for open pore foam. However, the production of high-pressure moulded closed-pore foam is much different particularly in terms of the curing process. This production makes use of a two-step cure process. Firstly, rubber compounds are filled completely in the

mould, and high pressure is applied to partially set the rubber compounds and to activate the blowing agent. The mould is opened in the second step to release the internal gas pressure and to allow the expansion of rubber foam within the mould. Then, the rubber foam is post-cured. In the case of the continuous extrusion method, rubber compounds are extruded through a die in the extruder and cured rapidly using hot air, liquid curing medium or microwave. At this stage, extruded rubber expands at ambient pressure without restriction as it is not being produced in a closed-mould. However, this method needs good process control particularly in terms of the rates of curing and blowing to produce a continuous rubber foam with unvarying density [53].

Table 2.6
Major chemical types of organic blowing agents [56].

Chemical name	Abbreviation	Decomposition temperature (°C)	Gas yield (ml/g)	Properties
Azodicarbonamide, Azo-bis(formamide)	ADC	160 to 180	180	Medium efficiency. Odourless. Accelerates cure.
N, N'-dinitrosopenta-methylenetetramine	DNPT	120 to 125	260	High efficiency. Low cost. Fishy smell. Discolours rubber.
Benzene sulphonylhydrazide	BSH	90 to 100	130	Medium efficiency. Non-toxic. No odour. Non-discolouring.

2.5.3 Research status of dry rubber foam

Natural rubber foam produced from latex is generally used in commercial applications such as mattresses and pillows. However, latex has low homogeneity as it contains only 30% to 40% rubber particles in the medium and remaining compositions are organic substances and inorganic minerals [7]. Moreover, latex requires chemical stabilization for the stable colloidal dispersion, as it is easily affected by the environment so that the storage and handling are critical. On contrary, dry natural rubber foam is more homogeneous and it is less affected by difficulties related to the latex processing [4]. Dry natural rubber foams have great potential for numerous commercial applications such as in the automotive industry, footwear, sports equipment, packaging and toys. However, there has been little attention

given to the production of dry natural rubber foams [57], and only a few studies have been reported on these foams production. For example, Metherell [58] presented information on the physical properties of natural rubber foams made from natural rubber, ENR-25 and ENR-50. The blowing agents used were organic blowing agents: azodicarbonamide (ADC); benzene sulphonylhydrazide (BSH); and *p*-toluene sulphonylhydrazide. The mixing process of the rubber compounds was carried out in a laboratory Banbury mixer at 100°C and the two-step cure process was applied. The rubber compounds were filled in the mould with 102% mould loading and cured at 140°C. The foaming pressure and curing time were 12 MPa and three minutes, respectively. Then, the second step of curing was carried out in air oven for 1 hour at 125°C. The author found that the foam densities were in a range of 240 to 280 kg/m^3 and all the foams produced had very fine closed-pore structures as shown in Figure 2.24. A water absorption testing on the foams was also carried out. The results indicated that all these foams had low water absorption were basically closed pore materials.
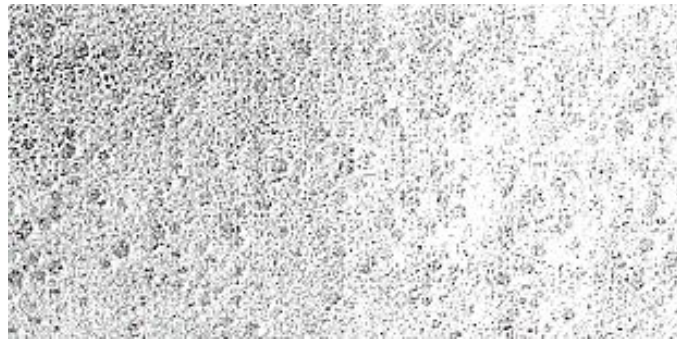
Figure 2.24: Micrograph of the pore structure of ENR-50 foam [58].

Another recent study by Kim *et al.* explored the effects of the foaming pressure [59] and curing temperature [60] on natural rubber foam produced by a one-step cure process. The blowing agent used was N, N'-dinitrosopentamethylenetetramine (DNPT). All the ingredients listed in ref. [59] and [60] were mixed using a two-roll mill machine. The compounded rubber was left for at least 24 hours prior to the curing process. Then, the rubber compound was filled in the closed-mould. The mould was then transferred into an electrically heated hydraulic press. The curing process was taken place to convert the rubber compound inside the mould into natural rubber foam. The authors investigated four different foaming pressures of 1.5 MPa, 2.5 MPa, 3.5 MPa and 4.5 MPa in ref. [59] and three different curing temperatures of 145°C, 150°C and 155°C in ref. [60]. They found that the density of the natural rubber foam increases with the increasing foaming pressure. The apparent density

was increased from 460 kg/m^3 at foaming pressure of 1.5 MPa to 590 kg/m^3 at foaming pressure of 4.5 MPa. It was also observed that increasing in foaming pressure resulted in higher thickness of pore wall as shown in Figure 2.25. They have stated that high foaming efficiency can be obtained with a low foaming pressure at 1.5 MPa. In contrast, the density of natural rubber foam decreases with the increasing curing temperature. The apparent density of foam decreased from 600 kg/m^3 at curing temperature of 145°C to 470 kg/m^3 at curing temperature of 155°C. The authors were also found that increasing in curing temperature leading to lower thickness of pore wall as shown in Figure 2.26, and high foaming efficiency can be obtained with high curing temperature at 155°C.
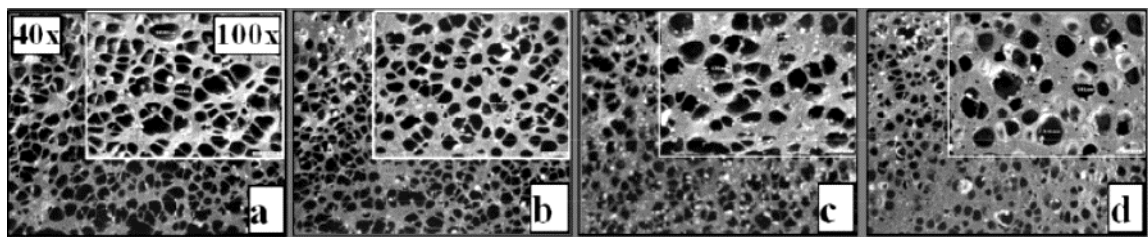
Figure 2.25: Microscopy images of natural rubber foam at different foaming pressures of (a) 1.5 MPa, (b) 2.5 MPa, (c) 3.5 MPa and (d) 4.5 MPa [59].
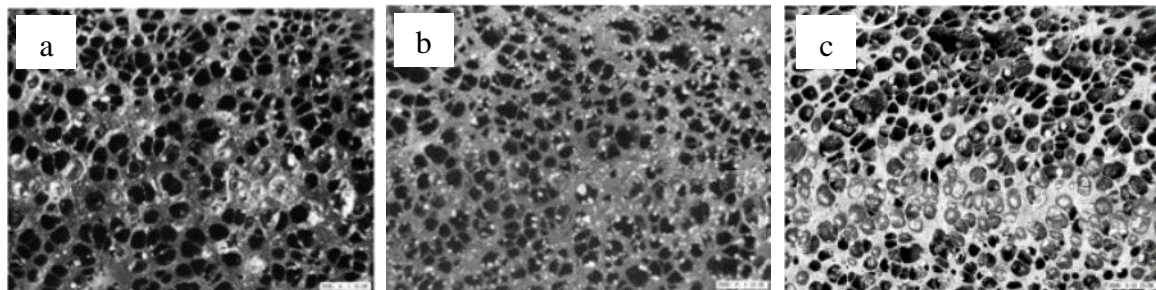
Figure 2.26: Microscopy images of natural rubber foam at different curing temperatures of (a) 145°C, (b) 150°C, and (c) 155°C [60].

Effect of curing temperature on the production of natural rubber foams were also studied by Najib *et al.* [4] and Ariff *et al.* [54]. They have investigated the physical properties and morphological study of natural rubber in ref. [4] and ENR-25 in ref. [54] at different curing temperatures of 140°C, 150°C and 160°C. Both studies use sodium bicarbonate as the blowing agent in the production of natural rubber foams. The methods to manufacture the foams were also similar with the utilization of a two-roll mill machine and implementation of a two-step cure process. The ingredients were mixed at room temperature and the mixing time was kept below 30 minutes. The rubber compounds were moulded in the compression

mould at a temperature of 100°C for 2 minutes as the first step. It was then cured in an air-oven for 20 minutes at three different temperatures of 140°C, 150°C and 160°C. They were also observed that the density of natural rubber foams decreased and average pore size increased with the increasing curing temperature. The density measured decreased approximately 30% and 10% for the natural rubber foam and the ENR-25 foam, respectively. At higher curing temperature, carbon dioxide decomposed from the blowing agent promotes the pore walls to expand further and to reduce the pore wall thicknesses of natural rubber foam and ENR-25 foam as shown in Figure 2.27 and Figure 2.28, respectively. This expansion of the pore walls can also be ruptured to form larger pores and resulted in foam with a lower density [4, 54]. However, the density changes for ENR-25 foam was not significant as the curing temperature increased. This is due to the presence of epoxide groups in ENR matrix that can accelerate the crosslinking of the rubber chains during the curing process. Therefore, this immediate reaction can possibly restrict the pore expansion process and resulted in small density reduction [54].
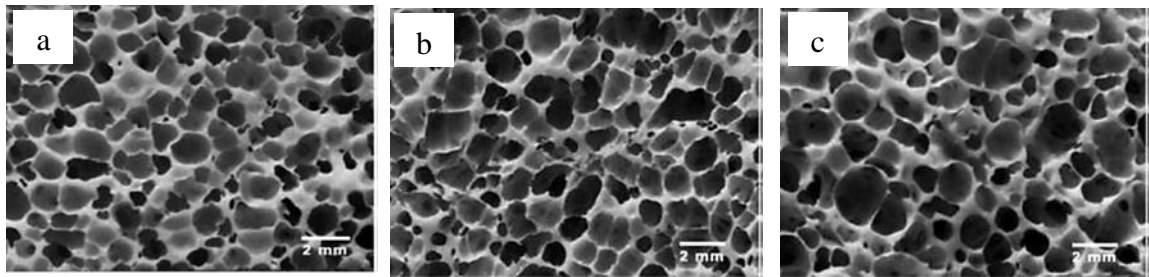
Figure 2.27: Microscopy images of natural rubber foam at different curing temperatures of (a) 140°C, (b) 150°C, and (c) 160°C [4].
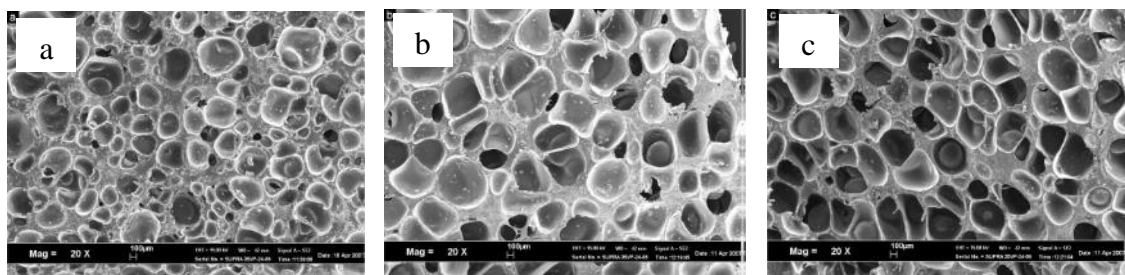
Figure 2.28: Microscopy images of ENR-25 foam at different curing temperatures of (a) 140°C, (b) 150°C, and (c) 160°C [54].

The work reported in ref. [4] focused on the dynamic and acoustic properties of dry natural rubber foams. The authors measured the storage modulus and the tan δ of natural rubber

foam for different curing temperatures of 140°C (NR 140), 150°C (NR 150) and 160°C (NR 160) as shown in Figure 2.29 and Figure 2.30, respectively. The dynamic behaviour of foam was carried out over the temperature range of -100°C to 100°C at 1 Hz excitation. The authors observed that the storage modulus decreased and the tan δ increased with the increasing curing temperature. They stated that the NR 160 foam had the lowest elastic behaviour and the highest damping behaviour as compared to the NR 140 and NR 150 foams. All the foams tested were exhibited with high storage modulus in the low temperature region. Then, the storage modulus value decreased with the increasing temperature and finally converged for all the three foams at around below -40°C. The storage modulus of the NR 160 foam was found lower than that of NR 140 foam because it had lower amount of solid phase. This result was correlated with the reduction of density and increasing of curing temperature.
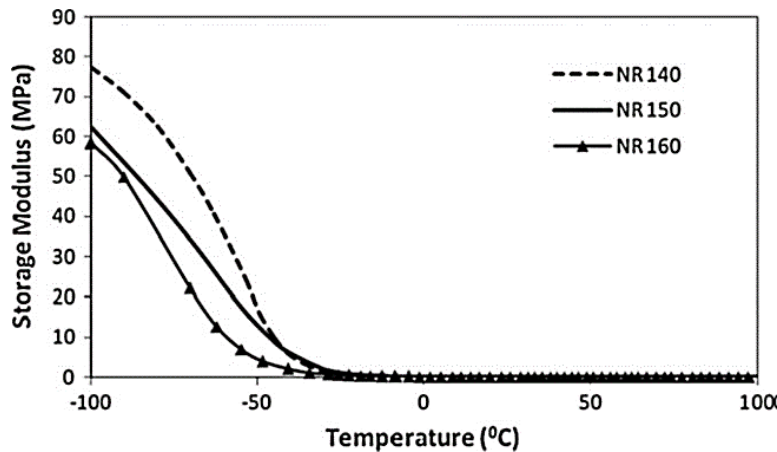
Figure 2.29: The dependence of the storage modulus for NR 140, NR 150 and NR 160 foams as a function of temperature at 1 Hz [4].
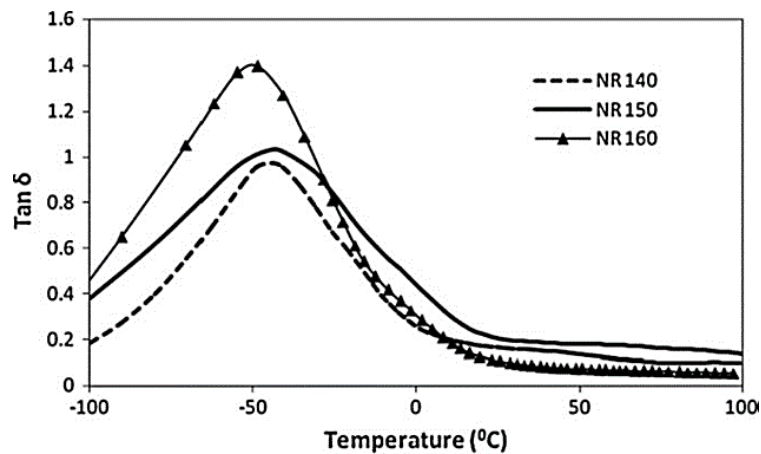
Figure 2.30: The dependence of the tan δ for NR 140, NR 150 and NR 160 foams as a function of temperature at 1 Hz [4].

35

The maximum of tan δ increased with the increasing curing temperature. The authors stated that increasing of curing temperature resulted in foam with a lower amount of solid phase. This factor contributed to a decrease in the value of the elastic modulus and produced foam with a higher tan δ value.

The authors of [4] have also presented the sound absorption coefficient of natural rubber foam developed at different curing temperatures. These data are shown in Figure 2.31. The authors found natural rubber foams were relatively efficient as sound absorbing materials in the frequency range of 1000 Hz to 2000 Hz. These observations were controlled by the physical properties of foam such as pore size and density.
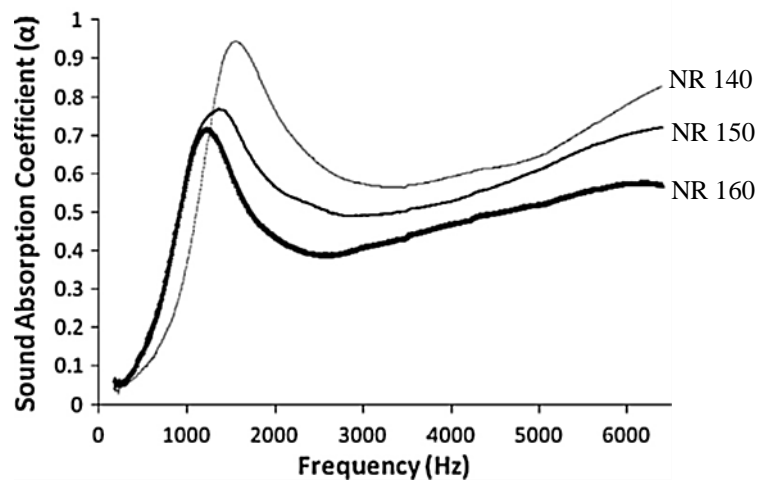
Figure 2.31: Sound absorption coefficient for NR 140, NR150 and NR 160 foams as a function of frequency [4].

2.6 Vibro-acoustic of porous material

A porous material contains porous structure which acts as an acoustic absorber. The performance of porous materials is influenced by the porosity and pore size. The porosity allows sound waves to penetrate the porous structure while the pore size is responsible for the energy dissipation in the sound wave that penetrates the porous structure. If the pore size is relatively small, then the energy dissipation from the sound waves is relatively high, but limited proportion of sound waves can penetrate to the porous structure. However, if the pore size is relatively large, more sound energy can penetrate the porous structure, but the energy dissipation from the sound waves is relatively low [61]. The relationship between the pore size and the sound absorption of porous materials is shown in Figure 2.32.
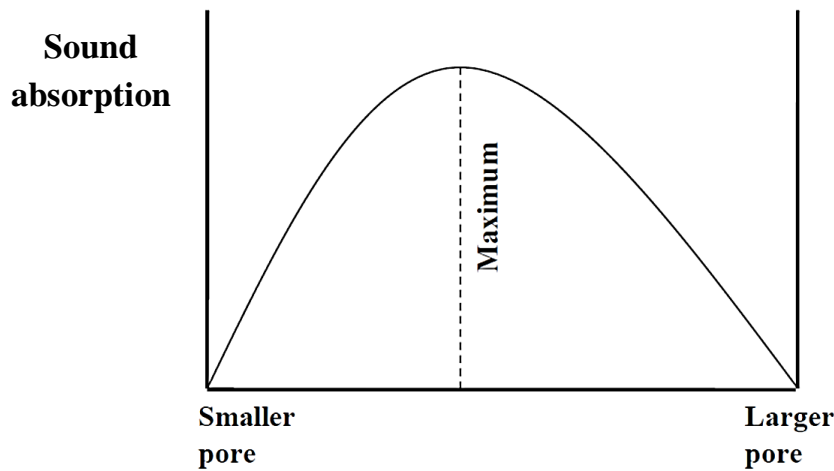
Figure 2.32: The relationship between the pore size and the sound absorption of porous materials [61].

2.6.1 Sound attenuation and sound propagation of porous material

The human ears are sensitive to sound waves with the frequency in the range of 20 Hz to 20,000 Hz, equivalent to the wavelengths in air between 17 m to 17 mm. The sound waves produce a change of air pressure in between 10^{-4} Pa to 10 Pa. The sound velocity, v, in porous medium can be expressed as [62]:

$$v = \sqrt{\frac{E}{\rho}}, \tag{2.5}$$

where E is Young's modulus and ρ is the density. Generally, there are three mechanisms for sound attenuation: absorbing, insulation and damping. A sound absorbing material is needed if the sound is generated within the enclosed space such as an office room, while the sound insulating material is essential to keep out the sound from outside comes to the office room. If a sound wave comes from a source of the vibrations that transmitting through the wall of a room, then vibration isolation and damping material is required. In the case of the porous materials, they can be really efficient as absorbing materials, and they can also combine with other materials for the vibration isolation and damping purposes. The sound insulation is related to the mass of the material which sound has to penetrate. The material with relatively high mass can insulates against sound effectively. Lightweight porous materials are not

recommended to be applied for this purpose but can be used in combination with other more denser materials [62].

Porous materials have two phases; the solid porous structure referred to as the frame and the fluid (air) which is contained in the pores confined by the frame. The sound absorption of a porous material can be described by two mechanisms. The first mechanism is the viscous losses which happen through the friction between the fluid and frame. This frictional force is then converting the sound waves or sound energy into heat. The second mechanism is the thermal losses which happen through the irreversible heat flow within the porous space [4].

In general, porous materials can be categorised as follows;

a. Rigid: The frame does not move significantly with the motion of the fluid. This is due to the frame has high stiffness or the density of the frame is higher than the density of the fluid [63].

b. Limp: The frame can move freely with the motion of the fluid. This is resulting to the density of the porous material is comparable with the density of the fluid or the frame is not self-supporting.

c. Elastic: The expanded frame has higher bulk modulus of elasticity than the fluid. The frame interacting with the motion of the fluid and the resultant structure vibrations need to be considered [61].

The sound propagation in a porous material is a mechanism that is governed by acoustic and non-acoustic properties that relate to the porous structure of the material. Key material properties of porous media are listed in Table 2.7. The procedure details of each property are presented in section 5.2.

Table 2.7
Acoustic and non-acoustic properties of porous materials.

Acoustic	Non-acoustic
• Sound absorption coefficient	• Porosity
	• Airflow resistivity
	• Dynamic properties

2.6.2 Determination of the dynamic measurement of porous material

The dynamic behaviour of porous materials is similar to the behaviour exhibited by solid viscoelastic materials. The stiffness of porous materials is relying on the force loading and a hysteresis is also can be observed upon the application of cyclic loading [64].

As an example, the viscoelastic behaviour of a porous material was investigated in ref. [65]. They were studied the stress versus strain for a melamine foam, and the stress-strain plot is illustrated in Figure 2.33. There are three regions of the viscoelastic behaviour for a porous material. The first region is the linear bending region. The stress increases drastically with strain. The porous material is started to bend and stretch and there is limited small strains in this region. The second region is the buckling region. In this region, the stress increases slowly with strain due to the buckling of the porous material. Finally, the third region is the densification region. The porous material collapses and acts as a solid material [62].
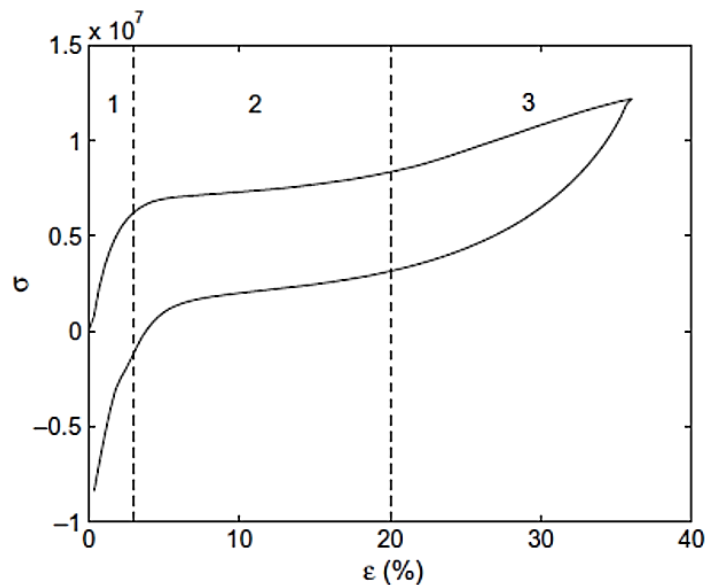
Figure 2.33: The stress-strain plot for a melamine foam at 24°C and the three viscoelastic regions [65].

The recent study reported by Bonfiglio *et al.* [66] investigated the accuracy of various testing methods using five different porous materials in several laboratories worldwide (round robin test). In total, there were 14 laboratories involved in this study as listed in Table 2.8.

Table 2.8

Fourteen laboratories involved in the measurement of dynamic properties of porous materials [66].

No.	Laboratory
1	University of Ferrara (Italy)
2	Adler Pelzer Holding GmbH (Italy-Germany)
3	STS-Acoustics (Italy)
4	Polytechnic of Milan (Italy)
5	University of Sheffield (UK) and Tun Abdul Razak Research Centre (UK)
6	Matelys Research Lab/ENTPE (France)
7	Laboratoire d'Acoustique de l'Universite du Maine (France)/LMSSC/Bourgogne
8	Cnam/PIMM (France)
9	Laboratoire Roberval de l'Universite de Technologie de Compiegne (France)
10	Saint-Gobain Isover (France)
11	Katholieke Universiteit Leuven (Belgium)
12	Autoneum (Switzerland)
13	IRSST/Ecole de Technologie Superieure (Canada)
14	Sherbrooke University (Canada)

Five different porous materials were tested as shown in Figure 2.34. These were (A) reticulated foam, (B) glass wool, (C) porous felt, (D) closed cell polyurethane foam and (E) reconstituted porous rubber. The physical properties of these porous materials are given in Table 2.9. According to ref. [66], the selection of these materials can represents typical porous materials used in vibration and noise control applications.
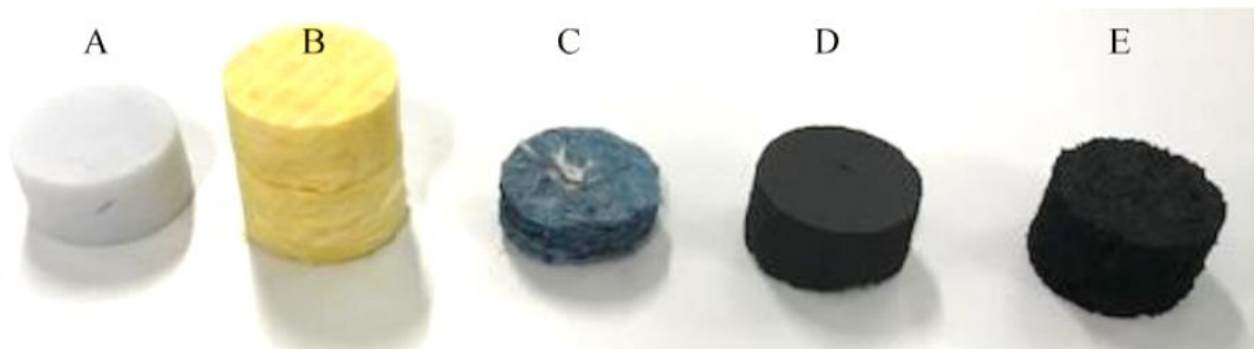
Figure 2.34: The tested porous materials; (A) reticulated foam, (B) glass wool, (C) porous felt, (D) closed cell polyurethane foam and (E) reconstituted porous rubber [66].

Table 2.9
The physical properties of the tested porous materials [66].

Material	Description	Nominal thickness (mm)	Nominal density (kg/m^3)
A	Reticulated foam	25	10
B	Glass wool	50	80
C	Porous felt	20	40
D	Closed cell polyurethane foam	25	48
E	Reconstituted porous rubber	25	240

The reproducibility of five methods to determine the dynamic properties of porous materials was studied. There was quasi-static uniaxial compression method, resonant method, lamb wave propagation method, transfer function/transfer matrix method and dynamic mechanical analysis. The procedure of each method is presented in section 5.2.2.

The measurement methods used by each laboratory is summarised in Table 2.10. The laboratory names were randomised and denoted as a number of one to fourteen. Therefore, these laboratories are referred as Laboratory 1 to Laboratory 14.

Table 2.10
Summary of measurement methods used by the 14 laboratories [66].

Measurement method	Laboratory
Quasi-static uniaxial compression method	2,3,6,8,9,10
Resonant method	1,4,7,11
Lamb wave propagation method	5
Transfer function/transfer matrix method	3B[1]
Dynamic mechanical analysis	12,13,14

[1]Laboratory 3 used two different measurement methods. 3B is the second method.

Figures 2.35 to 2.39 show the storage moduli and loss factors of each porous material measured by all the 14 laboratories. Generally, closed cell polyurethane foam and reconstituted porous rubber displayed strong viscoelastic behaviour as the storage moduli and loss factors increase with the increasing frequency. However, the overall dynamic behaviour of each porous material shows poor reproducibility between the 14 laboratories. It can be seen clearly from the results that the dynamic properties of porous materials have high dependency on the measurement method. The authors were also observed that the storage moduli of glass wool, porous felt and reconstituted porous rubber have a strong dependence on the varying static preload.

The authors in ref. [66] suggested that there is a need for the measurement standardisation to determine the dynamic properties of porous material. There are several aspects that need to be standardised such as the test preparation and installation of the porous materials, test calibration procedures, and number of samples to be tested. Therefore, a new international standard for dynamic properties measurement of porous material is required.
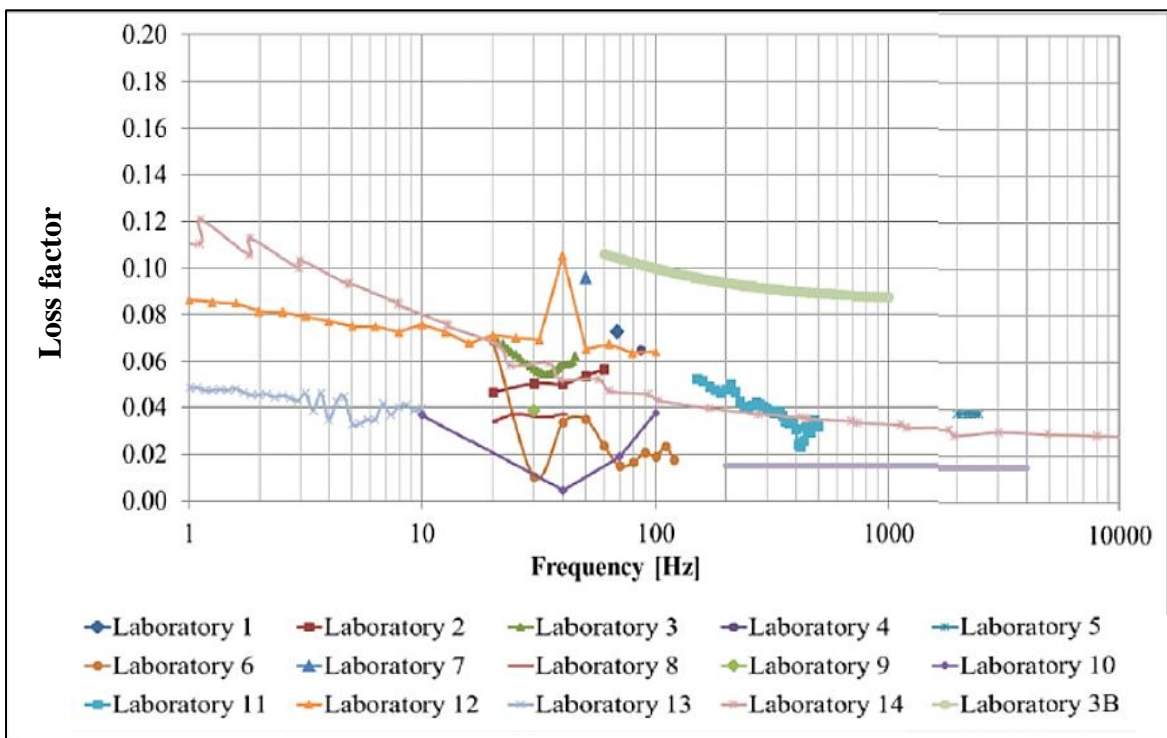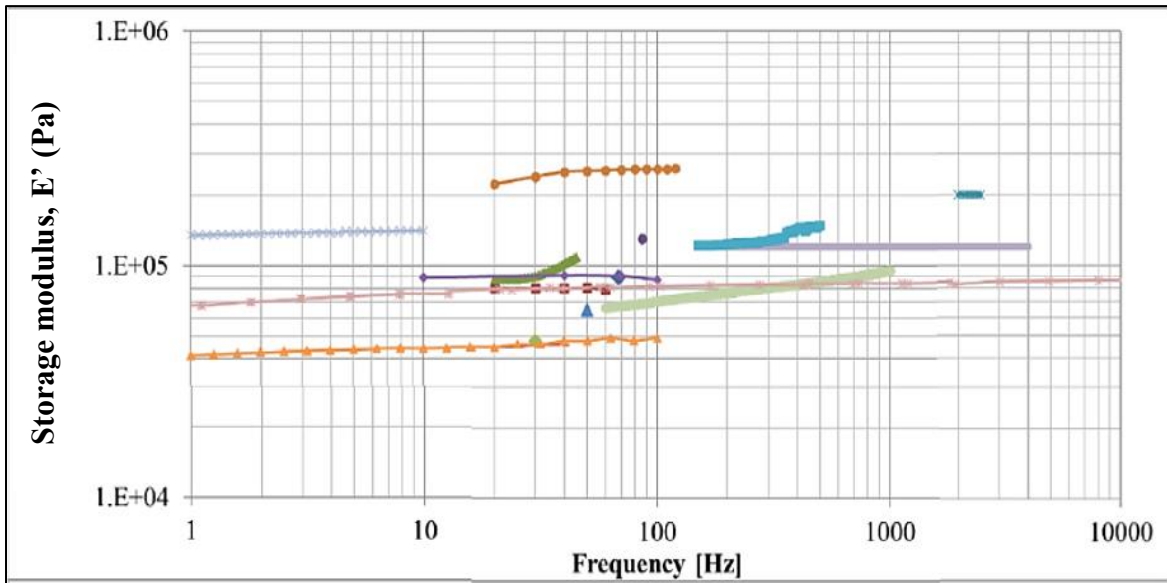
Figure 2.35: The dependence of the storage moduli and loss factors for reticulated foam [66].
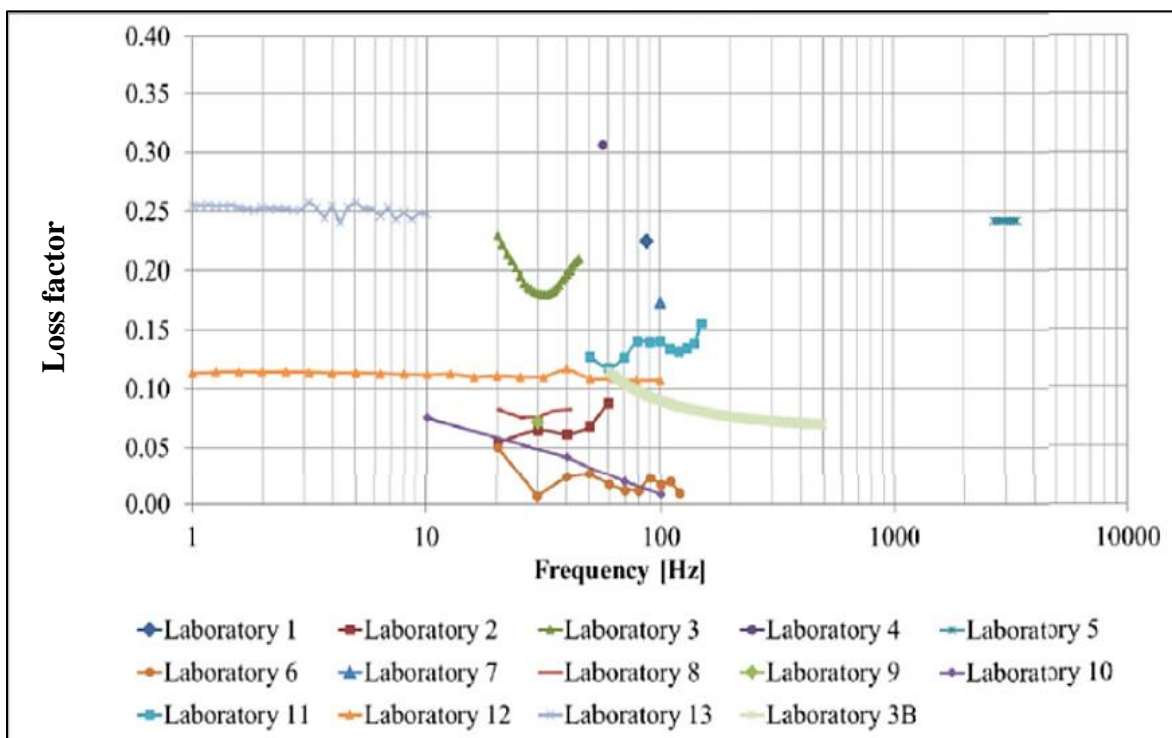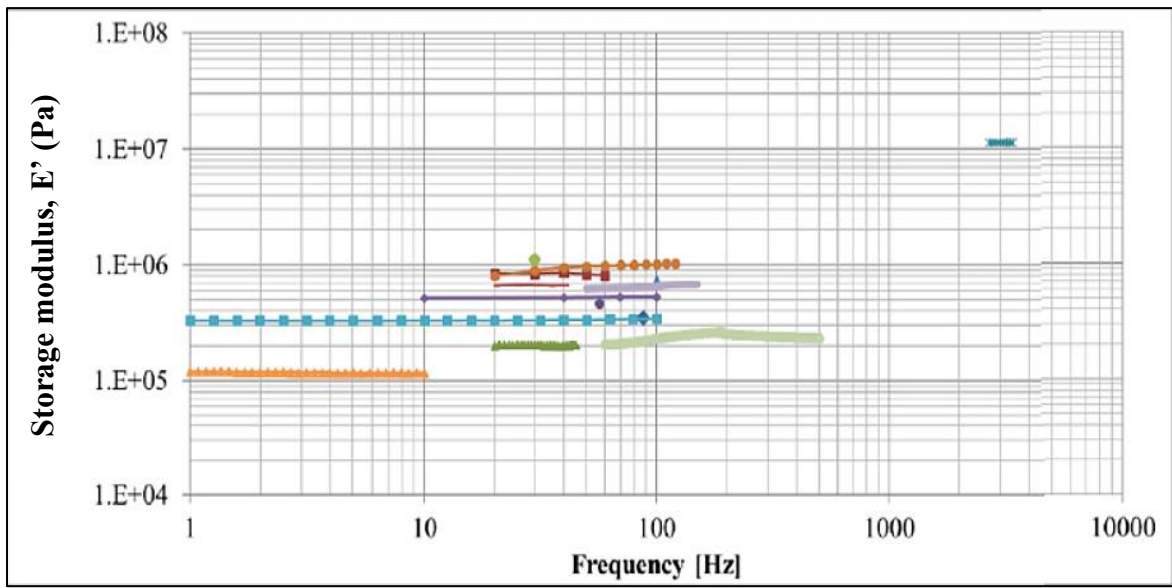
Figure 2.36: The dependence of the storage moduli and loss factors for glass wool [66].
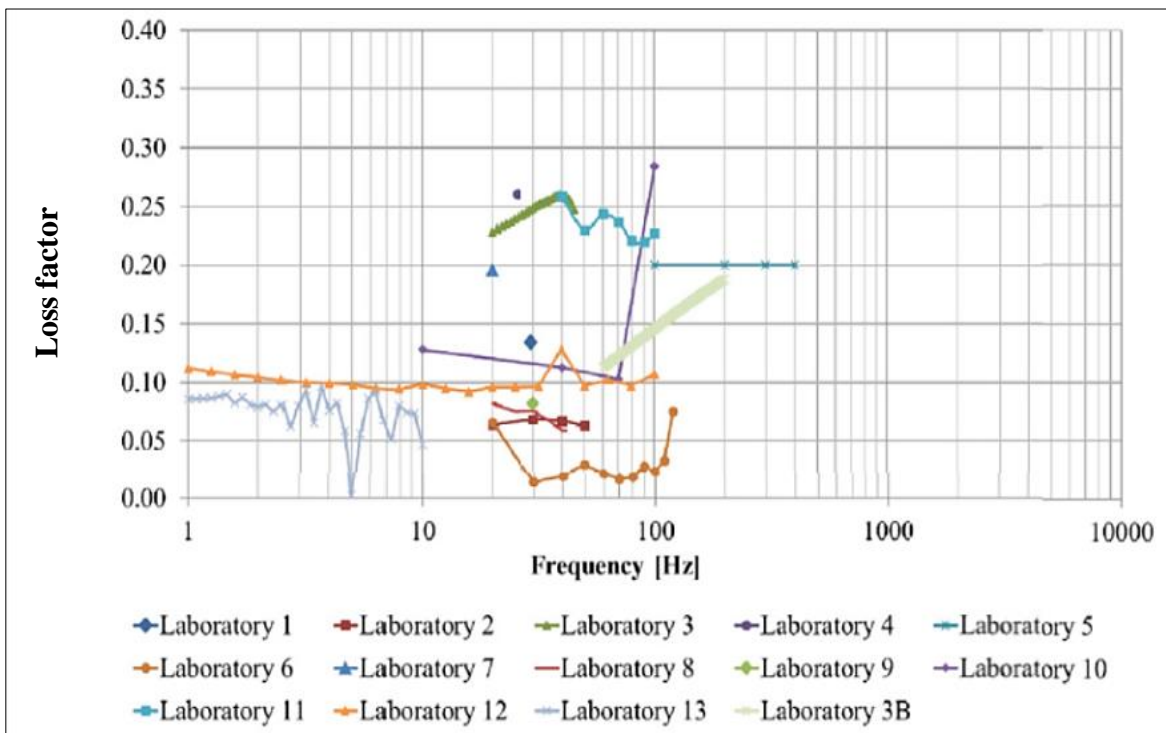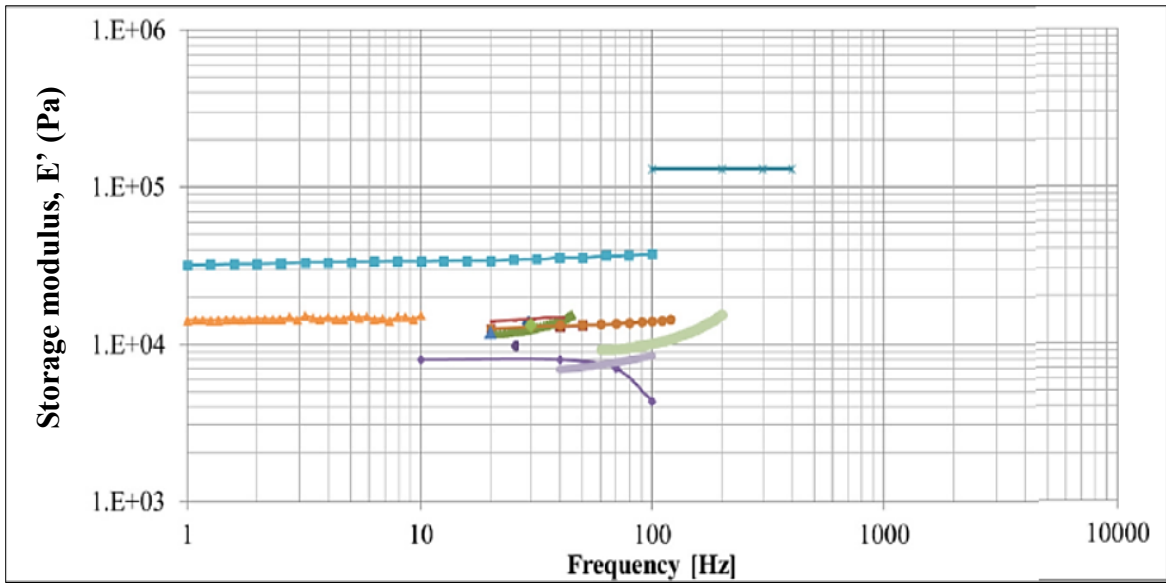
Figure 2.37: The dependence of the storage moduli and loss factors for porous felt [66].
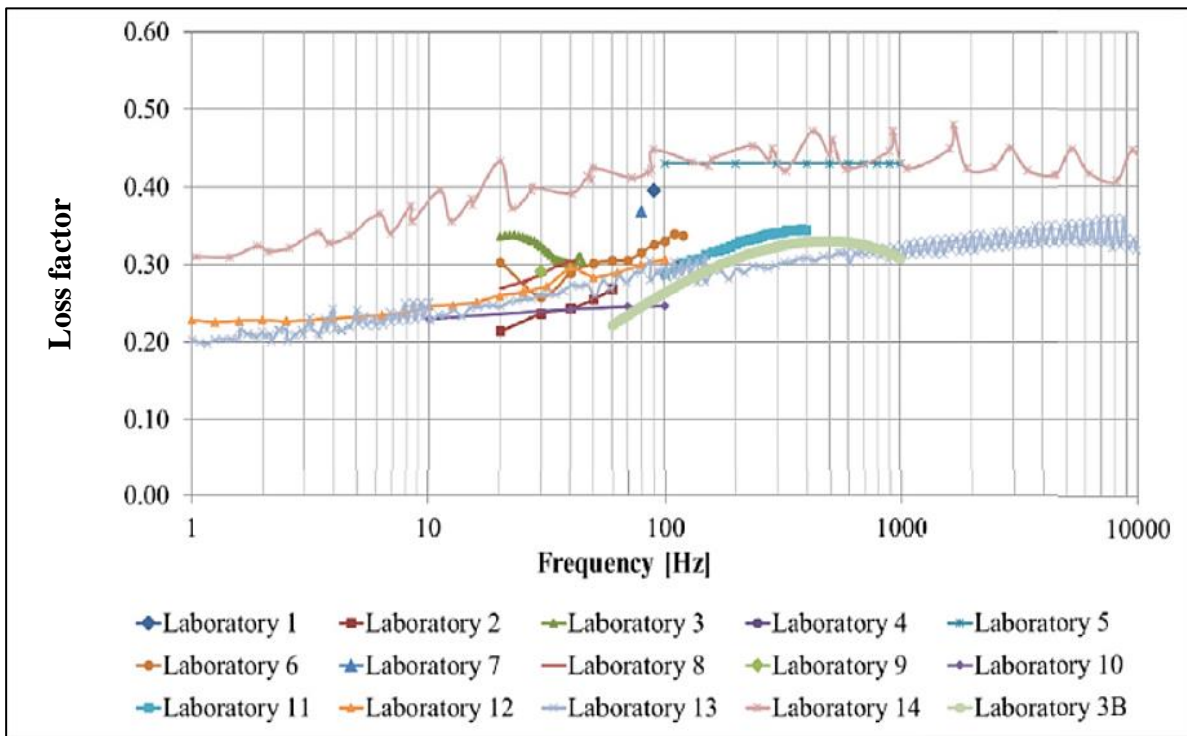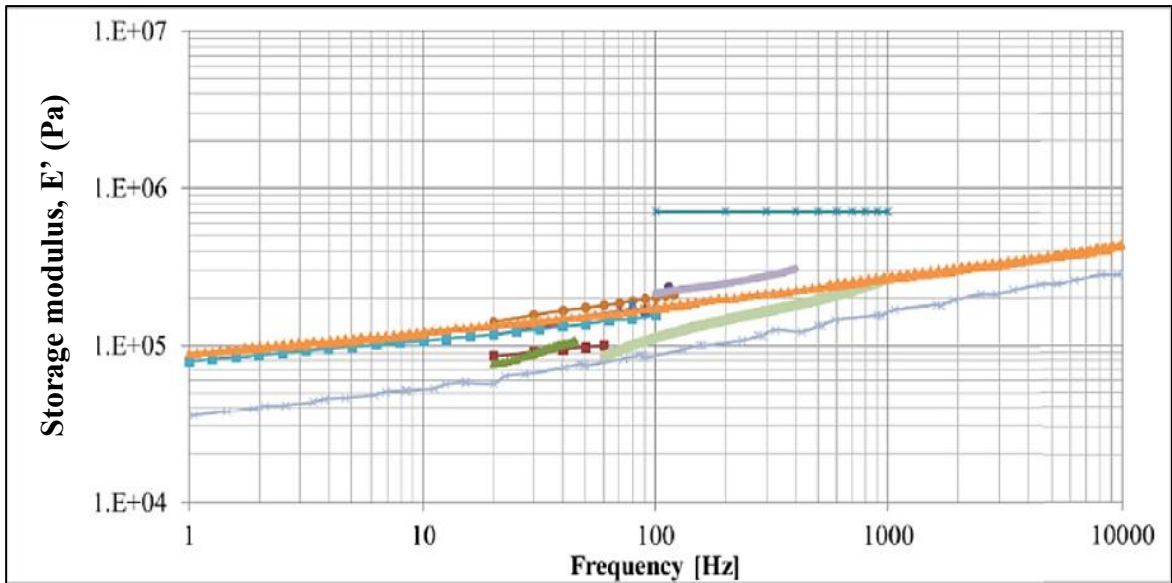
Figure 2.38: The dependence of the storage moduli and loss factors for closed cell polyurethane foam [66].
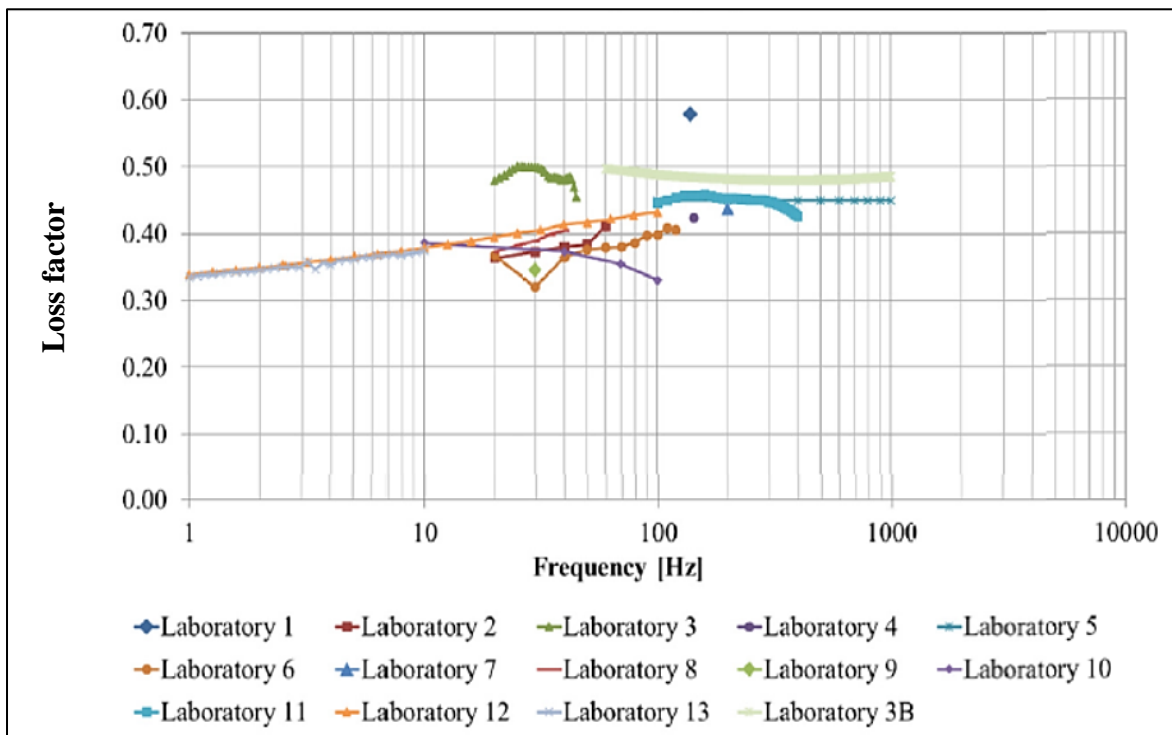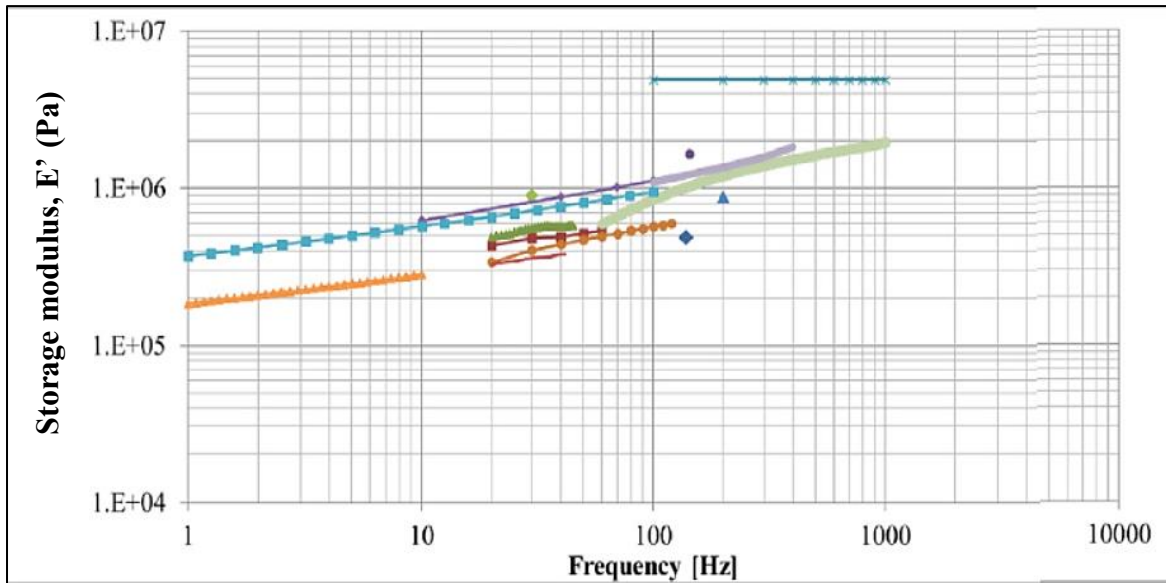
Figure 2.39: The dependence of the storage moduli and loss factors for reconstituted porous rubber [66].

2.6.3 Determination of the acoustical characterisation of porous material

The acoustical characterisation of porous material is crucial to determine the acoustic behaviour of this material and also to predict the non-acoustic properties data that are related to their porous microstructure. A standard method to measure the acoustical properties of porous material is the impedance tube method. The measurement of this method can provide the sound absorption coefficient and surface impedance of porous material [63]. The procedure of this method is presented in section 5.2.4.

The recent study reported by Pompoli *et al.* [67] evaluated the accuracy of the acoustical characterisation of porous material. They were investigated three different porous materials in seven laboratories worldwide (round robin test) as listed in Table 2.11.

Table 2.11
Seven laboratories involved in the acoustical characterisation of porous materials [67].

No.	Laboratory
1	University of Ferrara (Italy)
2	University of Perugia (Italy)
3	University of Bradford (UK)
4	Matelys Research Lab/ENTPE (France)
5	Katholieke Universiteit Leuven (Belgium)
6	Sherbrooke University (Canada)
7	Gesellschaft fur Akustikforschung Dresden (Germany)

Three different porous materials were tested as shown in Figure 2.40. These were (A) reticulated foam, (B) consolidated flint, and (C) reconstituted porous rubber. The thickness and density of these porous materials are given in Table 2.12.
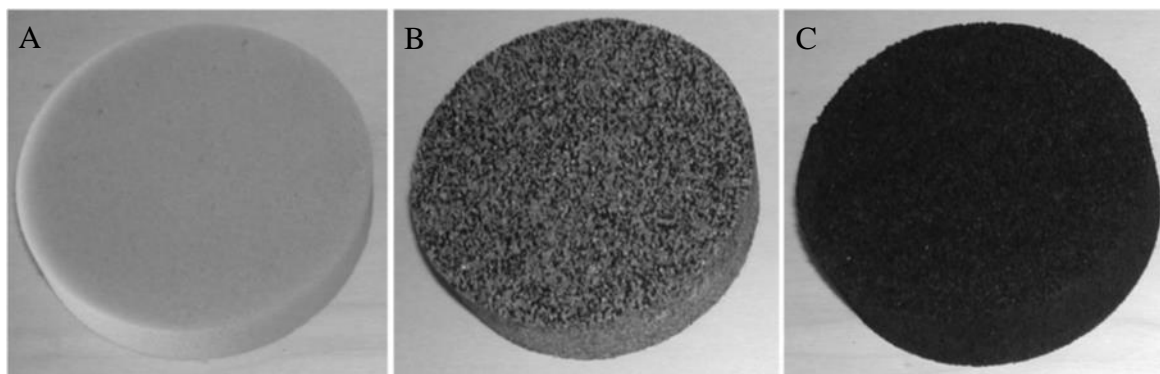
Figure 2.40: The tested porous materials; (A) reticulated foam, (B) consolidated flint, and (C) reconstituted porous rubber [67].

Table 2.12

The thickness and density of the tested porous materials [67].

Material	Description	Nominal thickness (mm)	Nominal density (kg/m³)
A	Reticulated foam	20	8.8
B	Consolidated flint	31	1500
E	Reconstituted porous rubber	28	242

The reproducibility of the acoustical characterisation of porous materials was studied. Types of the acoustical characterisation and laboratories involved in which these characterisations were measured are listed in Table 2.13. The laboratory names were randomised and denoted as a number of one to seven. Therefore, these laboratories are referred as Partner 1 to Partner 7. The procedure of each acoustical characterisation are discussed in ref. [67].

Table 2.13

Types of the acoustical characterisation used by the seven laboratories [67].

Acoustical characterisation	Partner
Sound absorption coefficient, α	1,2,3,4,5,6 and 7
Airflow resistivity, σ	1,2,3,4,5 and 6
Porosity, ϕ	1,2,3,4 and 6
Tortuosity, α_∞	1,2,4 and 6
Characteristic lengths, Λ and $\Lambda\prime$	1,2,4 and 6

Figures 2.41 to 2.43 show the sound absorption coefficient of materials A, B and C, respectively. In the case of material A, a significant dispersion in the sound absorption coefficient can be seen in the frequency above 2000 Hz. The dispersion of this material presence due to the frame resonance which can be observed for low density and soft porous materials. The dispersion in the sound absorption coefficient for material B can be observed particularly for frequencies above 1000 Hz. The dispersion of this material attributed to its relatively high rigidity and effect the differences in the mounting condition. Some of the partners wrapped the edges of the samples in tape to avoid any leakage around the edge

during testing and some of the partners did not require the sample to be wrapped in tape because a good fit between sample and the testing tube can be achieved. The same situation also applied for material C which one of the partners wrapped the edges of the samples in tape and this action resulting to increment in airflow resistivity and causes to an underestimation data for sound absorption coefficient.
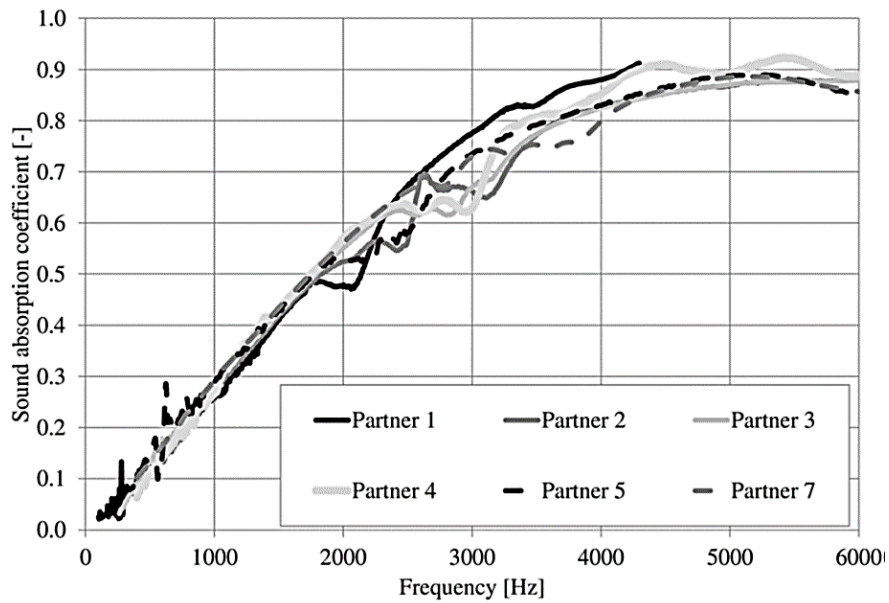
Figure 2.41: The sound absorption coefficient for material A (reticulated foam) as a function of frequency [67].
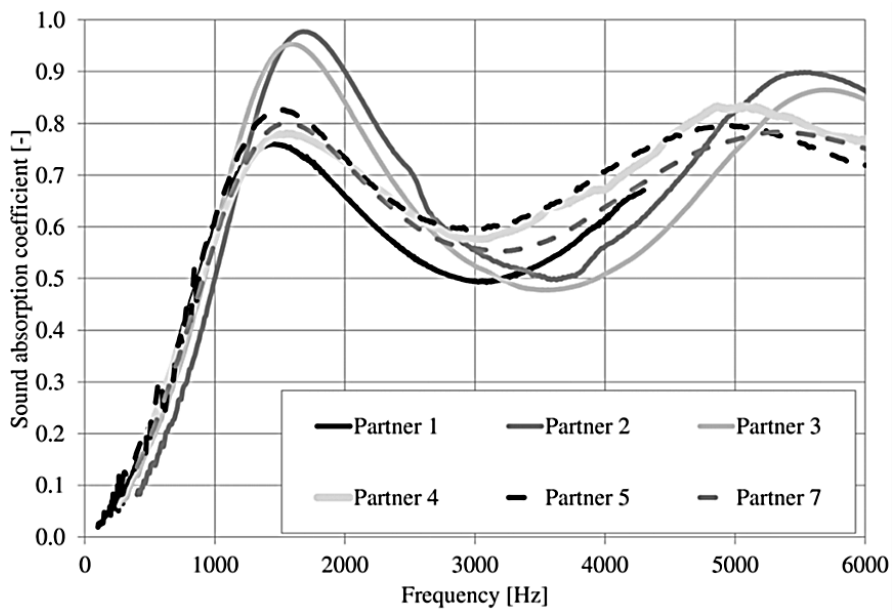
Figure 2.42: The sound absorption coefficient for material B (consolidated flint) as a function of frequency [67].
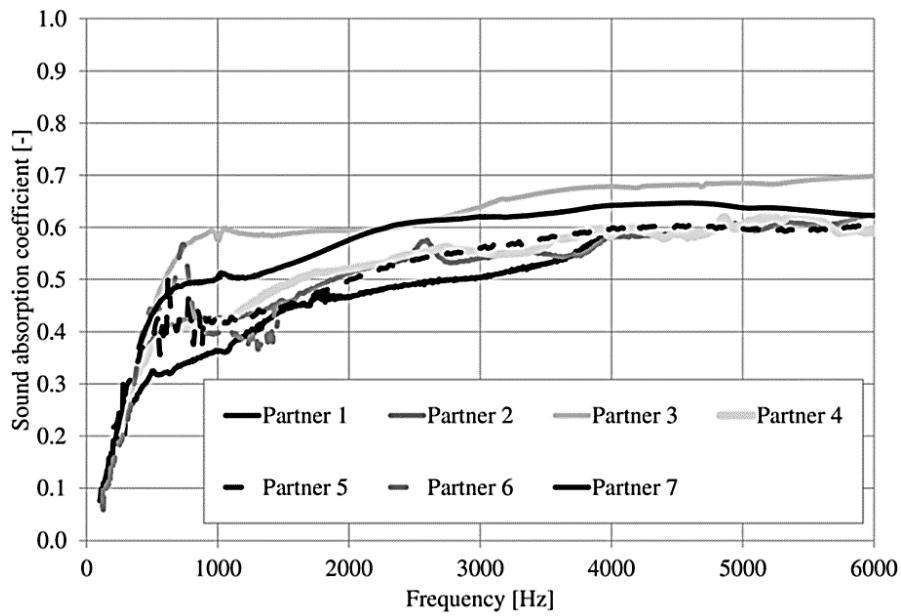
Figure 2.43: The sound absorption coefficient for material C (reconstituted porous rubber) as a function of frequency [67].

Figures 2.44 and 2.45 show the average values of airflow resistivity and porosity of materials A, B and C, respectively. The reproducibility for the airflow resistivity is relatively satisfactory for material A and the reproducibility is low for materials B and C. In contrast, high reproducibility for the porosity of materials A, B and C can be obtained. However, different porosity measurements on material C from partner 6 appears to underestimate the porosity value.
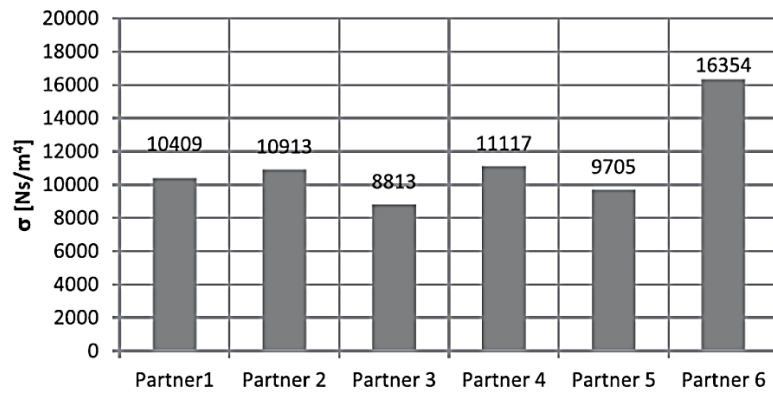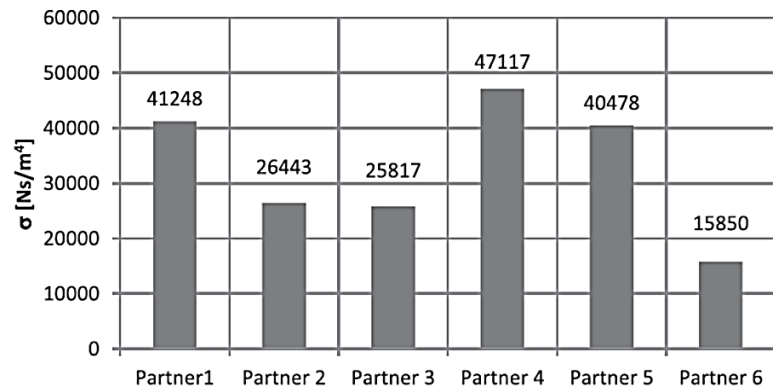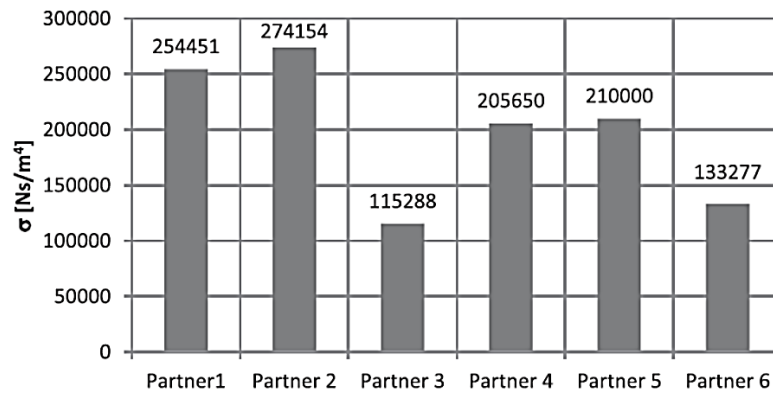
Figure 2.44: The average values of the airflow resistivity for material A (reticulated foam), material B (consolidated flint) and material C (reconstituted porous rubber) [67].
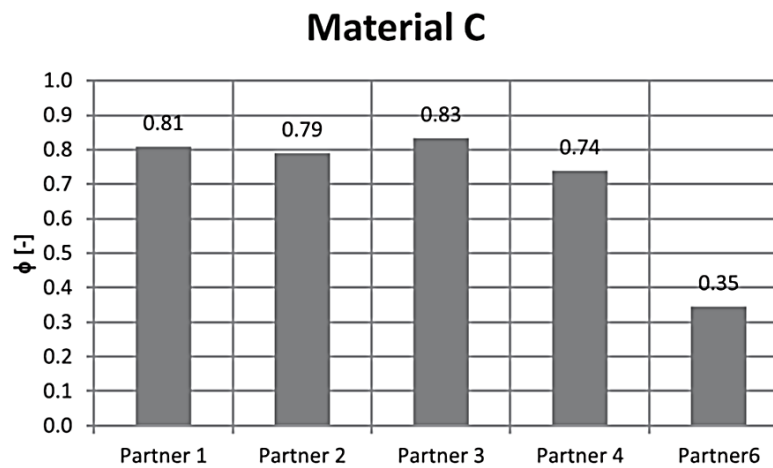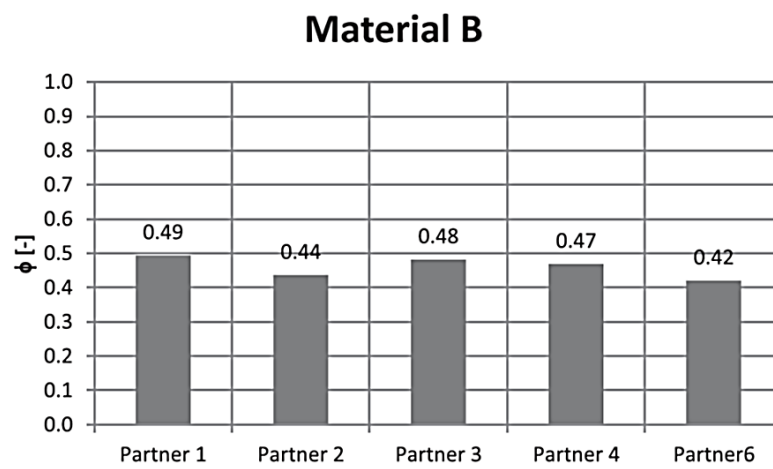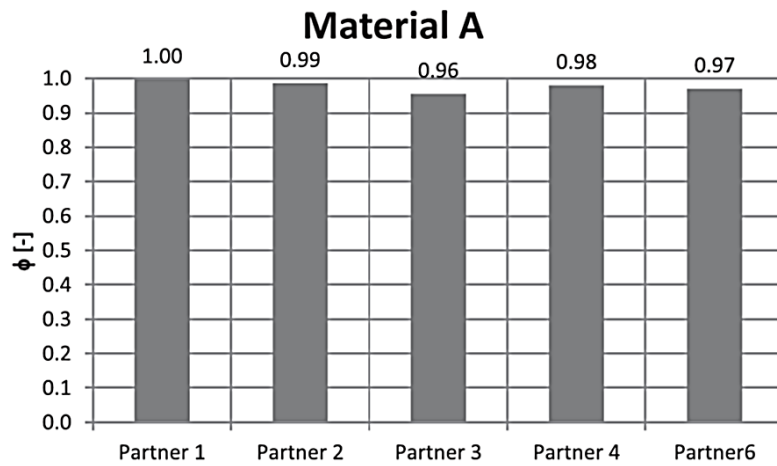
Figure 2.45: The average values of the porosity for material A (reticulated foam), material B (consolidated flint) and material C (reconstituted porous rubber) [67].

Figure 2.46 shows the average values of tortuosity, viscous characteristic length and thermal characteristic length for materials A, B and C. In the case of tortuosity, the high reproducibility is achieved for materials A and B and low reproducibility can be seen for material C. As for the characteristic lengths (viscous and thermal), the dispersion were between 20% to 80%.
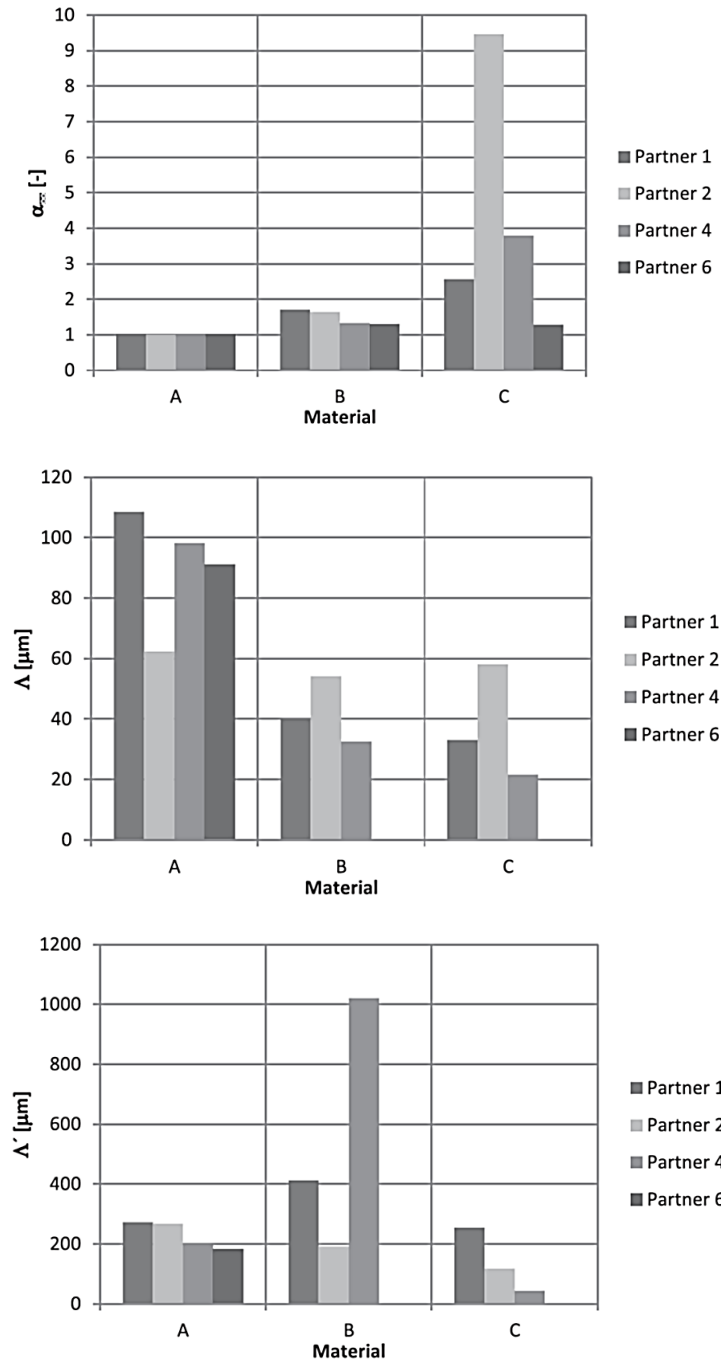
Figure 2.46: The average values of the tortuosity (top), viscous characteristic length (middle) and thermal characteristic length (bottom) for material A (reticulated foam), material B (consolidated flint) and material C (reconstituted porous rubber) [67].

54

The overall acoustical characterisation shows poor reproducibility between the 7 laboratories particularly for the acoustical properties of highly resistive materials. This observation suggests that these porous materials tested has natural inhomogeneity. Apart from that, differences in the sample preparation, mounting condition in the impedance tube and measurement method were also attributed to the poor reproducibility.

The authors in ref. [67] suggested that there is a need for revision of the measurement standardisation to determine the acoustical characterisation of porous material. There are several aspects that need to be standardised such as the potential measurement problems, test installation of the porous materials, test calibration procedures, number of samples to be measured, and acceptability of a certain standard deviation on the tests performed. Therefore, a new measurement standardisation for acoustical characterisation of porous material is required.

2.6.4 Modelling sound propagation of porous material

The most commonly used modelling on sound propagation of porous materials is based on the Biot theory. This theory describes sound propagation in a porous saturated medium that is fully saturated with a fluid which is resulting to the existence of compressional wave and transversal wave. In this three-dimensional theory, several non-acoustic parameters are considered such as fluid density, airflow resistivity, porosity and tortuosity. However, modelling through this Biot theory is considerably complex. Therefore, it has been common in a theoretical model to introduce semi-empirical model with inversion on non-acoustic parameters, but it appears that most theoretical models are not capable to fully characterised the complexity of real porous materials [61]. A clear physical model proposed by Johnson Champoux Allard [68, 69] is based on knowledge of the viscous and thermal characteristic lengths but these parameters are not straightforward to determine. Therefore, a few of simple empirical models have been introduced such as Delany and Bazley [70], Miki [71] and Voronina [72].

The viscous and thermal dissipation from the sound propagation through a porous material is shown to be related to a relaxation characteristic. Based on this situation, another theoretical model known as a relaxation model or Wilson model [73] for dynamic density

and dynamic bulk modulus is proposed to describe the viscous and thermal processes, respectively. Moreover, there is a theoretical model which is not considering the viscous and thermal characteristic lengths as parameters namely as a Padé approximation [74, 75]. This model is based on the microstructure properties of porous materials which can be used together with other non-acoustic properties to predict the acoustical behaviour of complex porous materials.

The ability to predict sound absorption of porous material is important or noise control applications. Most of the acoustic models that are used to determine the sound absorption behavior are equivalent fluid models. This fluid behaviour is described by the frequency dependent sound characteristic impedance, $z_c(\omega)$ and by the frequency dependent sound wavenumber in a porous material, $k_c(\omega)$, where ω is the angular frequency expressed as $\omega = 2\pi f$, where f is the sound frequency in Hertz. The sound characteristic impedance relates to the ability of sound waves to penetrate a porous material and propagate in it, whereas the sound wavenumber relates to the sound speed in the porous space and the rate at which the sound is attenuated. These properties can be predicted theoretically or empirically [76].

Models relate the sound characteristic impedance, z_c and the sound wavenumber, k_c to the dynamic density, ρ_b and compressibility, C_b of the equivalent fluid by the following equations:

$$z_c = \frac{1}{\rho_0 c_0} \sqrt{\frac{\rho_b}{C_b}} \tag{2.6}$$

and

$$k_c = 2\pi f \sqrt{\rho_b C_b}, \tag{2.7}$$

where ρ_0 is the fluid equilibrium density and c_0 is the sound speed in the fluid. Theoretical models consider the viscous losses and the thermal losses in a porous material. The viscous losses in a porous material are influenced by the dynamic density of the fluid, ρ_b. The

viscous losses are also noticeable at frequencies lower than viscous frequency, ω_v and it can be expressed as:

$$\omega_v = \frac{8\eta_0}{s^2\rho_0}, \tag{2.8}$$

where η_0 is the dynamic viscosity of the fluid and s is the pore size. However, the viscous losses are relatively low at frequencies higher than viscous frequency and the inertial effects are dominant. The difference between the viscous losses and inertial effects in the material pores can be differentiated by the viscous characteristic frequency that is controlled by the pore size. In the case of thermal losses in a porous material, they are influenced by the compressibility of the equivalent fluid, C_b. The thermal losses are noticeable at frequencies below than thermal frequency, ω_t and it can be expressed as:

$$\omega_t = \frac{\kappa}{s^2\rho_0 C_p}, \tag{2.9}$$

where κ is the thermal conductivity of the fluid and C_p is the heat capacity of the fluid. However, the thermal losses are relatively low at frequencies higher than thermal frequency where no heat transfer occurs.

Empirical model tends to estimate the sound characteristic impedance, z_c and the sound wavenumber, k_c directly. The equations in empirical models are based on the measured values of non-acoustic parameters. These models are validated with experimental data for the acoustic behaviour of porous material. Acoustical property that can measured directly is the normalised surface impedance, z_s, of a hard-backed porous material of thickness, d. Here z_s can be expressed as [76]:

$$z_s = z_c \coth(-ik_c d), \tag{2.10}$$

where, $i = \sqrt{-1}$.

Numerous works studied on the comparison of measurement data and prediction of acoustical characterisation of porous materials. For example, Horoshenkov [77] investigated the effect of consolidation on the acoustic properties of loose rubber granulates. In this paper, the authors compared the acoustic performance of the rubber granulates (loose and consolidated) obtained from the measurement data and several established models; Miki model, Wilson model, Voronina model and Padé approximation. Mixes of two different granule sizes; 0.71 to 1.0 mm and 1.41 to 2.0 mm were studied for the comparison purposes. Each granule size was separated into loose granular mix and consolidated granular mix with the compaction ratio (CR) 35%.

Figure 2.47 shows a comparison between the measurement data and predictions for the surface impedance of the loose granular mix. There was good correlation between the measured and predicted results in the frequency range below 3000 to 3500 Hz. The predictions by the Padé approximation, Wilson model and Miki model were almost the same. However, the disagreement between the measured and predicted results becomes more pronounced in the frequency range above 3000 to 3500 Hz as the models were more sensitive to any variations of the non-acoustic parameters.

Figure 2.48 shows a comparison between the measurement data and predictions for the surface impedance of the consolidated granular mix. There was good correlation between the measured and predicted results at lower frequencies and remain poor at higher frequencies. The predictions by the Padé approximation and Miki model had good agreement with the measured data for frequencies below than 2500 Hz.
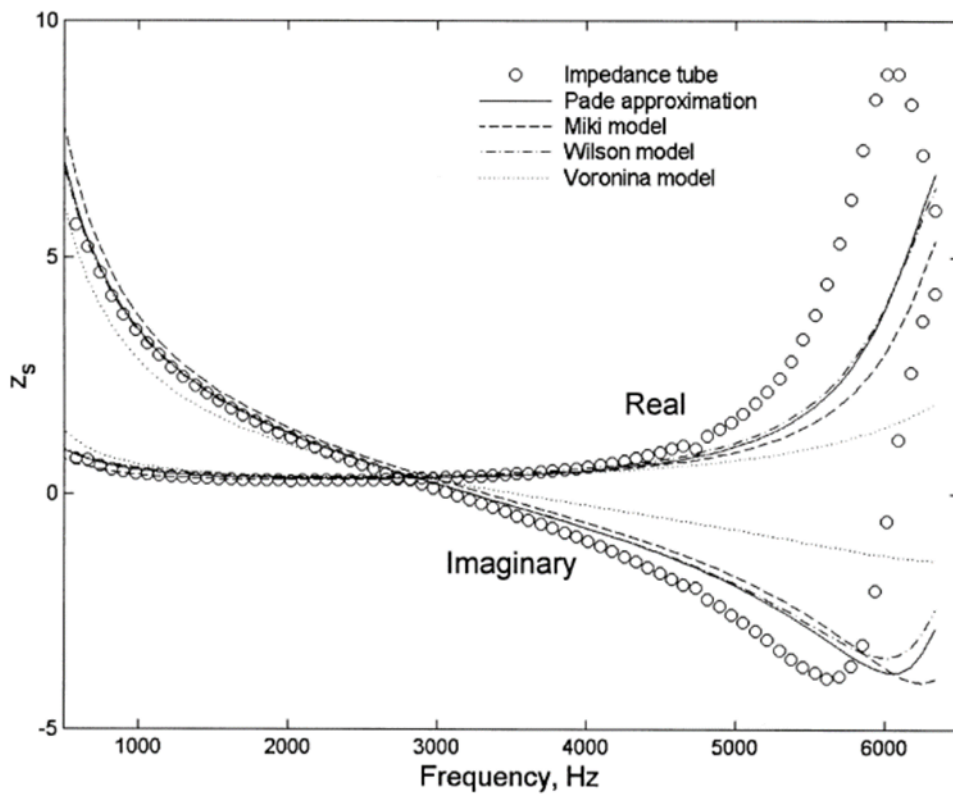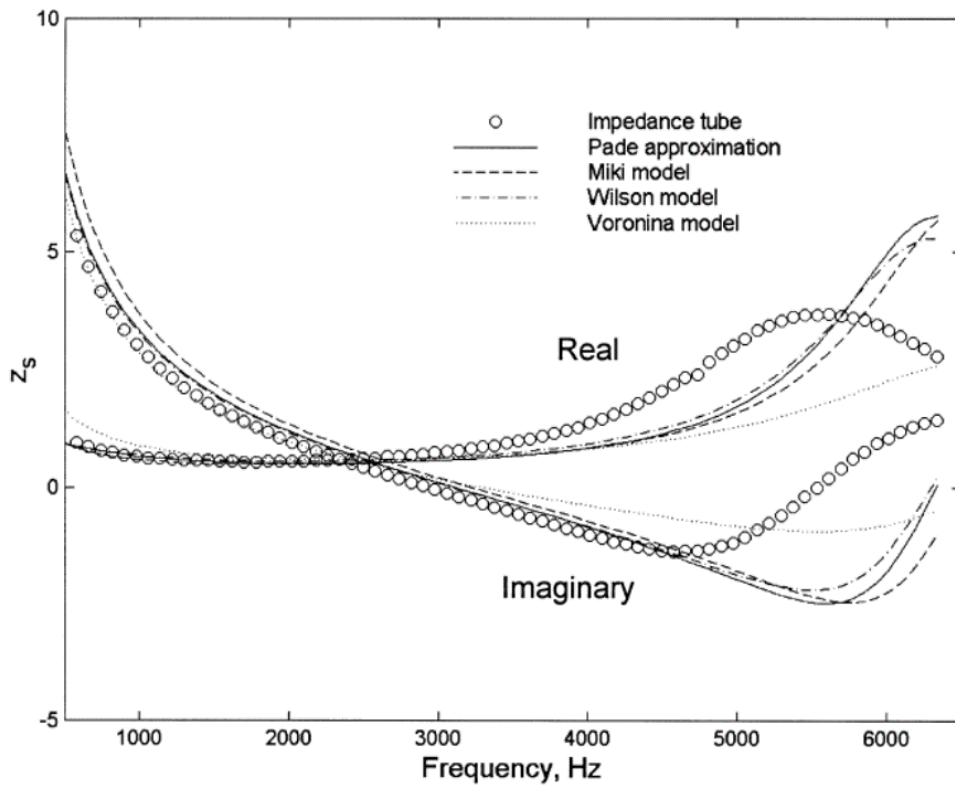
Figure 2.47: A comparison between the measurement data and predictions for the surface impedance of the 0.71 to 1.0 mm (top) and 1.41 to 2.0 mm (bottom) loose granular mix [77].
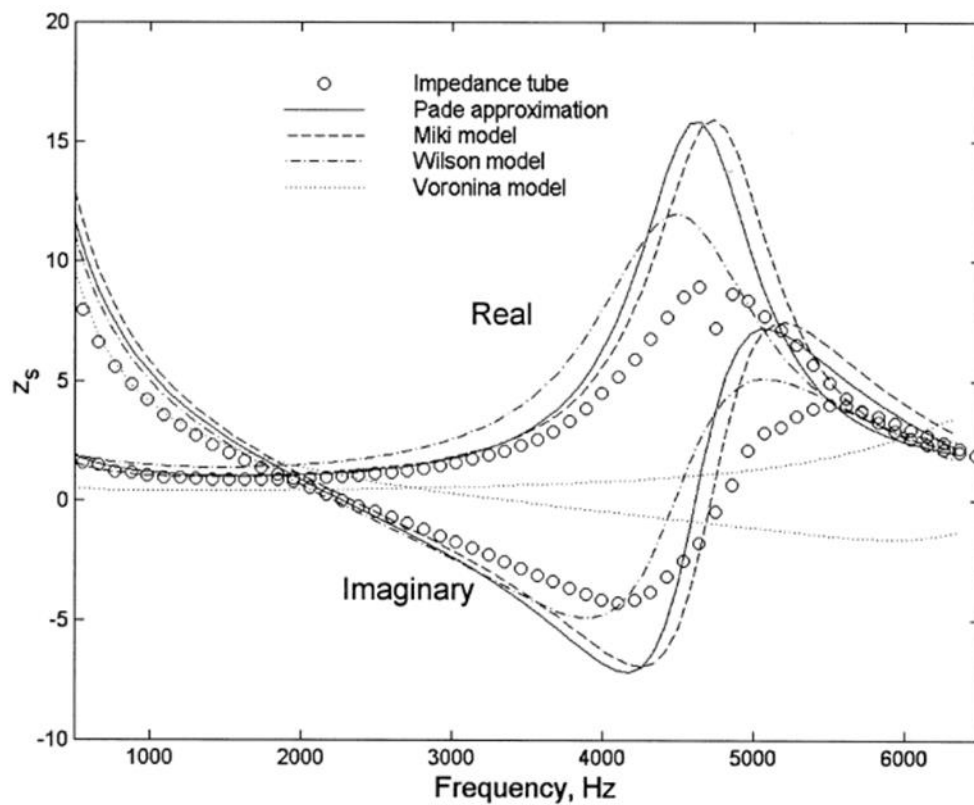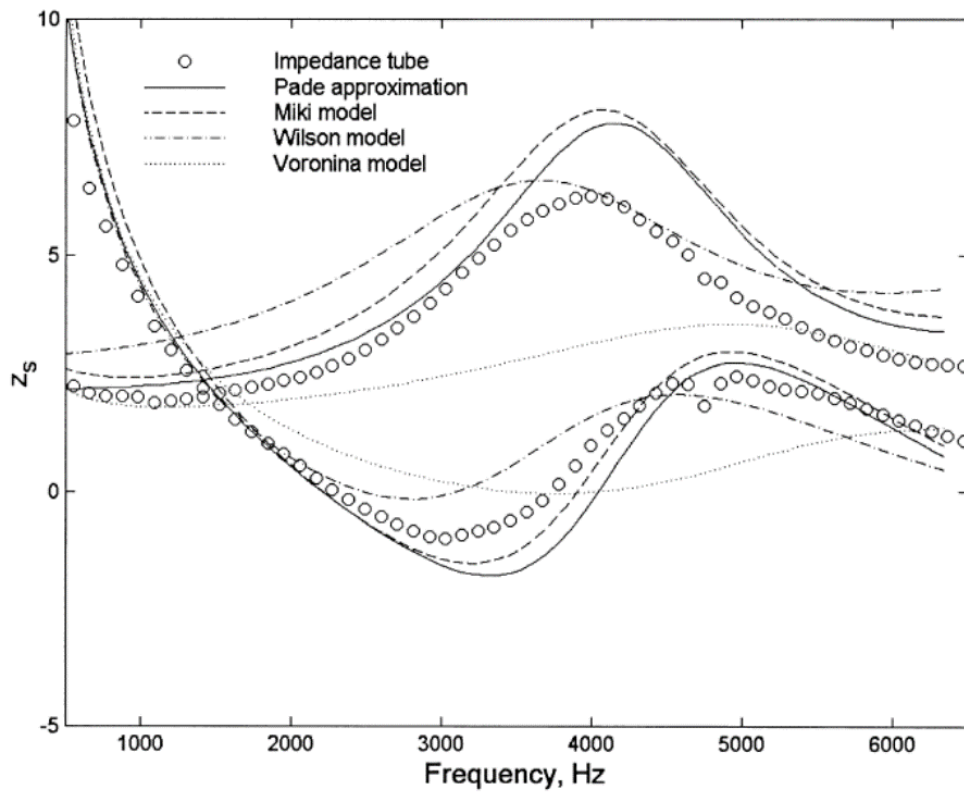
Figure 2.48: A comparison between the measurement data and predictions for the surface impedance of the 0.71 to 1.0 mm (top) and 1.41 to 2.0 mm (bottom) consolidated granular mix [77].

The authors in ref. [77] stated that agreement between the measurement data and predictions can be improved if the non-acoustic parameters used in those models are adjusted. They have used the Nelder-Mead simplex method to minimise the difference of the measured surface impedance value and those predicted by the theoretical models; Padé approximation and Wilson model. In the adjustment process, the minimisation analysis

$$F(\bar{x}) = \int_{\omega_{min}}^{\omega_{max}} \left| z_s^{exp}(\omega, \bar{x}) - z_s^{th}(\omega, \bar{x}) \right| d\omega \tag{2.11}$$

was carried out to adjust the non-acoustic parameters by fitting the predicted values of surface impedance, z_s^{th}, to the measured data, z_s^{exp}, obtained at the frequencies ω, where $\bar{x}$ is the design variable vector. The adjustment values for the non-acoustic parameters and the percentage of the required adjustment are shown in Table 2.14.

Table 2.14
Measured and adjusted values of the non-acoustic parameters for the prediction of the acoustic properties of loose and consolidated granular mixes [77].

Mix		Airflow resistivity, σ (N.s/m^4)	Porosity, ϕ	Tortuosity, α_∞	Standard deviation in pore size, σ_s (mm)
Loose 0.71 to 1.0 mm	Measured	10 900	0.605	1.201	0.41
	Adjusted	18 560 (+70%)	0.75 (+25%)	1.32 (+10%)	1.33 (+324%)
Loose 1.41 to 2.0 mm	Measured	4 960	0.622	1.201	0.40
	Adjusted	4 910 (-1%)	0.68 (+9%)	1.31 (+9%)	0.18 (-222%)
Consolidated 0.71 to 1.0 mm	Measured	92 200	0.364	1.681	0.27
	Adjusted	94 600 (+3%)	0.43 (+18%)	1.65 (-2%)	0.53 (+96%)
Consolidated 1.41 to 2.0 mm	Measured	19 800	0.36	1.679	0.35
	Adjusted	18 990 (-4%)	0.47 (+30%)	1.67 (-1%)	0.62 (+77%)

Figure 2.49 shows the improved agreement between the measured and predicted results of the surface impedance by the Padé approximation and Wilson model for the loose and consolidated granular mixes. The adjusted values of the non-acoustic parameters were implemented, and those parameter variations can result in an excellent agreement with the measurement data.
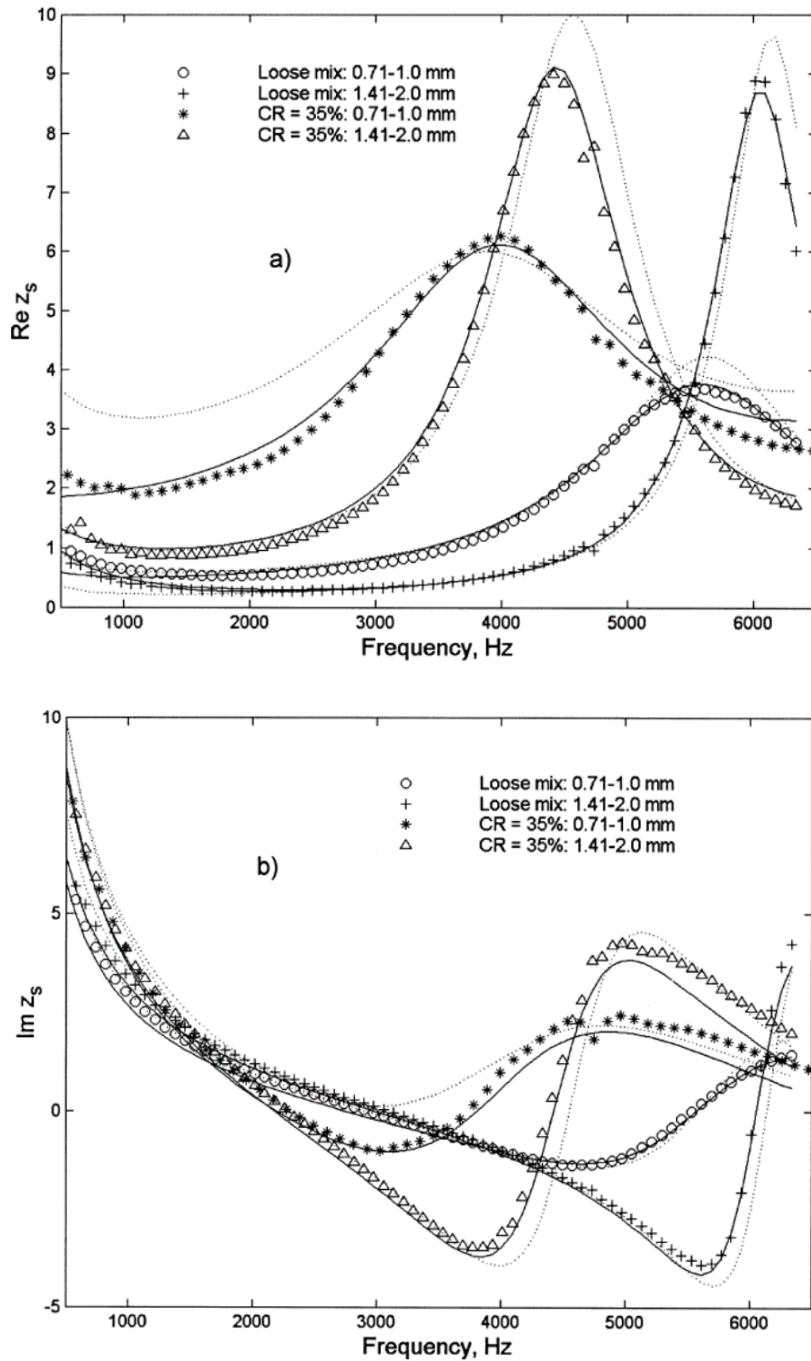
Figure 2.49: A comparison between the measurement data and predictions using the Padé approximation (solid line) and Wilson model (dotted line) for the (a) real and (b) imaginary parts of the surface impedance of the loose and consolidated granular mixes [77].

2.7 Summary

The commercial use of ENR is expected to grow drastically especially in the tyre industry. There are many other specialized applications for ENR which have not been investigated extensively. In the case of vibro-acoustic applications, there is a relatively small amount of published work that can be related to ENR. Most of the studies are focused on the physical and dynamic characteristics of ENR blending with other polymers, and less research work has been done on vibro-acoustic properties on ENR alone. The effect of the epoxidation level on these properties of ENR has not been fully investigated. Natural rubber foam can be produced from latex or dry rubber. However, the homogeneity of the latex composition is doubtful as it contains other residual substances. Latex handling is also critical as it is easily affected by the environment. On contrary, the production of natural rubber foam from dry rubber can eliminate difficulties that are associated with latex. There has been little attention given to the production of natural rubber foam from dry rubber. In fact, no exact theory is currently known that describes the use of natural rubber foam in vibro-acoustic applications. All these points deserve further investigation to understand how to design natural rubber and ENR that can be used in vibration and noise control applications. This requires developing the relationship between the non-acoustical and acoustical properties of natural rubber foam so that it can be designed as a noise control material.

Chapter 3

Dynamical Properties of Epoxidized Natural Rubber

3.1 Introduction

This chapter focuses on the dynamic mechanical characterisation of solid epoxidized natural rubber (ENR) and solid natural rubber. The effect of different epoxidation levels on the dynamic behaviour of ENR as a single matrix is investigated for a wide range of temperatures and frequencies. Three types of natural rubber with different epoxidation levels of 0, 25 and 50 mol% are studied. The master curves of the dynamic properties of the rubbers are generated and nomogram relating the reduced frequency to the complex moduli at different temperatures is presented. The influence of the epoxidation level on the relationship between the two dynamic moduli of the material is also studied using a Cole-Cole plot. Finally, the dynamic properties obtained are fitted by fitting the 5-parameter fractional derivative model by Pritz [6] to the master curves for the complex dynamic modulus.

3.2 Experimental procedures

Three types of natural rubber, SMR-CV60, ENR-25 and ENR-50 were obtained from the Malaysian Rubber Board. The basic details of the materials are shown in Table 3.1.

Table 3.1
Rubber materials used in the experiments.

Material	Type	Characteristic	
		Epoxidation Level[2] (%)	Glass Transition Temperature, T_g[3] (°C)
Natural rubber	SMR-CV60[1]	0	-72.0
Epoxidized natural rubber	ENR-25	29.4	-45.5
	ENR-50	52.1	-25.1

[1] Standard Malaysian Rubber constant viscosity: grade 60
[2] as analysed by Proton Nuclear Magnetic Resonance (^{1}H NMR)
[3] estimated based on the epoxide levels analysed by ^{1}H NMR from relationship described by Davey and Loadman [13]

All other ingredients were provided by Tun Abdul Razak Research Centre (TARRC), Hertford. All of the materials were commercial grade. The formulations used are given in Table 3.2. The formulations are denoted by R0, R25 and R50, where the numbers stand for the epoxidation level of the rubber. Parts per hundred of rubber (phr) of each ingredient was calculated based on the weight of rubber used in single formulation. For example, if 1000 g of SMR-CV60 raw rubber used in R0 formulation, the weight of other ingredients can be calculated as 25 g for sulfur, 40 g for zinc oxide and stearic acid, 10 g for Wingstay L and CBS and 3 g for PVI.

Table 3.2
R0, R25 and R50 formulations in parts per hundred of rubber (phr).

Ingredient	R0	R25	R50
SMR-CV60	100	-	-
ENR-25	-	100	-
ENR-50	-	-	100
Sulfur	2.5	2.5	2.5
Zinc Oxide	4	4	4
Stearic Acid	4	4	4
Wingstay L	1	1	1
CBS[1]	1	1	1
PVI[2]	0.3	0.3	0.3

[1]Benzothiazyl-2-cyclohexyl-sulfenamide
[2]Prevulcanisation inhibitor

All the mixing process and dynamic testing were also carried out at TARRC, Hertford. The materials were compounded on a laboratory two-roll-mill machine maintained below 40°C (Figure 3.1(a)). This is a mill that consists of two metal cylinders rotating towards each other. Raw rubber was loaded at the beginning of the compounding process (Figure 3.1(b)). The other ingredients were mixed together and then loaded gradually onto the two-roll-mill. Finally, a smooth and uniform sheet was obtained (Figure 3.2). The compounding time was kept below 20 minutes.

The compounded natural rubber was left for 24 hours before being compression moulded in the rubber disc shaped mould (Figure 3.3) for 20 minutes using an electrically heated hydraulic press at 150°C (Figure 3.4). The curing time was selected according to the

crosslinking time at which 95% of cure has taken place observed in the rheometer curve. The curve was analysed using a Monsanto Rheometer, MDR 2000. The rheometer curve will be discussed in section 4.3.2.
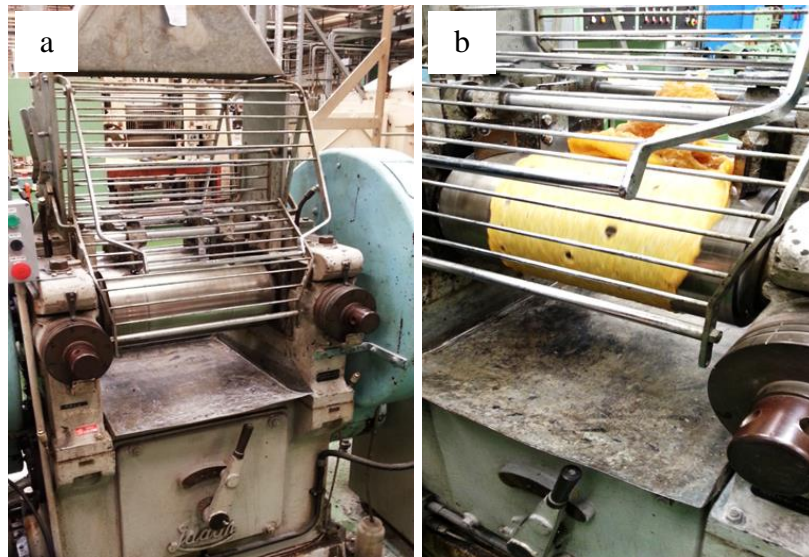
Figure 3.1: (a) A two roll-mill machine; (b) The compounding process.
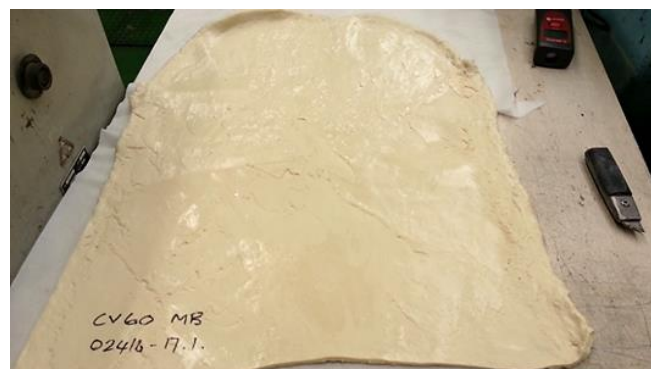
Figure 3.2: A compounded natural rubber sheet.

Figure 3.3: A rubber disc shaped mould.

Figure 3.4: An electrical heated hydraulic press.

The rubber pieces were bonded to stainless-steel surfaces during the curing process. The first step for bonding was to clean the stainless steel by dry sandblasting (air-blasting) as shown in Figure 3.5. Then, the stainless steel was immersed in acetone to remove the loose particles for 5 minutes. Finally, a rubber-metal bonding system, Chemosil® 211 (primer) and Chemosil® 225 (covercoat) were applied to the stainless-steel surfaces which was to be bonded to the rubber pieces during the curing process. Drying time of 30 minutes at room temperature for primer bonding agent was allowed before applying the covercoat bonding agent.
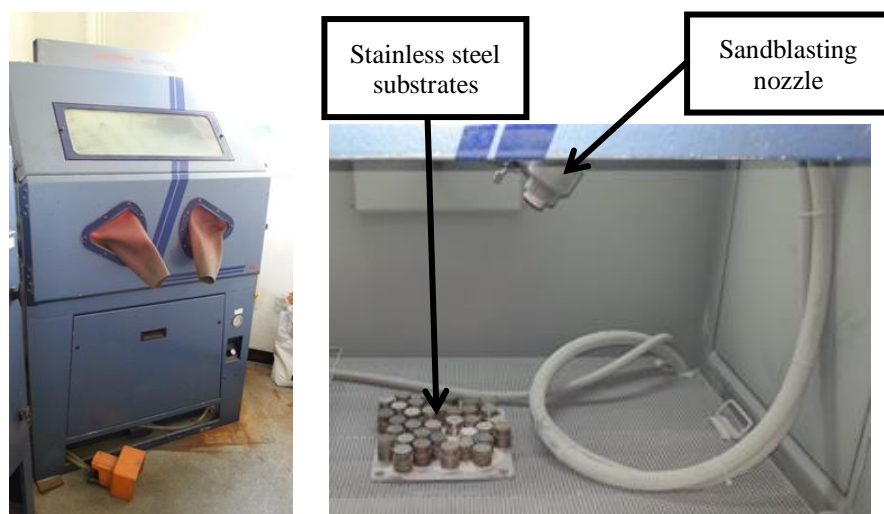
Figure 3.5: A dry sandblasting machine.

The dynamic properties of the three vulcanizates were measured using a Metravib DMA+1000 dynamic mechanical analyser (Figure 3.6). Tests were carried out over a frequency range of 0.1 to 170 Hz and a temperature range of -40 to 50°C with a dynamic strain of 0.1%. Double bonded shear test pieces (Figure 3.7) were used. The nominal dimensions of the rubber discs were 10 mm in diameter and 2 mm thickness.

Figure 3.6: A Metravib DMA+1000 dynamic mechanical analyser.
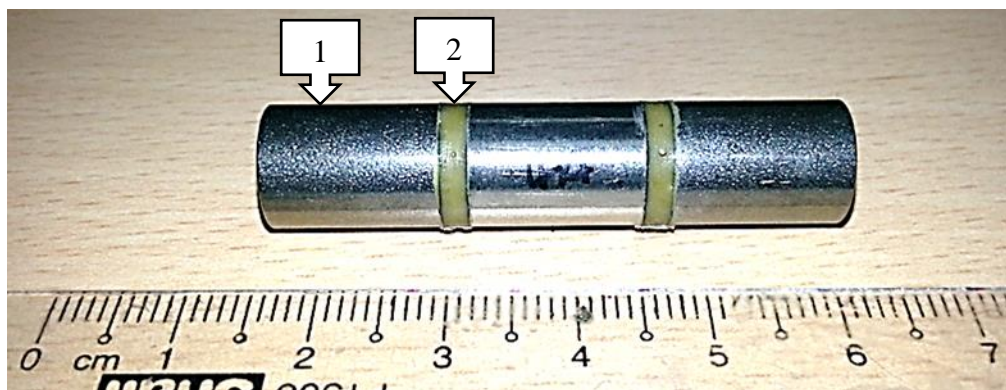
Figure 3.7: A double bonded shear test piece. 1: stainless steel; 2: rubber.

3.3 Dynamic mechanical properties

3.3.1 Effect of temperature

Figure 3.8 illustrates the dependence of the storage modulus (G') as a function of temperature in the range of -40°C to 50°C for natural rubber with different epoxidation levels. These data were taken at 170 Hz excitation. This choice of frequency is the best to capture the development of the loss factor peak for the R0, R25 and R50 rubbers studied in this work.
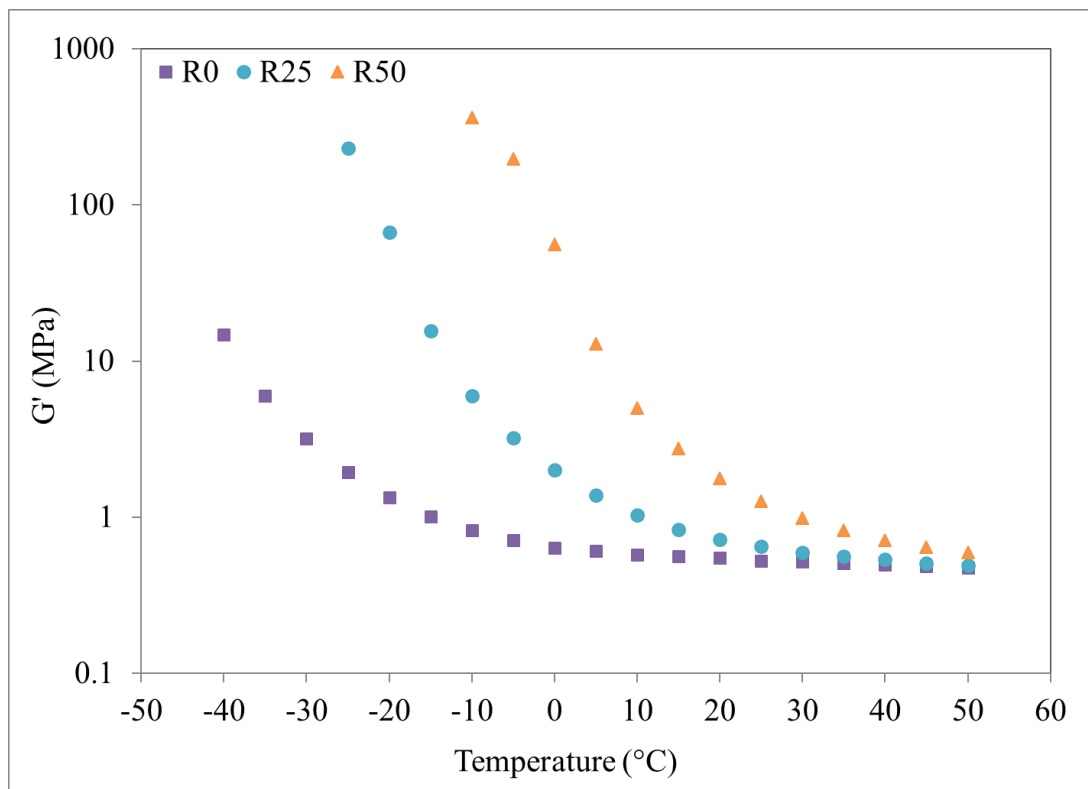
Figure 3.8: The dependence of the storage modulus for R0, R25, and R50 rubbers as a function of temperature at 170Hz.

It can be seen that all the materials exhibit high G' in the low temperature region. G' decreases with the increasing temperature. In this region the mobility of the polymer chains was increasing [78], so that a reduction in the material stiffness was expected. The storage modulus eventually converges for all three materials at around 50°C.

Figure 3.9 shows the loss factor ($\tan \delta$) curves under the same conditions. This parameter gives a measure of the energy loss in the material due to the molecular rearrangement and

internal friction in the natural rubber matrix. Above 5°C, $\tan\delta$, and therefore damping, increases with the increasing epoxidation level. Figure 3.9 also indicates that T_g increases as the epoxidation level is increased, suggesting that the epoxide groups result in restricting movement the natural rubber chains. As a result, a higher temperature is needed to overcome the chain rigidity and interactions and allow rubbery behaviour.
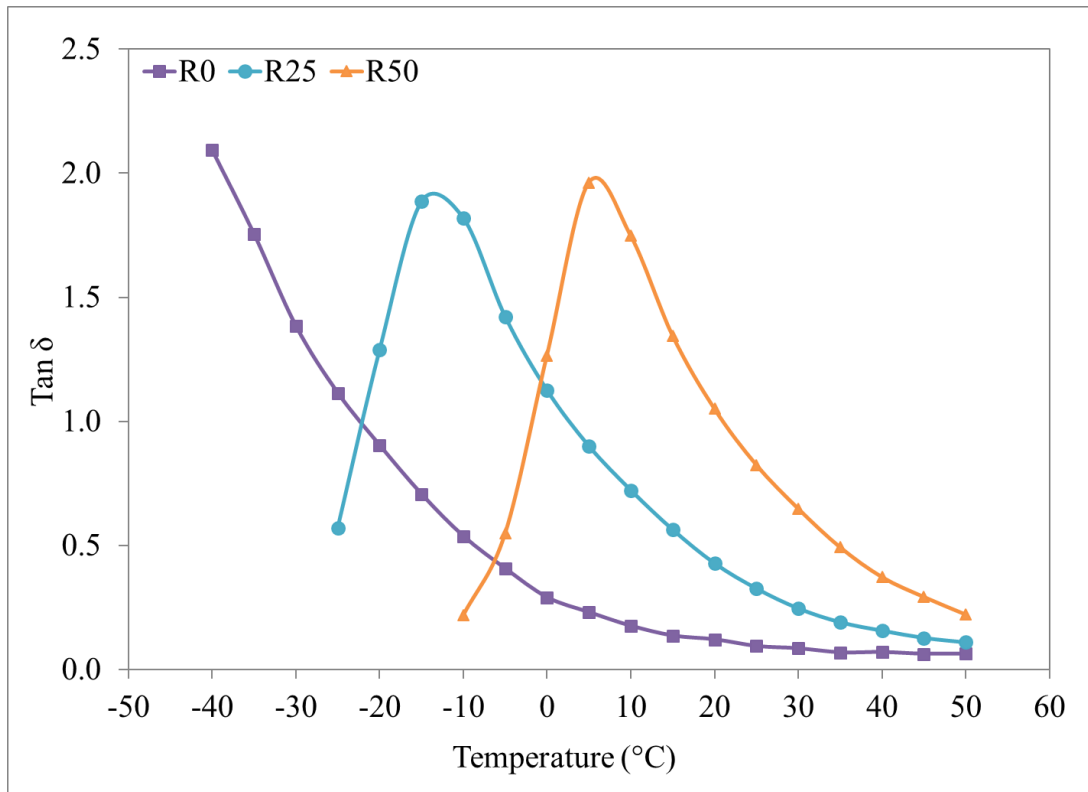
Figure 3.9: The dependence of the loss factor ($\tan\delta$) for R0, R25 and R50 rubbers as a function of temperature at 170Hz.

3.3.2 Effect of frequency

The storage modulus, G', of the three materials as a function of frequency and temperature is plotted in Figures 3.10 to 3.12. It is frequency dependent, with its value increasing with frequency at all measured temperatures. However, at higher temperatures the storage modulus is relatively frequency independent. It becomes progressively more dependent on frequency as the temperature decreases. Well above the T_g, the molecules are free to move and experience relatively little resistance, so that a relatively low modulus can be observed. As a result, similar storage modulus values are obtained at high temperatures for all three compounds. However, as the temperature approaches the T_g, the frequency dependence of the properties becomes more pronounced, as shown in Figures 3.10 to 3.12.
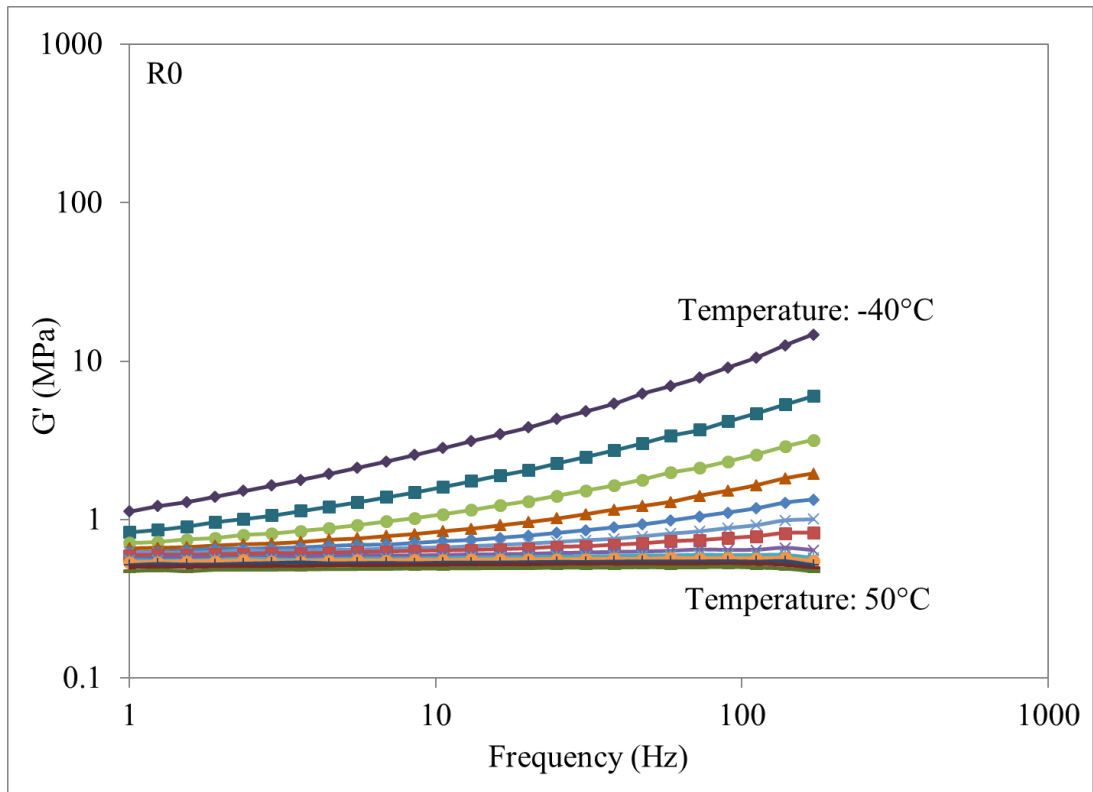
Figure 3.10: The frequency dependence of the storage modulus of R0 rubber for a range of temperatures: -40°C to 50°C with 5°C interval.
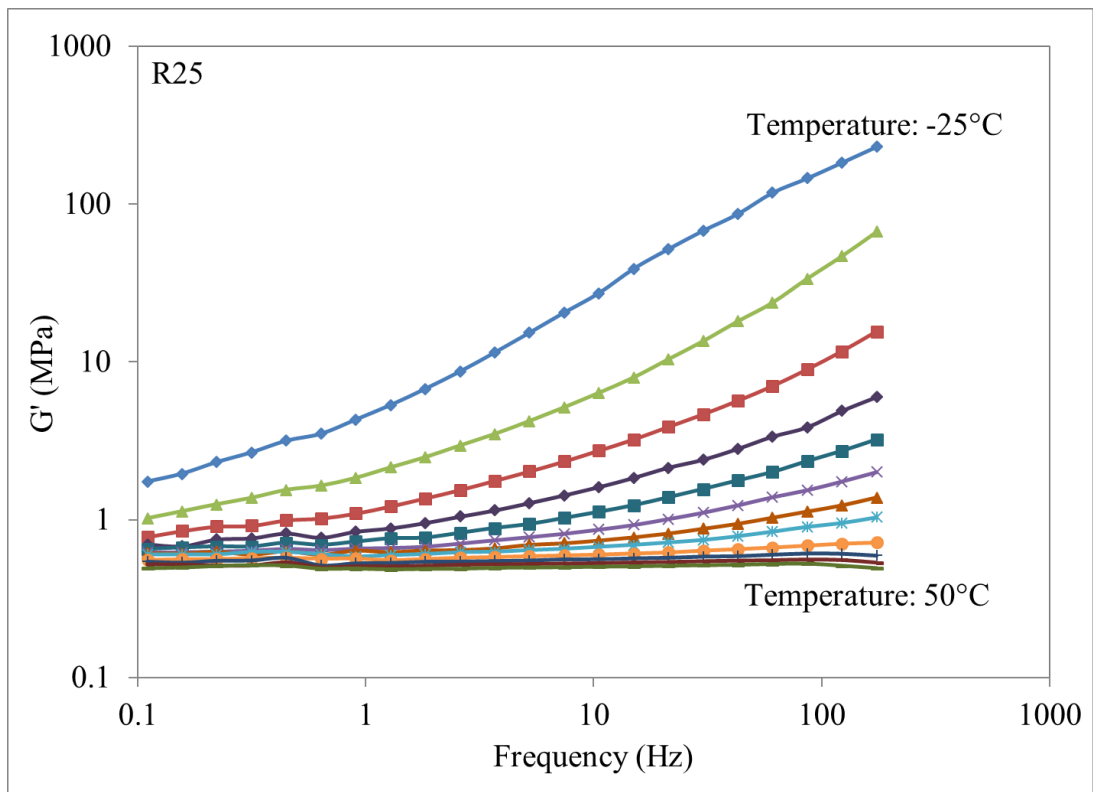
Figure 3.11: The frequency dependence of the storage modulus of R25 rubber for a range of temperatures: -25°C to 50°C with 5°C interval.
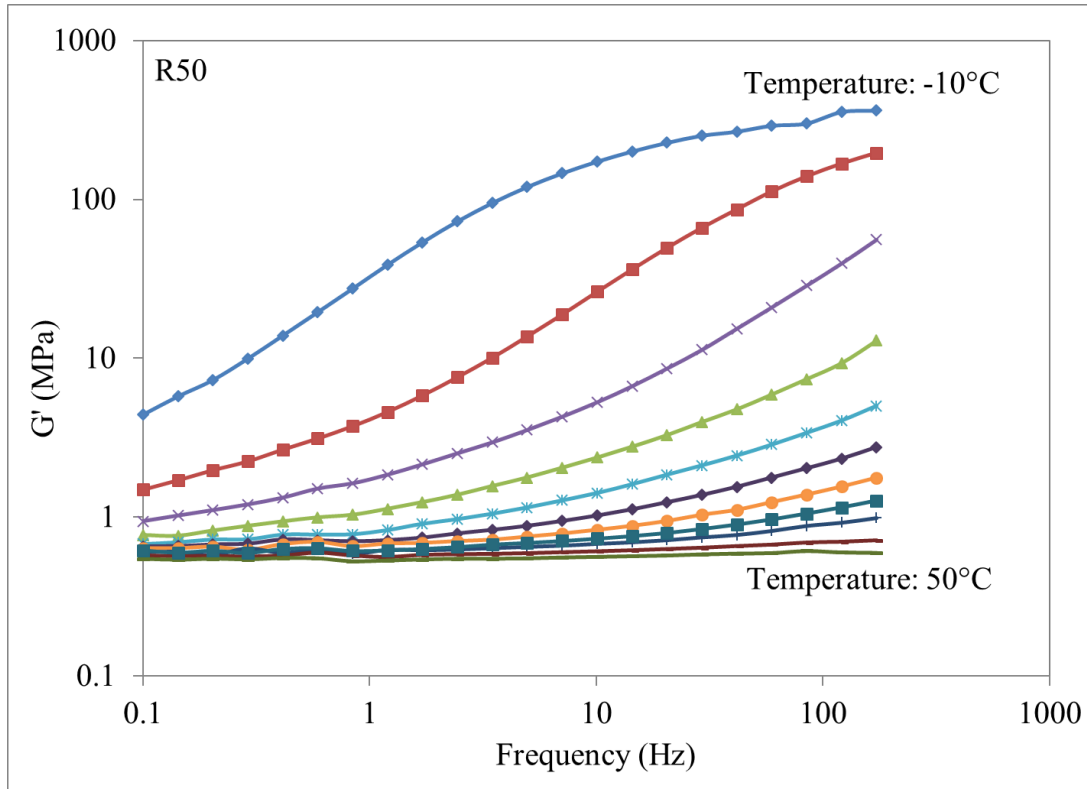
Figure 3.12: The frequency dependence of the storage modulus of R50 rubber for a range of temperatures: -10°C to 50°C with 5°C interval.

3.3.3 Time-temperature superposition

The isothermal curves plotted in Figures 3.10 to 3.12 can be shifted along the frequency axis and storage modulus axis to obtain superposition. In practice, the dynamic mechanical properties of the rubber materials can be tested in a limited frequency range. However, it is possible to infer the dynamic mechanical properties of the rubber over a wider frequency range using the time-temperature superposition principle. The time-temperature superposition is expressed in the following equation [46, 79]:

$$G_{T_0}(a_T\omega) = \frac{\rho_0 T_0}{\rho T} G_T(\omega), \tag{3.1}$$

where G_{T_0} and G_T are the shear modulus at the reference temperature, T_0 and at a given temperature, T, respectively. a_T is the horizontal shift coefficient along the frequency axis, ω, while ρ_0 and ρ are the density of the material at T_0 and T, respectively, and:

$$\frac{\rho_0 T_0}{\rho T} = b_T, \tag{3.2}$$

b_T being the vertical shift coefficient.

The horizontal shift coefficient, a_T, is used to adjust the horizontal position of the isothermal curve along the frequency axis, whereas the vertical shift coefficient, b_T, is used to adjust the vertical position of the isothermal curve. The vertical shift coefficient, b_T, for all isothermal curves were determined using Equation 3.2. It was assumed that the material density did not change significantly with temperature, so that the density value was kept constant.

The transition behaviour occurs in the range up to 100°C above T_g [48]. In this temperature range the frequency-temperature dependence of the dynamic properties of rubber can be inferred empirically. The approach suggested by Williams, Landel and Ferry (WLF) [80] expresses the shift factor, a_T, as the following:

$$\log a_T = -\frac{C_1(T - T_s)}{C_2 + T - T_s}. \tag{3.3}$$

Here, C_1 and C_2 are viscoelastic coefficients and T_s is the reference temperature estimated as:

$$T_s = T_g + 50°C. \tag{3.4}$$

Williams, Landel and Ferry suggested that the viscoelastic coefficients, $C_1 = 8.86$ and $C_2 = 101.6$. These values were selected based on the chosen reference temperature, T_s, of -30°C for polyisobutylene. If a different reference temperature, T_0 is chosen instead of T_s, then the new viscoelastic coefficients $C_1{}^0$ and $C_2{}^0$ are calculated based on the following equations:

$$C_1{}^0 = \frac{C_1 C_2}{C_2 + T_0 - T_s} \tag{3.5}$$

and

$$C_2{}^0 = C_2 + T_0 - T_s. \tag{3.6}$$

In this work, the chosen reference temperature, T_0, was 20°C, where the T_g of each rubber was estimated based on the epoxide levels analysed by nuclear magnetic resonance (NMR). The T_g of R0, R25 and R50 rubbers were -72.0°C, -45.5°C and -25.1°C respectively. The new viscoelastic coefficients for R0, R25 and R50 at a reference temperature of 20°C are summarised in Table 3.3.

Table 3.3
The new viscoelastic coefficients for the reference temperature of 20°C.

Viscoelastic Coefficients	R0	R25	R50
$C_1{}^0$	6.27	7.69	9.31
$C_2{}^0$	143.6	117.1	96.7

The horizontal shift factor is calculated using:

$$\log a_T = -\frac{C_1{}^0(T - T_0)}{C_2{}^0 + T - T_0} \tag{3.7}$$

and their values for all rubbers are listed in Table 3.4.

3.3.4 Relationship of dynamic properties of different epoxidation levels

For a single homogenous polymer, plotting storage modulus, G' against the loss modulus, G'', known as Cole-Cole plot [81], would show the relationship between the two moduli without any information on the temperature and frequency at which the measurements were taken. The data collapses on an arc of a circle presenting the dynamic properties of the polymer from the rubbery to glassy phase. Figure 3.13 shows this data for the natural rubber and ENR formulations tested. A full semicircle is not plotted as tests were not carried out at low enough temperatures approaching the glass transition temperature for these materials. The data for R0, R25 and R50 fall on a single arc suggesting that all the rubbers are correlated and the epoxidation does not influence the relationship between storage modulus and loss modulus.

74

Table 3.4

The horizontal shift coefficients for the reference temperature of 20°C.

Temperature (°C)	Horizontal shift coefficients, a_T		
	R0	R25	R50
-40	31551.529	-	-
-35	7786.905	-	-
-30	2231.669	-	-
-25	726.004	62785.932	-
-20	263.222	9731.792	-
-15	104.780	1892.968	-
-10	45.232	444.355	15379.298
-05	20.960	122.083	1761.166
00	10.336	38.315	267.527
05	5.385	13.470	51.181
10	2.946	5.221	11.849
15	1.683	2.202	3.218
20[1]	1.000	1.000	1.000
25	0.615	0.484	0.349
30	0.391	0.248	0.134
35	0.255	0.134	0.056
40	0.171	0.076	0.025
45	0.118	0.044	0.012
50	0.083	0.027	0.006

[1] Reference temperature, T_0

Figure 3.14 shows the G' master curves for R25 and R50 rubbers shifted to the right to match the master curve for R0 rubber at reference temperature of 20°C. This has been done by applying a multiplication factor to shift horizontally the curves for R25 and R50 rubbers. The multiplication factors for R25 and R50 rubbers were found to be 17 and 500, respectively. The same multiplication factors were applied to the master curves for G'' in Figure 3.15.
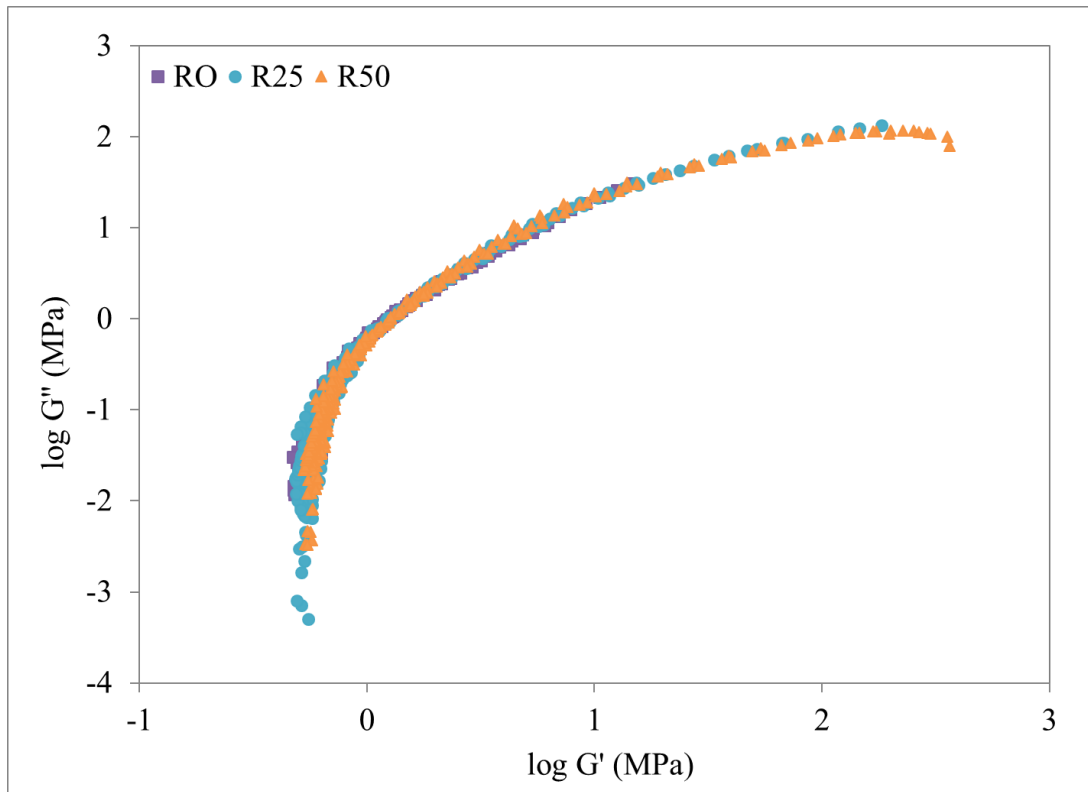
Figure 3.13: The Cole-Cole plots for R0, R25 and R50 rubbers.
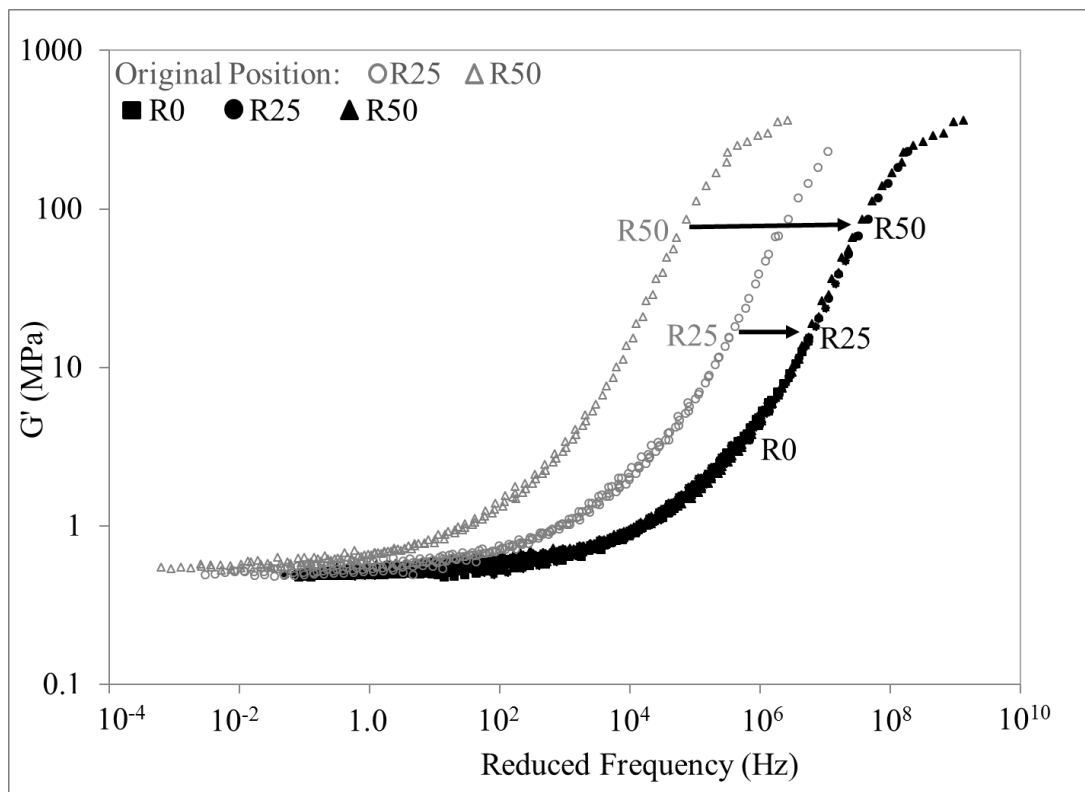
Figure 3.14: A comparison of the master curves for the storage modulus of R0, R25 and R50 rubbers as a function of the reduced frequency.

76
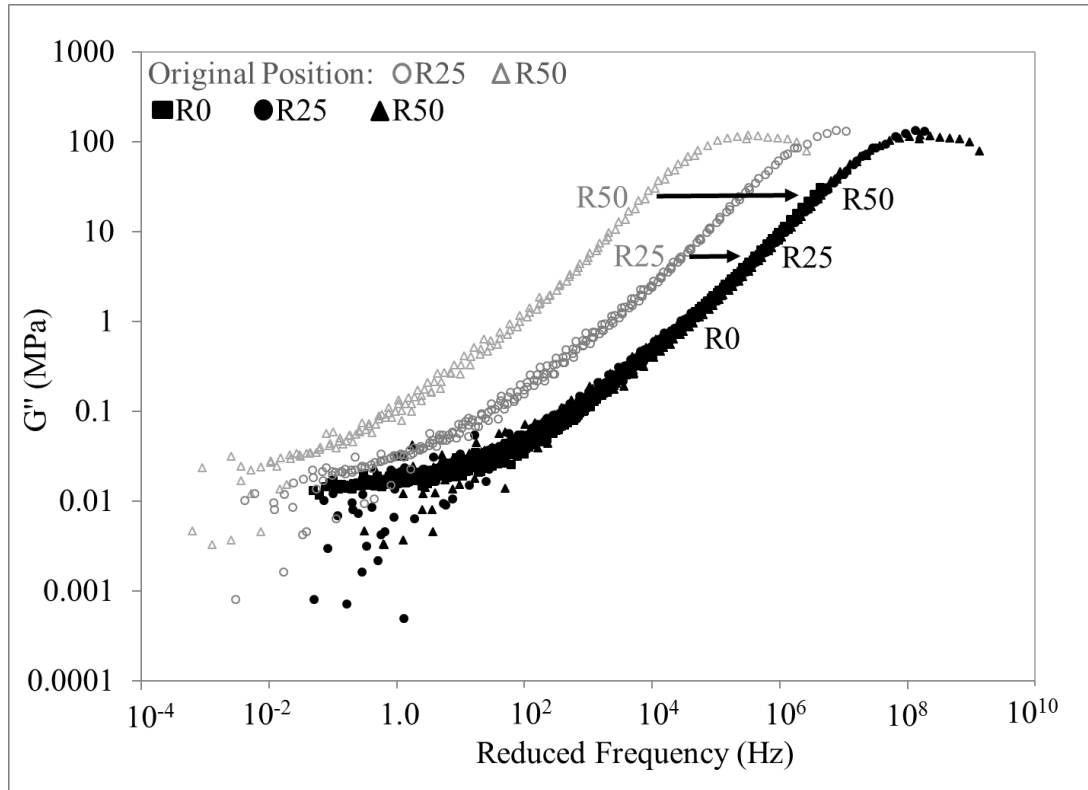
Figure 3.15: A comparison of the master curves for the loss modulus of R0, R25 and R50 rubbers as a function of the reduced frequency.

It is also possible to shift the curves for R0 and R50 by altering the reference temperature from 20°C to -3°C for R0 and to 38°C for R50 so that they overlap with the R25 curve at 20°C. The temperature differences between the reference temperature for R25 (20°C) and the new reference temperatures for R0 and R50 (23°C between R25 and R0 and 18°C between R25 and R50) were similar to the differences in their T_gs (26.5°C between R25 and R0 and 20.4°C between R25 and R50). It was observed that $C_1{}^0$ and $C_2{}^0$ were very similar for R0, R25 and R50 when the curves overlapped. This is to be expected as they have the same G' versus G'' relationship demonstrated by the Cole-Cole plot (Figure 3.13).

The implications of these observations are interesting from a practical perspective. Let us consider the case where it is desired to have an ENR having a particular dynamic property at a temperature T_ref. This may be achieved by shifting the master curves for the dynamic properties of natural rubber by a horizontal multiplication factor (x_r) to a new frequency range so that the desired modulus at the required frequencies is obtained. Then, the change required in the T_g of natural rubber can be calculated, and hence the epoxidation level required to obtain the dynamic properties under the desired conditions. Knowledge of the original three (before the application of x_r) shift factors (a_{T1}, a_{T2} and a_{T3}) and their

77

respective temperatures (T_1, T_2 and T_3) is required to form three simultaneous equations to solve for T_0 and $C_2{}^0$. It should be noted that T_0 is reference temperature for the natural rubber master curve shifted by x_r, whereas T_{ref} is the reference temperature for the ENR curve i.e. the temperature at which the desired properties are required.

$$\alpha = \log x_r\, a_{T1} = -\frac{C_1{}^0(T_1 - T_0)}{C_2{}^0 + T_1 - T_0} \tag{3.8}$$

$$\beta = \log x_r\, a_{T2} = -\frac{C_1{}^0(T_2 - T_0)}{C_2{}^0 + T_2 - T_0} \tag{3.9}$$

$$\gamma = \log x_r\, a_{T3} = -\frac{C_1{}^0(T_3 - T_0)}{C_2{}^0 + T_3 - T_0} \tag{3.10}$$

which leads to:

$$T_0 = \frac{\alpha\gamma T_2(T_3 - T_1) + \beta\gamma T_1(T_2 - T_3) + \alpha\beta T_3(T_1 - T_2)}{\alpha\gamma(T_3 - T_1) + \beta\gamma(T_2 - T_3) + \alpha\beta(T_1 - T_2)} \tag{3.11}$$

$$C_2{}^0 = \frac{(\alpha - \beta)(T_1 - T_0)(T_2 - T_0)}{\beta(T_1 - T_0) - \alpha(T_2 - T_0)} \tag{3.12}$$

Alternatively, if T_s of the original polymer (natural rubber) is known, then the following equation can be used instead of Equation 3.12:

$$C_2{}^0 = 101.6 + T_0 - T_s\,. \tag{3.13}$$

As mentioned earlier, the viscoelastic coefficients for overlapping NR and ENR compounds were found to be the same. The T_g of the ENR compound which gives the desired properties at T_{ref} can therefore be found:

$$T_g = 101.6 + T_{ref} - 50°C - C_2{}^0\,. \tag{3.14}$$

For example, using x_r as 0.06 (shifting R0 to match R25), T_1, T_2 and T_3 as -40°C, -35°C and -30°C, and a_{T1}, a_{T2} and a_{T3} as 31552, 7787 and 2232, the T_g for R25 is calculated, using Equations 3.11, 3.12 and 3.14 to be -48.5°C.

Another way of visualizing this data is to use a nomogram (Figure 3.16). This nomogram has been constructed from the data for R0, but it is generalised to apply to any ENR compounds with known T_g. The generalisation is approximate, but useful for design purposes. It could be employed in two ways.
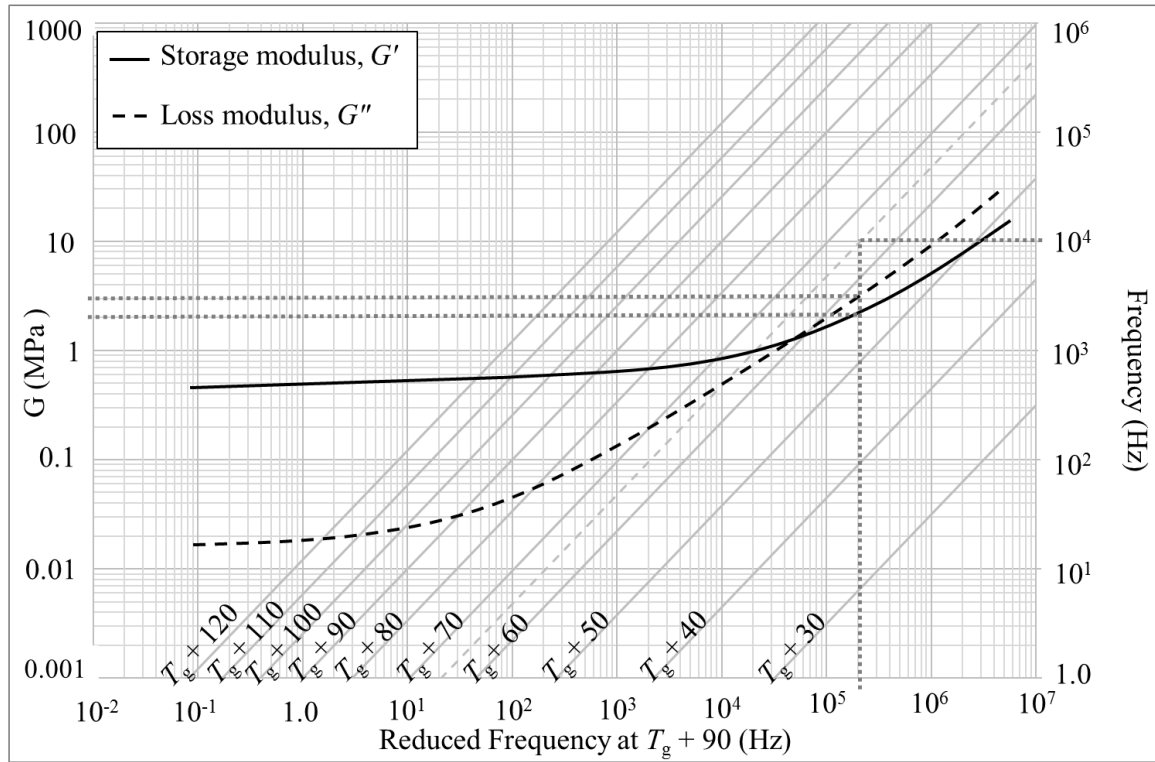
Figure 3.16: A nomogram relating the reduced frequency to G' and G'' at different temperatures. The data is for NR (R0). The temperature in this nomogram has been standardised such that it is applicable to other ENR compounds with knowledge of the T_g.

The first is estimation of the modulus at different temperatures and frequencies. For example, if one needs to know the properties of a rubber at 10000 Hz and T_g+65 then, from the right-hand vertical axis 10000 Hz is chosen. This line is followed until the T_g+65 line is reached. The horizontal axis value at the point (~200000 Hz) is the corresponding frequency for T_g+90 (or the 20°C reference temperature of R0) and where the G' and G'' curves intersect this vertical line are the corresponding values for this frequency and temperature. The value of G' is ~2 MPa and G'' is ~3 MPa. T_g+65 is approximately 20°C for R25, so the figures for G' and G'' can be confirmed by comparing with Figures 3.14 and 3.15. The second is to choose a suitable ENR compound based on desiring particular values of G' (or G'') at a particular frequency and temperature. To achieve this, a horizontal line is drawn

79

from the desired frequency and a vertical line through the desired value of G'. The point of the intersection gives an estimate of the temperature above T_g at which these properties could be achieved. From the knowledge of the temperature for the application the T_g, and therefore the level of epoxidation can be estimated.

3.3.5 Application of 5-Parameter Fractional Derivative Pritz Model

The 5-parameter fractional derivative model by Pritz, referred here to as the 5-parameter fractional model, is the generalization of the conventional viscoelastic Zener model [6]. This model has been developed and used successfully to fit experimental data on some polymeric damping materials, especially over a wide frequency range [82]. It is also known that the model describes the asymmetrical broadening peak of the loss factor and the low increment of dynamic modulus at high frequencies [6]. However, in this paper the model is fitted to the experimental data at low and medium frequencies only because the dynamic mechanical analysis was not performed at low enough temperatures to go well below the glass transition temperature for natural rubber. It is show in this part of the paper that the model satisfies the dynamic properties of natural rubber with different epoxidation levels over a wide frequency range.

The differential equation for the 5-parameter fractional model is [6]:

$$\sigma(t) + \tau^\beta \frac{d^\beta}{dt^\beta}\sigma(t) = G_0\varepsilon(t) + G_0\tau^\beta \frac{d^\beta}{dt^\beta}\varepsilon(t) + (G_\infty - G_0)\tau^\alpha \frac{d^\alpha}{dt^\alpha}\varepsilon(t). \qquad (3.15)$$

This equation has five parameters, $G_0, G_\infty, \alpha, \beta$ and τ which describe the dynamic behaviour of the material over a broad frequency range. The parameters G_0 and G_∞ are the low-frequency and high-frequency storage moduli, respectively. α is the parameter that determines the rate of change in the real and imaginary parts of the dynamic modulus in the low frequency range, i.e. below the peak in the loss factor. The parameter β is the correction to the conventional 4-parameter fractional derivative Zener model that controls the asymmetry of the loss peak and the high-frequency behaviour of the real and imaginary parts of the dynamic modulus. The parameter τ is the relaxation time that controls the position of the peak in the loss factor.

The complex modulus for the 5-parameter fractional model is derived in the form of the following equation (Equation 38 in ref. [6])

$$\bar{G}(\omega) = G_0 + G_0(d-1)\frac{(i\omega\tau)^\alpha}{1+(i\omega\tau)^\beta} \ , \tag{3.16}$$

where

$$d = \frac{G_\infty}{G_0} \tag{3.17}$$

and the normalised frequency is

$$\omega_n = \omega\tau. \tag{3.18}$$

In this work the values for the 5-parameter fractional model were determined directly from the experimental master curves. Since no dynamic properties data were obtained at the low temperatures below the glass transition temperature, the minimisation analysis

$$F(\boldsymbol{x}) = \sum_{n=1}^{N} |\bar{G}^{exp}(\omega_n, \boldsymbol{x}) - \bar{G}^{th}(\omega_n, \boldsymbol{x})| \rightarrow \min, \tag{3.19}$$

was carried out to invert the five parameters by fitting the predicted values of complex modulus, $\bar{G}^{th}(\omega_n, \boldsymbol{x})$, to the experimental data, $\bar{G}^{exp}(\omega_n, \boldsymbol{x})$, obtained at the frequencies ω_n. The design variable vector in Equation 3.19 is $\boldsymbol{x} = \{G_0, G_\infty, \alpha, \beta, \tau\}$. The inverted values of the five parameters are shown in Table 3.5.

Table 3.5
Optimized parameter values calculated for the 5-parameter fractional model.

Rubber	G_0 (Pa)	G_∞ (Pa)	α	β	τ (s)	d
R0	5.73 x 10^5	1.11 x 10^9	0.6828	0.6826	1.59 x 10^{-10}	1940
R25	5.84 x 10^5	4.03 x 10^8	0.7412	0.7388	1.78 x 10^{-8}	690
R50	6.60 x 10^5	3.21 x 10^8	0.7726	0.6926	9.95 x 10^{-7}	486

The predictions were performed for the inverted values of the five parameters and the results were compared with the experimental master curves. The results for the storage modulus and the loss modulus of R0, R25 and R50 rubbers are shown in Figure 3.17 and Figure 3.18. The master curves for the storage modulus suggest that there is a good correlation between the experimented and predicted results along the frequency range. The experimental master curves and that predicted by the 5-parameter fractional model are almost identical. The loss modulus of the rubbers exhibits similar behaviour by showing a good agreement from the top to middle part of the master curves (at and around the loss peak). However, as the frequency decreases, the disagreement between the data and the predictions becomes more pronounced. This disagreement may lead to considerable design errors if this model is used to predict the dynamic behaviour of the natural rubber that well above the glass transition temperature or for $\omega_n < 1$. Above this frequency range, the model accuracy is high with the maximum relative error being 5-8% for the storage modulus and 4-9% for the loss modulus. This observation suggests that the model proposed can provide a close agreement to the experimental master curves below the glass transition temperature or above $\omega_n > 1$.
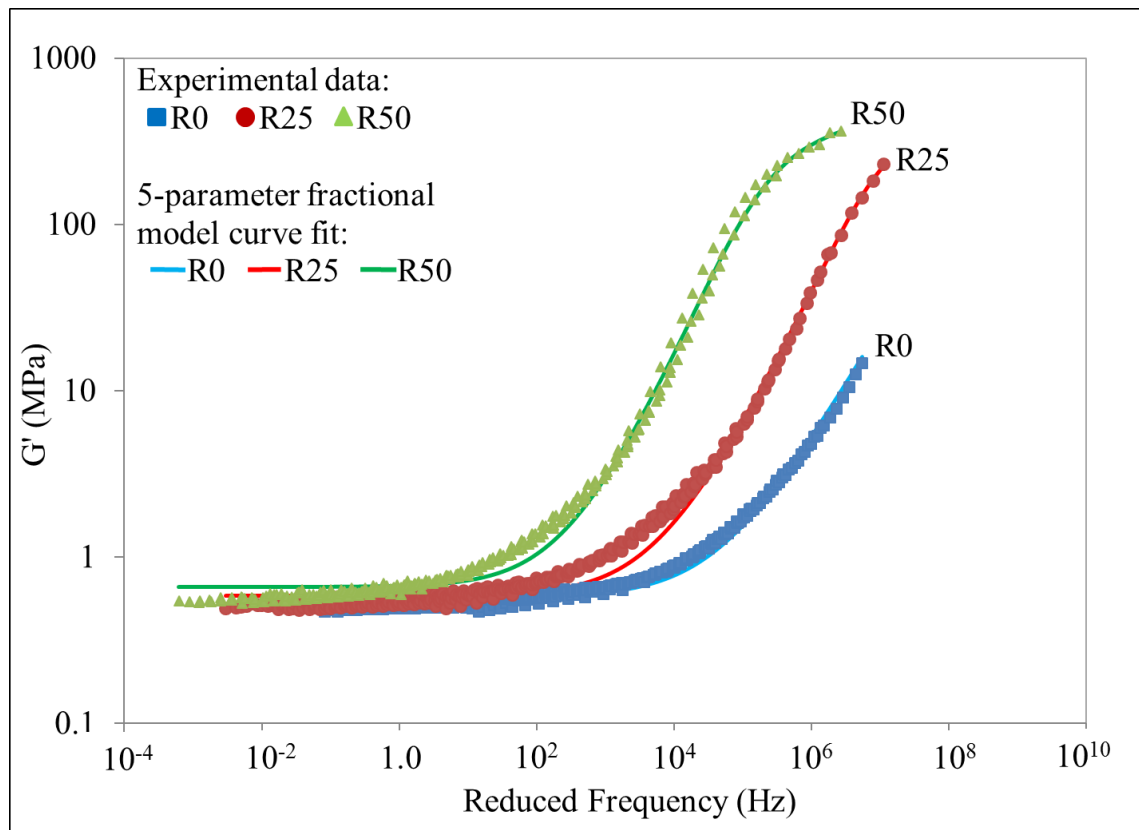
Figure 3.17: A comparison between the master curves and predictions from the 5-parameter fractional model for the storage modulus of R0, R25 and R50 rubbers as a function of the reduced frequency.
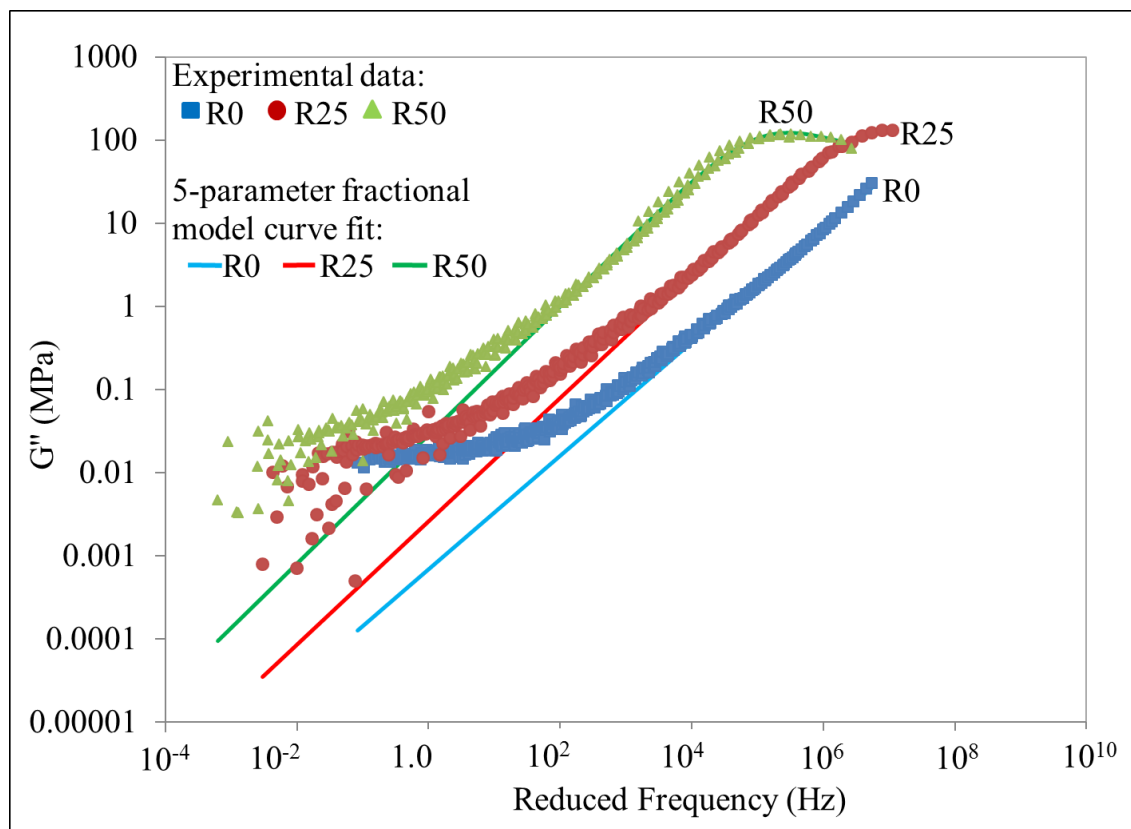
Figure 3.18: A comparison between the master curves and predictions from the 5-parameter fractional model for the loss modulus of R0, R25 and R50 rubbers as a function of the reduced frequency.

3.4 Summary

Three types of rubber with different epoxidation levels: SMR-CV60 (0 mol%), ENR-25 (25 mol%), and ENR-50 (50 mol%) were the focus of this study. The master curves for their dynamic properties were constructed based on the time-temperature equivalence principle using Williams-Landel-Ferry (WLF) relationship for amorphous polymers. Cole-Cole plots for all three vulcanizates fall on a single curve regardless of the level of epoxidation suggesting that the epoxidation does not influence the relationship between the storage modulus and loss modulus, but merely shifts the master curves for natural rubber along the frequency axis. The results obtained in this work provide the basis for determining the optimal epoxidation level to achieve specific dynamic property requirements over a range of temperature and frequencies. A nomogram has been constructed for predicting the appropriate epoxidation level for such purposes. In addition, the 5-parameter fractional model for the dynamic properties of natural rubber with different epoxidation levels has been fitted to the experimental data. This model can fit well the experimentally obtained master curves with the maximum relative error of 4-9%. The dynamic mechanical properties of

solid ENR and solid natural rubber were investigated. Consequently, the next step is to develop a manufacturing process for ENR foams and natural rubber foams based on dry rubber. The optimisation parameters in the manufacturing process of rubber foams need to be studied and understood so that they can be manufactured and used in vibration and noise control applications.

Chapter 4

Manufacturing Process of Epoxidized Natural Rubber Foam

4.1 Introduction

This chapter focuses on the development of a new manufacturing process for the dry rubber foams so that they can be used in vibration damping and noise control applications. Several manufacturing processes were performed to achieve optimum epoxidized natural rubber (ENR) foams and natural rubber foams formulations. The formulations, mixing process and curing procedures to produce vibro-acoustic foams are explained in detail. In addition, the Mooney viscosity measurement, cure characteristic analysis and morphology study on the rubber foams are discussed in this chapter.

4.2 Materials

The same materials and formulations as presented in section 3.2 were used to produce the natural rubber foam and ENR foams. The difference was only the addition of blowing agents to the formulations. Three types of natural rubber, SMR-CV60, ENR-25 and ENR-50 were obtained from the Malaysian Rubber Board. These three different epoxidation levels of natural rubber were used to study the effect of epoxidation levels on the manufacturing process of rubber foams. All other ingredients were provided by Tun Abdul Razak Research Centre (TARRC), Hertford while the blowing agents, sodium bicarbonate and ammonium bicarbonate were supplied by Sigma Aldrich. The foams are denoted as F0, F25 and F50, where the numbers stand for the epoxidation level of the rubber foam: 0, 25 and 50 mol%. All the manufacturing processes were carried out at TARRC, Hertford.

4.3 Manufacturing process 1: Introduction

4.3.1 Effect of different amount of sodium bicarbonate

Firstly, natural rubber with no epoxidation level was selected to study the possibility of the rubber to be produced as foam. The ultimate objective here was to obtain foam with an open pore structure and density being approximately below than 300 kg/m^3. Many vibration and

noise control applications require foams with open pore structure to provide a relatively low Young's modulus and higher damping properties. Foams with closed pore structure typically yield higher Young's moduli and can be used in application that require stiffer materials. The formulations shown in Table 4.1 were the initial formulations. These new formulations are denoted as DRF-8 and DRF-20. DRF-8 foam corresponds to the formulation with the same amount of sodium bicarbonate (8 phr) as used in ref. [4] and DRF-20 foam corresponds to the formulation with the maximum amount of sodium bicarbonate (20 phr) as proposed in ref. [56].

Table 4.1
DRF-8 and DRF-20 formulations in parts per hundred of rubber (phr).

Batch	Formulation	DRF-8	DRF-20
1	SMR-CV60	100	100
	Zinc Oxide	4	4
	Stearic Acid	4	4
	Wingstay L	1	1
2	Sulfur	2.5	2.5
	CBS[1]	1	1
	PVI[2]	0.3	0.3
	Sodium Bicarbonate	8	20

[1]Benzothiazyl-2-cyclohexyl-sulfenamide
[2]Prevulcanisation inhibitor

Most of the ingredients were based on the previous research [4]. The ingredients used in ref. [4] were chosen because of the same blowing agent, sodium bicarbonate, was used to produce the natural rubber foam. The sodium bicarbonate is one of the inorganic blowing agents. These kind of blowing agents are typically used to produce open pore foams, and they are non-hazardous materials [56]. The advantages of this blowing agent are presented in section 2.5.2.1.

Several modifications were made to the formulations shown in Table 4.1. The amount of stearic acid was increased slightly as this weak acid can help bicarbonate to decompose uniformly into carbon dioxide gas [56]. The amount of sulfur was also increased to avoid

any pore collapses due to insufficient crosslinking. Besides that, the addition of Wingstay L as an antioxidant to the formulations can protect rubber foams against degradation caused by oxidation. The addition of prevulcanisation inhibitor (PVI) increased the time to incipient the crosslinking process of a rubber formulation, so that bicarbonate can decompose into carbon dioxide gas in adequate time before the crosslinking process started. Finally, the influence of sodium bicarbonate itself in this study was also investigated.

All ingredients were compounded on a laboratory two-roll-mill machine. Raw rubber and other ingredients in Batch 1 (see Table 4.1) were loaded at the beginning of the compounding process and maintained below 40°C. The remaining ingredients in Batch 2 were mixed together and then loaded gradually onto the two-roll-mill. Finally, a compounded rubber sheet of rubber was obtained. The compounding time was kept below 20 minutes. The rubber sheet was left for 24 hours before being compression moulded for 20 minutes using an electrically heated hydraulic press at 150°C and the foaming pressure of 7 MPa. The stages for the preparation of compounded rubber before the curing process and for the production of rubber foam after the curing process are illustrated in Figure 4.1.
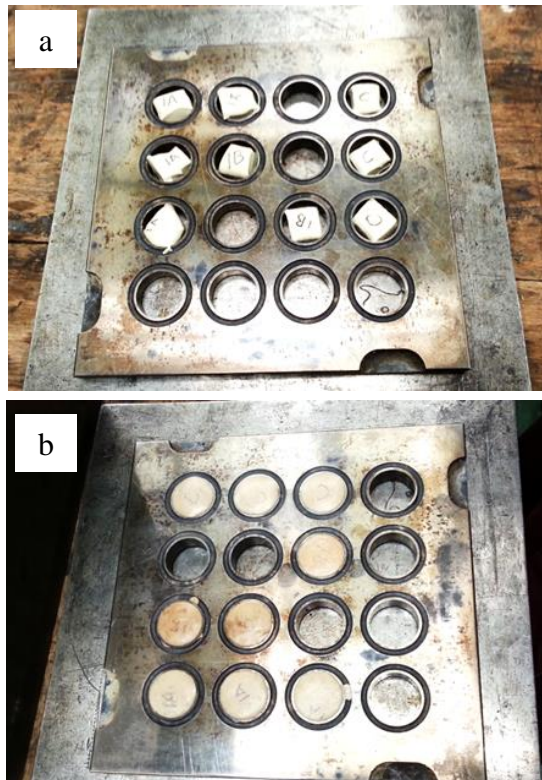
Figure 4.1: (a) The compounded rubber is ready to be compressed at predetermined time and temperature; (b) Rubber foam produced from the compression moulding process.

A preliminary study of the foam morphology was then performed. Light micrographs of razor-cut surfaces of DRF-8 and DRF-20 foams are shown in Figure 4.2. The surface was cut perpendicular to its foaming direction. The micrographs of the foam pores were then analysed using Image J software to determine their average pore size. This parameter was determined from the measurements of approximately more than 1000 different pores that were studied from a micrograph for each foam sample produced in this work.
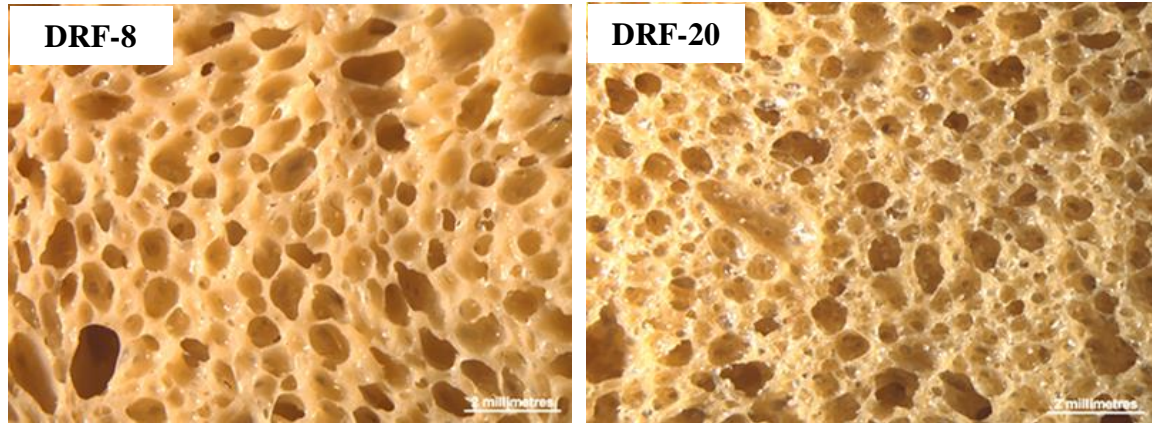
Figure 4.2: Light micrographs of DRF-8 and DRF-20 foams.

These micrographs were also analysed in terms of expansion ratio (ER) of the rubber foam [57] and number of pores per unit volume (N) [4]. These parameters can be expressed as:

$$ER = \frac{1}{\rho_x/\rho_y} \tag{4.1}$$

and

$$N = \frac{6}{\pi d^3}\left(\frac{\rho_y}{\rho_x} - 1\right) \tag{4.2}$$

where ρ_x is the density of the rubber foam, ρ_y is the density of the solid rubber and d is the average pore size or equivalent to diameter in mm. Density (ρ) measurements were performed by dividing the weight of each solid rubber or rubber foam with their corresponding volume as outlined in the ISO 6916-1:1995 [83]. The effect of adding different amounts of sodium bicarbonate on key physical properties of dry rubber foam are summarised in Table 4.2.

Table 4.2

Effect of different amount of sodium bicarbonate on the physical properties of dry rubber foam.

Physical properties	DRF-8	DRF-20
Density of solid rubber, ρ_y (kg/m^3)	967	967
Apparent density of rubber foam, ρ_x (kg/m^3)	390	260
Expansion ratio	2.48	3.72
Average pore size (mm)	0.55	0.42
Number of pores per unit volume (cm^{-3})	17,155	72,876

The density of dry rubber foam decreases with increasing amount of sodium bicarbonate. This observation suggests that a higher amount of sodium bicarbonate used in DRF-20 foam generates more carbon dioxide gas and allows this foam to expand more than DRF-8 foam. This statement is supported by the expansion ratio values which were 2.48 for DRF-8 foam and 3.72 for DRF-20 foam. According to the previous research [84], foam with a higher amount of sodium bicarbonate had more gas phase than the solid phase due to a higher amount of carbon dioxide present in the foam. Therefore, thinner pore walls in the matrix were created resulting to the production of the foam sample with lower density.

The results also indicate that the average pore size slightly decreased with increasing amount of sodium bicarbonate and the number of pores per unit volume increased by four-fold. This suggests that more small pores were developed in DRF-20 foam. These results were also observed in previous research [84] which stated that a higher amount of gas decomposed in the foaming process could resulted in smaller and more uniform pores. They also found that decreasing in the average pore size can lead to an increase in the number of pores per unit volume.

Figure 4.2 shows that thinner pore walls can be observed in the DRF-20 foam structure. These pore walls can be ruptured in the process to produce larger pores. However, this physical process was restricted by the high viscosity of raw rubber. This, in turn, restricted carbon dioxide gas from expanding more in the foam structure. Therefore, a mastication process (scissoring process) was introduced to obtain lower viscosity raw rubber. This

process was implemented successfully in the production of moulded rubber foam in ref. [85] and it is discussed in section 4.4.

4.3.2 Effect of compounding ingredients

The ingredients in the formulation have their own purposes and influence the end product. For example, sulfur is added to crosslink loose individual rubber chain molecules and to convert viscous and tacky raw rubber into an elastic rubber. Other ingredients used in the formulation such as activators (zinc oxide and stearic acid), accelerators (CBS; N-cyclohexyl-2-benzothiazole sulfonamide) and prevulcanisation inhibitor (PVI; N-(cyclohexylthio) phthalimide) also have their own functions in the formulation. These functions are explained in terms of their effect on the curing process. Table 4.3 shows the formulations studied. All these formulations contain the same amount of sulfur and antioxidant (Wingstay L). No blowing agent was applied for this observation study.

Table 4.3
R0-Raw, R0-Activator, R0-Accelerator and R0 formulations in parts per hundred of rubber (phr).

Batch	Formulation	R0-Raw	R0-Activator	R0-Accelerator	R0
1	SMR-CV60	100	100	100	100
	Zinc Oxide	-	4	-	4
	Stearic Acid	-	4	-	4
	Wingstay L	1	1	1	1
2	Sulfur	2.5	2.5	2.5	2.5
	CBS[1]	-	-	1	1
	PVI[2]	-	-	0.3	0.3
	Sodium Bicarbonate	-	-	-	-

[1]Benzothiazyl-2-cyclohexyl-sulfenamide
[2]Prevulcanisation inhibitor

These formulations are denoted as R0-Raw, which was a basic formulation with no activators and accelerators, R0-Activator, a formulation with activators only, R0-Accelerator, a formulation with accelerators only and R0, a formulation with the complete ingredients. The mixing process was the same as described in the previous section. Cure

characteristics were analysed using a Moving Die Rheometer, MDR 2000 (Figure 4.3(a)). The principle of the rheometer's operation is to apply a cyclic strain to the test sample and to measure the force (torque) developed as a function of time at a constant predetermined temperature. Five grams of each formulation was used in this experiment at the temperature of 150°C.
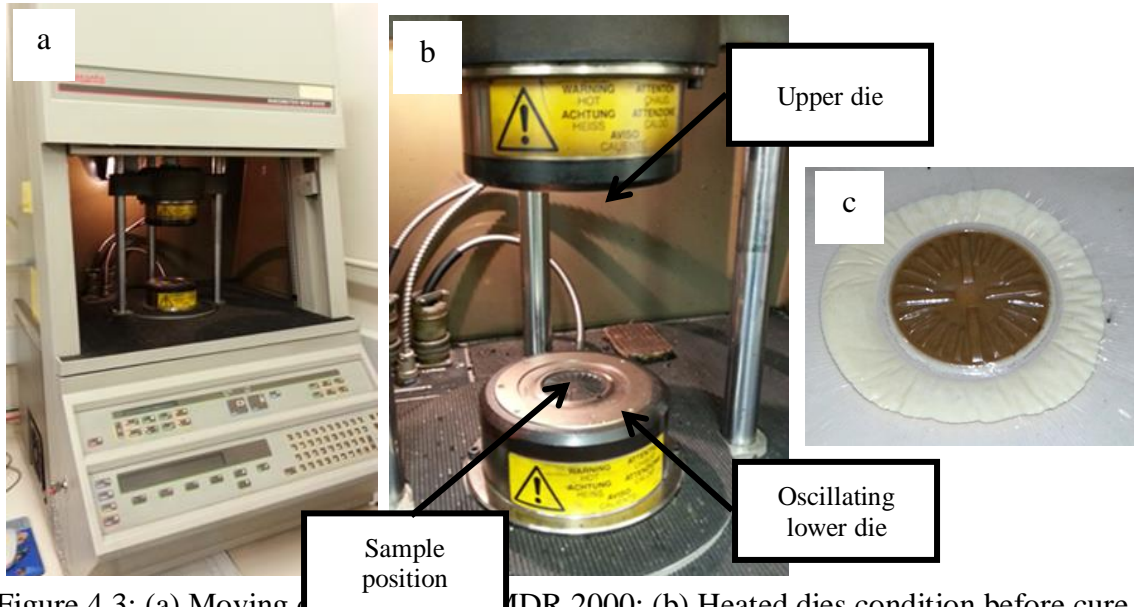
Figure 4.3: (a) Moving Die Rheometer, MDR 2000; (b) Heated dies condition before cure measurement; (c) Tested sample after cure measurement.

The rheometer curve (Figure 4.4) was obtained from this experiment in which the torque was plotted against time.
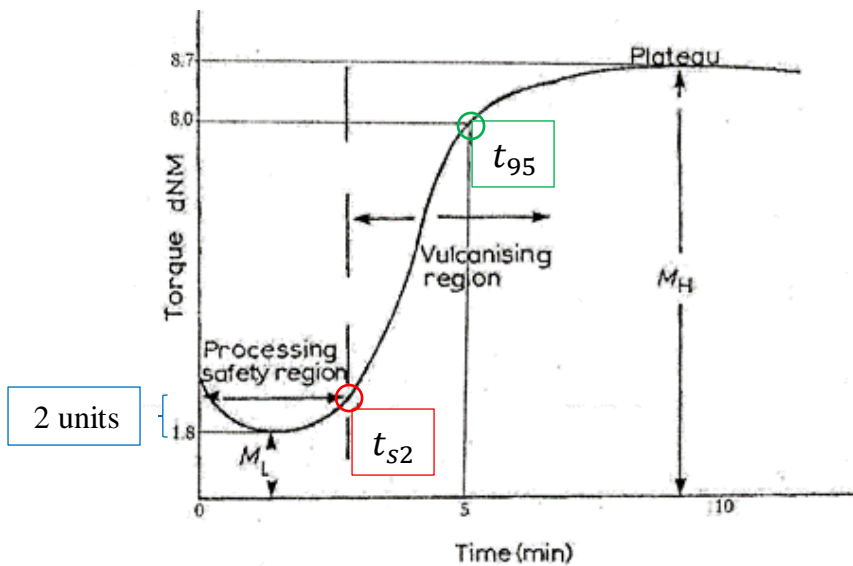
Figure 4.4: A rheometer curve [7].

91

The scorch time (t_{s2}), time to 95% cure (t_{95}), minimum torque (ML), and maximum torque (MH) were obtained from the rheometry data. Scorch is premature vulcanisation or crosslinking of rubber compound. The scorch time (t_{s2}) is the time taken for minimum torque value to increase by two units (ML + 2 units), and it is a measurement time for premature vulcanisation to start in the curing process, while t_{95} is the crosslinking time at which 95% of cure has taken place. The minimum torque (ML) relates to the viscosity of non-crosslinking natural rubber (unvulcanised natural rubber) taken at the minimum point of the rheometer curve, while the maximum torque (MH) is a viscosity measurement of crosslinked natural rubber (vulcanised natural rubber) taken at the maximum point of the rheometer curve.

The rheometer curve of the formulations is plotted in Figure 4.5 and their cure characteristics are given in Table 4.4.
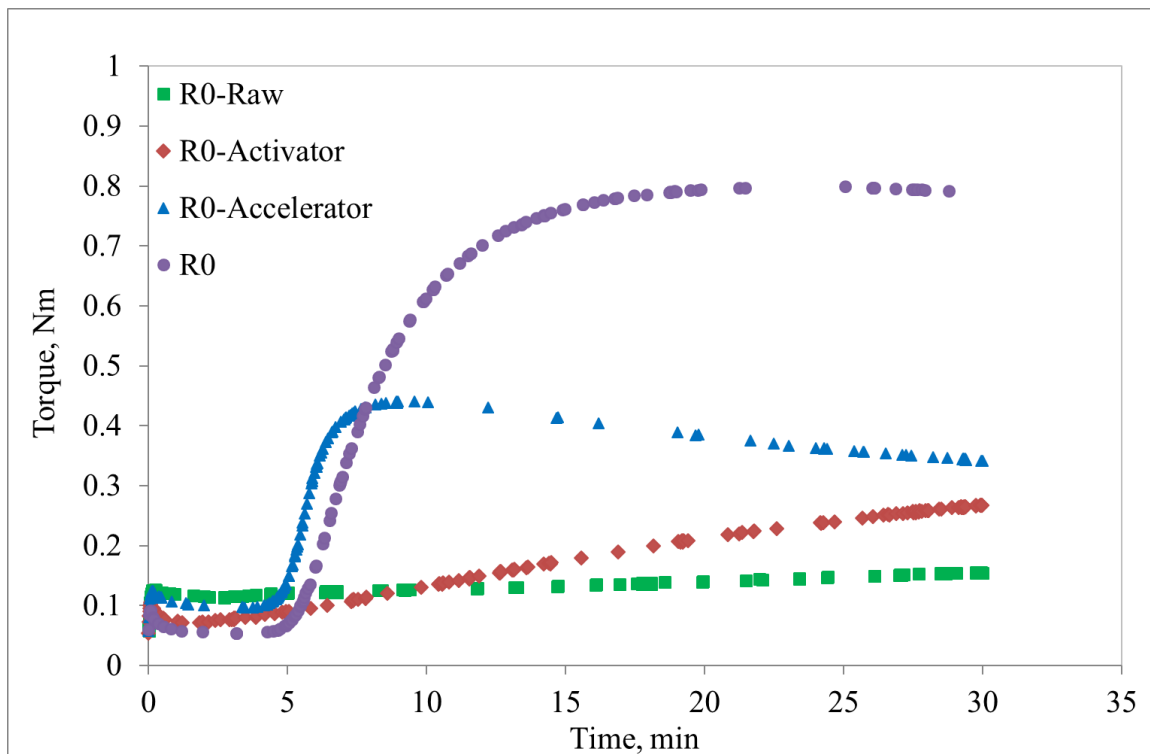
Figure 4.5: The rheometer curve for R0-Raw, R0-Activator, R0-Accelerator and R0 formulations at 150°C.

Table 4.4

The cure characteristics of R0-Raw, R0-Activator, R0-Accelerator and R0 formulations at 150°C.

Cure characteristics	R0-Raw	R0-Activator	R0-Accelerator	R0
a. Scorch time, t_{s2} (min)	Not available	31	6	7
b. Curing time, t_{95} (min)	Not available	52	8	15
c. Minimum torque, ML (Nm)	0.11	0.07	0.10	0.05
d. Maximum torque, MH (Nm)	0.16	0.35	0.44	0.80

R0-Raw formulation shows that data for the scorch time and the curing time were not able to be recorded. This observation may be attributed to the fact that no crosslinking happened within this time period. These parameters could be recorded after the activators were added to the R0-Activator formulation. The crosslinking process was too long with the time taken were 31 minutes for the scorch time and 52 minutes for the curing time.

After accelerators were introduced in R0-Accelerator formulation, the scorch time was measured and recorded at a realistically short time period of 6 minutes. This suggests that an accelerator is a compounding material which can be used with a sulfur to increase the speed of vulcanisation. For this formulation, the curing time of 8 minutes was found too short and too close to the scorch time. The cure system of the compound with the blowing agent must be capable of allowing the blowing agent to decompose into gas in adequate time so that the blown rubber can be set up steadily. Therefore, its pores structure does not collapse prior to vulcanisation [53]. Besides that, a decrease in torque can be seen after the maximum torque has been reached (see R0-Accelerator in Figure 4.5). This situation indicates a reversion of crosslinking process in the natural rubber compound. Reversion refers to the loss of crosslinking as a result of thermal aging [7].

The scorch time and the cure time of R0 formulation were recorded at 7 minutes and 15 minutes, respectively. This experiment provided an ample time for the gas in blowing agent to decompose sufficiently. In addition, the maximum torque was recorded at the highest value among the other formulations with 0.80 Nm with no reversion observed. The data show that the formulation had high viscosity and it was thermally stable. In this formulation,

an activator functioned very well by increasing the effectiveness of an accelerator. As a result, this formulation was the right formulation to be used in the natural rubber foam development

4.3.3 Effect of curing temperature

The study on curing temperature was performed to understand the relationship between the curing temperature and the cure characteristics in the rubber compounding process. This study was also extended to natural rubber with 25 mol% and 50 mol% epoxidation level and no blowing agent was applied. Four different curing temperatures were studied, 130°C, 140°C, 150°C and 160°C. Table 4.5 shows the formulations used in this study. These are denoted as R0, R25 and R50, where the numbers stand for the epoxidation level of the rubber: 0, 25 and 50 mol%, respectively.

Table 4.5
R0, R25 and R50 formulations in parts per hundred of rubber (phr).

Batch	Formulation	R0	R25	R50
1	SMR-CV60	100	-	-
	ENR-25	-	100	-
	ENR-50	-	-	100
	Zinc Oxide	4	4	4
	Stearic Acid	4	4	4
	Wingstay L	1	1	1
2	Sulfur	2.5	2.5	2.5
	CBS[1]	1	1	1
	PVI[2]	0.3	0.3	0.3
	Sodium Bicarbonate	-	-	-

[1]Benzothiazyl-2-cyclohexyl-sulfenamide
[2]Prevulcanisation inhibitor

The mixing process and cure characterisation procedures were the same as described in the previous section. The rheometer curve of R0, R25 and R50 formulations at different curing temperatures is plotted in Figures 4.6 to 4.8, respectively, and their cure characteristics are given in Table 4.6. The scorch time and the curing time decreased with the increasing curing temperature for all the formulations. These observations suggest that the crosslinking

process became shorten at higher curing temperature and the prevulcanisation might be happened earlier along with the rising curing temperature. A decreasing trend of the minimum torque and the maximum torque were also observed with the increasing curing temperature. These observations may be attributed to the increase in the curing temperature which caused in lower viscosity of the rubber formulation. At this point, the curing temperature of 150°C was considered as it provides realistically scorch time and reasonable curing time for all rubbers with different epoxidation levels. Moreover, the formulations at this curing temperature were thermally stable within 20 minutes curing process (see Figures 4.6 to 4.8).
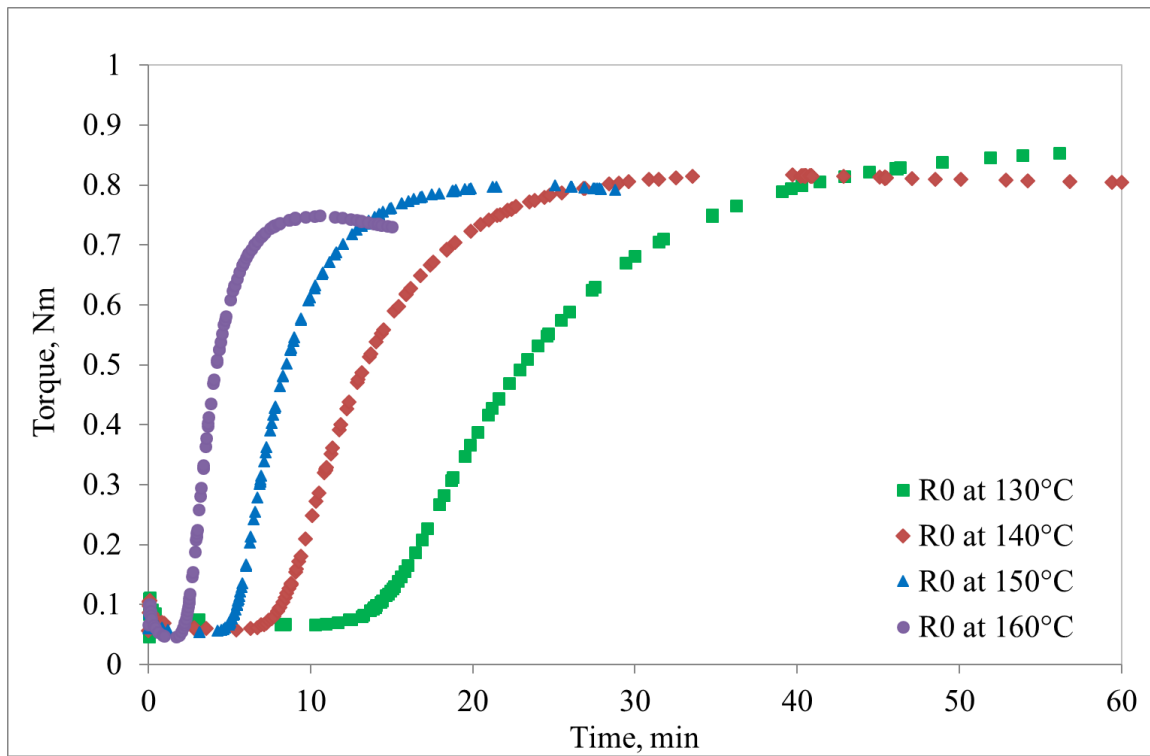
Figure 4.6: The rheometer curve for R0 formulation at different curing temperatures.
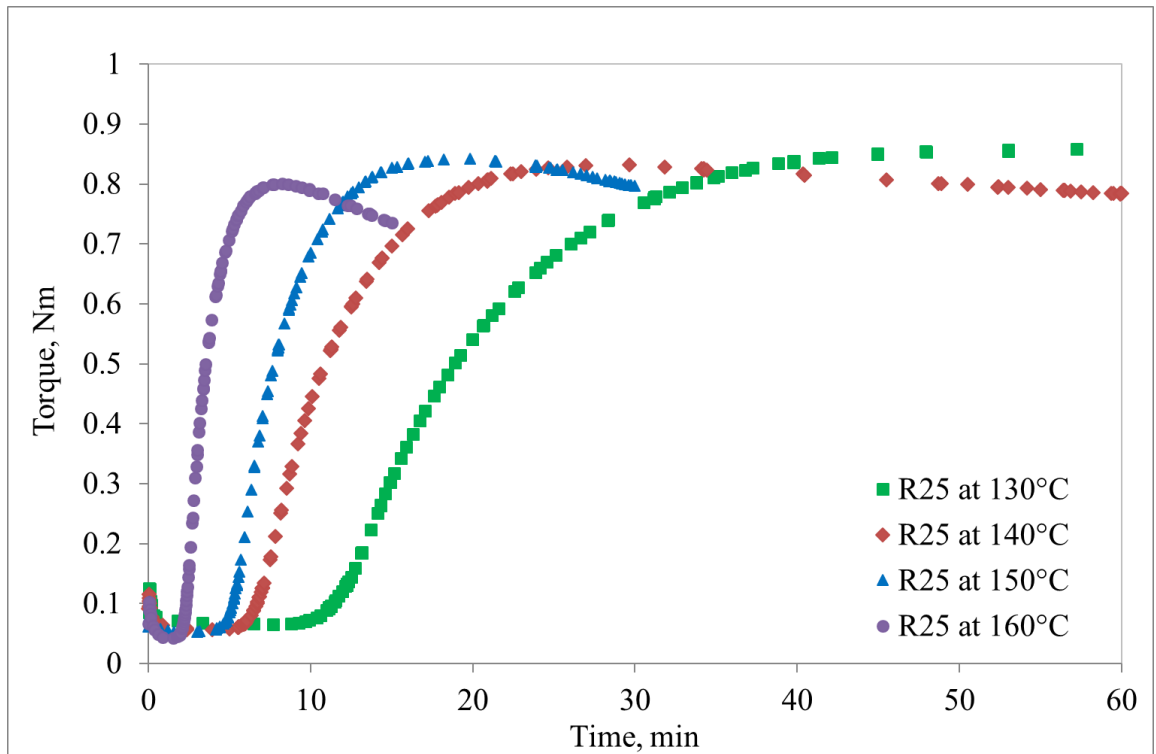
Figure 4.7: The rheometer curve for R25 formulation at different curing temperatures.
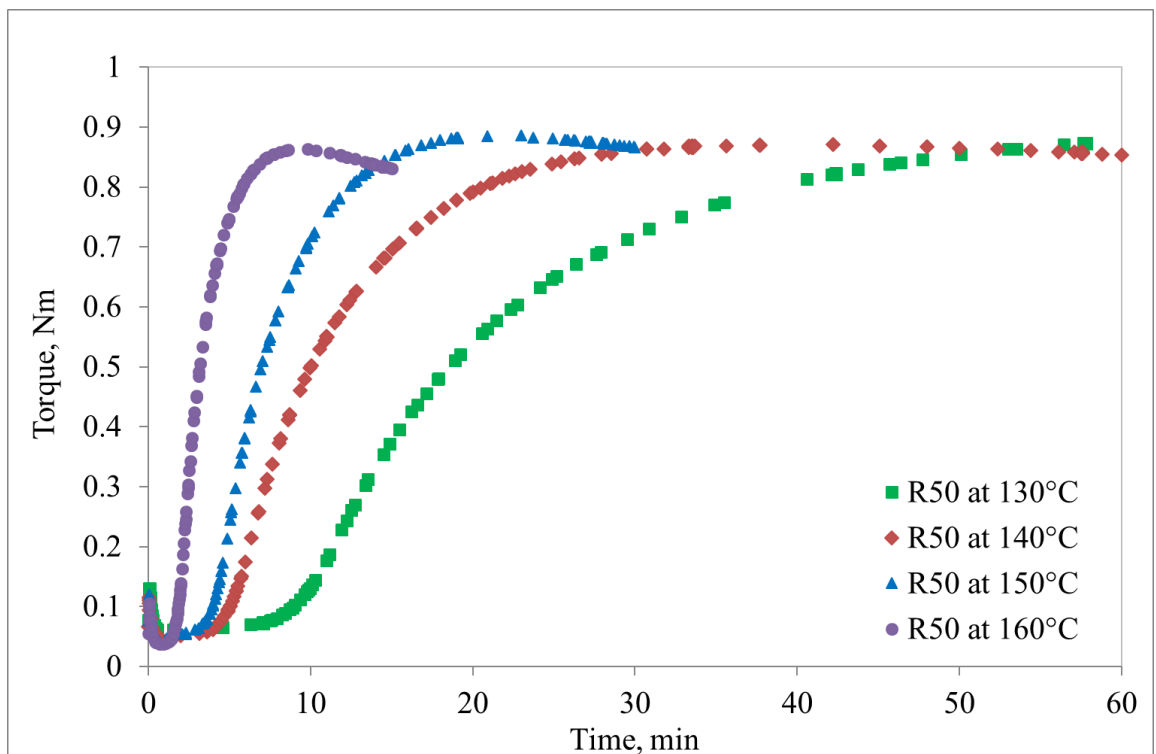
Figure 4.8: The rheometer curve for R50 formulation at different curing temperatures.

Table 4.6

The cure characteristics for R0, R25 and R50 formulations at different curing temperatures.

Curing temperature (°C)	R0				R25				R50			
	130	140	150	160	130	140	150	160	130	140	150	160
Scorch time, t_{s2} (min)	18	11	7	4	15	9	6	3	13	7	5	3
Curing time, t_{95} (min)	47	25	15	7	36	20	14	6	51	24	15	7
Minimum torque, ML (Nm)	0.07	0.06	0.05	0.05	0.07	0.06	0.05	0.04	0.06	0.05	0.05	0.04
Maximum torque, MH (Nm)	0.87	0.82	0.80	0.75	0.86	0.83	0.84	0.80	0.90	0.87	0.89	0.87

The rheometer curve of R0, R25 and R50 formulations at 150°C plotted in Figures 4.6 to 4.8 are replotted in Figure 4.9. No difference in terms of rheometer curve trend and no obvious reversion is taken place. However, it can be seen that the scorch time decreased slightly with the increasing epoxidation levels from 7 minutes for R0 formulation to 5 minutes for R50 formulation (see Table 4.6). The scorch time reduction can be explained by the presence of epoxide groups in the natural rubber matrix that contributes to the restriction of the polymer chains movement and initiation speed of the crosslinking process. These results were also observed in previous research [12] which found that the epoxidation can shorten the scorch time during the curing process. However, in terms of t_{95}, it was almost the same for all the formulations and it was in the range of 14 to 15 minutes.
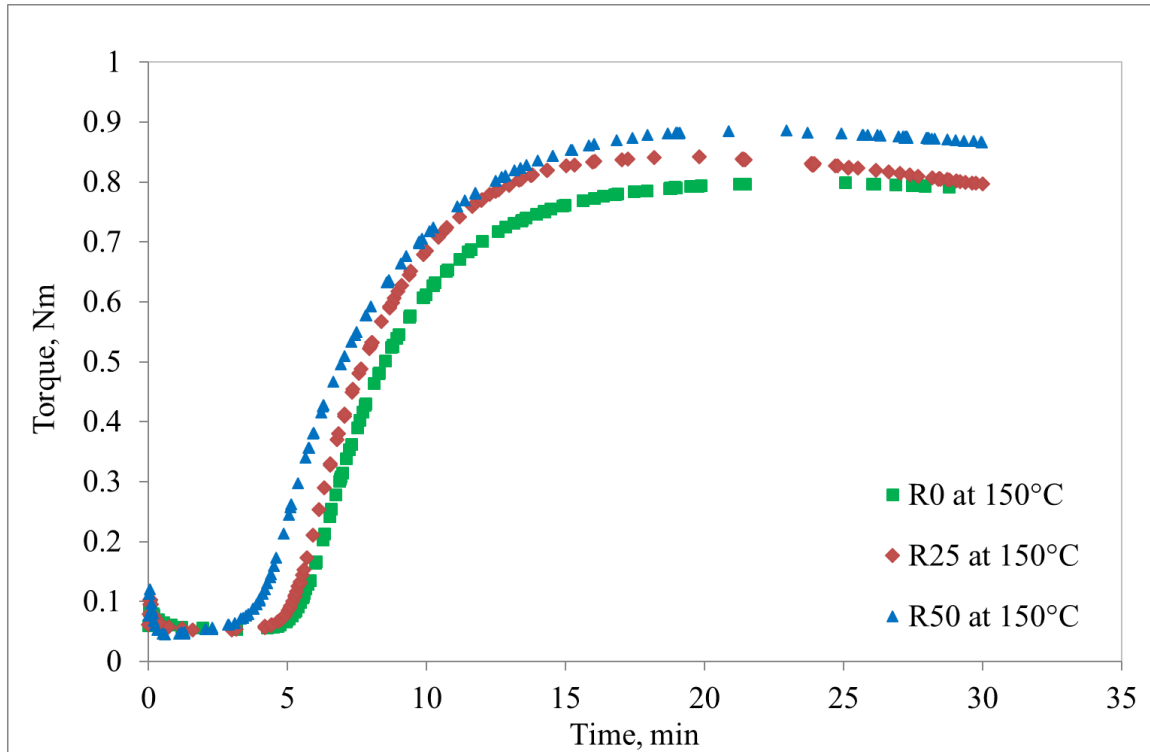
Figure 4.9: The rheometer curve for R0, R25 and R50 formulations at 150°C.

The minimum torques recorded were the same for all the formulations with the data measured were 0.05 Nm. This torque value indicates that the viscosity of unvulcanised material was the same for different epoxidation levels. The maximum torque increased with the increasing epoxidation levels. These data were obtained at 0.80 Nm, 0.84 Nm and 0.89 Nm for R0, R25 and R50 formulations, respectively. This was due to the presence of high polarity of epoxide groups in the rubber matrix which contributed to the higher viscosity of the vulcanised rubber.

Based on the rheometer curve presented in Figure 4.9, the curing time of 20 minutes was considered as the one at which the curing process was completed and no revision happened. This condition can be seen from the constant torque value on the rheometer curve of each formulation.

4.4 Manufacturing process 2: Mastication of raw rubber

In section 4.3.1, a mastication process was mentioned to reduce the viscosity of raw rubber. Raw rubber is a high molecular weight or high viscosity rubber. The purpose of the

mastication process is to reduce the average molecular weight of raw rubber by mechanical work. Therefore, the low viscosity of raw rubber can facilitate the combination of compounding ingredients and improves their dispersion in the rubber matrix [7]. In this study, the aim was to control the low viscosity of raw rubber, so that the raw rubber could allow the carbon dioxide gas produced from the thermal decomposition of sodium bicarbonate to expand more in the foam structure. Therefore, high porosity of rubber foam could be obtained. This process was implemented as suggested for the production of moulded rubber foam in ref. [85]. The viscosity of raw rubber in ref. [85] was masticated to 15 to 20 MV, where MV is stand for Mooney Viscosity, a viscosity index to measure the viscosity of raw rubber or rubber compound. The viscosity can be measured using the Mooney Viscometer at a standard prescribed elevated temperature, 100°C (Figure 4.10(a)).
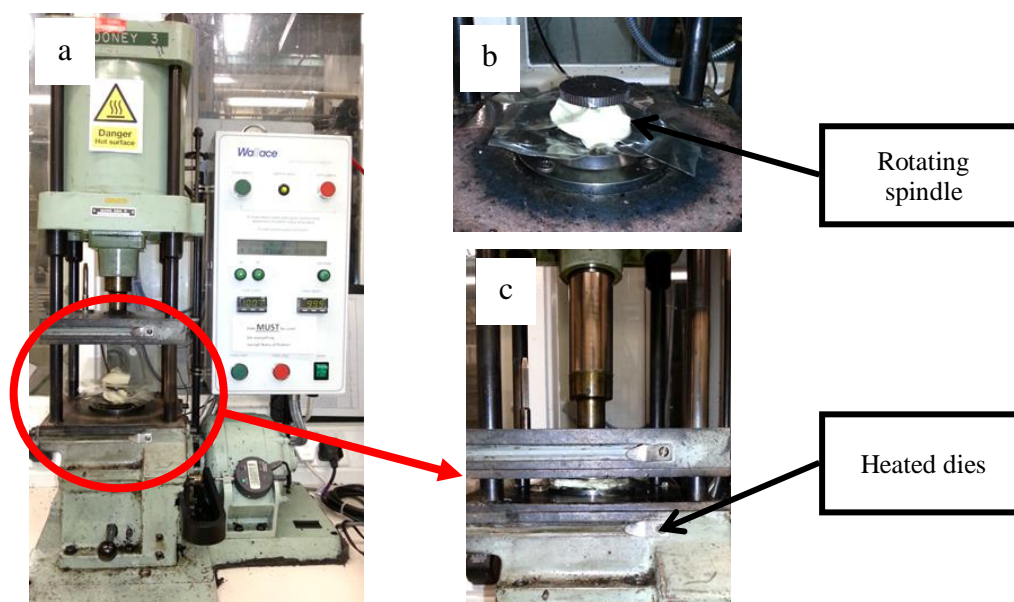
Figure 4.10: (a) Mooney viscometer; (b) Rotating spindle filled with the rubber sample; (c) The rubber sample within two heated dies.

This instrument measures torque on rotating spindle filled with 30 grams of rubber sample (Figure 4.10(b)). The pressure is then introduced to the sample within two heated dies for a minute to ensure the sample can reach the thermal equilibrium (Figure 4.10(c)). Next, the spindle is rotated by means of motor for four minutes measurement and finally a torque value is taken as viscosity index.

Table 4.7 shows the formulations studied and they are denoted as F0, F25 and F50, where the numbers stand for the epoxidation level of the foam: 0, 25 and 50 mol%, respectively.

Table 4.7
F0, F25 and F50 formulations in parts per hundred of rubber (phr).

Batch	Formulation	F0	F25	F50
1	SMR-CV60	100	-	-
	ENR-25	-	100	-
	ENR-50	-	-	100
	Zinc Oxide	4	4	4
	Stearic Acid	4	4	4
	Wingstay L	1	1	1
2	Sulfur	2.5	2.5	2.5
	CBS[1]	1	1	1
	PVI[2]	0.3	0.3	0.3
	Sodium Bicarbonate	20	20	20

[1]Benzothiazyl-2-cyclohexyl-sulfenamide
[2]Prevulcanisation inhibitor

The raw rubber was masticated for 10 minutes using a cracker mill machine (Figure 4.11) at room temperature. The machine has the same concept as the two-roll-mill machine but it larger in size. The mastication process using the two-roll-mill machine was not recommended as the process took 50 minutes to obtain the raw rubber with desired Mooney viscosity. The mixing process, cure characterisation procedures and curing process were the same as described in the previous section.

The Mooney viscosity in Table 4.8 indicates that the desired Mooney viscosity for the raw rubbers can be achieved within the first 10 minutes of the mastication process. At this stage, the viscosity of the raw rubber was kept around 20 MV. The Mooney viscosity of raw rubber can go lower than 20 MV as suggested in ref. [85]. However, this procedure was not recommended for this study as the raw rubber became tacky. It can be seen in Table 4.8 that the Mooney viscosity of compounded rubber were relatively low with the data measured were in the range of 8 to 12 MV for all formulations.

Figure 4.11: A cracker mill.

Table 4.8
The Mooney viscosity of F0, F25 and F50 formulations at different stages.

Mooney viscosity, 100°C (MV)	F0	F25	F50
Raw rubber	78.5	105.0	98.0
10 minutes mastication	21.0	21.5	20.0
Compounded rubber	8.0	12.0	12.0

The rheometer curves for F0, F25 and F50 formulations at the temperature of 150°C are plotted in Figure 4.12, and their cure characteristics are given in Table 4.9. The scorch time remain the same with the increasing epoxidation levels. This outcome is contradicted with the statement made in ref. [12] where the author observed that the epoxidation may shorten the scorch time in the curing process. However, these results suggest that the epoxidation may not influence significantly to the scorch time upon the addition of blowing agent to the formulations. These results were also observed correspondingly in previous research, e.g. [86]. The scorch time recorded in ref. [86] were similar with the increasing ratio of ENR in their binary formulation. In contrast, the curing time increased with the increasing epoxidation levels. The curing time for F0 formulation was 12 minutes and it increased to 18 minutes for F50 formulation.
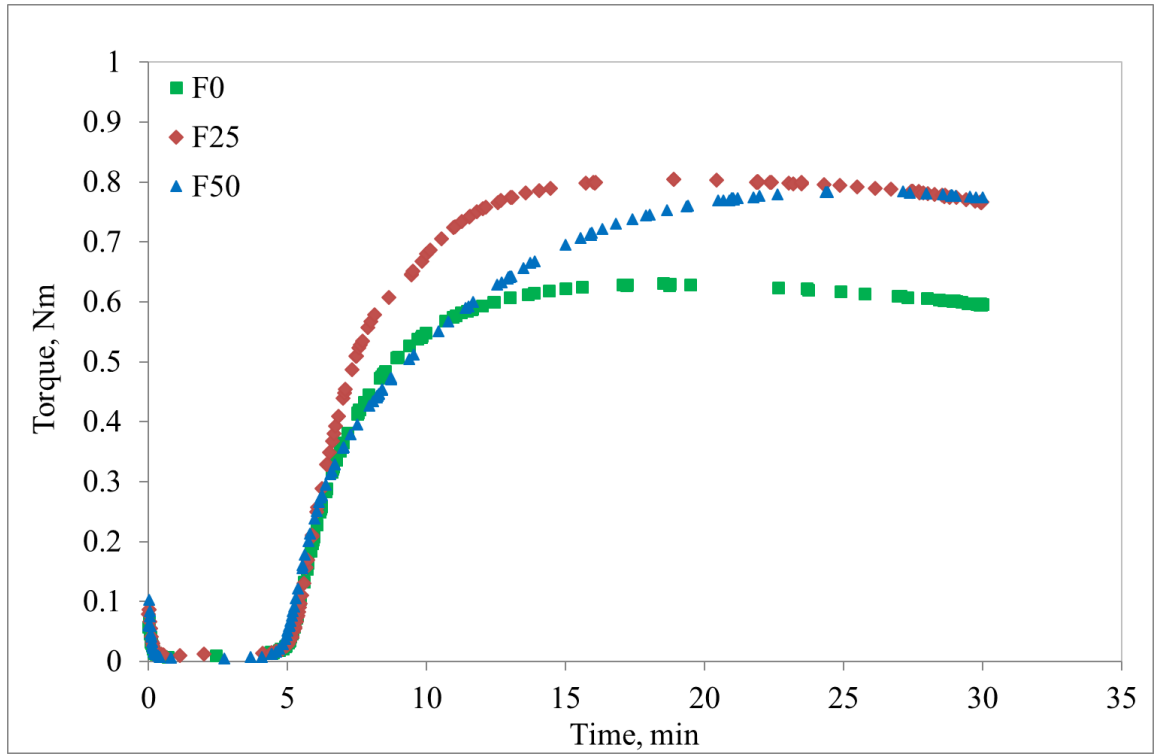
Figure 4.12: The rheometer curve for F0, F25 and F50 formulations at 150°C.

Table 4.9
The cure characteristics for F0, F25 and F50 formulations at 150°C.

Cure characteristics	F0	F25	F50
Scorch time, t_{s2} (min)	6	6	6
Curing time, t_{95} (min)	12	13	18
Minimum torque, ML (Nm)	0.01	0.01	0.01
Maximum torque, MH (Nm)	0.63	0.81	0.78

The minimum torques recorded were the same for all the formulations with the data measured were 0.01 Nm. However, the maximum torque shows different trend with the increasing epoxidation levels. The maximum torque for F50 formulation was lower than that for F25 formulation. This observation may be attributed to the lower viscosity of F50 raw rubber than F25 raw rubber used in this study (see Table 4.8).

The morphology study of F0 foam was performed. Light micrograph of razor-cut surfaces of F0 foam is shown in Figure 4.13. The micrograph processing procedures and the physical

102

properties studied were the same as described in section 4.3.1. The physical properties of F0 foam after the mastication process of raw rubber are summarised in Table 4.10.
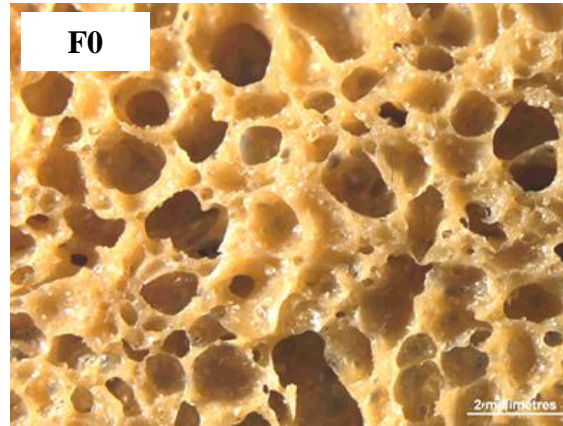
Figure 4.13: Light micrographs of F0 foam.

Table 4.10
The physical properties of F0 foam after the mastication process of raw rubber.

Physical properties	F0
Density of solid rubber, ρ_y (kg/m^3)	967
Apparent density of rubber foam, ρ_x (kg/m^3)	256
Expansion ratio	3.78
Average pore size (mm)	0.35
Number of pores per unit volume (cm^{-3})	126,090

The expansion ratio value of F0 foam after the mastication process of raw rubber was slightly higher than the expansion ratio value obtained for F0 20 foam (see Table 4.2). This result is attributed to the lower density of F0 foam. It shows here the mastication process which leading to the viscosity reduction of raw rubber can help the carbon dioxide gas to expand more in the foam structure even at the same amount of sodium bicarbonate. The results also indicate that the average pore size of the foam was slightly decreased and the number of pores per unit volume increased by 42% after the mastication process. This suggests that more small pores were produced in F0 foam.

However, no morphology study was performed on F25 and F50 foams as the production for both foams were not successful as illustrated in Figure 4.14. F25 and F50 foams collapsed during the curing process. This observation suggests that the carbon dioxide gas was not able

to penetrate through the ENR membranes even after the mastication process on ENR raw rubber. A few solutions were introduced by adding other ingredients in the formulation. These solutions are discussed in the following section.

F0 foam	F25 and F50 foams
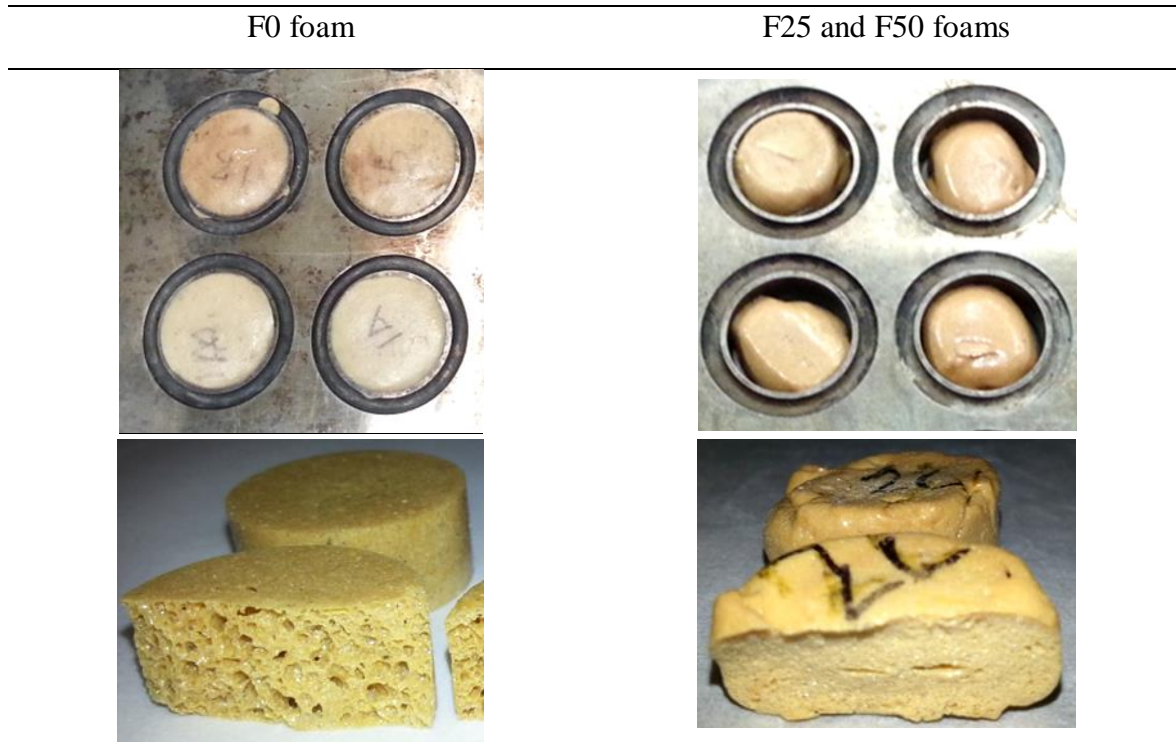
Figure 4.14: A comparison between the foam production after the mastication process for F0, F25 and F50 foams.

4.5 Manufacturing process 3: Addition of other ingredients

ENR has low gas permeability. This observation has been reported in previous research, e.g. [12]. The author found that the gas permeability decreased drastically with the increasing epoxidation levels. The presence of epoxide groups on the rubber backbone increase the degree of saturation in ENR and results in a reduction rate of gas permeability. Therefore, a few solutions were suggested to overcome the issue.

In this study, F50 foam was selected due its highest epoxidation level. Three new ingredients were added to F50 formulation. Table 4.11 shows the formulations used in this study.

Table 4.11
F50 CS, F50 AB and F50 PO formulations in parts per hundred of rubber (phr).

Batch	Formulation	F50 CS	F50 AB	F50 PO
1	ENR-50	100	100	100
	Zinc Oxide	4	4	4
	Stearic Acid	4	4	4
	Wingstay L	1	1	1
	Calcium Stearate	2	-	-
	Naphthenic Oil[1] (Strukthene 410)	-	-	10
	Talc	-	-	9
2	Sulfur	2.5	2.5	2.5
	CBS[1]	1	1	1
	PVI[2]	0.3	0.3	0.3
	Sodium Bicarbonate	20	10	20
	Ammonium Bicarbonate	-	10	-

[1]Benzothiazyl-2-cyclohexyl-sulfenamide
[2]Prevulcanisation inhibitor

These formulations are denoted as F50 CS, which is a formulation with addition of calcium stearate, F50 AB, a formulation with addition of ammonium bicarbonate and F50 PO, a formulation with addition of process oil. All these ingredients were added to ensure the gas in the F50 formulation can be expanded without any restriction by ENR membranes.

Calcium stearate is one of the lubricants used in the rubber compounding that can reduce the frictional forces between the rubber chains [7]. Therefore, this material was expected to reduce further the viscosity of the compounded rubber of F50 CS formulation. The lubricant coats the rubber and other ingredients in the first part of the mixing process. Then, it begins to melt with the increasing temperatures and starts to function in the rubber matrix by the shearing action of the two-roll-mill machine.

Ammonium bicarbonate (NH_4HCO_3) is another inorganic blowing agent. It is produced from the equilibrium reaction of ammonium carbonate ($(NH_4)_2CO_3$) and water (H_2O) as shown in the Equation 4.3 below [53]:

$$3(NH_4)_2CO_3 + H_2O \leftrightarrow 2\,NH_4HCO_3 + NH_2COONH_4 + 2\,NH_4OH \tag{4.3}$$
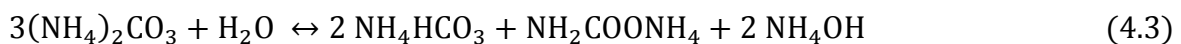
Ammonium bicarbonate starts to decompose the ammonia gas (NH_3) and the carbon dioxide gas (CO_2) when the temperature reaches 60°C as shown in the Equation 4.4.

$$NH_4HCO_3 \leftrightarrow NH_3 + CO_2 + H_2O \tag{4.4}$$

According to ref. [53], the thermal decomposition of ammonium carbonate can result in a formation of large broken pores in the foam structure. This is due to the production of large amounts of ammonia gas which contributed to the high rise in pressure during the decomposition process. This suggests that the ammonium bicarbonate has the same reaction, but it releases less ammonia gas and less rise in pressure is expected. Therefore, this mechanism was predicted and used to allow fair pores formation in ENR membranes with the assist of ammonia gas. Furthermore, the authors in ref. [53] stated that the low stability of this blowing agent can be improved by mixing it with the more stable blowing agent such as sodium bicarbonate. This can be achieved by mixing these two blowing agents with an equal weight in the F50 AB formulation (see Table 4.11).

Finally, the last suggested ingredient, process oil acts as a plasticiser and it provides softening effect to the compounded rubber by reducing its viscosity. The low viscosity process oil, naphthenic oil, was added to the F50 PO formulation and this type of process oil was also used in the suggested production of moulded rubber foam in ref. [85]. In F50 PO formulation, talc was also added to ensure the formulation does not contain an excessive oil which can make the mixing process difficult.

The mastication process of raw rubber was also implemented at the beginning of the mixing process for all the formulations. The viscosity measurement, cure characterisation procedures and curing process were the same as described in the previous sections. However, the mixing process for F50 PO formulation was slightly different because of the high dosage level of process oil used in the formulation. F50 PO formulation was not recommended to be mixed in the two-roll-mill machine as more practical mixing machine such as a Banbury mixer can be used as shown in Figure 4.15. This mixer can blend all the ingredients with the process oil in the close mixing condition.

Figure 4.15: A Banbury mixer.

The Banbury mixer has two intermeshing rotors that rotate side by side towards each other in a mixing chamber. The mixer has a door called hopper to insert the mixing ingredients. The Banbury mixer is operated by raising the ram completely and inserting the mixing ingredients to fill the chamber. The ram is then lowered under pressure to push the mixing ingredients to the mixing chamber before they are being blended by the rotors. After mixing process is completed by the shearing action of the rotors, the compounded rubber is discharged to the discharge tray. The mixing conditions and the mixing procedure of the F50 PO formulation are presented in Table 4.12.

Table 4.12
The mixing conditions and the mixing procedure of F50 PO formulation applied on the Banbury mixer.

Machine temperature:	40°C	Rotor speed:	100 rotation/minute

Mixing Time	Process
0 min	Ram up. Load the masticated raw rubber. Ram down.
1 min	Ram up. Load remaining ingredients in Batch 1 (see Table 4.11). Ram down.
6 min	Ram up. Load all the ingredients in Batch 2. Ram down.
8 min	Discharged.

The Mooney viscosity for F50 CS, F50 AB and F50 PO formulations are presented in Table 4.13. The desired Mooney viscosity for the raw rubbers was achieved within 10 minutes mastication process. The Mooney viscosity for all the compounded rubbers were relatively lower than F50 formulation (see Table 4.8). This observation suggests that the viscosity of F50 formulation can be reduced further with the addition of these ingredients. Therefore, the decomposition gas was expected to expand in the ENR membranes.

Table 4.13
The Mooney viscosity for F50 CS, F50 AB and F50 PO formulations at different stages.

Mooney viscosity, 100°C (MV)	F50 CS	F50 AB	F50 PO
Raw rubber	98.5	98.5	98.5
10 mins mastication	19.0	18.5	19.5
Compounded rubber	10.5	8.0	6.0

The rheometer curves for F50 CS, F50 AB and F50 PO formulations at the temperature of 150°C are plotted in Figure 4.16, and their cure characteristics are given in Table 4.14.
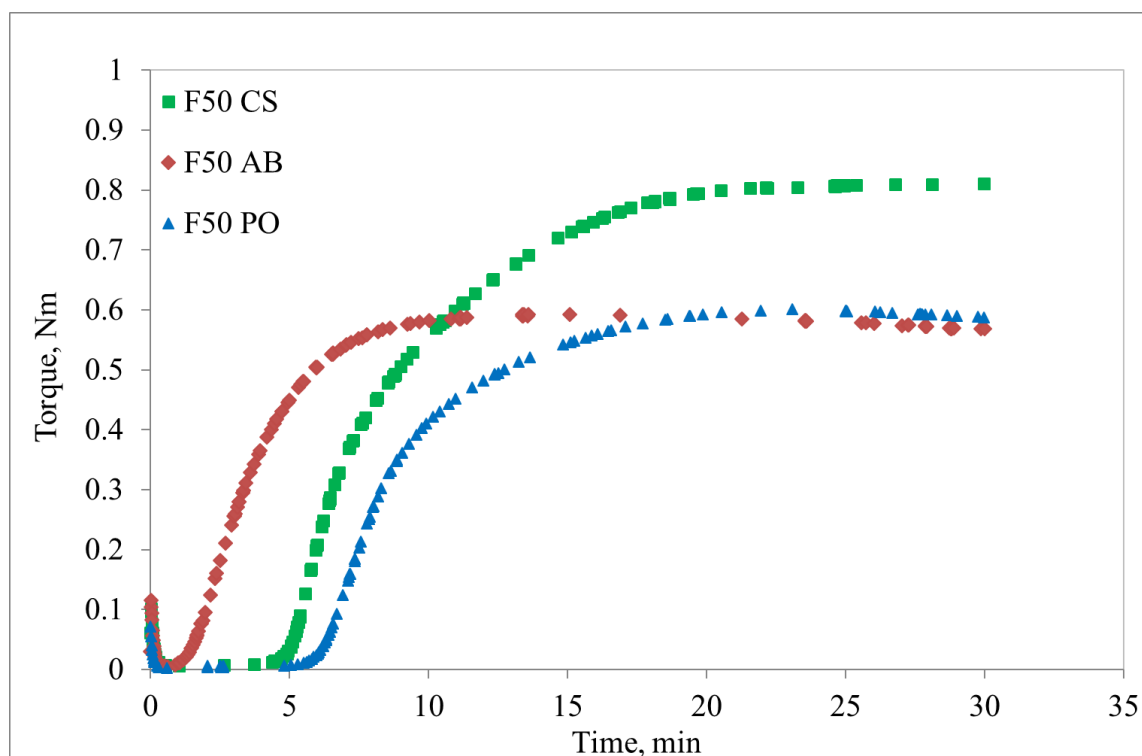
Figure 4.16: The rheometer curve for F50 CS, F50 AB and F50 PO formulations at 150°C.

Table 4.14
The cure characteristics for F50 CS, F50 AB and F50 PO formulations at 150°C.

Cure characteristics	F50 CS	F50 AB	F50 PO
Scorch time, t_{s2} (min)	6	3	8
Curing time, t_{95} (min)	18	9	18
Minimum torque, ML (Nm)	0.01	0.01	0.01
Maximum torque, MH (Nm)	0.81	0.60	0.60

The cure characteristics of F50 CS formulation were similar to F50 formulation (see Table 4.9). This suggests that the calcium stearate does not change the cure characteristics. The result was also predicted in the case of F50 PO formulation. The scorch time increased and maximum torque decreased when process oil was added. The softening effect delayed the crosslinking to occur during the curing process and it also reduced the F50 PO formulation stiffness by 23%.

In the case of F50 AB formulation, the scorch time and the curing time reduced by half as compared to F50 CS formulation, and the maximum torque also decreased with the presence of ammonium bicarbonate to the formulation. These observations suggest that ammonia gas decomposed strongly after the curing temperature reached at 60°C and relatively high pressure developed prior to the formation of the crosslinking process of the rubber. Therefore, the gas increases the speed of crosslinking process. The results can also be supported by the finding reported in ref. [53]. The authors found different pressure behaviour between ammonium carbonate $((NH_4)_2CO_3)$ and sodium bicarbonate $(NaHCO_3)$ as a function of temperature (Figure 4.17). The thermal decomposition of ammonium carbonate starts at lower temperatures and pressure increases drastically at temperatures above 80°C. In contrast, sodium bicarbonate decomposes at higher temperatures and it results in a relatively low in pressure rise. This comparison suggests that ammonium carbonate or bicarbonate are more active inorganic blowing agents as compared to sodium bicarbonate.

The morphology study of F50 AB foam was performed. A light micrograph of razor-cut surfaces of F50 AB foam is shown in Figure 4.18. The micrograph processing procedure and the physical properties studied were the same as described in the previous section. The physical properties of F50 AB foam are summarised in Table 4.15.
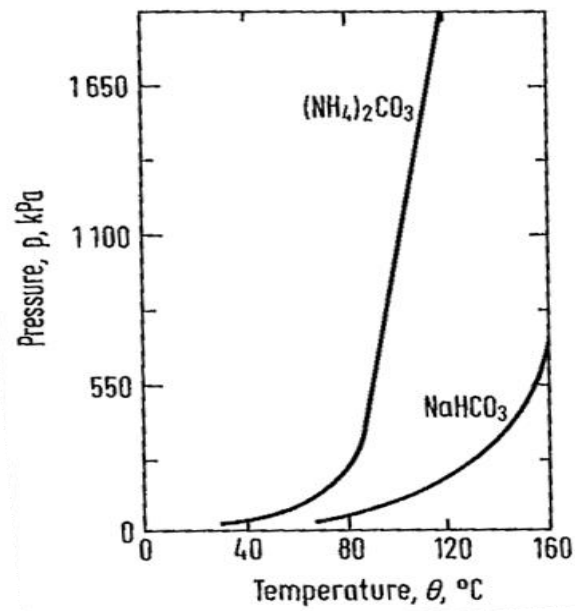
Figure 4.17: The pressure behaviour of ammonium carbonate ($(NH_4)_2CO_3$) and sodium bicarbonate ($NaHCO_3$) as a function of temperature [53].
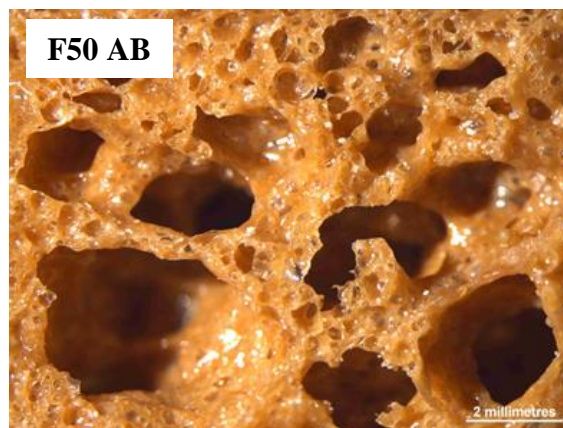
Figure 4.18: Light micrographs of F50 AB foam.

Table 4.15
The physical properties of F50 AB foam.

Physical properties	F50 AB
Density of solid rubber, ρ_y (kg/m^3)	1049
Apparent density of rubber foam, ρ_x (kg/m^3)	266
Expansion ratio	3.94
Average pore size (mm)	0.48
Number of pores per unit volume (cm^{-3})	49,985

The expansion ratio value of F50 AB foam was comparable to the expansion ratio value obtained for F0 foam (see Table 4.10). This observation suggest that the ammonia gas produced from the thermal decomposition of ammonium bicarbonate was able to expand in ENR membranes allowing pores formation in the foam structure. The results also indicate that the average pore size of foam increased and that the number of pores per unit volume decreased upon the addition of ammonium bicarbonate. This suggest that more larger pores were produced in F50 AB foam as compared to F0 foam. Ammonium bicarbonate was producing a relatively high pressure at temperatures above 80°C and contributed to the formation of larger pores in the foam structure. The results also show that ammonia gas decomposed just before the scorch time was reached and that the expansion occurred immediately to rupture the ENR membranes before the crosslinking process could have stabilised them.

No morphology study was performed on F50 CS and F50 PO foams because these foams were not considered promising enough because of their relative low porosity as shown in Figure 4.19. F50 CS and F50 PO foams were not fully blown foam by the curing process. This observation suggests that the calcium stearate and process oil were not fully able to assist carbon dioxide gas to expand completely and to penetrate through the ENR membranes. At this point, the addition of ammonium bicarbonate to the formulation was considered. The comparative study on the effect of different ratios of ammonium bicarbonate and sodium bicarbonate in the rubber foam production is presented in the following section.

F50 CS foam	F50 AB foam	F50 PO foam
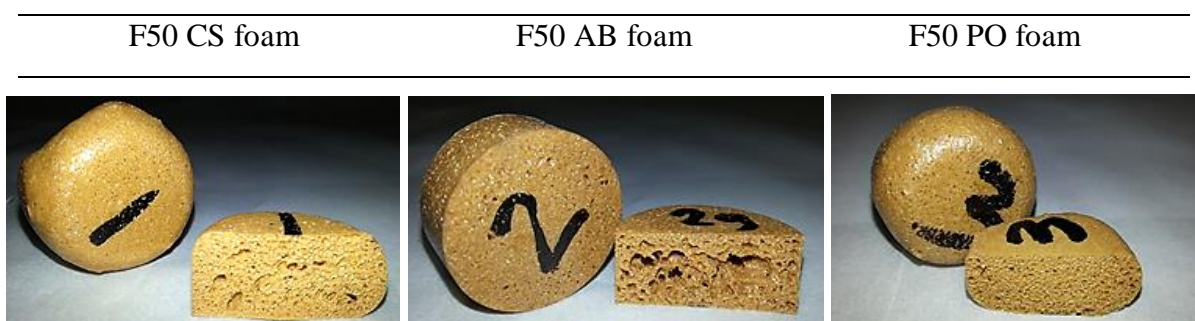
Figure 4.19: A comparison between the foam production for F50 CS, F50 AB and F50 PO foams.

4.6 Manufacturing process 4: Finalising

The introduction of ammonium bicarbonate showed some improvement in the ENR foam production. Besides that, the authors of ref. [53] recommended a mixture of ammonium carbonate (or bicarbonate) and sodium bicarbonate because this mixture does not decompose immediately during the curing process so that foam with uniform structure could be produced. Therefore, the effect of different ratios of ammonium bicarbonate and sodium bicarbonate in the rubber foam with different epoxidation levels was investigated.

At this stage, a relatively low foaming pressure of 2 MPa was applied in the production of rubber foams. The purpose was to improve the production of ENR foams especially the ones with sodium bicarbonate alone (see Figure 4.14). This mechanism was expected to assist the carbon dioxide gas to expand in the ENR membranes at low foaming pressure. The effect of foaming pressure on the rubber foam production was observed in previous research [59]. The authors found that the foaming efficiency decreased with the increasing foaming pressure, resulting in a high density, low expansion ratio and thicker pore walls. Therefore, rubber foam at a low foaming pressure had higher foaming efficiency.

Table 4.16 shows the formulations studied and they are denoted as F0, F25 and F50, where the numbers stand for the epoxidation level of the rubber foam. Each rubber foam was formulated with two different blowing agent contents, namely as 20:0, 15:5 and 10:10, where the numbers stand for the ratio of sodium bicarbonate to ammonium bicarbonate in parts per hundred rubber (phr) used in the formulation. At this point, F0, F25 and F50 formulations in Table 4.7, as well as F50 AB formulation in Table 4.11 are denoted as F0 20:0, F25 20:0, F50 20:0 and F50 10:10, respectively. The production and analysis of these formulations were repeated to ensure a consistency in terms of the viscosity of raw rubber and application of the same foaming pressure. In this way a direct comparison could be made of all formulations with different ratios of blowing agents.

The mixing process, viscosity measurement, cure characterisation procedures and curing process were the same as described in the previous sections. The Mooney viscosity in Table 4.17 indicates that the desired Mooney viscosity for the raw rubbers can be achieved within 10 minutes mastication process.

Table 4.16
F0, F25 and F50 formulations with different ratios of sodium bicarbonate to ammonium bicarbonate in parts per hundred of rubber (phr).

Batch	Formulation	F0 20:0	F0 15:5	F0 10:10	F25 20:0	F25 15:5	F25 10:10	F50 20:0	F50 15:5	F50 10:10
1	SMR-CV60	100	100	100	-	-	-	-	-	-
	ENR-25	-	-	-	100	100	100	-	-	-
	ENR-50	-	-	-	-	-	-	100	100	100
	Zinc Oxide	4	4	4	4	4	4	4	4	4
	Stearic Acid	4	4	4	4	4	4	4	4	4
	Wingstay L	1	1	1	1	1	1	1	1	1
2	Sulfur	2.5	2.5	2.5	2.5	2.5	2.5	2.5	2.5	2.5
	CBS[1]	1	1	1	1	1	1	1	1	1
	PVI[2]	0.3	0.3	0.3	0.3	0.3	0.3	0.3	0.3	0.3
	Sodium Bicarbonate	20	15	10	20	15	10	20	15	10
	Ammonium Bicarbonate	-	5	10	-	5	10	-	5	10

[1]Benzothiazyl-2-cyclohexyl-sulfenamide
[2]Prevulcanisation inhibitor

Table 4.17
The Mooney viscosity for F0, F25 and F50 formulations with different ratios of blowing agents at different stages.

Mooney viscosity, 100°C (MV)	F0 20:0	F0 15:5	F0 10:10	F25 20:0	F25 15:5	F25 10:10	F50 20:0	F50 15:5	F50 10:10
Raw rubber	79.0	79.0	79.0	99.0	99.0	99.0	98.5	98.5	98.5
10 mins mastication	17.5	17.5	17.5	18.0	18.0	18.0	19.0	19.0	19.0
Compounded rubber	9.5	10.0	8.5	13.5	12.0	11.0	13.5	13.0	11.0

The results also showed that the Mooney viscosity for all compounded rubbers reached their lowest Mooney viscosity at 10:10 formulation, where the ratio of ammonium bicarbonate was at maximum. These observations suggest that some amount of ammonia bicarbonate might have been decomposed, and that ammonia gas expanded during the mixing process even at the mixing temperature of 40°C. Therefore, the reduction in viscosity was observed.

The rheometer curve of F0, F25 and F50 formulations with different ratios of blowing agents at the temperature of 150°C is plotted in Figures 4.20 to 4.22, and their cure characteristics are given in Table 4.18. As expected, the scorch time for F0, F25 and F50 formulations decreased by half with the addition of 5 phr ammonium bicarbonate. However, no further reduction in scorch time was observed upon the addition of 10 phr ammonium bicarbonate. The same decreasing trend was also observed for the curing time. These observations suggest that ammonia bicarbonate increases the speed of the crosslinking process by producing a relatively high pressure and high rate thermal decomposition at the beginning of the curing process. Beyond this point no significant difference was observed in the scorch time and the curing time with the increasing amount of ammonium bicarbonate.
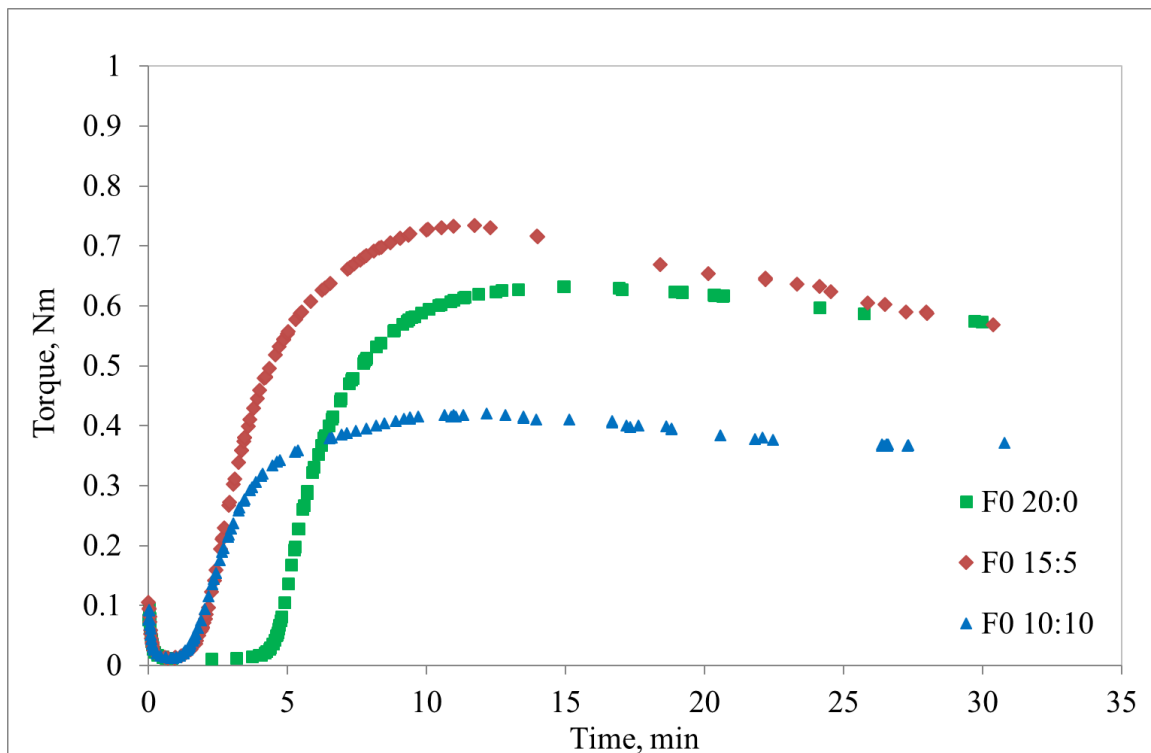
Figure 4.20: The rheometer curve for F0 formulation with different ratios of blowing agents at 150°C.
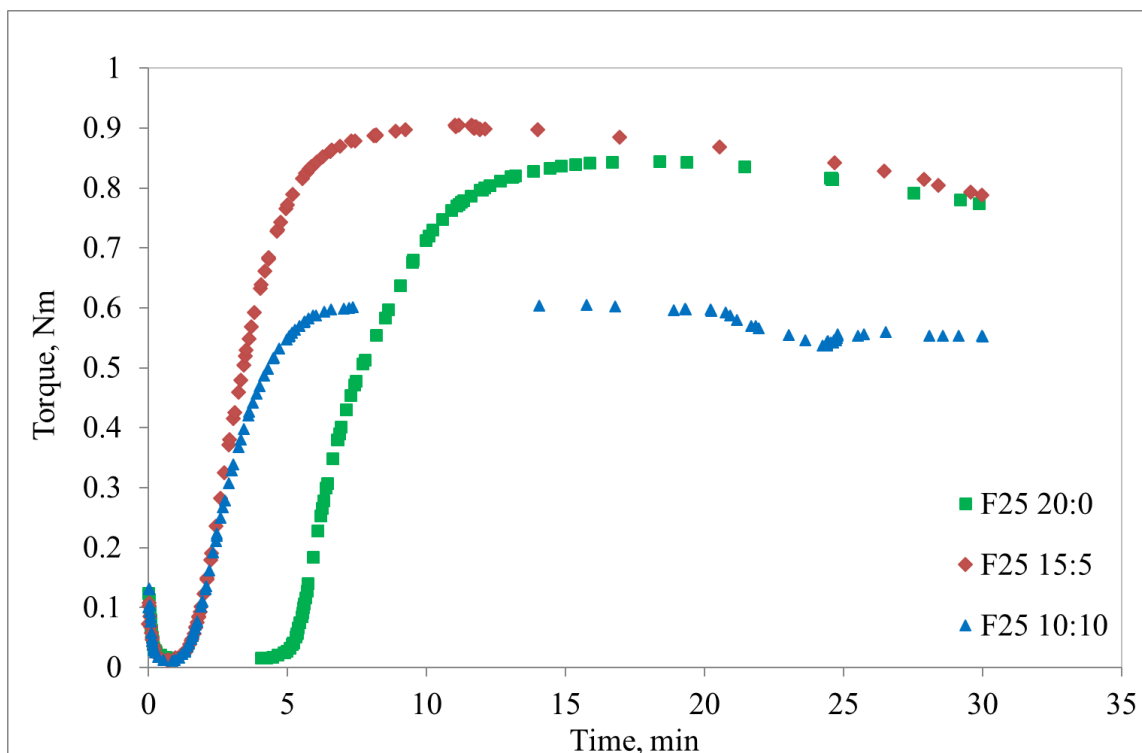
Figure 4.21: The rheometer curve for F25 formulation with different ratios of blowing agents at 150°C.
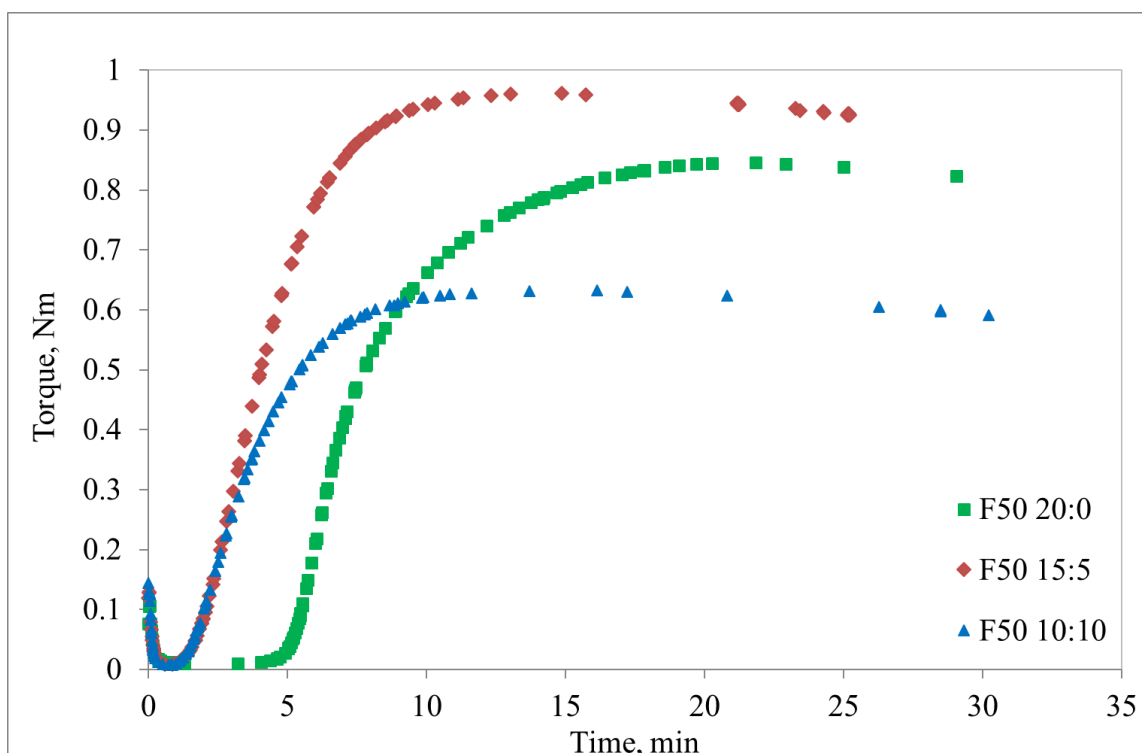
Figure 4.22: The rheometer curve for F50 formulation with different ratios of blowing agents at 150°C.

Table 4.18
The cure characteristics for F0, F25 and F50 formulations with different ratios of blowing agents at 150°C.

Cure characteristics	F0 20:0	F0 15:5	F0 10:10	F25 20:0	F25 15:5	F25 10:10	F50 20:0	F50 15:5	F50 10:10
Scorch time, t_{s2} (min)	6	3	3	6	3	3	6	3	3
Curing time, t_{95} (min)	11	9	9	13	7	6	16	9	9
Minimum torque, ML (Nm)	0.01	0.01	0.01	0.02	0.01	0.01	0.01	0.01	0.01
Maximum torque, MH (Nm)	0.63	0.73	0.42	0.85	0.91	0.61	0.85	0.96	0.63

The minimum torque for all the formulations was the same and in the range of 0.01 to 0.02 Nm. However, the maximum torque for F0, F25 and F50 formulations reached its highest values with the addition of 5 phr ammonium bicarbonate before it reduced to its lowest values as ammonium bicarbonate was continuously added. It shows that the mixture with 15:5 formulation can support the crosslinking process between the rubber chains, resulting in a considerable improvement in the torque values. However, the increasing amount of ammonium bicarbonate to 10 phr had decreased the torque values due to the possibility of the ammonia bicarbonate being partially decomposed during the mixing process resulting in a low viscosity for the mixture with 10:10 formulation.

No morphology study was performed on foams with the 10:10 formulation because the production of F0 10:10 and F25 10:10 foams were not successful (see their structure in Figure 4.23). The decomposition of ammonia bicarbonate starts at 60°C [53]. However, it is possible for ammonia bicarbonate to partially decompose in the mixing process at 40°C before the curing process starts. This observation can be seen clearly for F0 10:10 foam. The natural rubber with no epoxidation level is not the same as ENR. This rubber has relatively high gas permeability [12], so that there was a possibility for ammonia gas to escape from this natural rubber during the mixing process. In contrast, the application of a low foaming pressure was successful in the production of F25 20:0 and F50 20:0 foams. These foams were fully blown during the curing process and comparable in their properties to F0 20:0 foam.

Formulation	20:0	15:5	10:10
F0			
F25			
F50			

Figure 4.23: A comparison between the foam production for F0, F25 and F50 formulations with different ratios of blowing agents.

The morphology study was performed on F0 20:0, F0 15:5, F25 20:0, F25 15:5, F50 20:0 and F50 15:5 foams. A light micrograph of razor-cut surfaces of each foam is shown in Figure 4.24. The micrograph processing procedure and the physical properties studied were the same as discussed in the previous sections. The physical properties of each foam are summarised in Table 4.19. The expansion ratio value of F0 foam decreased with the addition of ammonium bicarbonate, resulting in some reduction in the average pore size and increased number of pores per unit volume. In contrast, the expansion ratio value of F25 and F50 foams increased with the addition of ammonium bicarbonate leading to a larger average pore size and smaller number of pores per unit volume produced in the foam structure. These observations suggest that more large pores were produced in ENR foams with the addition of ammonium bicarbonate. The same results were seen and discussed earlier for F50 AB in section 4.5.

In contrast, this process did not provide the same result for F0 15:5 foam upon the addition of ammonium bicarbonate. This also attributed to the same reason observed for F0 10:10 foam discussed earlier. There was a possibility some of ammonia bicarbonate to decompose during the mixing process at 40°C and ammonia gas produced escaped from this compounded rubber due to its relatively high gas permeability.
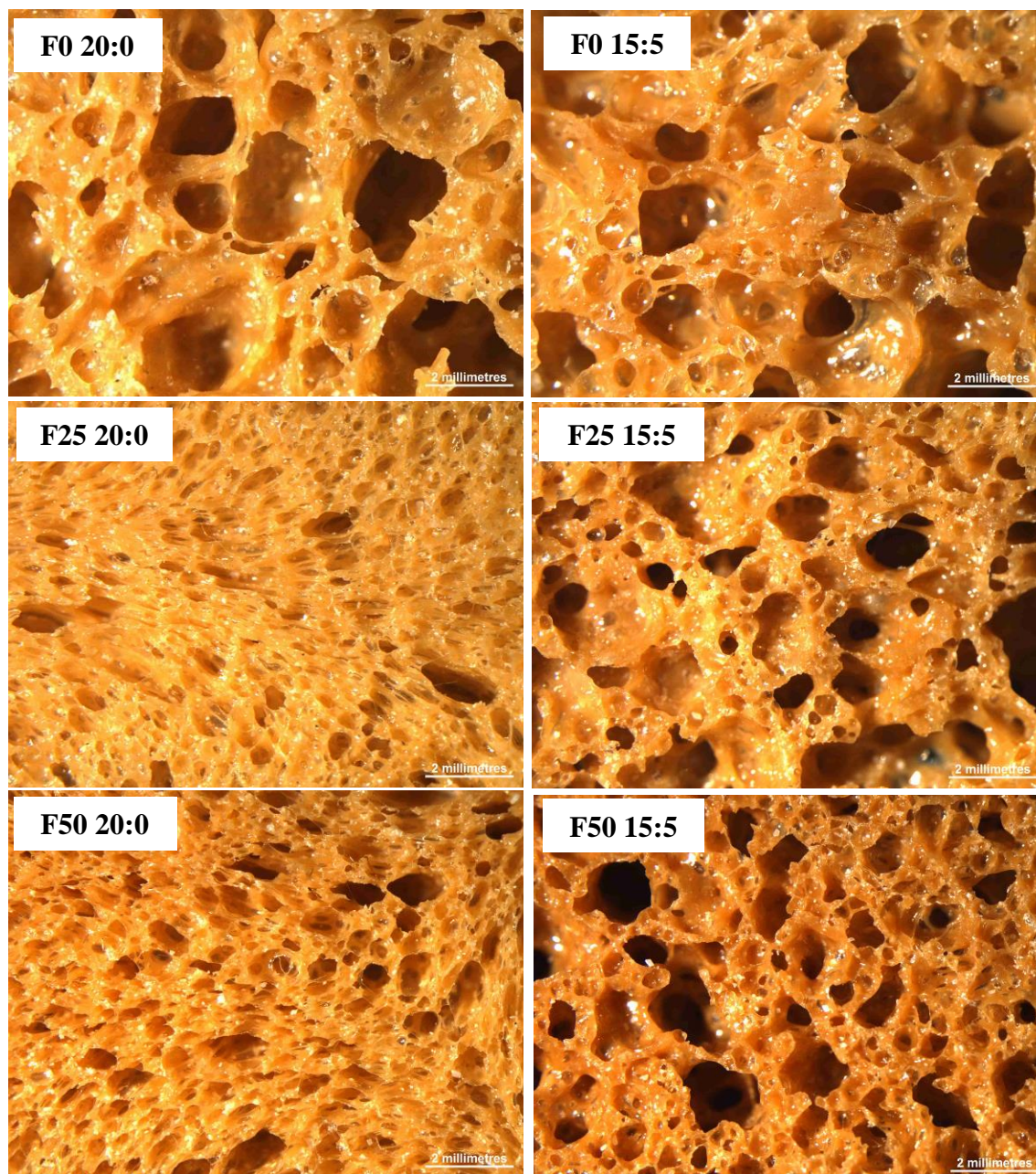
Figure 4.24: Light micrographs of F0 20:0, F0 15:5, F25 20:0, F25 15:5, F50 20:0 and F50 15:5 foams.

Table 4.19
The physical properties of F0 20:0, F0 15:5, F25 20:0, F25 15:5, F50 20:0 and F50 15:5 foams.

Physical properties	F0 20:0	F0 15:5	F25 20:0	F25 15:5	F50 20:0	F50 15:5
Density of solid rubber, ρ_y (kg/m^3)	967	967	1010	1010	1049	1049
Apparent density of rubber foam, ρ_x (kg/m^3)	260	270	309	294	331	304
Expansion ratio	3.72	3.58	3.27	3.44	3.17	3.45
Average pore size (mm)	0.49	0.34	0.30	0.42	0.34	0.42
Number of pores per unit volume (cm^{-3})	44,701	125,010	159,407	63,152	106,800	64,955

4.7 Summary

This chapter focused on a new manufacturing process of ENR foams and natural rubber foams produced from dry rubber. Sodium bicarbonate was initially implemented as a blowing agent in the production of rubber foam as it is commonly used in the production of open pore foams. A higher amount of sodium bicarbonate generates more carbon dioxide gas and allows higher expansion efficiency. Therefore, rubber foam with lower density can be produced. However, carbon dioxide gas expansion was restricted by the high viscosity of raw rubber and this restriction can be solved by reducing the viscosity of raw rubber through a mastication process. A natural rubber foam with the right pore structure can be produced using the mastication process of raw rubber. However, this technique does not work in the production of ENR foams. This observation suggests that carbon dioxide gas was not able to penetrate through ENR membranes. Therefore, three alternative ingredients were added separately to the ENR formulation: ammonium bicarbonate (an inorganic blowing agent), calcium stearate (a lubricant) and process oil (a plasticiser). All these ingredients were added to ensure the gas in the ENR formulation can be expanded without any restriction by ENR

membranes. The ammonia gas produced from the thermal decomposition of ammonium bicarbonate was able to expand in ENR membranes and resulting in pores formation in the foam structure. This is due to the production of ammonia gas which contributed to the high rise in pressure during the decomposition process. In contrast, the calcium stearate and process oil were not fully able to assist carbon dioxide gas to expand completely and to penetrate through ENR membranes. At this point, the addition of ammonium bicarbonate to the ENR foams was considered. The low stability of ammonium bicarbonate can be improved by mixing it with the more stable blowing agent such as sodium bicarbonate. Therefore, the effect of different ratios of ammonium bicarbonate and sodium bicarbonate in the rubber foam with different epoxidation levels was investigated. The expansion ratio value of natural rubber foam decreased with the addition of ammonium bicarbonate, resulting in some reduction in the average pore size. In contrast, the expansion ratio value of ENR foams increased with the addition of ammonium bicarbonate leading to a larger average pore size in the foam structure. These observations suggest that more large pores were produced in ENR foams with the addition of ammonium bicarbonate. This process did not provide the same result for natural rubber foam upon the addition of ammonium bicarbonate. There was a possibility some of ammonia bicarbonate to decompose during the mixing process and ammonia gas produced escaped from this compounded rubber due to its relatively high gas permeability. The manufacturing process of natural rubber foams and ENR foams was optimised thoroughly. Therefore, it is now essential to characterise these dry rubber foams in terms of their non-acoustical and acoustical properties, so that their behaviour in vibration and noise control applications can be fully understood.

Chapter 5

Characterisation of Epoxidized Natural Rubber Foam

5.1 Introduction

This chapter focuses on characterisation of the physical, dynamical, microstructure and acoustical properties of dry rubber foams produced in this study. The foams are denoted as F0, F25 and F50, where the numbers stand for the epoxidation level of the rubber foam: 0, 25 and 50 mol%. Each rubber foam was formulised with two different blowing agent contents namely as 20:0 and 15:5, where the numbers stand for the ratio of sodium bicarbonate (SB) to ammonium bicarbonate (AB) in parts per hundred rubber (phr) used in the formulation. The characterisation of the latex foams with different epoxidation levels produced by Malaysian Rubber Board [23] are also presented. The latex foams are denoted as LF0, LF25 and LF50 where the numbers represent the epoxidation level. The properties obtained are discussed and compared with that of commercially available foams. Two commercially available foams are reconstituted rubber foam (RRF) which is produced by Armacell [87], and polyurethane foam (PUF) which is produced by CMS Danskin Acoustics [88]. This chapter also discusses the modelling tools that are potentially can be applied to describe the acoustical behavior of epoxidized natural rubber (ENR) foams and natural rubber foams. The availability of modelling tools is crucial to understand the acoustic wave propagation in the porous medium so that optimization in designing a vibro-acoustic system for engineering applications is achievable. The models presented in this chapter depend on the information of physical, dynamic and microstructure parameters which can relate to the acoustic absorption of the developed foams. These parameters can be determined with standard experimental procedures which are outlined in this chapter.

5.2 Experimental procedures

5.2.1 Physical characterisation

Density (ρ) measurements of the foam were performed by dividing the weight of each foam with its corresponding volume as outlined in the ISO 6916-1:1995 [83].

5.2.1.1 Porosity characterisation

The porosity of a porous material is equivalent to the total volume of the fluid in the pores divided by the volume of the test specimen. It is one of the non-acoustical parameters that is important in the acoustic modelling of the porous material. There are various methods for measuring porosity such as buoyancy, mercury porosimetry or methods based on density measurements. A commonly used technique to determine the porosity is immersing the test specimen in the water. The volume of the test specimen is measured based on rising of the water level upon immersion of the test specimen in a measuring cylinder. However, this technique is less appropriate as the morphological properties of the porous materials can easily damage by the water [89].

A method to determine the porosity without immersing the test specimen in the water was proposed by Beranek [90]. The porous material of volume V_s is contained in an airtight chamber of volume V_c that is connected to a U-tube manometer as shown in Figure 5.1. The ambient temperature is held constant. The valve is opened and the initial height of the water (h) in the two sides of the manometer is observed. Then, the valve is closed, and the height of the water have changed for each side of the manometer from h to h_1 and h_2. The difference between h_1 and h_2 is the change of pressure, ΔP. The heights difference from h to h_1 and h to h_2 can be read accurately by a cathetometer and a graduated scale, respectively. The porosity, ϕ is given by:

$$\phi = \frac{P_0 \Delta V_a}{V_s \Delta P} + 1 - \frac{V_c}{V_s} \tag{5.1}$$

where P_0 is atmospheric pressure and ΔV_a is the reduction of air volume in the chamber and equals $(h_1 - h)S$, where S is the cross-sectional area of the tube.
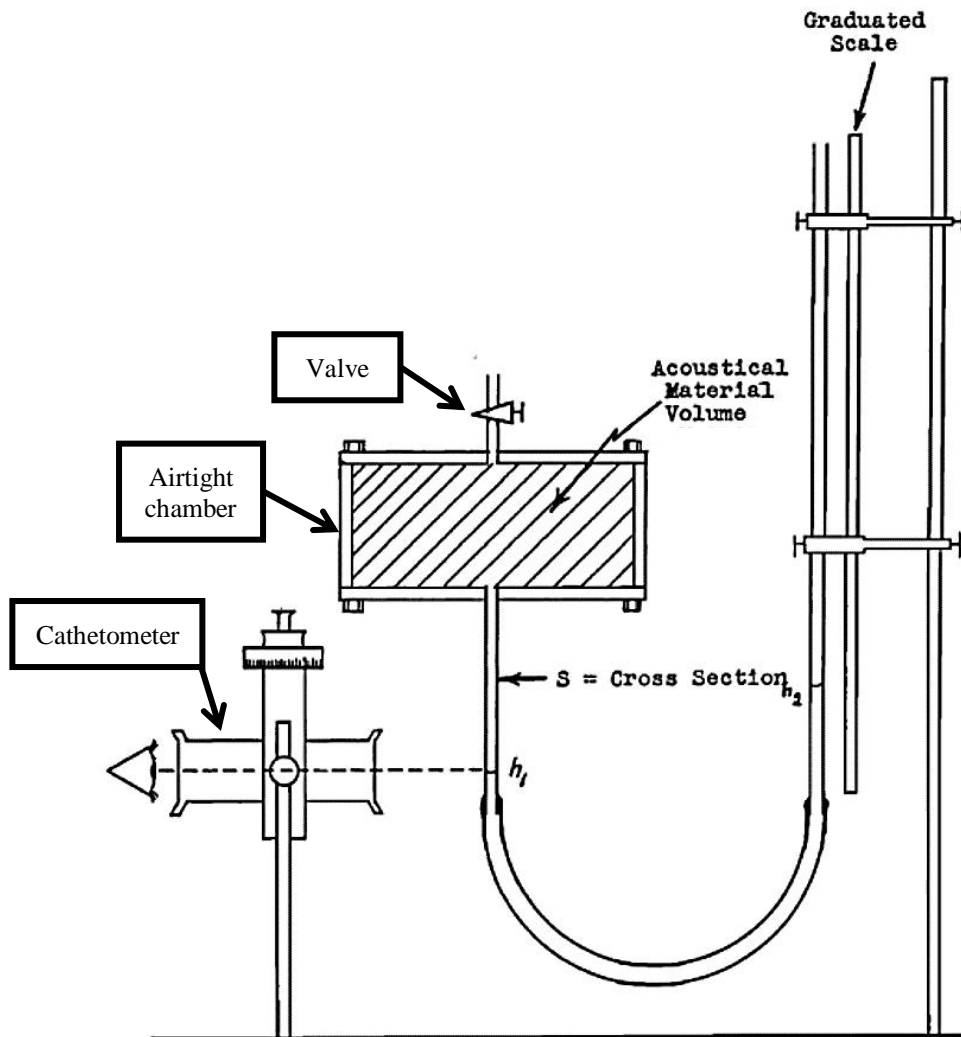
Figure 5.1: Experimental setup for measuring the porosity based on Beranek's method [90].

Champoux *et al.* [91] proposed a similar porosity measurement setup. Their method can provide results with high precision in a wider range of porosities. The authors proposed a system that includes a micrometer drive for measuring volume variations in the chamber, a differential pressure transducer to replace the U-tube manometer and an air reservoir to separate the system from atmospheric pressure fluctuation (Figure 5.2).
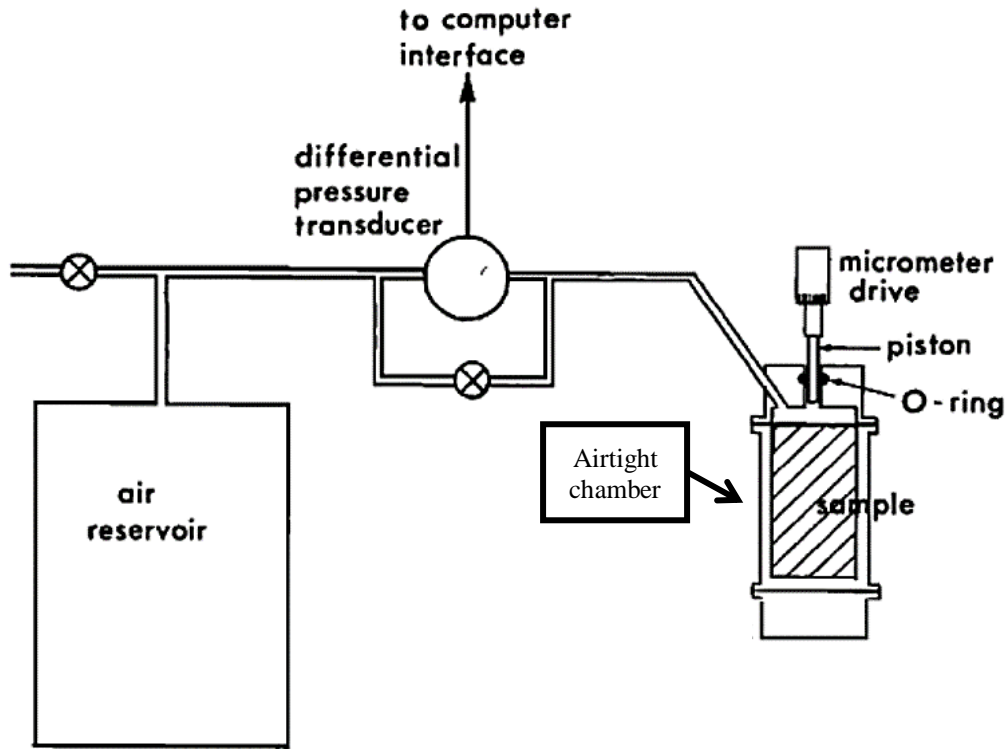
Figure 5.2: Experimental setup for measuring the porosity based on Champoux *et al.*'s method [91].

The porosity measurement in this method is given by:

$$\phi = \frac{V_a}{V_s},$$
(5.2)

where V_s is a total volume of porous material situated in an airtight chamber and V_a is an air-filled volume in the porous material.

Another recent study by Leclaire *et al.* [89] proposed an alternative method based on volume comparison between two chambers. This experimental setup for measuring the porosity is shown in Figure 5.3. This method consists of a reference chamber and a measurement chamber that are connected to the glass U-tube manometer containing water. The air volume in both chambers are controlled by a piston and the volume of the water in the manometer is controlled by a water-drawing piston. The uniqueness of this method is based on the less influence of the temperature and atmospheric pressure that can affect the porosity measurement. The air volumes of the reference chamber and the measurement chamber are

compared and equalized so that any temperature variations or atmospheric pressure fluctuations act concurrently on both chambers.
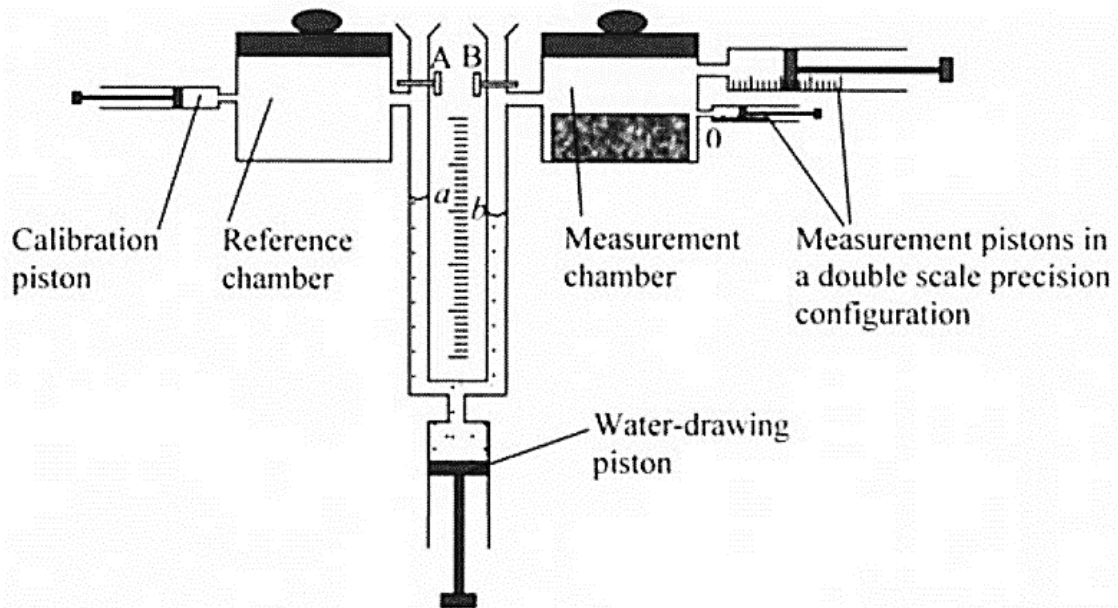
Figure 5.3: Experimental setup for measuring the porosity based on Leclaire *et al.*'s method [89].

The porosity (ϕ) in this study was measured using the method proposed by Leclaire [89]. The in-house experimental setup (Figure 5.4) consists of two 60 mL air-tight chambers known as a reference chamber and a measurement chamber. Both chambers are connected to the glass U-tube manometer containing water with an inner diameter of 5 mm. The air volume in both chambers are controlled by pistons with 27.5 mL capacity for the measurement chamber and 25 mL capacity for the reference chamber. The volume of the water in the manometer is controlled by a 50 mL water-drawing piston.
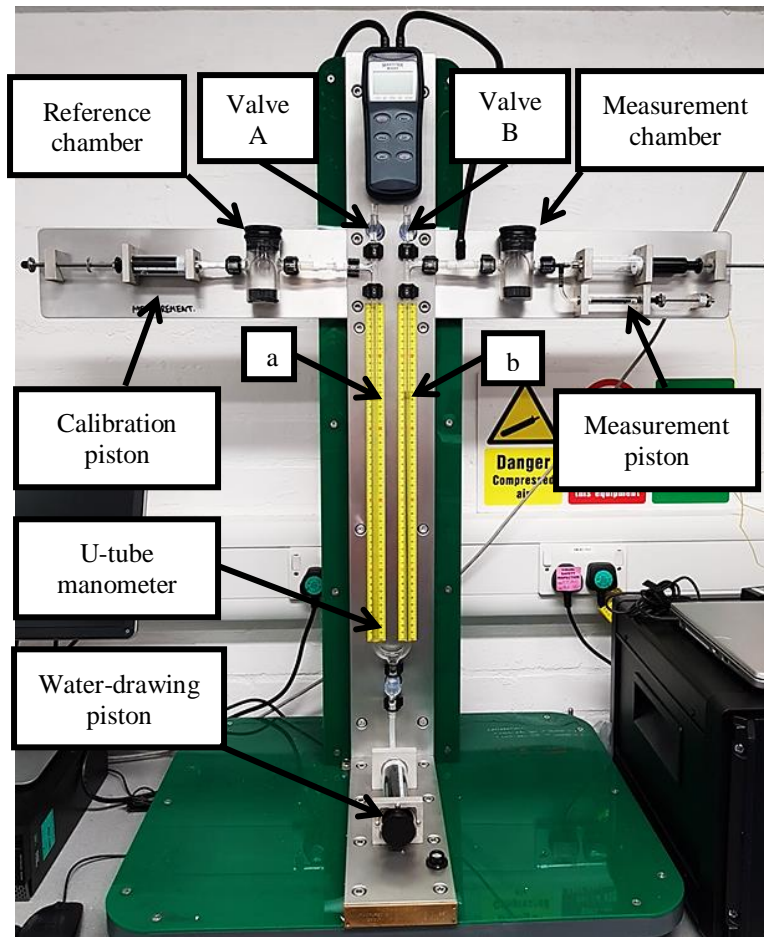
Figure 5.4: An in-house manufactured porosimeter.

Firstly, a calibration is carried out to equalize the volumes of the reference chamber and the measurement chamber with no test specimen in the chambers and the calibration piston and measurement piston are set at zero value. Valve A and B are opened to set the chambers at atmospheric pressure and a level of water is at maximum in both branches. Then, valve A and B are closed, and water is drawn by water-drawing piston. If the volumes of the two chambers are the same, the pressure difference (a - b) is close to zero. If the volumes of the two chambers are not the same, then these volumes can be equalised by increasing the volume in the calibration piston until the pressure difference (a - b) approaches zero. After the calibration is completed, a foam (20 mm in diameter and 25 mm in thickness) is placed in the measurement chamber with valve A and B are opened. The reduction of air volume due to the introduction of the foam is compensated by increasing the volume of the measurement piston from the zero position. The measurement piston should be moved only when valve B is opened. Then, water is drawn with valve A and B are closed. This procedure is carried out several times until the pressure difference (a – b) approaches zero. The final volume of the measurement piston indicates the difference in air volume between the two

chambers. As the experiment was assumed to be as an isothermal process, the Boyle's law [91] was used to calculate the difference in air volume between the two chambers. This can then be used to calculate the porosity of the foam using Equation 5.2.

5.2.1.2 Airflow resistivity characterisation

Airflow resistivity of a porous material can be determined by measuring the differential pressure across the porous material and volume airflow. This method is described in the ISO 9053 [92]. Principally, there are two methods to determine the airflow resistivity: the direct airflow method; and the alternating airflow method. The direct airflow method has a controlled unidirectional airflow penetrating through a porous material. The measurement of the differential pressure between the two free faces of the porous material is determined (Figure 5.5), while the alternating airflow method has a slowly alternating airflow penetrating through a porous material. The measurement of the alternating component of the pressure in a test volume confined by the porous material is obtained (Figure 5.6).
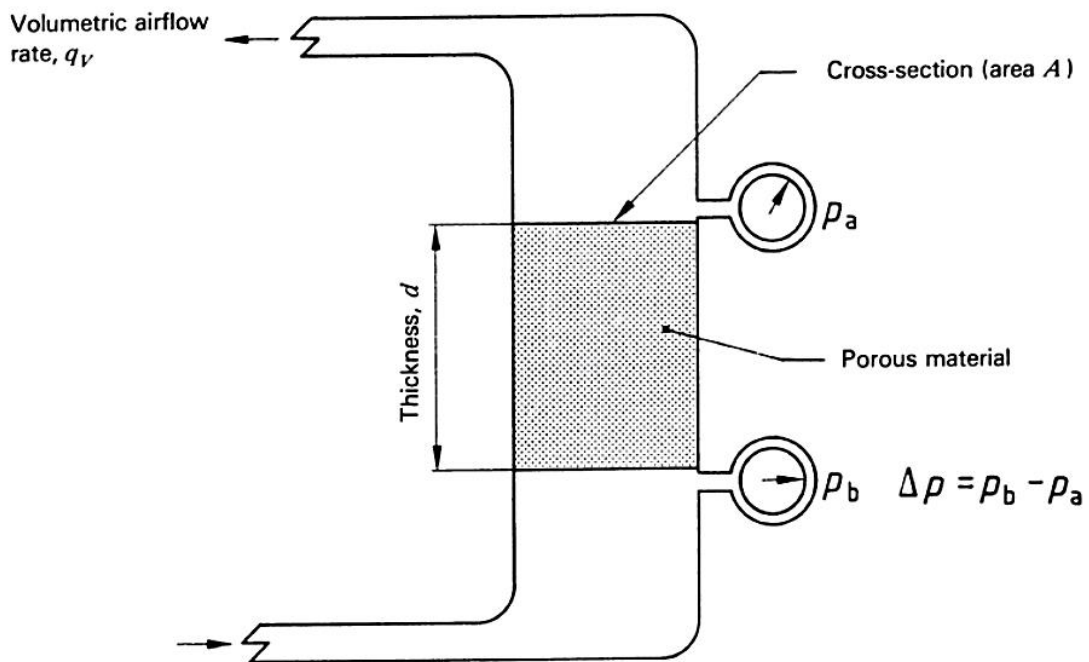
Figure 5.5: Basic principle of direct airflow method [92].
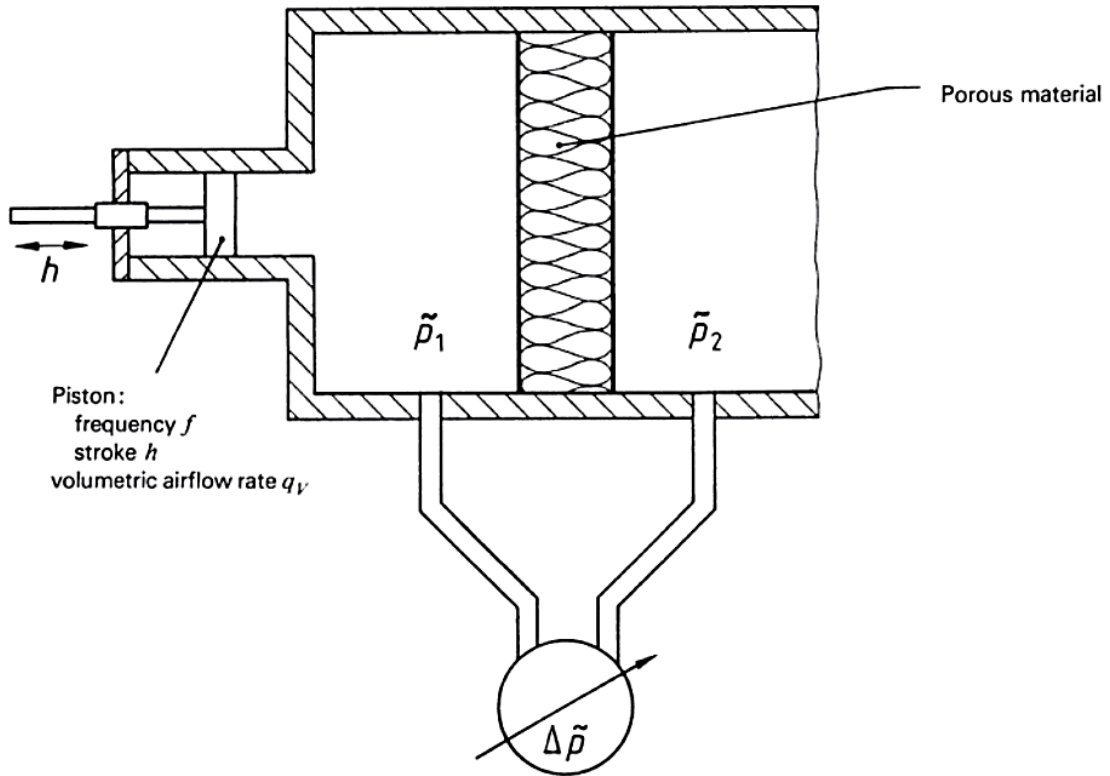
Figure 5.6: Basic principle of alternating airflow method [92].

The airflow resistivity, σ represents the ability of sound waves to penetrate the porous material and it is related to sound attenuation. The airflow resistivity can be expressed as:

$$\sigma = \frac{A\Delta P}{q_v t} ,$$

(5.3)

where A is the area of the porous material, ΔP is the differential pressure across the porous material, q_v is the volumetric airflow rate and t is the thickness of the porous material.

The measurement was performed using an AFD 300 Acoustiflow® (Figure 5.7) supplied by Akustikforschung Dresden [93]. The equipment measures the pressure drop across the foam as a function of the volume airflow. This technique determines the airflow resistance of the foam based on the direct airflow method. A foam sample with the diameter of 100 mm and thickness of 25 mm was placed in a 100 mm diameter sample holder and tested at room temperature.

128
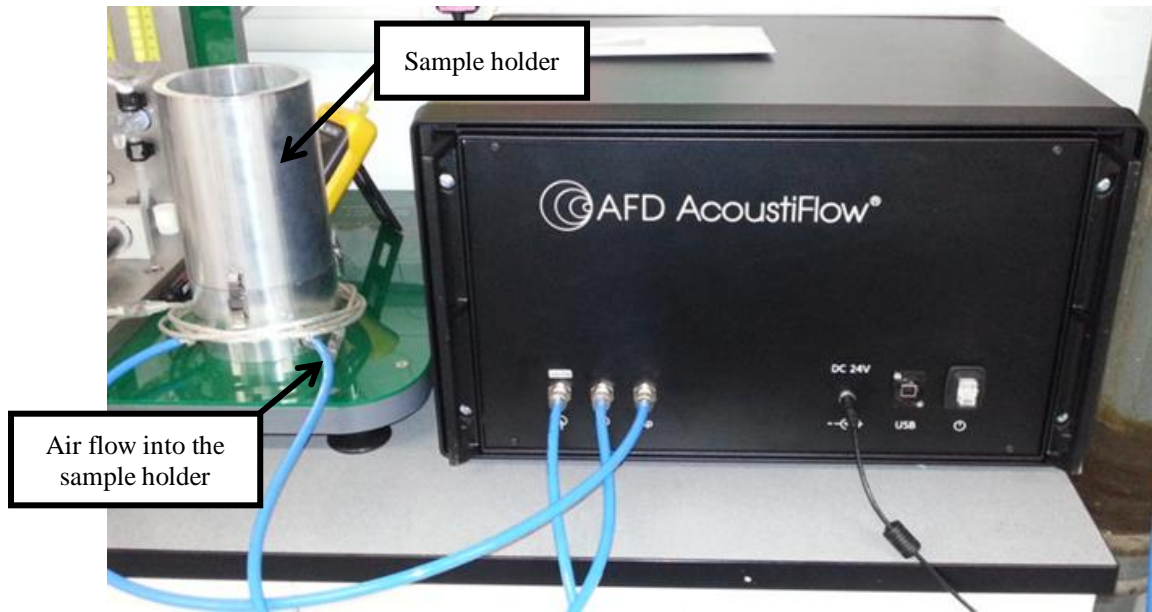
Figure 5.7: An AFD 300 Acoustiflow®.

5.2.2 Dynamic characterisation

The acoustic performance of a porous material can be influenced by its dynamic properties. Therefore, it is important to determine parameters such as dynamic modulus and loss factor of the porous material. Various methods are available to measure the dynamic properties such as uniaxial compression, torsion and shear (see Jaouen *et al.* [65]). The authors of [65] stated that porous materials typically display a noticeable phase transition of their dynamic behaviour in the audible frequency range of 20 Hz to 8000 Hz and over the temperature range of -50°C to 50°C.

The recent study reported by Bonfiglio *et al.* [66] reviewed method to measure the dynamic properties of porous materials. The first method is a quasi-static uniaxial compression method. The porous material is placed in between two rigid plates as shown in Figure 5.8(a). The lower plate is excited by an electrodynamics shaker and the upper plate is fixed. Generally, there are three quantities measured as a function of frequency: (a) the vertical displacement that is measured by an accelerometer, (b) the lateral displacement that is measured by a laser vibrometer and (c) the force applied to the tested material that is measured by a force transducer. These quantities can be used to determine the dynamic modulus and loss factor of porous materials.

a

b

c

d

e

Number description:

1. Porous material
2. Accelerometer
3. Force transducer
4. Torque transducer
5. Angular displacement transducer
6. Laser vibrometer
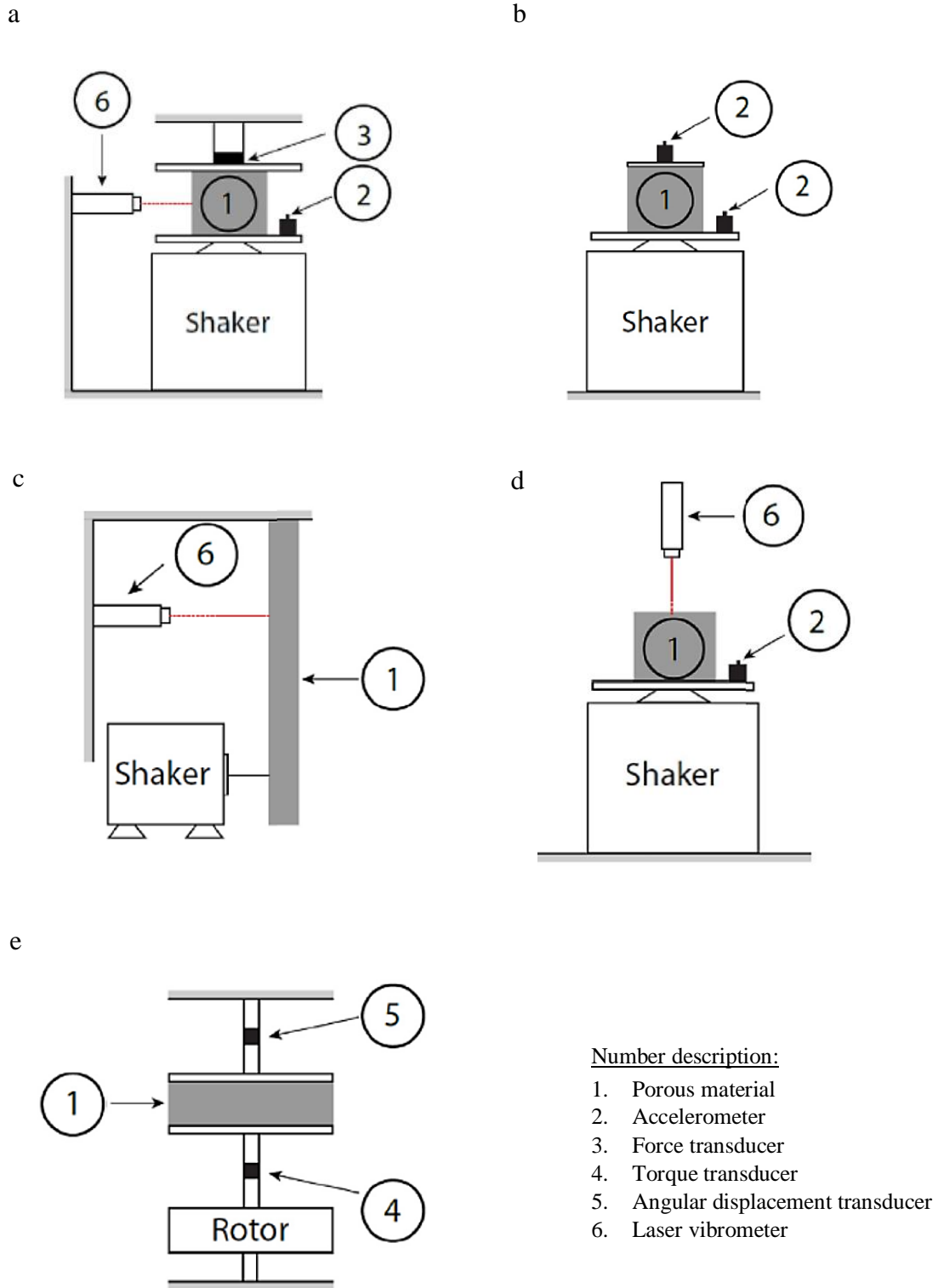
Figure 5.8: Methods to measure the dynamic properties of porous materials: (a) quasi-static uniaxial compression method; (b) resonant method; (c) lamb wave propagation method; (d) transfer function/transfer matrix method and (e) dynamic torsional method [66].

The second method is a resonant method. The top of a rectangular porous material is loaded with a mass and the bottom of the material is attached to a rigid rectangular plate that is excited by a shaker as shown in Figure 5.8(b). The amplitude measurement of the transmissibility function between the top and the bottom accelerations is determined as a function of frequency. Then, the dynamic modulus and loss factor can be related through the resonance frequency obtained from this frequency dependent transmissibility function.

The third method is a lamb wave propagation method. In this method, a slab of porous material is fixed on one side and another side is left free to vibrate (Figure 5.8(c)). An electromagnetic shaker is used to excite the porous material and the displacement is measured at different distances from the excitation source by a laser vibrometer. The lamb wave propagation is accounted for with a model that allow to determine the dynamic properties of the porous material.

The fourth method is a transfer function/transfer matrix method. The porous material is placed on a rigid plate that is excited by an electromagnetic shaker (Figure 5.8(d)). The rigid plate acceleration is measured using an accelerometer and the velocity at the top surface of the porous material is measured using a laser vibrometer. The dynamic properties can be determined through the plane wave propagation using the measured velocity transfer function across the porous material.

The fifth method is a dynamic mechanical analysis. This method is commonly used to study the dynamic behavior of viscoelastic materials at different temperatures and frequencies. The setup of this method is similar to the quasi-static uniaxial compression method. This method is also can be used to predict dynamic properties of porous materials over a wider frequency range by generating the master curve with the implementation of the time-temperature superposition principle. One of the laboratories in this study had performed this method differently with the porous material was excited in torsion as shown in Figure 5.8(e).

The dynamic properties of the foam in this study were measured using a Viscoanalyseur VA2000 dynamic mechanical analyser (DMA) supplied by Metravib [94] as shown in Figure 5.9.
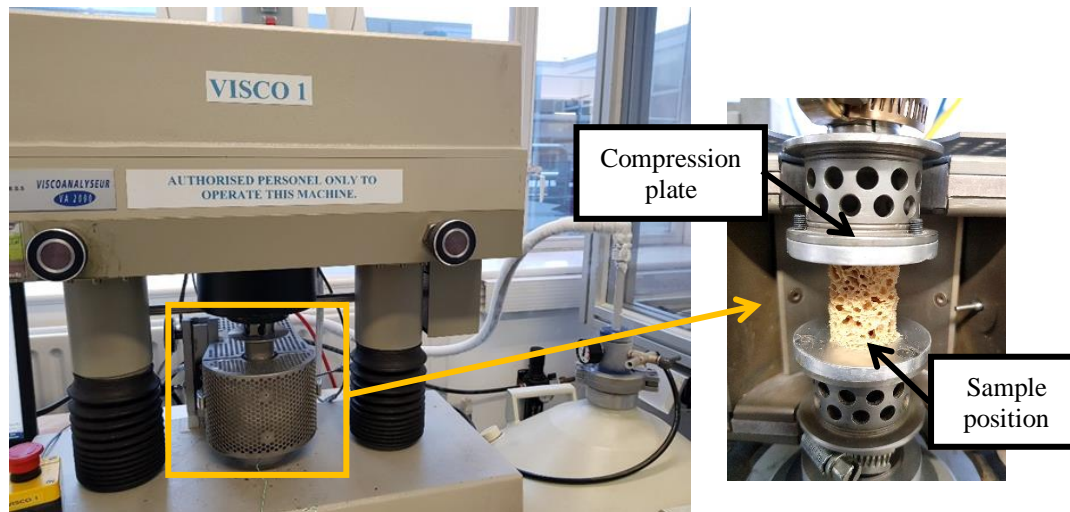
Figure 5.9: A Viscoanalyseur VA2000 dynamic mechanical analyser.

The foams were prepared in the form of cylinders with the diameter of 20 mm and thickness of 25 mm. Tests were performed in a compression mode of deformation over a frequency range of 1 to 100 Hz and at ambient temperature, with a static strain of 1% and a dynamic strain of 0.1%. The viscoelastic properties including storage modulus, loss modulus, and tan δ were measured as a function of frequency.

It is also possible to determine the viscoelastic properties of the foams over an extended range of frequencies. The time temperature superposition as discussed in section 3.3.3 was applied to generate the master curve for the dynamic modulus of foam. In this case, the rubber foams which formulised with sodium bicarbonate was selected to observe their dynamic behaviour. For this testing purposes, other foams were prepared in the form of cylinders with the same diameter but with reduced thickness of 8 mm. Tests were performed in a compression mode of deformation over a temperature range of -30°C to 30°C with the same frequency range, static strain and dynamic strain conditions.

5.2.3 Microstructure characterisation

The micrographs of the foam sample with the diameter of 10 mm and thickness of 25 mm were obtained using a Micro Computer Tomography (Micro-CT) scanner, model Bruker SkyScan 1172 (Figure 5.10). The scanner obtains multiple x-ray transmission images of the foam sample from multiple angular views as the sample rotates on a high-precision stage. From these images, 938 cross-section layers of foam sample were reconstructed to create a complete set of micrographs. A full representative measurement of pore size in diameter is very difficult to obtain as the pore shape is irregular. Therefore, the pore diameter in each micrograph was analysed using Computer Tomography Analysis (CTAn) software. This parameter was used to define the mean pore size of the foam sample. The results were determined from the measurements of 1000 different connected pores displayed in the reconstructed micrographs.

Figure 5.10: A Micro Computer Tomography (Micro-CT) scanner.

5.2.4 Acoustic characterisation

The acoustic characterisation of sound absorbing materials is carried out according to the ISO 10534-2:2001 [95]. The standard involves the use of an impedance tube, microphones and a frequency analysis system. The airtight impedance tube as shown in Figure 5.11 consists two ends, with one end has a sound source that provides the sound signal and the test specimen is placed in the tube at the other end to receive the sound signal. Two microphones mounted within the top wall of the tube and these microphones are used to measure the sound pressures [95]. The acoustic properties of the test specimen such as the normalised absorption coefficient, normalised reflection coefficient and normalised surface impedance can be measured with this equipment [96].
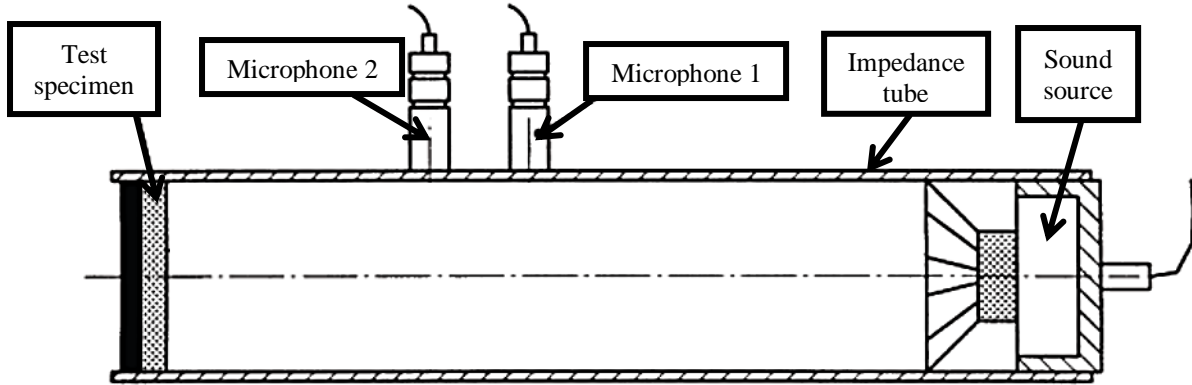
Figure 5.11: The schematic of the impedance tube [95].

The sound absorption coefficient of a material is frequency dependent and it represents the ability of the material to absorb sound. A material with a coefficient of one is a perfectly absorbing material, while a material with coefficient of zero is purely reflective. Therefore, a material with coefficient of 0.7 can absorbs 70% of the sound and reflects remaining 30% of the sound.

The two microphones measure the sound pressure of the incident wave, P_I and the reflected wave, P_R [95]. These parameters can be expressed as:

$$P_I = \hat{P}_I e^{ik_0 x} \tag{5.4}$$

and

$$P_R = \hat{P}_R e^{-ik_0 x}, \tag{5.5}$$

where $\hat{P}_I$ and $\hat{P}_R$ are the magnitudes of P_I and P_R at the reference plane ($x = 0$), while k_0 is a wavenumber and can be expressed as:

$$k_0 = \omega/c_0 = 2\pi f/c_0, \tag{5.6}$$

where ω is the angular frequency, f is the frequency and c_0 is the sound speed in air. The sound absorption coefficient, α and the surface impedance, z_s of the test specimen can be determined from the following equations:

$$\alpha = 1 - |r|^2 \qquad (5.7)$$

and

$$\frac{z_s}{\rho_0 c_0} = \frac{1+r}{1-r}, \qquad (5.8)$$

where $r = P_R/P_I$ and ρ_0 is the air equilibrium density.

The sound absorption coefficient (α) was measured using a two-microphone impedance tube supplied by Materiacustica [97] as depicted in Figure 5.12. A cylindrical foam sample with the diameter of 45 mm and thickness of 25 mm was prepared for each foam and its sound absorption coefficient was calculated over the frequency range of 50 to 4000 Hz.
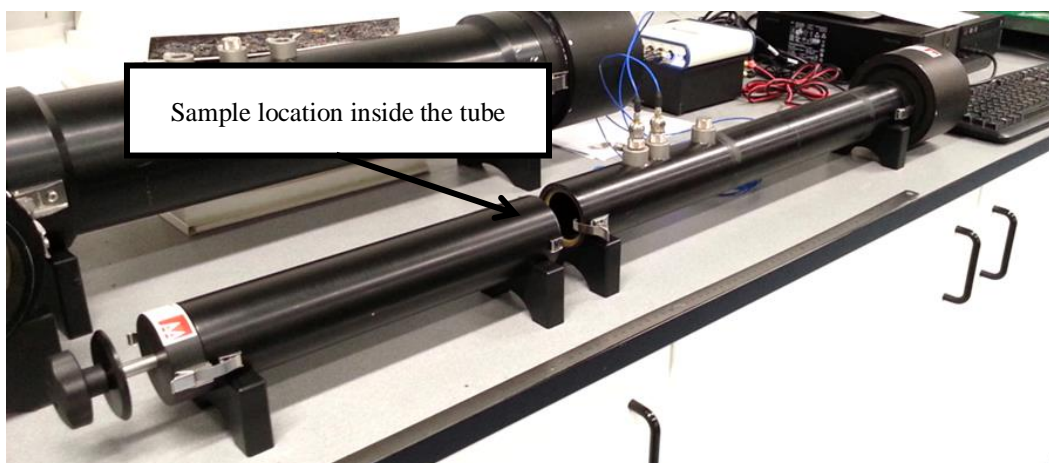
Figure 5.12: A two-microphone impedance tube.

5.3 Physical properties

The physical properties of the foam samples are summarised in Table 5.1. The density of foam increases with increasing epoxidation levels. The recorded density data from 0 to 50 mol% epoxidation level showed an increment of 21%, 11% and 33% for dry rubber foam with SB, dry rubber foam with SB & AB and latex foam, respectively. The porosity of foam decreases with increasing epoxidation levels. The porosity of dry rubber foam with SB at 0 mol% epoxidation level was 0.69 and it dropped to 0.41 when the epoxidation level increased to 50 mol%. In the case of dry rubber foam with SB & AB, the porosity values were between 0.68 and 0.46 and the porosity values of latex foam were between 0.82 and 0.77.

The airflow resistivity of dry rubber foam with SB at 0 mol% epoxidation level was 43,580 N.s/m^4. Then, the airflow resistivity values increased drastically with increasing epoxidation levels with the data measured were 261,135 N.s/m^4 for F25 20:0 foam and 173,571 N.s/m^4 for F50 20:0 foam, respectively. The airflow resistivity value of dry rubber foam with SB & AB was slightly decreased with increasing epoxidation levels from 0 mol% to 25 mol%. The data obtained was 31,869 N.s/m^4 for F0 15:5 foam and 29,808 N.s/m^4 for F25 15:5 foam, respectively. Then it rose to 75,348 N.s/m^4 for F50 15:5 foam. The same trend is also observed for latex foam with the airflow resistivity values were 26,709 N.s/m^4, 19,741 N.s/m^4 and 80,008 N.s/m^4 for LF0, LF25 and LF50 foams, respectively.

The non-acoustical properties of RRF were also investigated in previous research [67]. The density and porosity values obtained in ref. [67] were similar with the values obtained in this work. However, the airflow resistivity values obtained in this work were not comparable and lower than the airflow resistivity values shown in ref. [67]. This observation suggested that the airflow resistivity measurement in this study might be presented a limitation of the circumferential gap between the foam sample and the sample holder. The air gap might be small but the airflow resistivity values in Table 5.1 suggested that they are less resistant in comparison. Therefore, the airflow resistivity values in this study might be differ and can influence the accuracy of the prediction of the acoustical properties of foams.

Table 5.1
Physical properties of foams used in the experiments.

Description	Foam	Density, ρ (kg/m^3)	Mean Porosity, ϕ	Mean Airflow Resistivity, σ (N.s/m^4)
Dry rubber foam with SB[1]	F0 20:0	260	0.69	43,580
	F25 20:0	309	0.37	261,135
	F50 20:0	331	0.41	173,571
Dry rubber foam with SB[1] and AB[2]	F0 15:5	270	0.68	31,869
	F25 15:5	294	0.67	29,808
	F50 15:5	304	0.46	75,348
Latex foam	LF0	172	0.82	26,709
	LF25	201	0.82	19,741
	LF50	256	0.77	80,008
Commercially available foam	RRF	316	0.81	63,816
	PUF	186	0.75	23,850

[1]Sodium Bicarbonate (SB)
[2]Ammonium Bicarbonate (AB)

The results suggest that the density, porosity and airflow resistivity of the natural rubber foams were influenced by the epoxidation levels. This dependence is reflected in the density data. The more epoxide groups presence in the natural rubber, the higher the value of density is obtained. These results were also observed in previous research [54]. The research presented in ref. [54] studied the properties of natural rubber foams based on different rubber grades namely as SMR-L, SMR-10 and ENR-25. The authors found natural rubber with epoxide group which is ENR-25 has the highest relative foam density value. They observed that thicker pore walls and more rubber matrix per unit area in ENR-25 foam contributed to a high value of density. The density is a key parameter that relates to the porosity and airflow resistivity. Therefore, natural rubber foam with a lower density is recommended to achieve a relatively high porosity and optimal low airflow resistivity values so that foams with a better noise control performance can be developed.

Generally, some of dry rubber foams developed such as F0 20:0, F0 15:5 and F25 15:5 as well as latex foam can show comparable performance with the results obtained by commercially available foams. These observations suggest that natural rubber foam with different epoxidation levels produced from dry rubber or latex can be used as an alternative option to the synthetic foams or polymeric foams in the commercial applications.

5.4 Dynamic properties

The storage modulus (E') of all the rubber foams at 1 to 100 Hz and at ambient temperature are plotted in Figures 5.13 to 5.15. The data on commercial foams, RRF and PUF were also included for comparison purposes. A logarithmic plot of E' as a function of frequency shows that the storage modulus of rubber foams with 0 and 25 mol% epoxidation level is generally less frequency dependent and the modulus increase with frequency only slightly. Rubber foams with 50 mol% epoxidation level are more frequency dependent. This is attributed to the glass transition temperature (T_g) of these foams which is close to the ambient temperature.
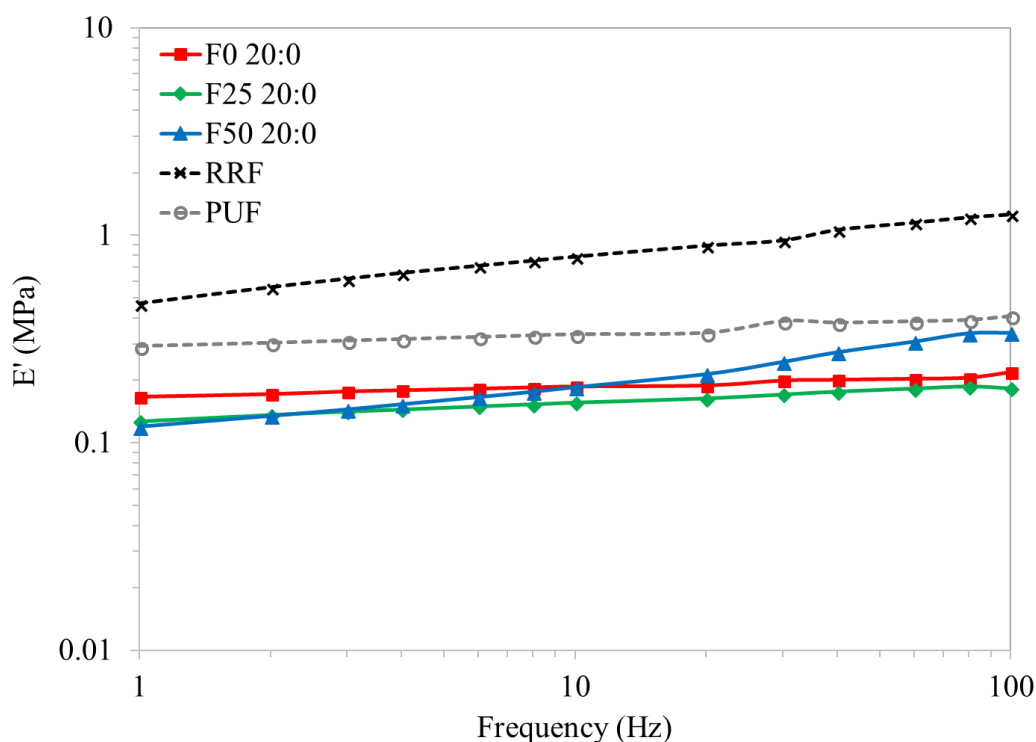
Figure 5.13: The dependence of the storage modulus for F0 20:0, F25 20:0, F50 20:0, RRF and PUF foams as a function of frequency at ambient temperature.

138
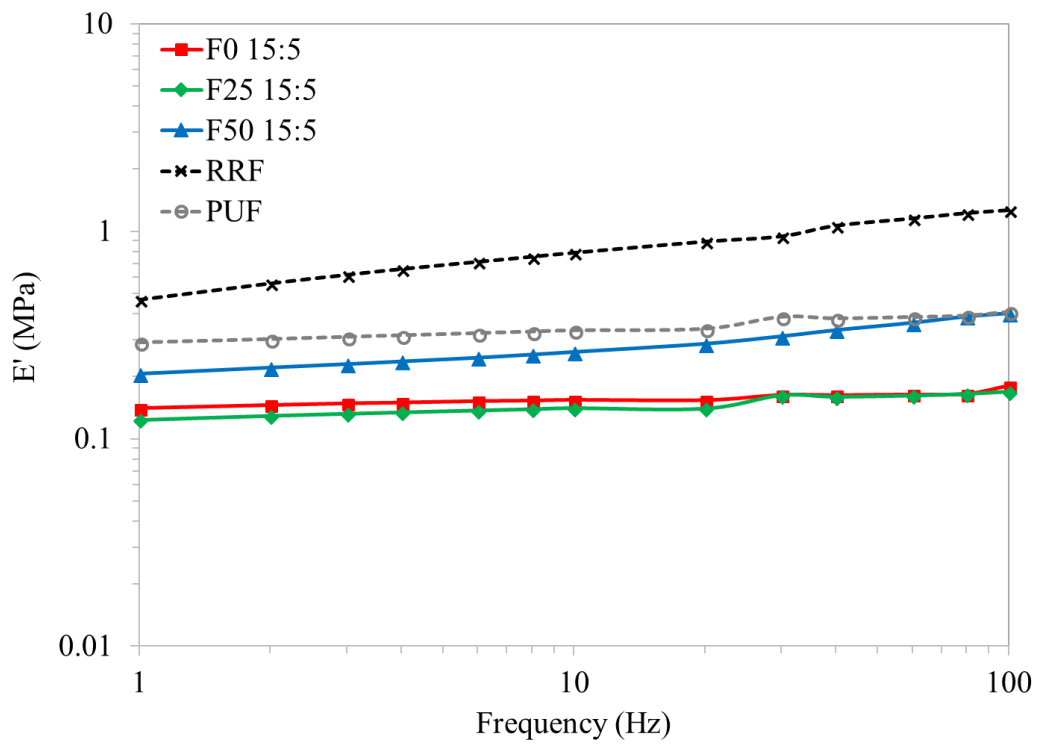
Figure 5.14: The dependence of the storage modulus for F0 15:5, F25 15:5, F50 15:5, RRF and PUF foams as a function of frequency at ambient temperature.
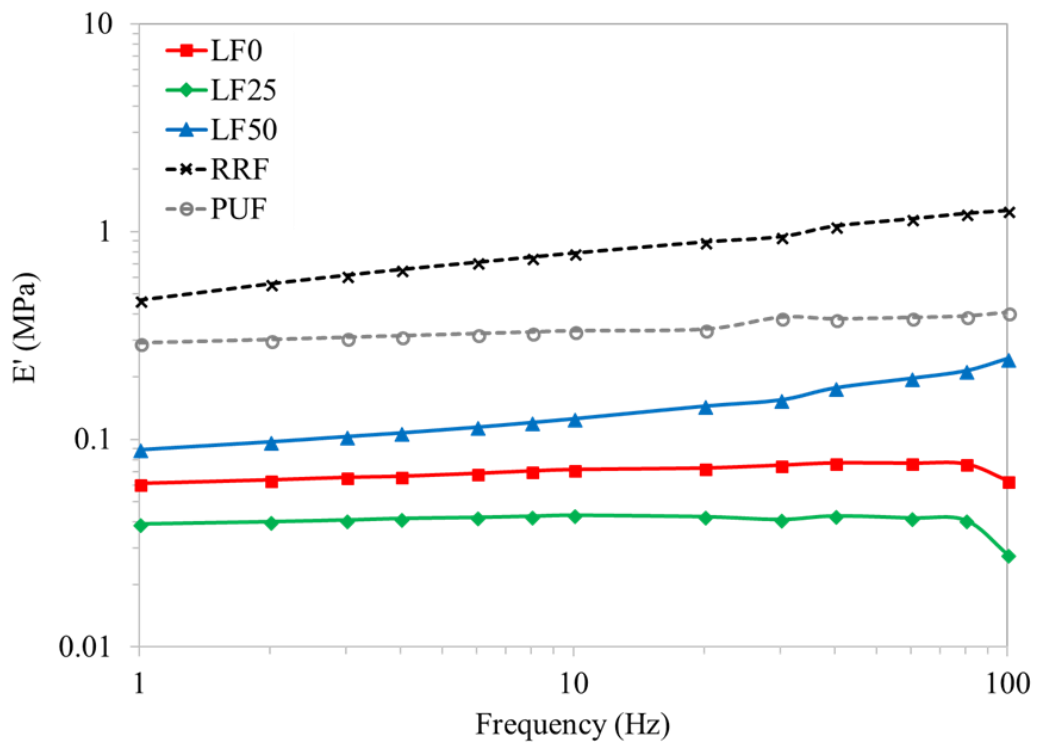
Figure 5.15: The dependence of the storage modulus for LF0, LF25, LF50, RRF and PUF foams as a function of frequency at ambient temperature.

Generally, all the rubber foams display lower storage modulus value than the commercial foams: RRF and PUF. The storage modulus value of latex foam is much lower with the average storage modulus of 0.07 MPa for LF0 foam, 0.04 MPa for LF25 foam and 0.15 MPa for LF50 foam. These observations suggest that the low storage modulus value of dry rubber foam and latex foam would be a value in designing the rubber foams in the vibro-acoustic isolation applications.

5.4.1 Time-temperature superposition of dry rubber foam

In this section, the dynamic properties for F0 20:0, F25 20:0 and F50 20:0 foams over a range of temperatures and frequencies are presented. These foams are selected based on a single blowing agent (sodium bicarbonate) used in the formulation and they are almost identical to the solid rubber formulation. A master curve for their dynamic properties is generated based on the time-temperature superposition principle as described in section 3.3.3.

Figure 5.16 shows the dependence of the storage modulus (E') as a function of temperature in the range of -30°C to 30°C and at 10 Hz excitation for F0 20:0, F25 20:0 and F50 20:0 foams. However, some data not able to be recorded as the machine was not sensitive enough to measure the dynamic behaviour of rubber foam at very low temperatures. As expected, all rubber foams show their highest E' at the lowest temperature tested and E' decreases with the increasing temperature. The storage modulus of F25 20:0 foam is slightly higher than F50 20:0 foam at 20°C and 30°C. This might be attributed to the changes in the structure of the rubber attained with the addition of blowing agent.

Figure 5.17 shows the loss factor (tan δ) curves under the same conditions. Tan δ decreases with the increasing temperature. Above 5°C, tan δ increases with the increasing epoxidation levels.
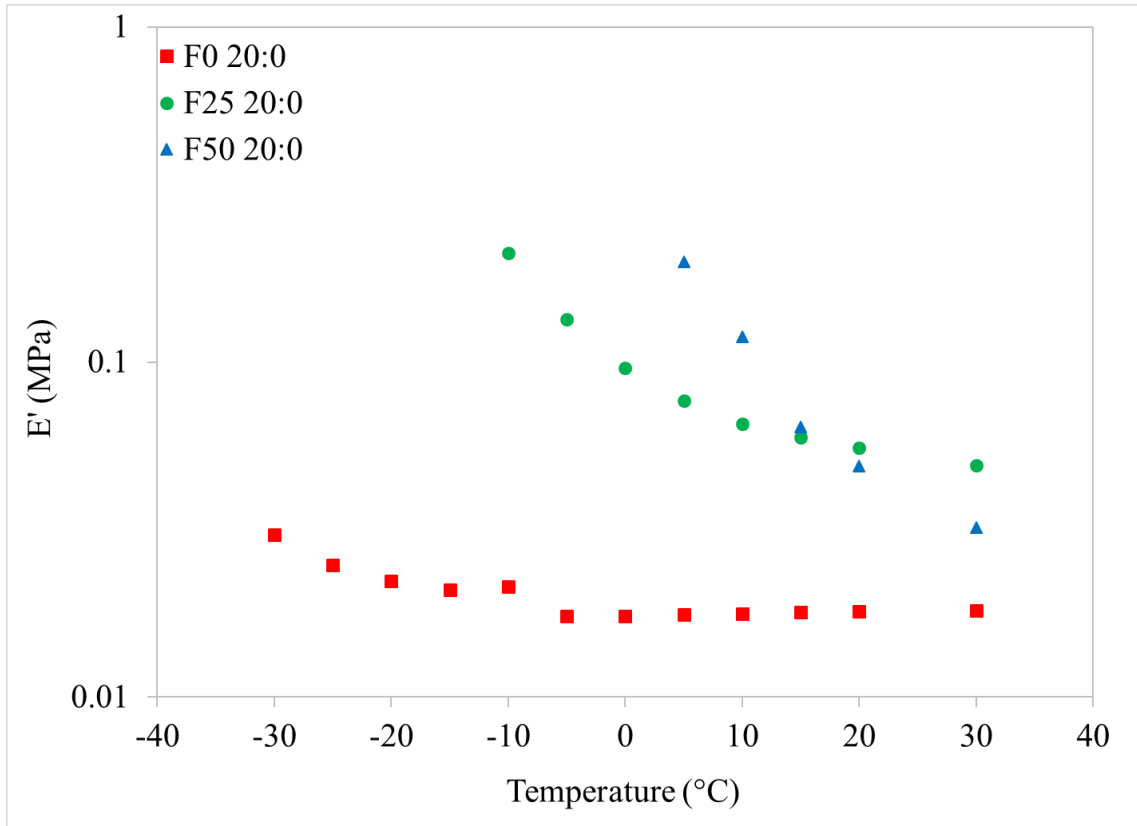
Figure 5.16: The dependence of the storage modulus for F0 20:0, F25 20:0 and F50 20:0 foams as a function of temperature at 10 Hz.
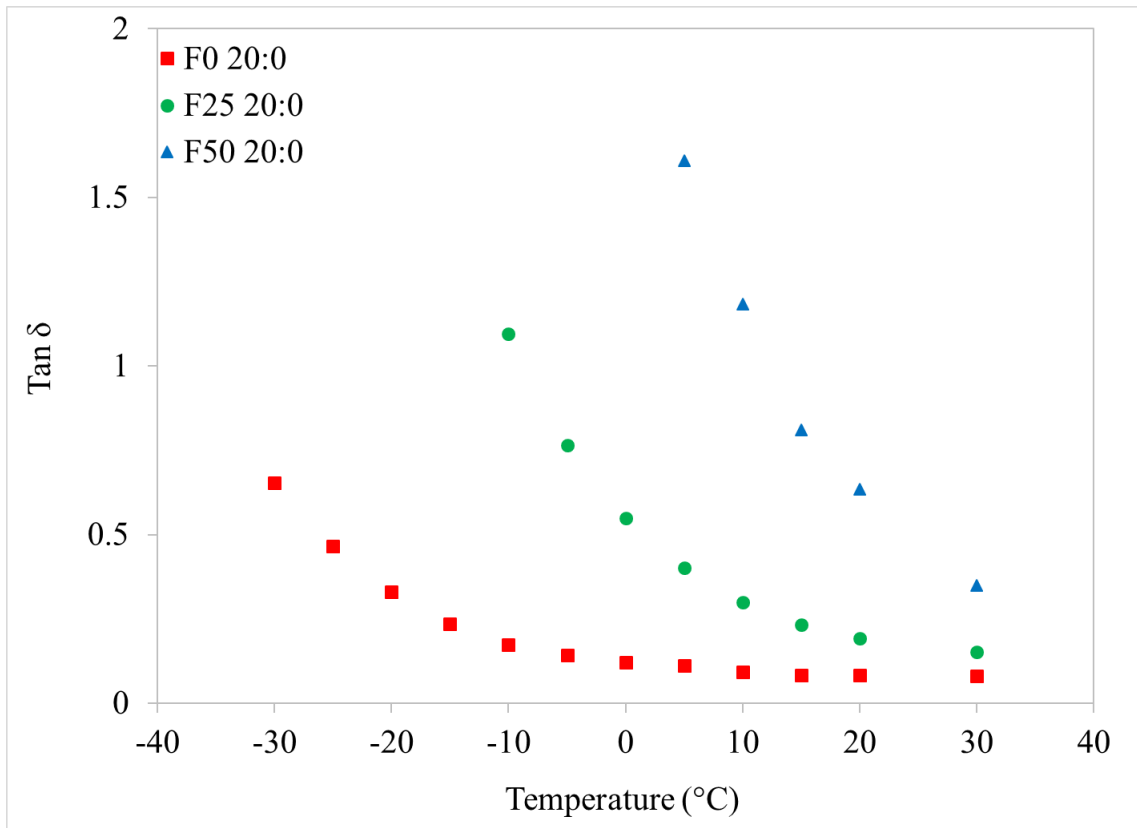
Figure 5.17: The dependence of the loss factor for F0 20:0, F25 20:0 and F50 20:0 foams as a function of temperature at 10 Hz.

The storage modulus, E', of the rubber foams as a function of frequency and temperature is plotted in Figures 5.18 to 5.20. E' increases with the increasing frequency at all measured temperatures. It becomes more dependent on frequency at lower temperatures. However, E' is less dependent on frequency as the temperature increases. The trend of the curves are in agreement with the research done on the effect of frequency on the dynamic behaviour of polyurethane foams [98].

The isothermal curves plotted in Figures 5.18 to 5.20 are shifted along the frequency axis and storage modulus axis to obtain superposition. The dynamic mechanical properties of rubber foam over a wider frequency range are generated using time-temperature superposition principle. In this work, the chosen reference temperature, T_0, was 20°C, where the T_g of each rubber foam was based on the T_g obtained for the solid rubber.
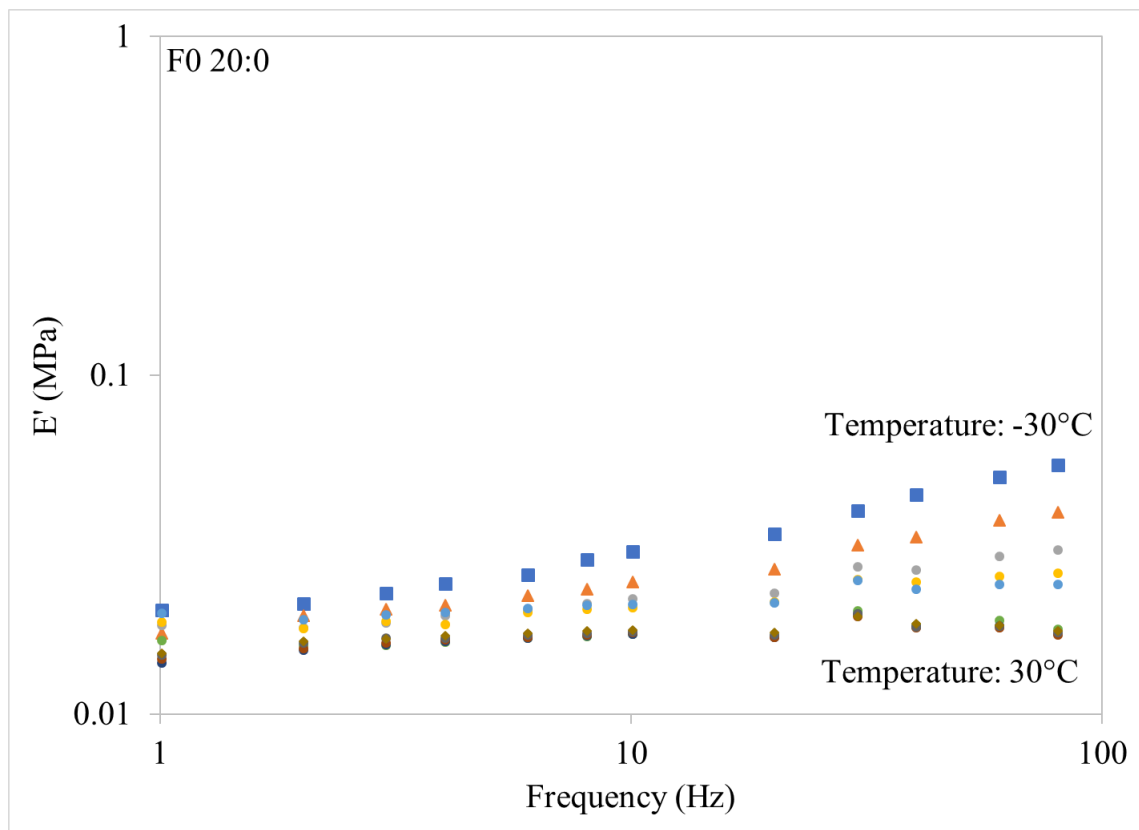
Figure 5.18: The frequency dependence of the storage modulus of F0 20:0 foam for a range of temperatures: -30°C to 30°C.

142
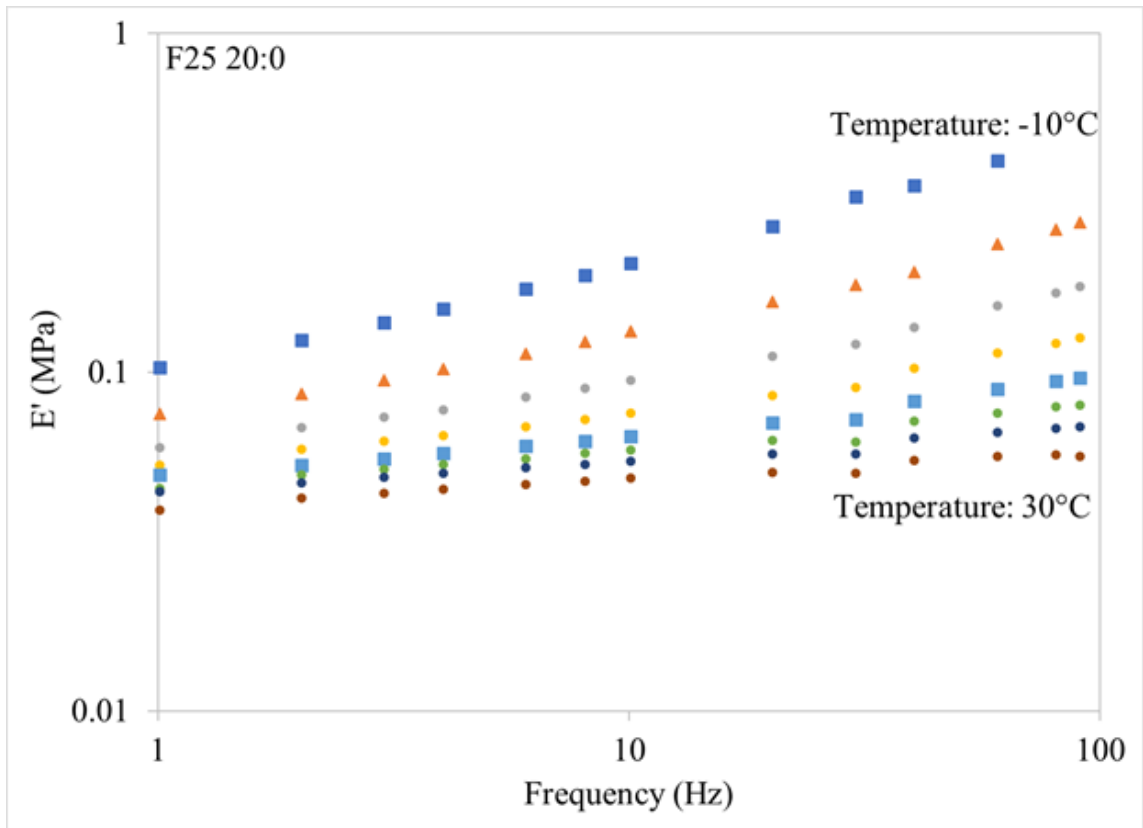
Figure 5.19: The frequency dependence of the storage modulus of F25 20:0 foam for a range of temperatures: -10°C to 30°C.
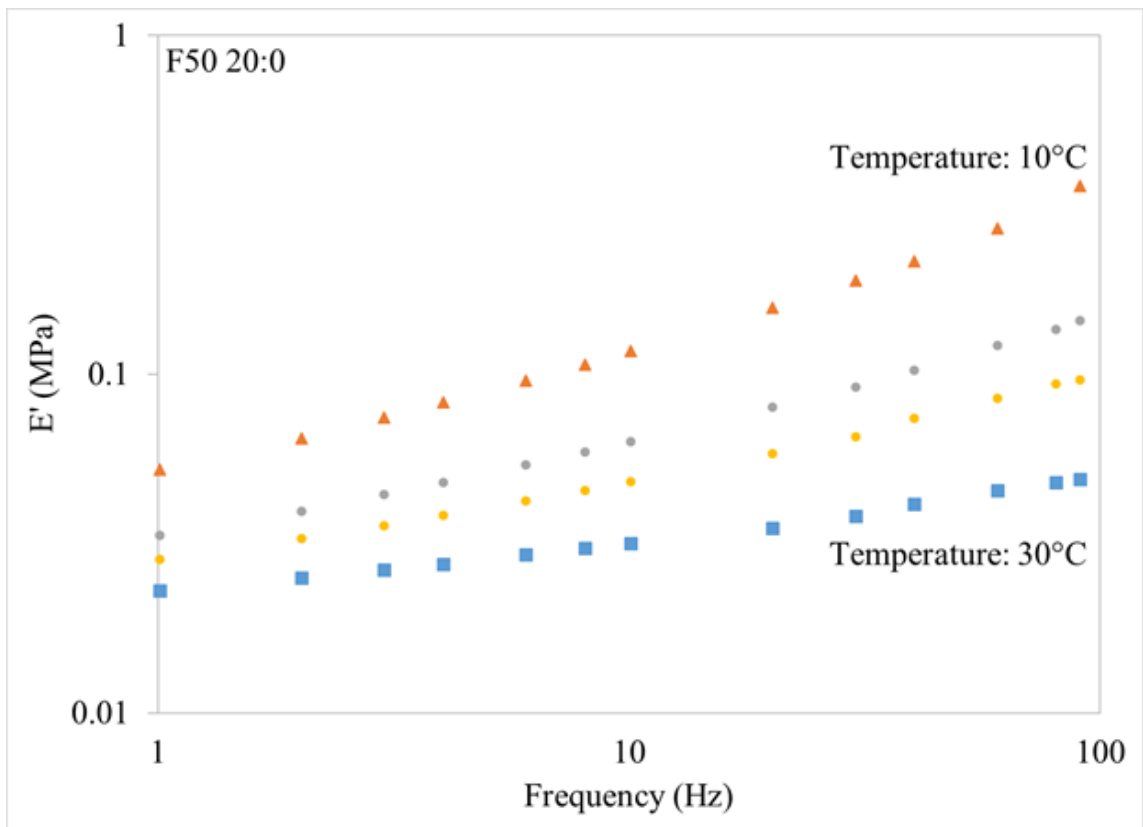
Figure 5.20: The frequency dependence of the storage modulus of F50 20:0 foam for a range of temperatures: 10°C to 30°C.

143

Figures 5.21 and 5.22 show the storage modulus master curves and the loss modulus master curves for F0 20:0, F25 20:0 and F50 20:0 foams, respectively. All the master curves plotted are frequency dependent and the dynamic moduli increase drastically with the increasing reduced frequency. The storage modulus master curve of F25 20:0 foam is slightly higher than F50 20:0 foam in the low frequency region. This observation is also can be seen earlier in Figure 5.16 in the higher temperatures.

The relationship of dynamic properties of rubber foam with different epoxidation levels known as Cole-Cole plot were also investigated. The relationship is described in section 3.3.4 and it is plotted for foams studied in this work in Figure 5.23. A full semicircle is not plotted as tests were not carried out at low enough temperatures approaching the glass transition temperature for these rubber foams. The data for F0 20:0, F25 20:0 and F50 20:0 foams is not collapse on a single arc. The results are different with the results obtained for solid rubbers for which the dynamic moduli data collapse on a single arc. This suggests that the addition of blowing agent to the solid rubber has changed the rubber structure and therefore the epoxidation of the rubber foam does influence the relationship between storage modulus and loss modulus.
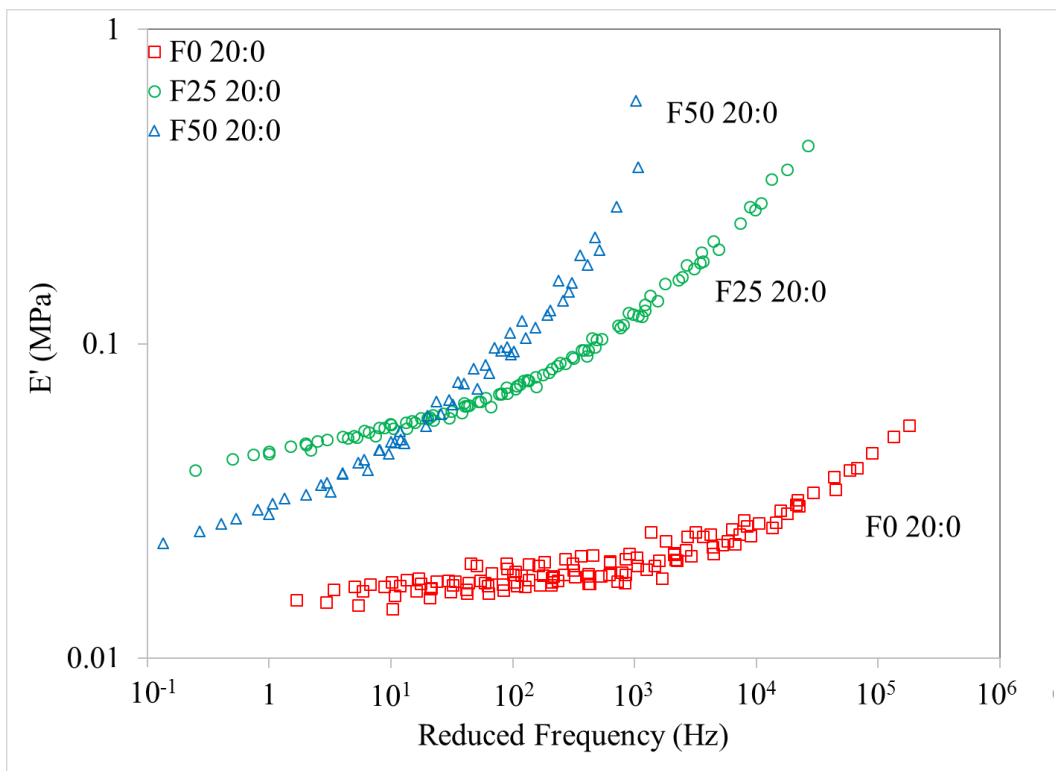
Figure 5.21: A comparison of the master curves for the storage modulus of F0 20:0, F25 20:0 and F50 20:0 foams as a function of the reduced frequency.

144
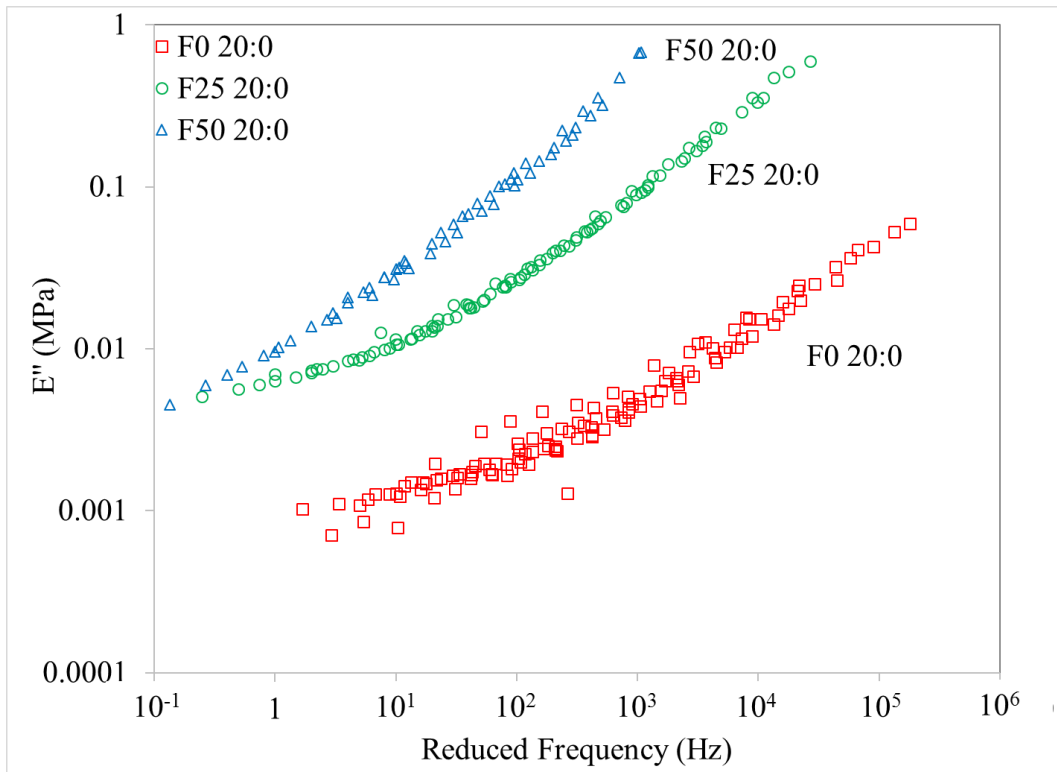
Figure 5.22: A comparison of the master curves for the loss modulus of F0 20:0, F25 20:0 and F50 20:0 foams as a function of the reduced frequency.
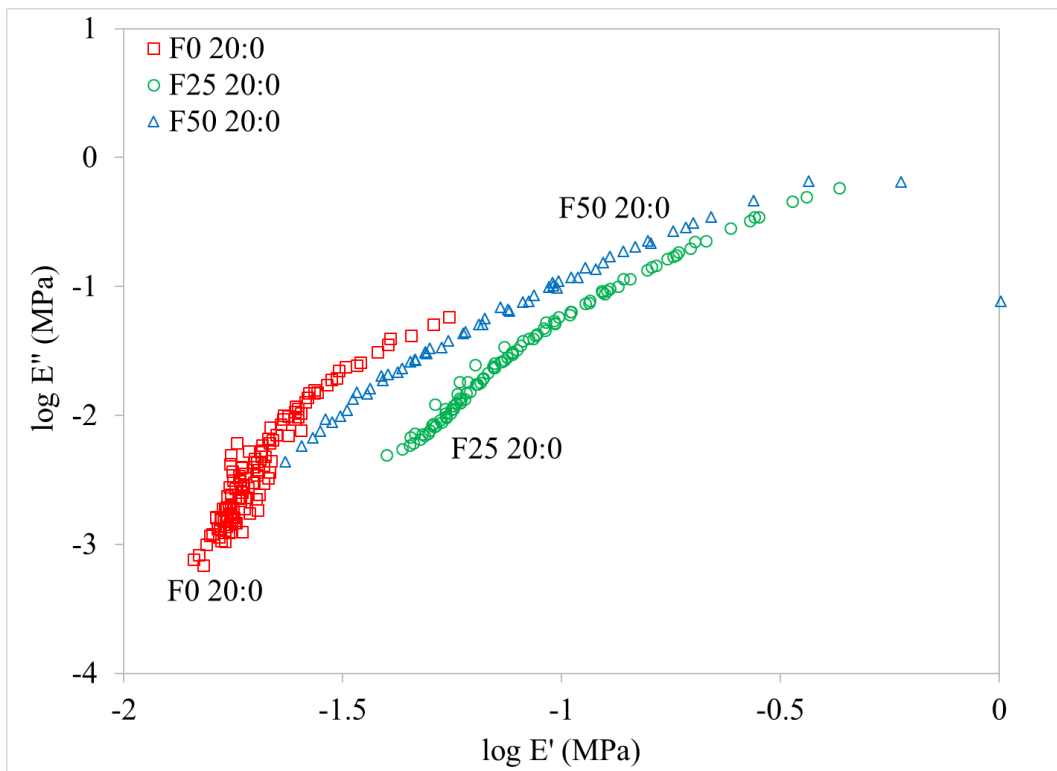
Figure 5.23: The Cole-Cole plots for F0 20:0, F25 20:0 and F50 20:0 foams.

5.5 Microstructure properties

The microstructure properties including the mean pore size and standard deviation in pore size were measured for all rubber foams. The data on commercial foams: RRF and PUF were also obtained and included in the analysis for comparison purposes.

The microstructure for F0 20:0, F25 20:0 and F50 20:0 foams is shown in Figure 5.24. The mean ($\bar{s}$) and the standard deviation (σ_s) in the pore size for the foams were $\bar{s} = 42.81$ µm and $\sigma_s = 44.47$ µm for F0 20:0 foam, $\bar{s} = 42.02$ µm and $\sigma_s = 40.15$ µm for F25 20:0 foam and $\bar{s} = 35.94$ µm and $\sigma_s = 27.44$ µm for F50 20:0 foam, respectively.

Foam	Mean	Standard Deviation
F0 20:0	42.81 µm	44.47 µm
F25 20:0	42.02 µm	40.15 µm
F50 20:0	35.94 µm	27.44 µm
RRF	40.74 µm	36.10 µm
PUF	21.66 µm	10.21 µm
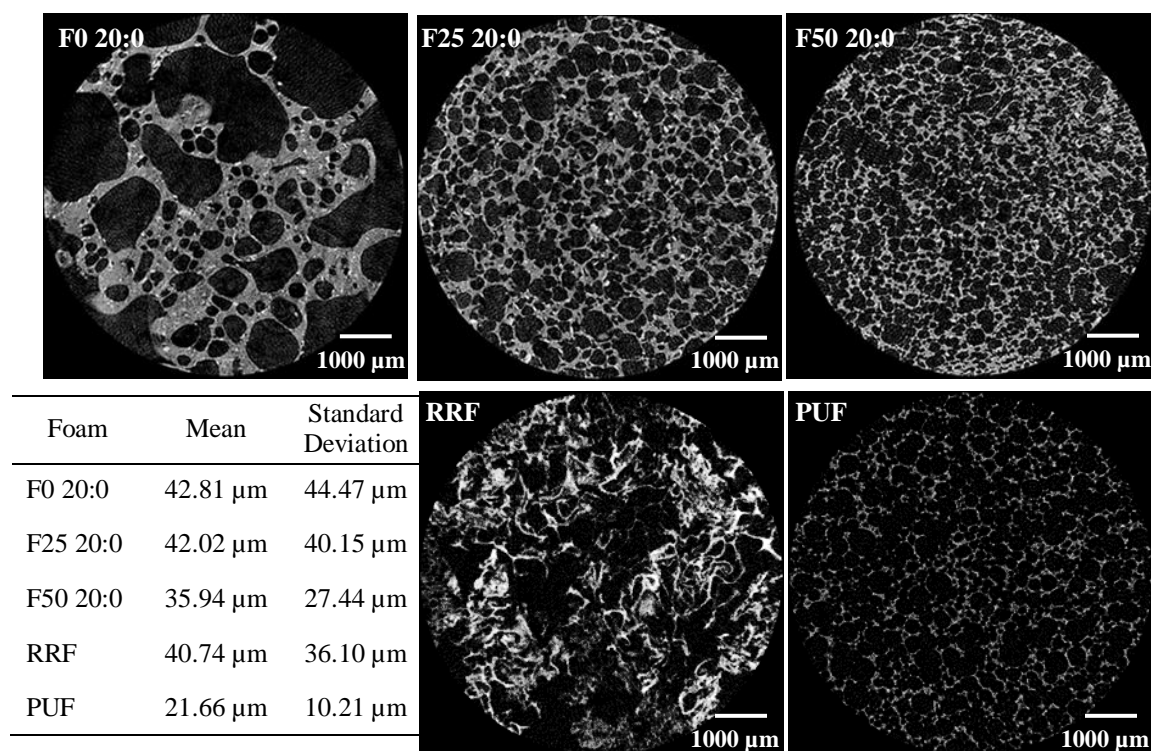
Figure 5.24: The microstructure, mean and standard deviation in the pore size for F0 20:0, F25 20:0, F50 20:0, RRF and PUF foams.

The microstructure results indicate that the pore sizes decrease with the presence of epoxide groups on the natural rubber backbone. ENR foams: F25 20:0 and F50 20:0 have a relatively low gas (or air) permeability as solid ENR [12] and close pores dominate. This finding is supported with the high airflow resistivity values (see Table 5.1). This observation suggests that the ENR foams in general have very high airflow resistivity or low air permeability. The gas decomposes from sodium bicarbonate that is carbon dioxide is might not be able to penetrate and expand enough through the wall of ENR and resulted in foam with a relatively

146

small pore size and isolated pores. These results were also observed in previous research [54]. At constant curing temperature and the same amount of sodium bicarbonate used in their formulations, ENR foam in the work reported in ref. [54] had the smallest pore size as compared with the other rubber foams. It was believed that the epoxide groups on the rubber main chain have contributed to the forceful crosslinking process. This condition has provided some extra crosslinking sites locations together with the carbon double bond, and therefore contributed to higher restriction to expansion in ENR foam. However, the standard deviation in the pore size of F25 20:0 and F50 20:0 foams were lower in comparison to F0 20:0 foam. These results show that the pore expansion restriction in ENR foams had generated uniform pore size in the matrix so that the porous structure in the foams becomes more homogenous.

The microstructure for F0 15:5, F25 15:5 and F50 15:5 foams is shown in Figure 5.25. The mean and the standard deviation in the pore size were similar for all the foams: F0 15:5 foam with $\bar{s} = 40.42$ µm and $\sigma_s = 32.93$ µm, F25 15:5 foam with $\bar{s} = 40.65$ µm and $\sigma_s = 38.28$ µm and F50 15:5 foam with $\bar{s} = 39.42$ µm and $\sigma_s = 30.89$ µm.

Foam	Mean	Standard Deviation
F0 15:5	40.42 µm	32.93 µm
F25 15:5	40.65 µm	38.28 µm
F50 15:5	39.42 µm	30.89 µm
RRF	40.74 µm	36.10 µm
PUF	21.66 µm	10.21 µm
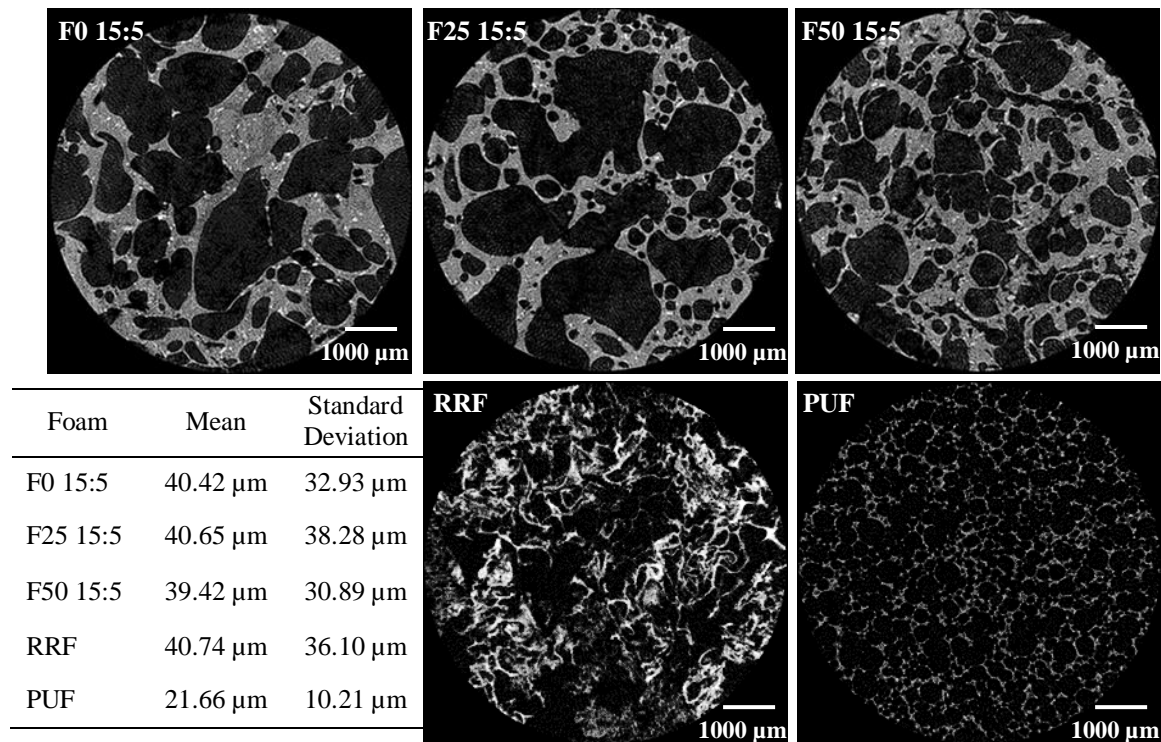
Figure 5.25: The microstructure, mean and standard deviation in the pore size for F0 15:5, F25 15:5, F50 15:5, RRF and PUF foams.

These results suggest that the addition of ammonium bicarbonate does not influence significantly the mean pore size of the foams with different epoxidation levels. However, observation on the microstructure results of F25 20:0 and F50 20:0 foams suggests that the addition of ammonium bicarbonate does influence the porous structure of F25 15:5 and F50 15:5 foams by expanding some of the pore size. These results show that the polar gas, ammonia, produced from the thermal decomposition of ammonium bicarbonate can help the foaming process of the high polarity of ENR foams by expanding some of the pore size. All these foams were showing non-uniform pore size distribution and heterogeneous pore structure with several much larger pores being produced within the foaming process.

The microstructure for LF0, LF25 and LF50 foams is shown in Figure 5.26. The mean and the standard deviation in the pore size for the foams were $\bar{s} = 35.40$ µm and $\sigma_s = 26.71$ µm for LF0 foam, $\bar{s} = 44.10$ µm and $\sigma_s = 31.22$ µm for LF25 foam and $\bar{s} = 38.88$ µm and $\sigma_s = 27.88$ µm for LF50 foam, respectively.

Foam	Mean	Standard Deviation
LF0	35.40 µm	26.71 µm
LF25	44.10 µm	31.22 µm
LF50	38.88 µm	27.88 µm
RRF	40.74 µm	36.10 µm
PUF	21.66 µm	10.21 µm
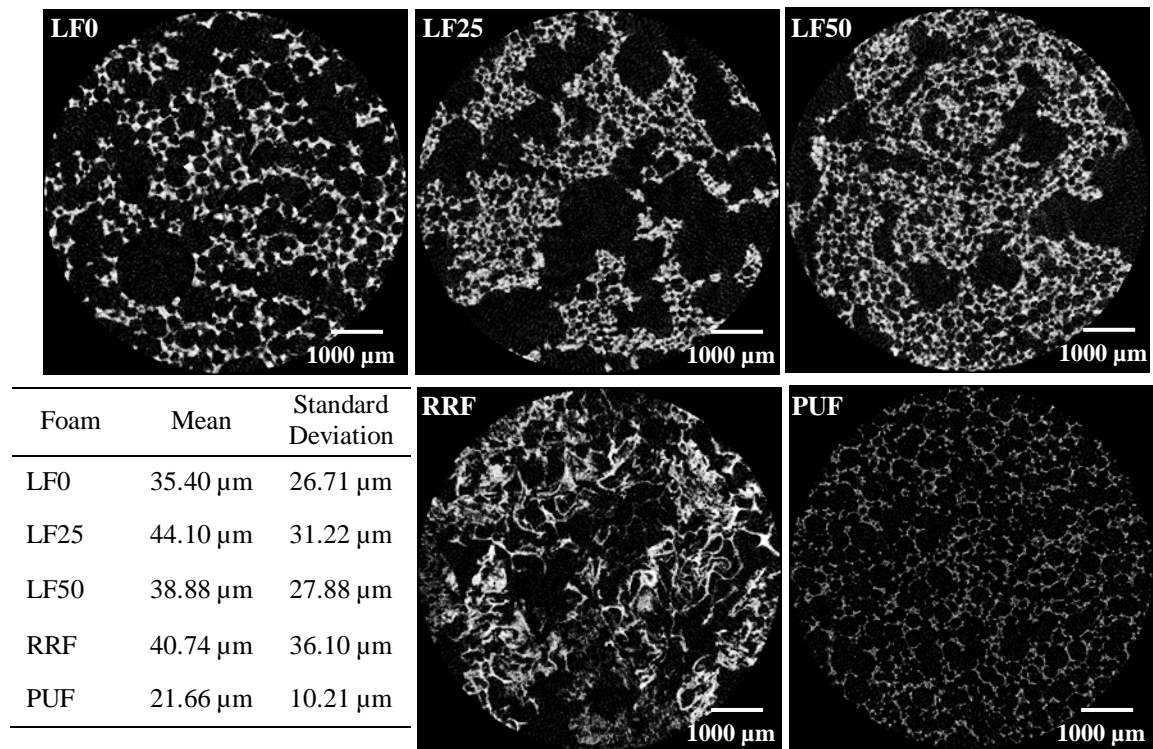
Figure 5.26: The microstructure, mean and standard deviation in the pore size for LF0, LF25, LF50, RRF and PUF foams.

The mean pore size of latex foams was generally similar with dry rubber foams. However, the standard deviation of latex foams was generally lower than dry rubber foams. These observations suggest that the mean pore size does not influenced by the different processes of producing natural rubber foam and ENR foams, but the standard deviation of all the latex foams were showing high homogeneity in their pore size.

The mean pore size of commercial foams was 40.74 µm for RRF and 21.66 µm for PUF, respectively. These foams show a low value in the standard deviation in pore size, 36.10 µm for RRF and 10.21 µm for PUF, and considered to be good acoustic absorbers. This observation is supported with the high porosity values for these foams (see Table 5.1). The porosity values of RRF and PUF were 0.81 and 0.75, respectively. The results suggest that a relatively small pore size, homogenous pore size distribution in a porous structure and high porosity are among the features that can contribute in producing a good noise control material.

The microstructure properties such as the mean pore size and the standard deviation in pore size are principles that can be used together with other non-acoustic properties to predict the acoustic absorption behavior of foams. In the case of dry rubber foams, the epoxidation levels and the blowing agent are the parameters that influence the microstructure properties. Therefore, the selection of these parameters is very crucial to obtain the optimum design of the rubber foam for noise control applications.

However, this microstructure characteristic presented several limitations. Firstly, only 60% of foam sample area were considered, therefore the results obtained may not be representative of these particular foams. Secondly, the pore shape in these foams is irregular. The pores were assumed to be spherical-shaped and the mean pore size was analysed using Computer Tomography Analysis (CTAn) software. These issues may influence the accuracy of the prediction of the acoustical properties of foams which are discussed in the following section.

5.6 Acoustic properties

The sound absorption coefficient for all rubber foams was measured. The results for commercial foams, RRF and PUF were also obtained and included for comparison purposes. Generally, the results indicate that the epoxidation level does influence the sound absorption coefficient in a broad frequency range. The sound absorption coefficient of all rubber foams is similar below 500 Hz, and above this frequency the acoustic absorption behaviour depends on the epoxidation level. Moreover, the absorption behaviour at higher frequencies might be due to the pore shape in rubber foam being irregular, many pores are closed or dead-ended which would amplify the so-called circumferential edge effects [99].

Figure 5.27 shows the sound absorption coefficient for F0 20:0, F25 20:0 and F50 20:0 foams. For F25 20:0 and F50 20:0 foams the absorption is generally low as a result of relatively low porosity (Table 5.1).
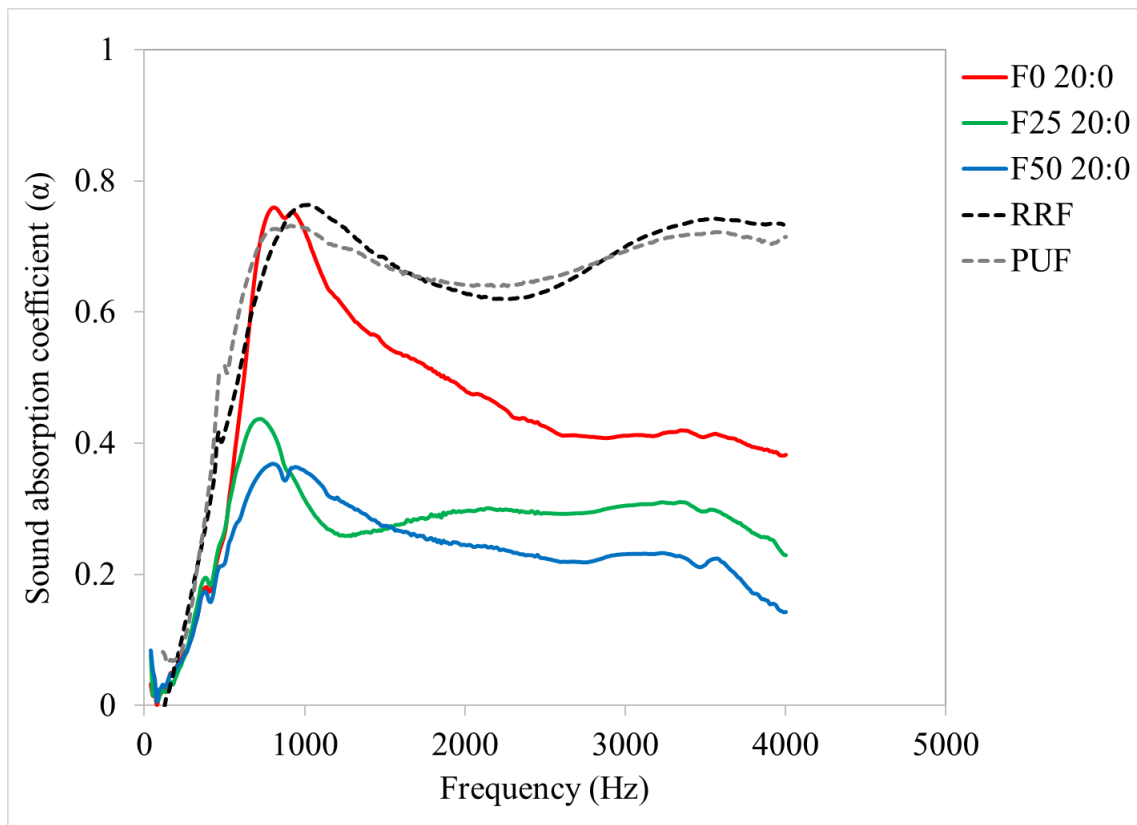
Figure 5.27: The sound absorption coefficient for F0 20:0, F25 20:0, F50 20:0, RRF and PUF foams.

The sound absorption peak relates to the resonance in the foam sample of given thickness. It is also controlled by the circumferential gap between the foam sample and the tube wall, and by the density and dynamic moduli of foam. This sound absorption peak does not significantly shift with a change in the epoxidation level. These peaks can be explored in noise control applications. The absorption coefficient of foam with no epoxidation level, F0 20:0, is relatively high at frequencies above the resonance peak as a result of its relatively high porosity. The amplitude of the resonance peak for this foam is almost doubles in comparison with that attained for F25 20:0 and F50 20:0. The two commercial foams outperform rubber foams throughout the entire frequency range because of their higher porosity values.

The sound absorption coefficient for F0 15:5, F25 15:5 and F50 15:5 foams in Figure 5.28 indicates a different acoustic absorption behaviour. F50 15:5 foam shows a slightly higher sound absorption upon the addition of ammonium bicarbonate. The sound absorption peak increases to 0.420 at 727 Hz.
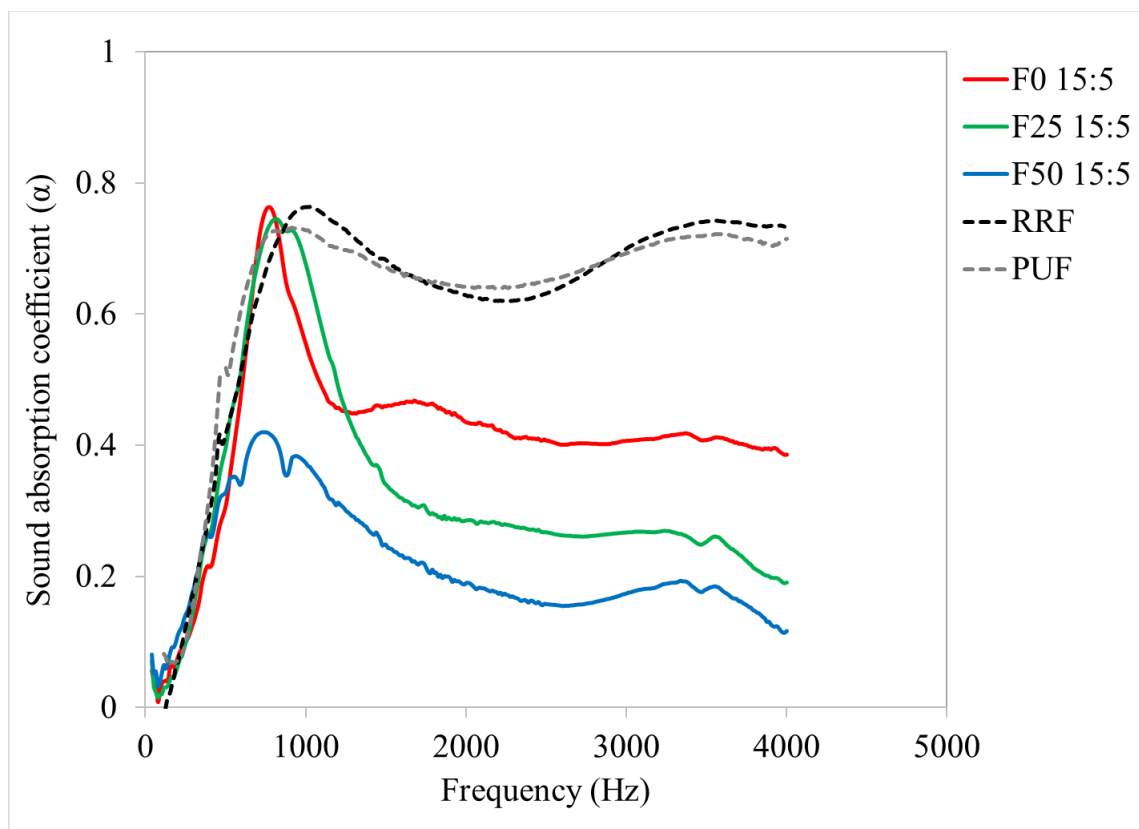
Figure 5.28: The sound absorption coefficient for F0 15:5, F25 15:5, F50 15:5, RRF and PUF foams.

However, the sound absorption peak increases dramatically to 0.745 at 815 Hz for F25 15:5 foam as a result of its relatively high porosity. Applying the ammonium bicarbonate in F25 15:5 foam improves its acoustic properties and yielding 40% increment in sound absorption around the peak. As for F0 15:5 foam, no significant different observed in sound absorption curve upon the addition of ammonium bicarbonate. The foam exhibits promising absorption coefficient peak of 0.764 at 765 Hz.

In this study, the sound absorption curve for all the dry rubber foams generally decreases above the resonance. They can generally absorb the sound effectively in a narrow frequency range. The sound absorption curve flattens above this resonance where the ability of these foams to absorb sound is limited. These observations are also can be seen in the research done on dry natural rubber foam produced with different foaming temperatures [4]. The sound absorption for all the foams decreased after reaching the sound absorption peak. They also stated that the natural rubber foam reaches its high sound absorption at the low frequency region. These results can be explained the limited value of porosity and by a relatively high proportion of closed and dead-end pores.

The results also suggest that the foams with no epoxidation level, F0 20:0 and F0 15:5, can produce rubber foam with the right density, porosity and airflow resistivity in contributing to the promising sound absorption coefficient. This can be seen also in F25 15:5 foam upon the addition of ammonium bicarbonate. This modification has changed the physical properties of F25 15:5 foam and resulted in a higher sound absorption coefficient. In contrast, F25 20:0, F50 20:0 and F50 15:5 foams have a relatively high density, lower porosity and higher airflow resistivity. A limited amount of sound energy is able to penetrate into these foams to be absorbed.

On contrary, the outcome of the sound absorption coefficient for LF0, LF25 and LF50 foams in Figure 5.29 shows promising acoustic absorption behaviour as being compared with commercial foams. The sound absorption of LF0 and LF25 foams is generally high as a result of their relatively high porosity. The absorption coefficient after the resonance peak remains relatively high being above 50% for both foam samples.

152
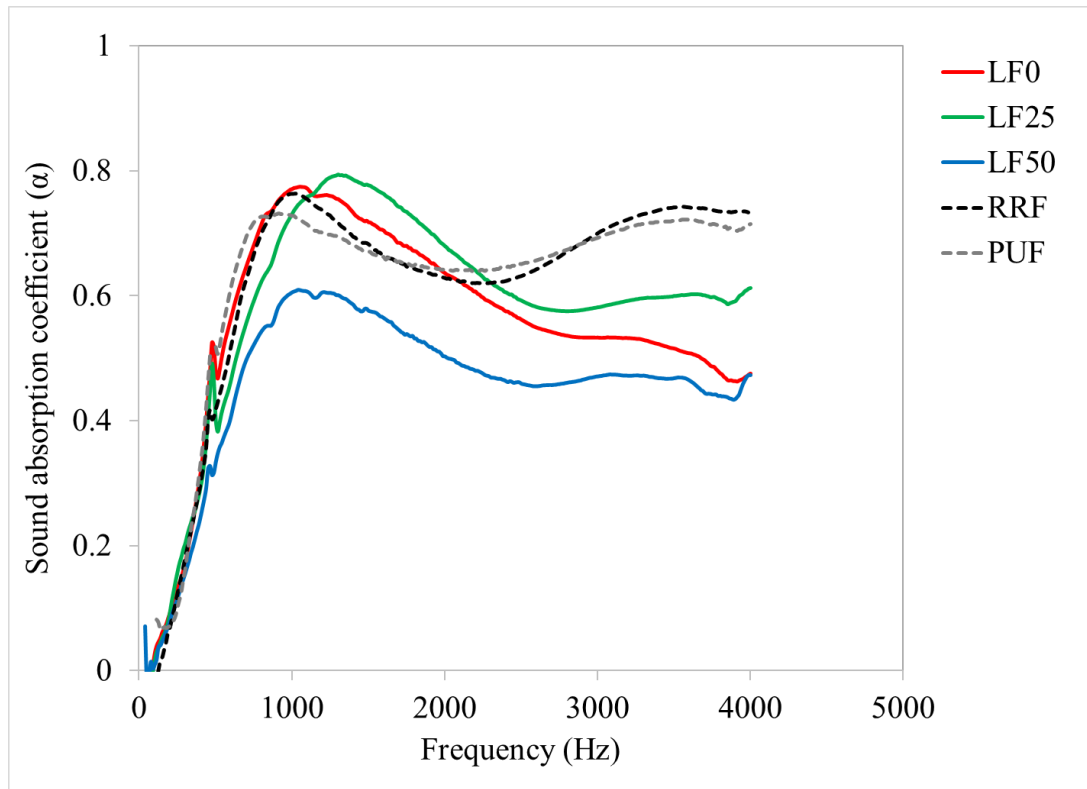
Figure 5.29: The sound absorption coefficient for LF0, LF25, LF50, RRF and PUF foams.

In the case of LF50 foam, the sound absorption peak is higher than the peaks obtained earlier for the dry rubber foam with the same epoxidation level, 50 mol%: F50 20:0 and F50 15:5 foams. The sound absorption peak of LF50 foam is 0.609 at 1040 Hz. This outcome is also attributed to the higher porosity of the LF50 foam than the porosity obtained for the F50 20:0 and F50 15:5 foams.

The first resonant frequency in the absorption range of all latex foams slightly shifts towards the higher frequencies, as being compared to the first resonant frequency of the dry rubber foam. These observations show that the latex foam can be used as a sound absorbing material in the higher frequency range. However, the sound absorption curves of all latex foams also decrease after the resonance. This suggests that the different processes of producing natural rubber foam and ENR foams do not influence the sound absorption curve trend along the frequency axis.

Based on the evaluation of acoustic absorption behaviour of natural rubber foam and ENR foams, it can be seen that most of the foams show promising sound absorption at the low frequency region, so that they are applicable as vibration damping materials. However, the

sound absorption of the foams is relatively low at the high frequency region. This observation suggests that the capability of these foams as noise control materials need to be improved further. This can be done by improving the physical, dynamic and microstructure properties of the foams as those properties are the main features in delivering their acoustic performance. Therefore, knowledge in predicting those properties is crucial to design and produce foams with an optimum acoustic performance. Therefore, model development needs to be carried out to understand better and to describe accurately the relationship between the non-acoustical and acoustical properties of these foams.

5.6.1 Modelling of dry rubber foam

In the previous sections it was shown that the acoustic absorption behavior of epoxidized natural rubber (ENR) foam and natural rubber foam depends on their non-acoustic properties. In order to validate experimental data, a heterogeneous model [100] was selected to describe the acoustic absorption behaviour of the equivalent fluid in the network of pores in rubber foams produced in this work. The heterogeneous model selected in this study treated the rubber foam installed in the two-microphone impedance tube as a porous composite. The consideration was based on the limitation of the circumferential gap between the rubber foam and the sample holder in the airflow resistivity measurement as shown in Figure 5.30.
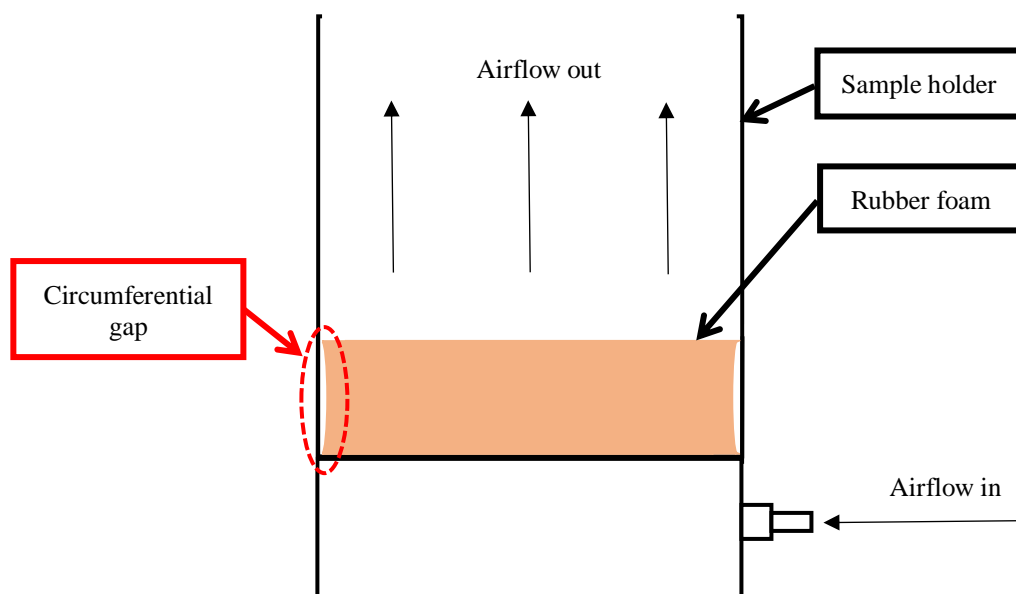
Figure 5.30: The limitation of the circumferential gap between the foam sample and the sample holder in the airflow resistivity measurement.

154

The microstructure properties indicated that rubber foams have many closed pores and this suggests that the foams were highly resistive porous material. However, the airflow resistivity measurement showed that they are less resistant in comparison. The application of the Teflon tape around the foam sample to fill the gap was also not provide significance difference to the results. These observations relate to the presence of circumferential gap. Therefore, the heterogeneous model is the right model to investigate and predict circumferential edge effects that might be happened during the acoustic measurement of the rubber foams in the impedance tube.

According to this model, sound waves penetration to porous material can be controlled by the perforation types [100] as shown in Figure 5.31. In this study, 'circle in circle' type was selected based on the circular shape of a foam sample being tested in the circular shape of the impedance tube.
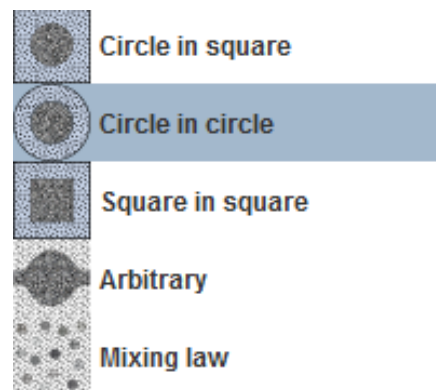
Figure 5.31: The perforation types in the heterogeneous model [100].

The perforation type is defined by the diameter of the two-microphone impedance tube, L_t and the diameter of the foam sample placed in the two-microphone impedance tube, L_p. These parameters are illustrated in Figure 5.32. The rubber foam edge effect was considered as the possibility of circumferential air gap occurred in between the rubber foam and the impedance tube.

155
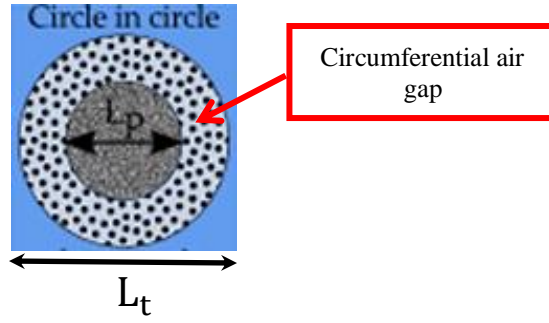
Figure 5.32: The diameter of the two-microphone impedance tube, L_t and the diameter of the foam sample, L_p. [100].

Two acoustic models were selected to predict the acoustic absorption behavior of foams. The first semi-empirical modelling approach was that proposed by Miki [101]. This model predicts the normalized characteristic impedance and sound wavenumber of a porous medium from the knowledge of three non-acoustical parameters: airflow resistivity; porosity; and tortuosity. The second model is the analytical model known as Padé approximation model [74]. It approximates the viscosity correction function in the expressions for the characteristic impedance and sound wavenumber in a porous medium with variable pore size distribution. This model depends on the five non-acoustical parameters: mean pore size; standard deviation in pore size; airflow resistivity; porosity; and tortuosity. All predictions by these two models were based on the measured values of non-acoustic parameters. The models were validated with the experimental data for the sound absorption coefficient.

5.6.2 Miki model

The Miki model [101] was introduced to improve the original model proposed by Delany and Bazley [70]. This simple model appears more causal and provides a more accurate estimation for the acoustic behavior of porous materials across a broader frequency range. According to this model, the normalised characteristic impedance (z_c) of a porous material can be calculated by the following equations:

$$z_c(f) = R(f) + iX(f), \tag{5.9}$$

$$R(f) = 1 + 0.0070 \left(\frac{f}{\sigma}\right)^{-0.632}, \tag{5.10}$$

$$X(f) = -0.107 \left(\frac{f}{\sigma}\right)^{-0.632}. \tag{5.11}$$

The sound wavenumber in a porous material (k_c) can also be calculated by the following equations:

$$k_c(f) = \alpha(f) + i\beta(f), \tag{5.12}$$

$$\alpha(f) = \frac{2\pi f}{c_0} \left[0.160 \left(\frac{f}{\sigma}\right)^{-0.618}\right], \tag{5.13}$$

$$\beta(f) = \frac{2\pi f}{c_0} \left[1 + 0.109 \left(\frac{f}{\sigma}\right)^{-0.618}\right]. \tag{5.14}$$

In the above equations, f is the frequency of sound, $i = \sqrt{-1}$, σ is the airflow resistivity of a porous material and c_0 is the sound speed in air (340 m/s). These two functions (z_c) and (k_c) can be used to calculate the normalised surface impedance (z_s) of a hard-backed porous material of thickness (d) and the sound absorption coefficient (α) with the following equations:

$$z_s = z_c \coth(-ik_c d) \tag{5.15}$$

and

$$\alpha = 1 - \left|\frac{z_s - 1}{z_s + 1}\right|^2. \tag{5.16}$$

5.6.3 Padé approximation

The acoustic behaviour of the porous material depends on the pore size and the prediction of this behaviour can be made with the information of the pore size distribution. In this study, foams produced had variable pore size distribution so that the Padé approximation model

[75] can be used to predict the dynamic density of the equivalent fluid in the foam pores (ρ_f) and compressibility of the equivalent fluid (C_f) to determine the acoustic behavior of the foam with non-uniform pores. The dynamic density can be expressed as:

$$\rho_f = 1 + \epsilon_\rho^{-2} \widetilde{F}_\rho(\epsilon_\rho),$$ (5.17)

where the viscosity correction function is given as:

$$\widetilde{F}_\rho(\epsilon_\rho) = \frac{1 + \theta_{\rho,3}\epsilon_\rho + \theta_{\rho,1}\epsilon_\rho}{1 + \theta_{\rho,3}\epsilon_\rho},$$ (5.18)

with $\epsilon_\rho = \sqrt{-i2\pi f \rho_0/\sigma_x}$, $\theta_{\rho,1} = 1/3$, which depends on the pore cross-sectional shape, $\theta_{\rho,3} = \theta_{\rho,1}/\theta_{\rho,2}$ and $\theta_{\rho,2} = e^{-1/2(\sigma_s \log 2)^2}/\sqrt{2}$, which depends on the pore cross-sectional shape and the width of pore size distribution. A similar procedure can be used for the bulk compressibility which can be expressed as:

$$C_f = \frac{1}{\gamma P_0}\left(\gamma - \frac{\gamma - 1}{1 + \epsilon_c^{-2}\widetilde{F}_c(\epsilon_c)}\right),$$ (5.19)

where γ is the specific heat ratio (1.4), P_0 is the air pressure (101.325 kPa), and:

$$\widetilde{F}_c(\epsilon_c) = \frac{1 + \theta_{c,3}\epsilon_c + \theta_{c,1}\epsilon_c}{1 + \theta_{c,3}\epsilon_c},$$ (5.20)

with $\epsilon_c = \sqrt{-i2\pi f \rho_0 N_{Pr}/\sigma'_x}$, $\theta_{c,1} = 1/3$, $\theta_{c,3} = \theta_{c,1}/\theta_{c,2}$ and $\theta_{c,2} = e^{3/2(\sigma_s \log 2)^2}/\sqrt{2}$. In the above equations, ρ_0 is the air equilibrium density (1.2 kg/m³), σ_x and σ'_x are the air flow resistivity and the thermal flow resistivity in the pore respectively, while N_{Pr} is the Prandtl number and σ_s is the standard deviation in the log-normal pore size. According to this model, these equations are for a single pore and therefore some parameters in the equations need to be replaced for porous material with multiple pores or the bulk medium. A bulk dynamic

density (ρ_b) and compressibility with its bulk characteristic (C_b) are given with the following equations:

$$\rho_b = \frac{\alpha_\infty}{\phi}\rho_f \qquad\qquad (5.21)$$

and

$$C_b = \phi C_f , \qquad\qquad (5.22)$$

where α_∞ is the tortuosity. The bulk air flow resistivity and the bulk thermal flow resistivity are also need to be introduced and expressed as $\sigma_b = \sigma_x \alpha_\infty/\phi$ and $\sigma'_b = \sigma'_x \alpha_\infty/\phi$, which replace the air flow resistivity (σ_x) and the thermal flow resistivity (σ'_x) of a single pore. Both parameters are also related to the mean pore size ($\bar{s}$) and standard deviation in pore size (σ_s):

$$\sigma_x = \frac{8\eta_0}{\bar{s}^2} e^{6(\sigma_s \log 2)^2} \qquad\qquad (5.23)$$

and

$$\sigma'_x = \frac{8\eta_0}{\bar{s}^2} e^{-6(\sigma_s \log 2)^2} , \qquad\qquad (5.24)$$

where η_0 is the dynamic viscosity of air (1.81 x 10^{-5} Pa.s). As a result, the frequency dependent parameter ϵ_ρ and ϵ_c must also be replaced with $\epsilon_\rho = \sqrt{-i2\pi f \alpha_\infty \rho_0/\sigma_b \phi}$ and $\epsilon_c = \sqrt{-i2\pi f \alpha_\infty \rho_0 N_{Pr}/\sigma_b'\phi}$.

Finally, ρ_b and C_b can be used to calculate the normalised characteristic impedance (z_c) and the sound wavenumber in foam (k_c) by using Equations 2.6 and 2.7 in section 2.6.4. Then, the normalised surface impedance (z_s) and the sound absorption coefficient (α) are determined as outlined in Equations 5.15 and 5.16.

Before continuing with the comparison of modelling approaches, the difference on the sound absorption coefficient of F0 20:0 foam between two ways of prediction were studied. First prediction was based on the Padé approximation with non-acoustic data measurement and second prediction was based on the heterogenous model and Padé approximation with circumferential gap consideration. These predictions were then compared with the measurement data as shown in Figure 5.33. The measured non-acoustic values and inverted values of the non-acoustical parameters with circumferential gap consideration in the heterogeneous model is listed in Table 5.2.
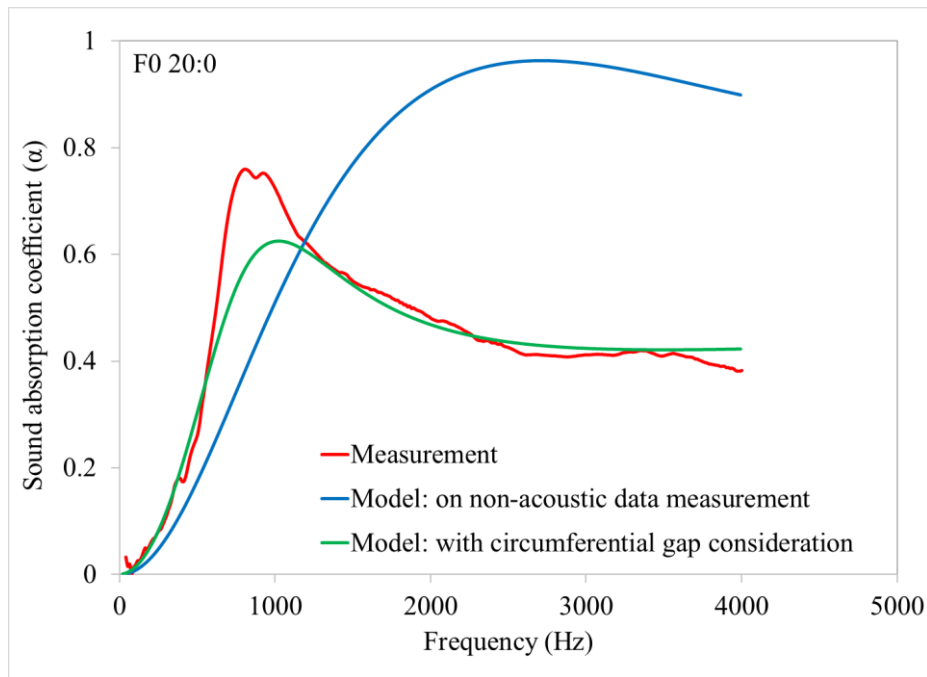
Figure 5.33: A comparison between the measurement data and predictions based on non-acoustic data measurement and with circumferential gap consideration of the sound absorption coefficient of F0 20:0 foam.

Table 5.2
The parameters comparison between the prediction based on non-acoustic data measurement and with circumferential gap consideration for F0 20:0 foam.

Prediction	Thickness (mm)	Porosity, ϕ	Airflow resistivity, σ (N.s/m^4)	Tortuosity	Mean pore size (µm)	Standard deviation in pore size (µm)
Non-acoustic data measurement	25	0.69	43,580	-	42.81	44.47
Circumferential gap consideration[1]	25	0.50[2]	549,840[2]	1.2	27.54[2]	44.47

[1] $L_t = 45.0$ mm and $L_p = 43.9$ mm was applied in the heterogeneous model.

[2] Inverted non-acoustic values.

It can be seen clearly that the sound absorption curves between the measurement data and the prediction based on the non-acoustic data measurement were not in agreement. This suggests that the non-acoustic data obtained were not fit to the measurement of the acoustic properties of F0 20:0 foam. However, the sound absorption curves for the F0 20:0 foam suggest that there is a good correlation between the measurement data and the prediction with circumferential gap consideration along the frequency range. The measurement curve and that predicted by the heterogeneous model are almost identical. This observation suggests that the model proposed can provide a close agreement to the acoustic measurement of rubber foam.

5.6.4 Comparison of modelling approaches

The measured and predicted acoustic properties of the rubber foam are presented in Figures 5.34 to 5.42. The agreement of the sound absorption curves between the measurement data and those predicted by the heterogeneous model and the acoustic models are presented below. The heterogeneous model is based on the diameter of the two-microphone impedance tube (L_t) and the diameter of the rubber foam sample (L_p). These diameters are difficult to make identical and it is common that $L_t > L_p$. This leads to the circumferential edge effects [99]. Four input parameters are needed for the Miki model: foam thickness, porosity, airflow resistivity and tortuosity. The Padé approximation is based on the foam thickness and the five measurable non-acoustic parameters: porosity, airflow resistivity, tortuosity, mean pore size and standard deviation in pore size. A majority of these parameters were obtained experimentally as described in the previous section. The tortuosity was estimated using Alphacell software [100]. Tables 5.3 to 5.11 present the measured and inverted values of the non-acoustical parameters which were used to predict the acoustic absorption behaviour of rubber foams. Some of the non-acoustic parameters were fitted to improve the agreement between the measurement and modelling curve. These parameters were: porosity and airflow resistivity (Miki model and Padé approximation); mean pore size and standard deviation in pore size (Padé approximation); and foam sample diameter (L_p) or air gap width.

Figure 5.34: A comparison between the measurement data and prediction using the Miki model and Padé approximation of the sound absorption coefficient of F0 20:0 foam.

Table 5.3
The parameters comparison between the measurement value and inverted value used in Miki model and Padé approximation for F0 20:0 foam.

F0 20:0	Thickness (mm)	Porosity, ϕ	Airflow resistivity, σ (N.s/m^4)	Tortuosity	Mean pore size (μm)	Standard deviation in pore size (μm)
Measurement value	25	0.69	43,580	-	42.81	44.47
Inverted value by Miki model	25	0.50 (28%)	700,000 (94%)	1.2	-	-
Inverted value by Padé approximation	25	0.50 (28%)	549,840 (92%)	1.2	27.54 (36%)	44.47 (0%)

L_t = 45.0 mm	L_p = 43.9 mm

a. Percentage in the bracket indicates the percentage difference between the measurement value and the inverted value by the acoustic models.

b. L_p was inverted value.

162

Figure 5.35: A comparison between the measurement data and prediction using the Miki model and Padé approximation of the sound absorption coefficient of F25 20:0 foam.

Table 5.4

The parameters comparison between the measurement value and inverted value used in Miki model and Padé approximation for F25 20:0 foam.

F25 20:0	Thickness (mm)	Porosity, ϕ	Airflow resistivity, σ (N.s/m^4)	Tortuosity	Mean pore size (µm)	Standard deviation in pore size (µm)
Measurement value	23	0.37	261,135	-	42.02	40.15
Inverted value by Miki model	23	0.37 (0%)	800,000 (67%)	1.2	-	-
Inverted value by Padé approximation	23	0.37 (0%)	700,180 (63%)	1.2	28.37 (32%)	40.15 (0%)

L_t = 45.0 mm	L_p = 44.6 mm

a. Percentage in the bracket indicates the percentage difference between the measurement value and the inverted value by the acoustic models.

b. L_p was inverted value.

Figure 5.36: A comparison between the measurement data and prediction using the Miki model and Padé approximation of the sound absorption coefficient of F50 20:0 foam.

Table 5.5

The parameters comparison between the measurement value and inverted value used in Miki model and Padé approximation for F50 20:0 foam.

F50 20:0	Thickness (mm)	Porosity, ϕ	Airflow resistivity, σ (N.s/m^4)	Tortuosity	Mean pore size (μm)	Standard deviation in pore size (μm)
Measurement value	25	0.41	173,571	-	35.94	27.44
Inverted value by Miki model	25	0.33 (20%)	1,300,000 (87%)	1.2	-	-
Inverted value by Padé approximation	25	0.30 (27%)	1,150,400 (85%)	1.2	24.58 (32%)	27.44 (0%)

$L_t = 45.0$ mm	$L_p = 44.6$ mm

a. Percentage in the bracket indicates the percentage difference between the measurement value and the inverted value by the acoustic models.

b. L_p was inverted value.

Figure 5.37: A comparison between the measurement data and prediction using the Miki model and Padé approximation of the sound absorption coefficient of F0 15:5 foam.

Table 5.6

The parameters comparison between the measurement value and inverted value used in Miki model and Padé approximation for F0 15:5 foam.

F0 15:5	Thickness (mm)	Porosity, ϕ	Airflow resistivity, σ (N.s/m^4)	Tortuosity	Mean pore size (μm)	Standard deviation in pore size (μm)
Measurement value	25	0.68	31,869	-	40.42	32.93
Inverted value by Miki model	25	0.50 (26%)	550,000 (94%)	1.2	-	-
Inverted value by Padé approximation	25	0.48 (29%)	470,050 (93%)	1.2	30.40 (25%)	32.93 (0%)

L_t = 45.0 mm L_p = 44.3 mm

a. Percentage in the bracket indicates the percentage difference between the measurement value and the inverted value by the acoustic models.

b. L_p was inverted value.
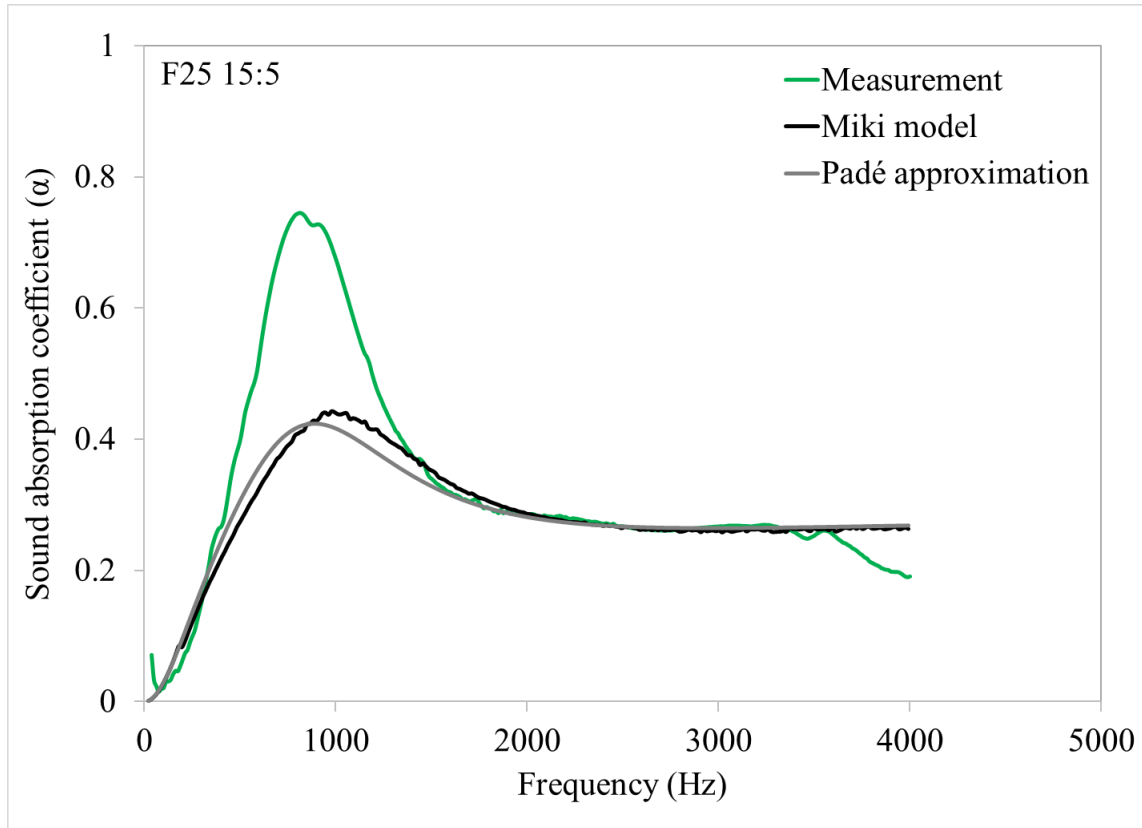
Figure 5.38: A comparison between the measurement data and prediction using the Miki model and Padé approximation of the sound absorption coefficient of F25 15:5 foam.

Table 5.7

The parameters comparison between the measurement value and inverted value used in Miki model and Padé approximation for F25 15:5 foam.

F25 15:5	Thickness (mm)	Porosity, ϕ	Airflow resistivity, σ (N.s/m^4)	Tortuosity	Mean pore size (μm)	Standard deviation in pore size (μm)
Measurement value	25	0.67	29,808	-	40.65	38.28
Inverted value by Miki model	25	0.50 (25%)	1,400,000 (98%)	1.2	-	-
Inverted value by Padé approximation	25	0.50 (25%)	1,249,300 (98%)	1.2	18.27 (55%)	38.28 (0%)
$L_t = 45.0$ mm			$L_p = 44.4$ mm			

a. Percentage in the bracket indicates the percentage difference between the measurement value and the inverted value by the acoustic models.
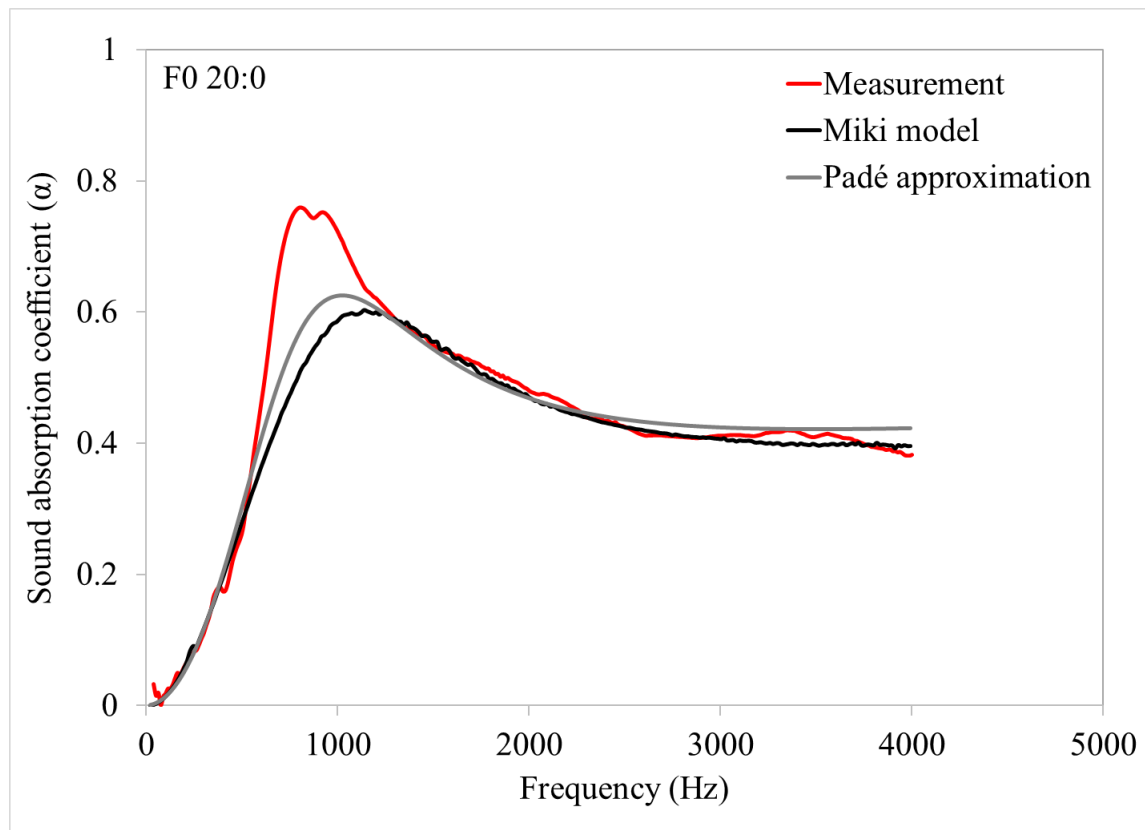
b. L_p was inverted value.

166
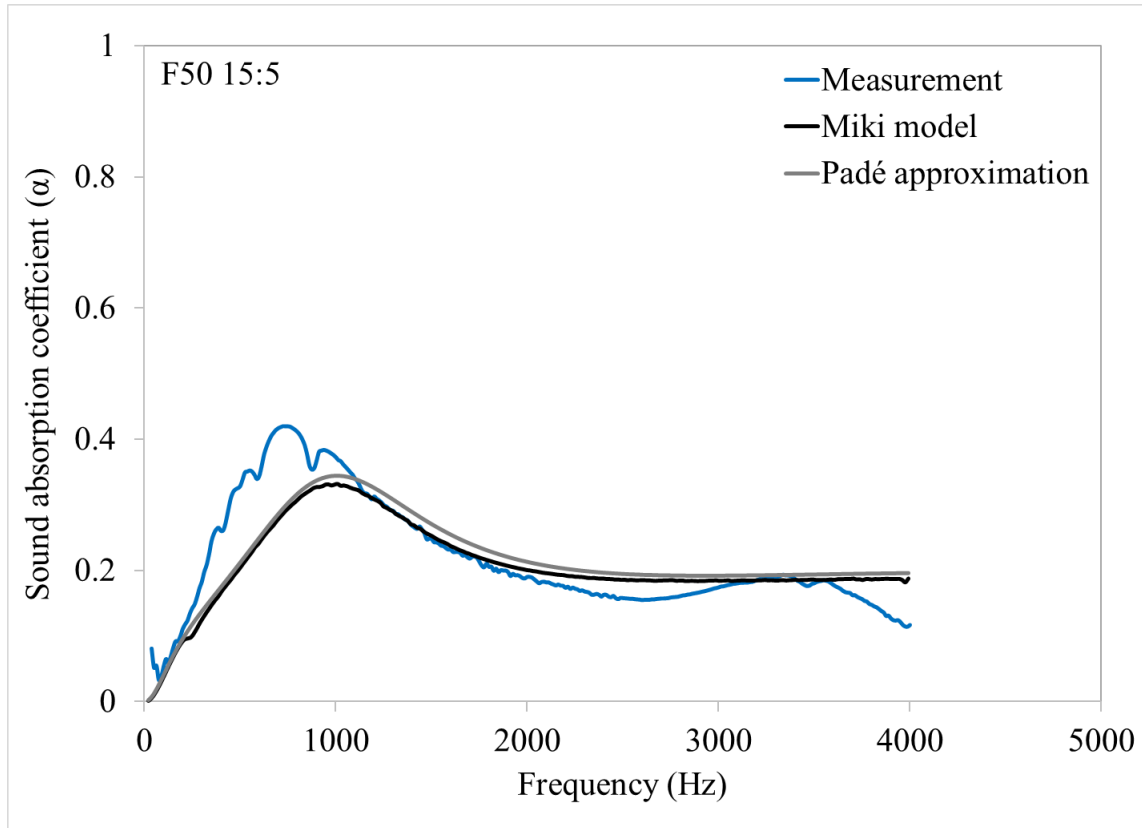
Figure 5.39: A comparison between the measurement data and prediction using the Miki model and Padé approximation of the sound absorption coefficient of F50 15:5 foam.

Table 5.8

The parameters comparison between the measurement value and inverted value used in Miki model and Padé approximation for F50 15:5 foam.

F50 15:5	Thickness (mm)	Porosity, ϕ	Airflow resistivity, σ (N.s/m^4)	Tortuosity	Mean pore size (µm)	Standard deviation in pore size (µm)
Measurement value	23	0.46	75,348	-	39.42	30.89
Inverted value by Miki model	23	0.46 (0%)	2,500,000 (97%)	1.2	-	-
Inverted value by Padé approximation	23	0.46 (0%)	2,498,300 (97%)	1.2	13.47 (66%)	30.89 (0%)

L_t = 45.0 mm L_p = 44.6 mm

a. Percentage in the bracket indicates the percentage difference between the measurement value and the inverted value by the acoustic models.
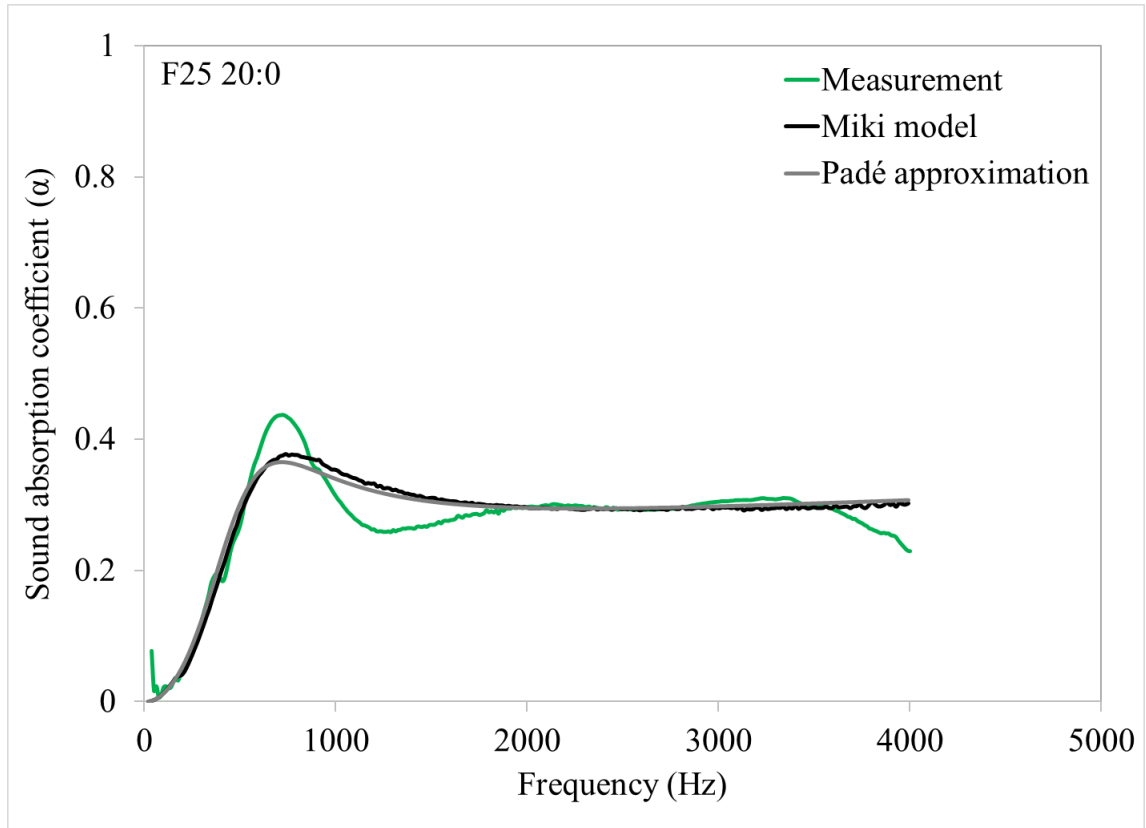
b. L_p was inverted value.

167
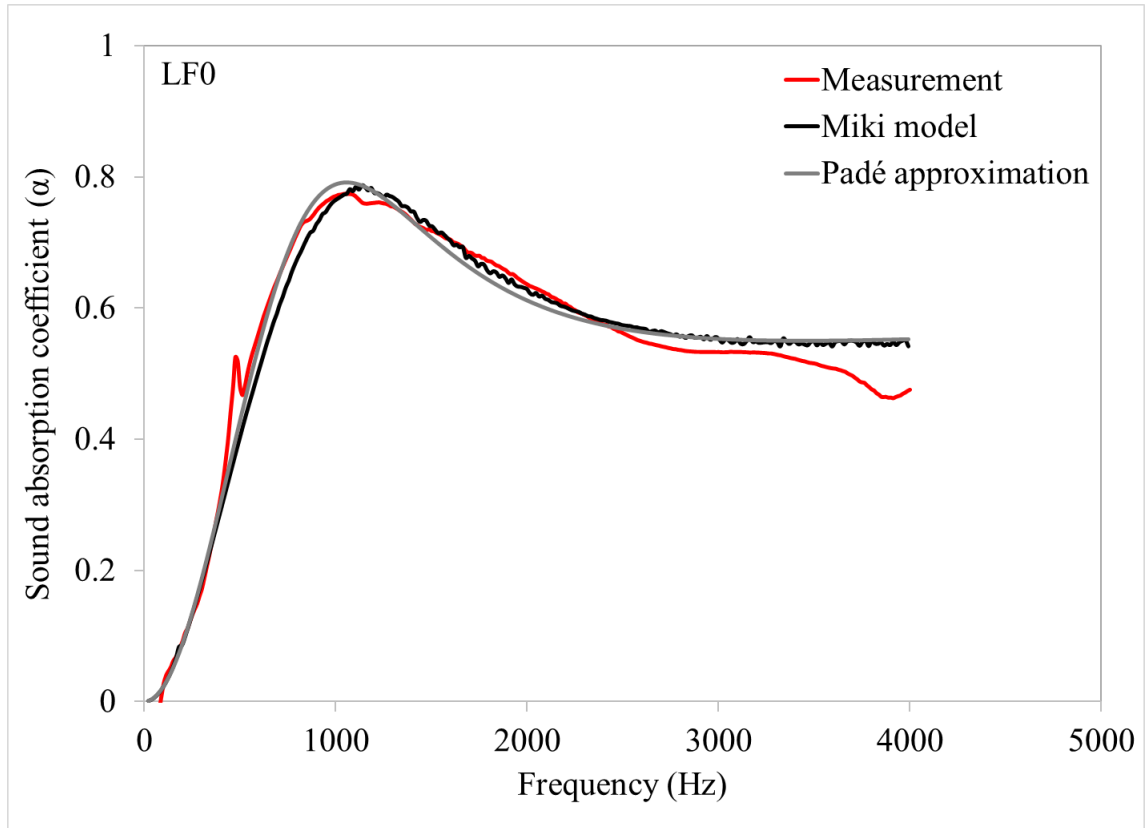
Figure 5.40: A comparison between the measurement data and prediction using the Miki model and Padé approximation of the sound absorption coefficient of LF0 foam.

Table 5.9

The parameters comparison between the measurement value and inverted value used in Miki model and Padé approximation for LF0 foam.

LF0	Thickness (mm)	Porosity, ϕ	Airflow resistivity, σ (N.s/m⁴)	Tortuosity	Mean pore size (μm)	Standard deviation in pore size (μm)
Measurement value	27	0.82	26,709	-	35.40	26.71
Inverted value by Miki model	27	0.82 (0%)	450,000 (94%)	1.2	-	-
Inverted value by Padé approximation	27	0.82 (0%)	400,100 (93%)	1.2	25.21 (29%)	26.71 (0%)

| L_t = 45.0 mm | | L_p = 43.3 mm | | | | |

a. Percentage in the bracket indicates the percentage difference between the measurement value and the inverted value by the acoustic models.
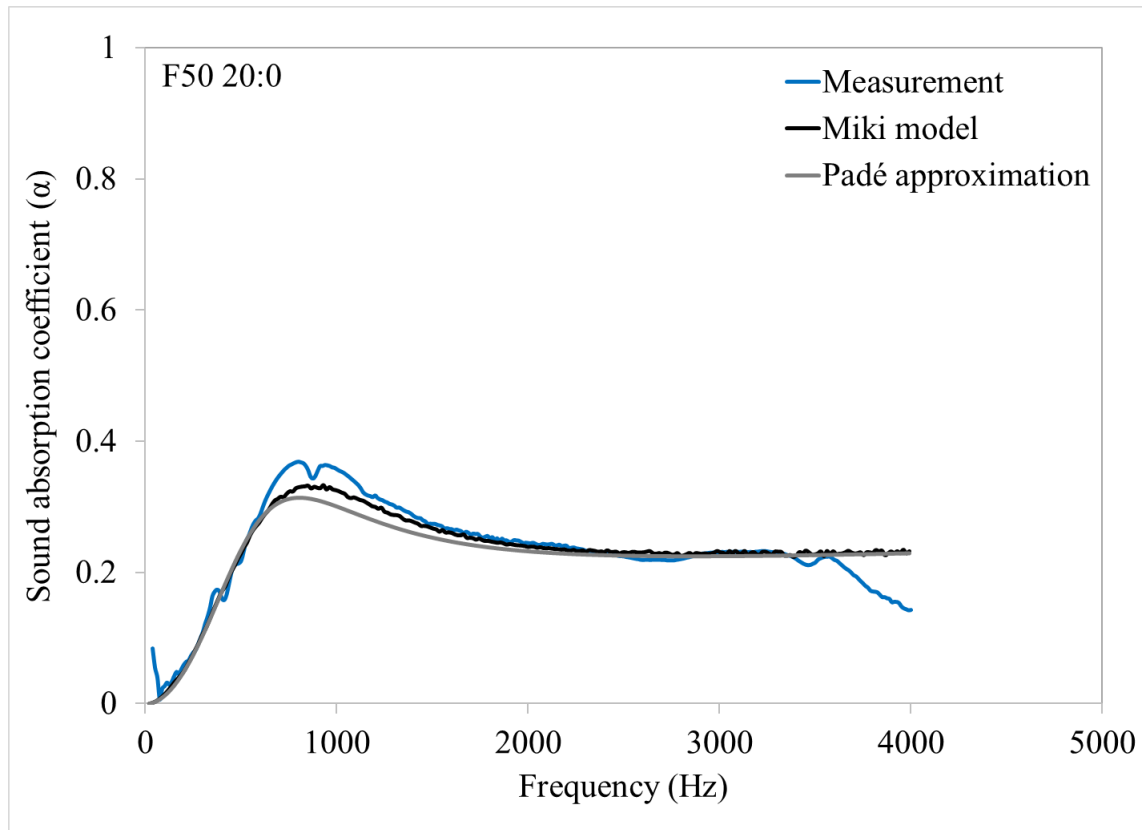
b. L_p was inverted value.
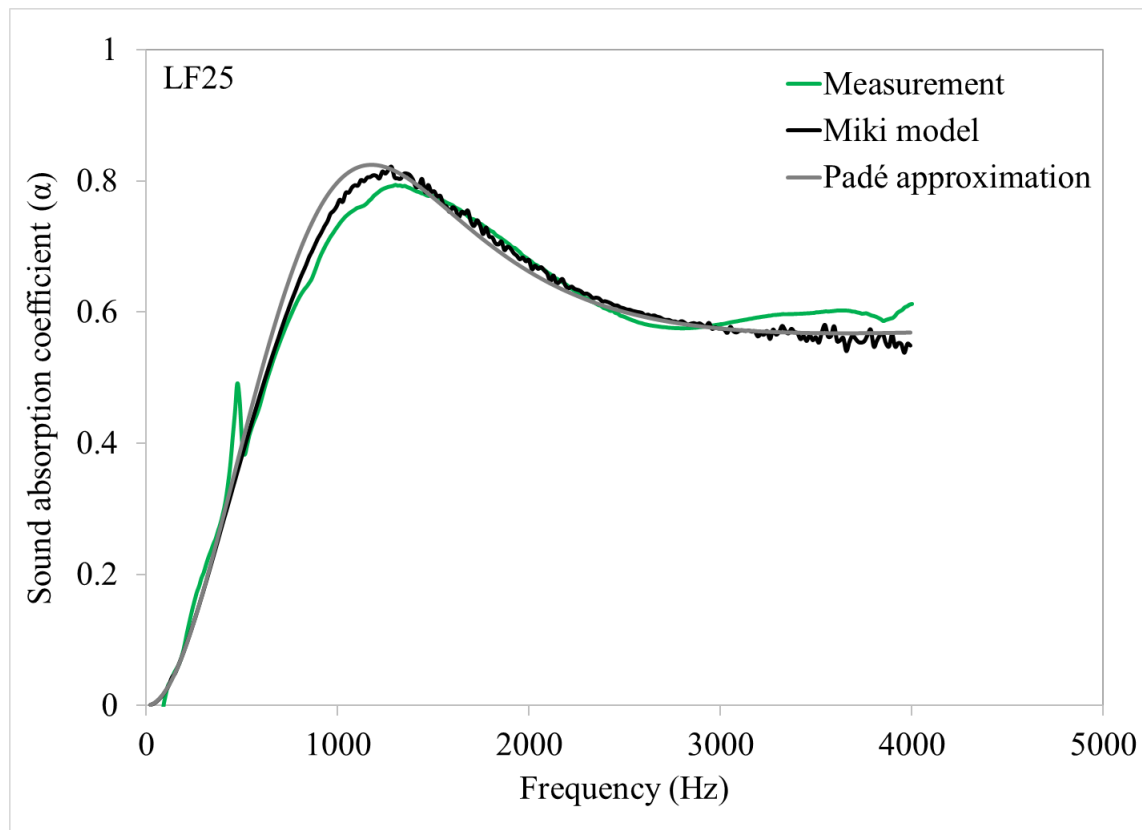
Figure 5.41: A comparison between the measurement data and prediction using the Miki model and Padé approximation of the sound absorption coefficient of LF25 foam.

Table 5.10

The parameters comparison between the measurement value and inverted value used in Miki model and Padé approximation for LF25 foam.

LF25	Thickness (mm)	Porosity, ϕ	Airflow resistivity, σ (N.s/m⁴)	Tortuosity	Mean pore size (μm)	Standard deviation in pore size (μm)
Measurement value	27	0.82	19,741	-	44.10	31.22
Inverted value by Miki model	27	0.82 (0%)	450,000 (96%)	1.2	-	-
Inverted value by Padé approximation	27	0.82 (0%)	400,100 (95%)	1.2	25.21 (43%)	31.22 (0%)
L_t = 45.0 mm			L_p = 43.0 mm			

a. Percentage in the bracket indicates the percentage difference between the measurement value and the inverted value by the acoustic models.
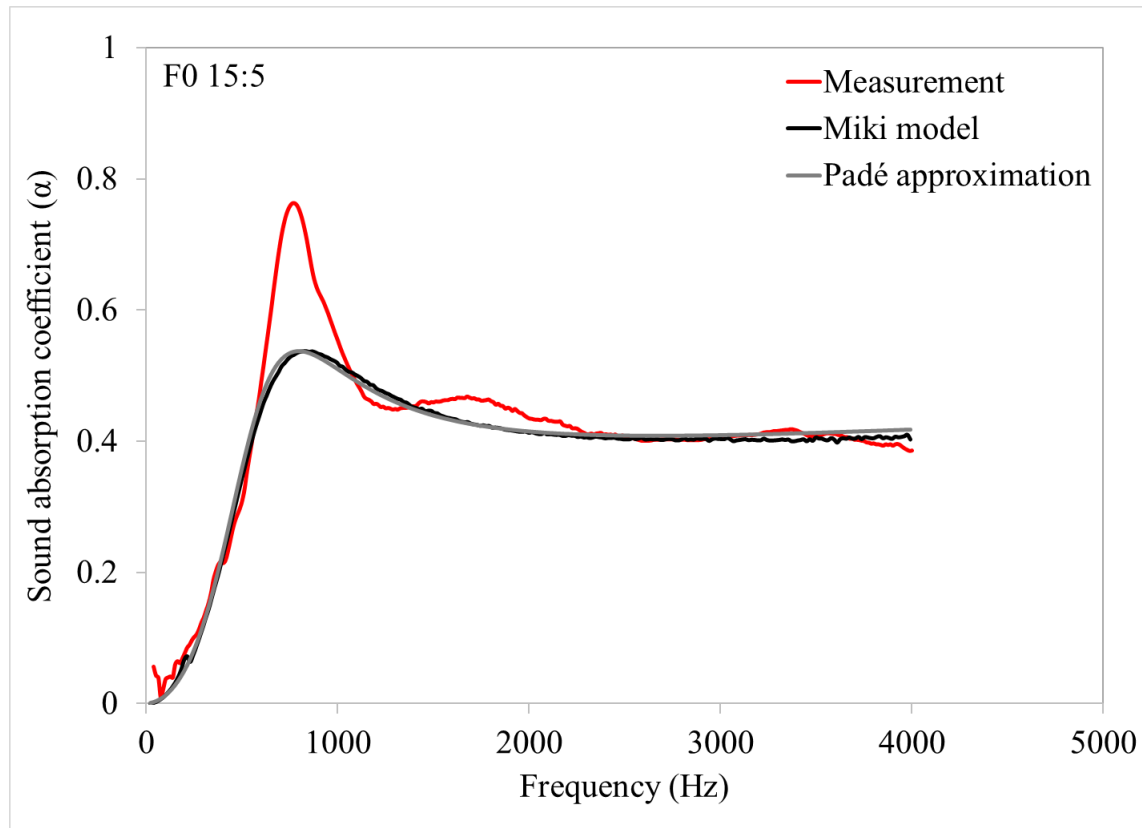
b. L_p was inverted value.
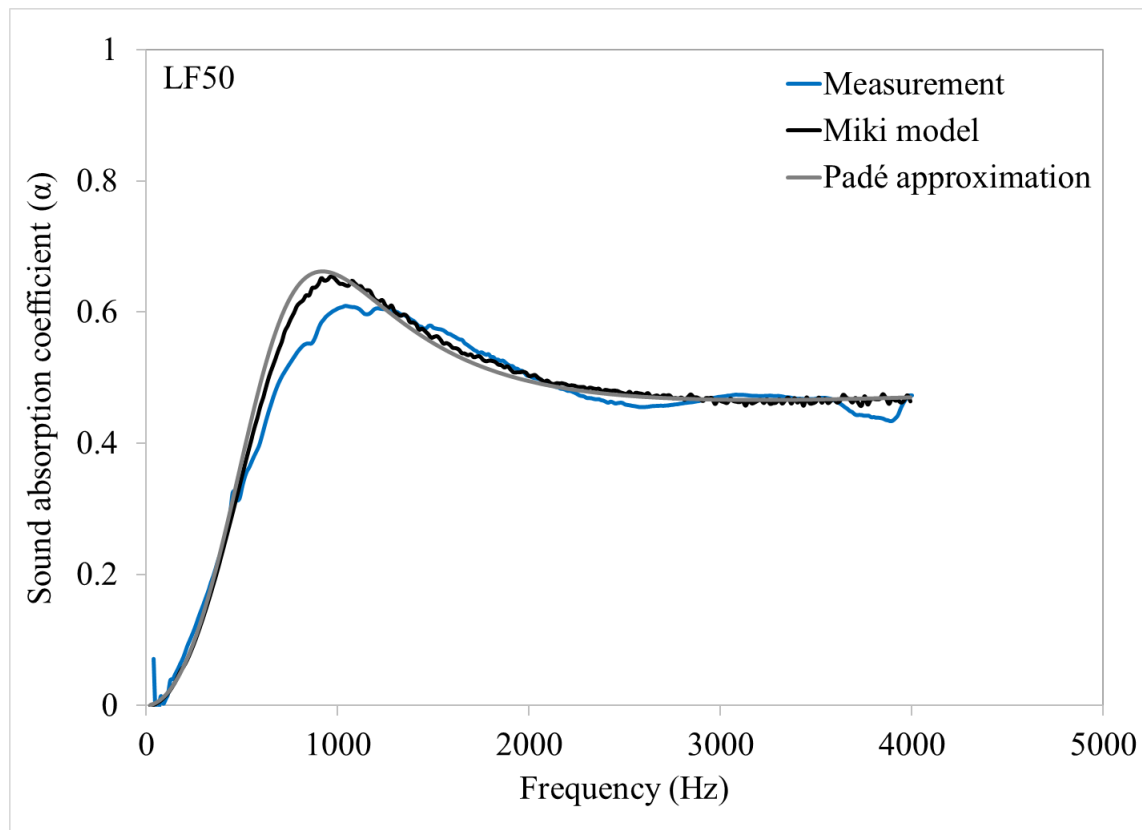
Figure 5.42: A comparison between the measurement data and prediction using the Miki model and Padé approximation of the sound absorption coefficient of LF50 foam.

Table 5.11

The parameters comparison between the measurement value and inverted value used in Miki model and Padé approximation for LF50 foam.

LF50	Thickness (mm)	Porosity, ϕ	Airflow resistivity, σ (N.s/m^4)	Tortuosity	Mean pore size (μm)	Standard deviation in pore size (μm)
Measurement value	21	0.77	80,008	-	38.88	27.88
Inverted value by Miki model	21	0.60 (22%)	500,000 (84%)	1.2	-	-
Inverted value by Padé approximation	21	0.60 (22%)	449,990 (82%)	1.2	27.79 (29%)	27.88 (0%)

L_t = 45.0 mm	L_p = 43.9 mm

a. Percentage in the bracket indicates the percentage difference between the measurement value and the inverted value by the acoustic models.

b. L_p was inverted value.

Referring to the inverted values by Miki model and Padé approximation, in particular cases the porosity and mean pore size values require some an adjustment between 20% to 29% and 25% to 66%. However, there is a huge difference between the measured and inverted values of airflow resistivity. The airflow resistivity values require massive adjustment between 63 to 98%. This is attributed to the circumferential gap between the foam sample and the sample holder during the airflow resistivity measurement. However, the sound absorption curve for rubber foams suggest that there is a good correlation between the measurement and predicted results along the frequency range, especially for latex foams with high homogeneity in their pore size. The model accuracy is generally high with the maximum relative error being 10-15%. However, the disagreement between the measurement data and the predictions becomes more pronounced if these models are used to predict the sound absorption coefficient of dry rubber foams with broad pore size distribution.

5.7 Summary

Experimental procedures used to study the physical, dynamic, microstructure and acoustic properties of the rubber foams were presented. The results of each experimental work were also discussed. Two modelling approaches, Miki model and Padé approximation were introduced to describe the acoustic absorption behaviour of rubber foams. The comparative study between the two models and the measurement data have been carried out in order to understand the relationship between the non-acoustic properties and the acoustic properties of rubber foams. A good correlation between the measurement data of acoustic properties and the predictions based on the non-acoustic properties can be achieved. It has been shown that the acoustic performance of rubber foams can be modelled, controlled and optimised by the non-acoustic properties. The adjustment of these properties can change the acoustic absorption behaviour of rubber foams to be used in vibro-acoustic isolation applications.

Chapter 6

Conclusions and Recommendations

6.1 Conclusions

Epoxidized natural rubber (ENR) is a new specialty grades of natural rubber that has greater market potential through innovation to compete the synthetic rubber. The usage of ENR is predicted to grow rapidly in commercial applications especially in the tyre industry. However, there is a relatively small amount of published work that can be related to ENR alone in vibration and noise control applications. Prior to this research the effect of the epoxidation level on vibro-acoustic properties of ENR not been fully investigated. Besides that, efficient production of open-cell ENR and natural rubber foam from dry rubber has remained a challenge. Little or no data exist on the use of these foams in vibration and noise control applications.

The aim of this thesis was to design ENR and natural rubber that can be used in vibration and noise control applications. First step was identification of the dynamical properties of solid ENR and solid natural rubber. Then, the development of a new manufacturing process of ENR foam and natural rubber foam based on dry rubber was carried out. These dry rubber foams produced were characterised in terms of their non-acoustical and acoustical properties. Finally, the acoustic absorption behaviour of ENR foam and natural rubber foam were predicted based on the key non-acoustical parameters.

Dynamic properties of solid natural rubber with different epoxidation levels: SMR-CV60 (0 mol%), ENR-25 (25 mol%), and ENR-50 (50 mol%) were carried out. The dynamic properties for all three rubbers were temperature and frequency dependent. The master curves of the dynamic properties obtained for each natural rubber were generated based on the time-temperature superposition principle using Williams-Landel-Ferry (WLF) relationship. Cole-Cole plots for all three rubbers fall on a single curve regardless of the epoxidation level. This suggests that the epoxidation level does not influence the relationship between the dynamic moduli. The results obtained provide evidence the optimal epoxidation level in natural rubber can be predicted to meet specific dynamic properties over a range of

temperatures and frequencies. A nomogram has been constructed for predicting the optimal epoxidation level for such purposes.

A new manufacturing process of natural rubber foam with different epoxidation levels: SMR-CV60 (0 mol%), ENR-25 (25 mol%), and ENR-50 (50 mol%) were performed. These foams were produced from dry rubber. A natural rubber foam (0 mol%) with the right pore structure can be produced using the mastication process of raw rubber. However, this technique does not work in the production of ENR foams. Carbon dioxide gas produced from the thermal decomposition of sodium bicarbonate was not able to penetrate through ENR membranes. Alternatively, another blowing agent known as ammonium bicarbonate was introduced. Ammonia gas produced from the thermal decomposition of ammonium bicarbonate can expand in ENR membranes and resulting in a formation of pores in the foam structure. This is due to the production of ammonia gas which contributed to the high rise in pressure during the decomposition process. The low stability of ammonium bicarbonate can be improved by mixing it with the more stable blowing agent such as sodium bicarbonate. For this purpose, the effect of different ratios of ammonium bicarbonate and sodium bicarbonate in the rubber foam with different epoxidation levels was studied. ENR foams with relatively large pores were produced upon the addition of ammonium bicarbonate. It was found that this process did not provide the same result for natural rubber foam upon the addition of ammonium bicarbonate. There was a possibility for some of ammonia bicarbonate to decompose during the mixing process and for some ammonia gas produced escaped from this compounded rubber due to its relatively high gas permeability.

The physical, dynamic, microstructure and acoustic properties of the dry rubber foams produced were measured. The characterisation of the latex foams with different epoxidation levels produced by Malaysian Rubber Board were also presented. The measured data were compared with that of commercially available vibration and noise control foams: reconstituted rubber foam and polyurethane foam. The acoustic absorption behaviour of rubber foams were described by two modelling approaches: Miki model and Padé approximation. A good correlation between the measured data for the acoustic properties of rubber foams and predicted values of the acoustic properties was found. It was shown that some parameters of these models need adjusting to account for the circumferential gap between a relatively low permeability sample of rubber foam and the wall of the impedance

tube. These observations suggest that the relationship between non-acoustic properties and acoustic behaviour of ENR and natural rubber foams can be used to develop new material with improved acoustic absorption and transmission loss performance.

6.2 Recommendations for future work

There remain many areas that can be investigated and improved for designing ENR and natural rubber foams that can be used in vibration and noise control applications. The points below are some recommendations for future work:

1. ENR and natural rubber are different in terms of their glass transition temperature, T_g. Each natural rubber exhibits effective damping in a narrow temperature range or around their T_g. Blends between ENR and natural rubber can exhibit effective damping in a wider temperature range. Therefore, investigation of the dynamic properties of ENR/natural rubber blends is a useful work to carry out. The production of natural rubber foam based on ENR/natural blends and its vibro-acoustic properties also can be discovered.

2. The comparative study on the usage of organic blowing agent and inorganic blowing agent in the production of dry rubber foam should be studied further. The effect of the production process and its parameters such as pressure and temperature on dry rubber foam production should be investigated further. This should include a study of an inorganic blowing agent used in combination with organic blowing agent on the properties of dry rubber foam. In fact, ammonium bicarbonate is already used as an additive to dinitrosopentamethylene-tetramine (DNPT) for manufacturing PVC foams [53].

3. In this study, ammonia gas produced from the thermal decomposition of ammonium bicarbonate resulted in a formation of larger pores in the dry rubber foam structure, especially in ENR foams. This is due to the production of large amounts of ammonia gas which contributed to the high rise in the gas pressure during the decomposition process. However, the microstructure properties of commercial foams, e.g. RRF and PUF, indicate that a relatively small pore size and homogeneous pore size distribution can contribute to

high absorption and damping. Therefore, the composition of ammonium bicarbonate needs to be reduced (less than 5 phr) in the future production of dry rubber foam.

4. The dynamic characterisation on dry rubber foam was not carried out at low enough temperatures approaching the T_g. As a result, data on the dynamic behaviour of rubber foam at very low temperatures are incomplete. The loss peak (maximum peak of $\tan \delta$) in the master curve obtained through the time-temperature superposition principle and a full semicircle in the Cole-Cole plot were not able to be plotted. Therefore, an improvement in the test preparation of the rubber foams and extended range of temperatures in a DMA experiment is required. A better standardisation to determine the dynamic properties of porous material is also requested in ref. [66].

5. The image scanned of F50 20:0 foam showed that there were two separate phases exist in foam (Figure 6.1). These phases indicate low pore connectivity and medium pore connectivity. The difference in pore connectivity occurred during the curing process of the foam in the closed-mould. The high temperature of the mould increased the crosslinking rate of the compounded rubber in the mould's wall area and resulted in small pores formation with low connectivity [5]. Therefore, the effect of pore connectivity on the acoustic behaviour of ENR foam and natural rubber foam is one of the future works that need to be considered.
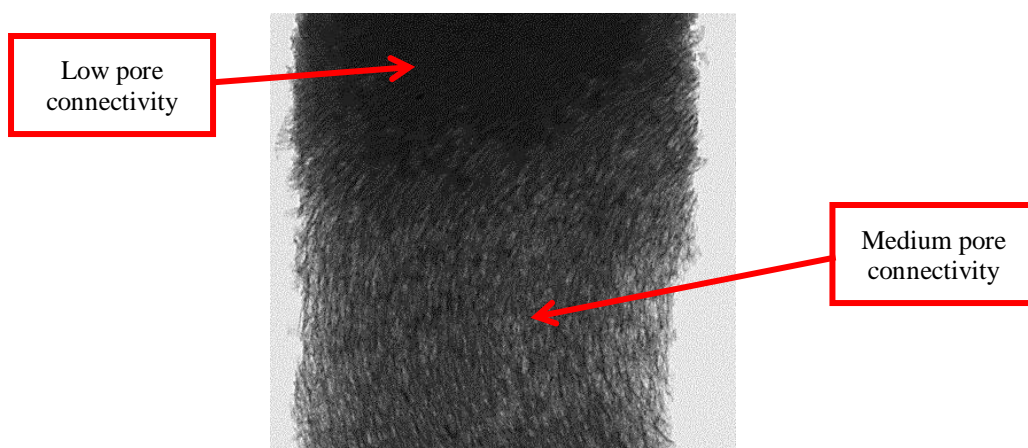

Figure 6.1: Image scanned of F50 20:0 foam.

Bibliography

[1]   Malaysian Rubber Exchange: Monthly prices [Online].

[2]   A. Ahmad and Z. M. Nor. (2012) EPP 4: Commercialisation of Ekoprena^{TM} and Pureprena^{TM}. *MRB Rubber Technology Developments*. 27-28.

[3]   "ETP Annual Report 2011: Palm Oil and Rubber," Jabatan Perdana Menteri, Malaysia2011.

[4]   N. N. Najib, Z. M. Ariff, A. A. Bakar, and C. S. Sipaut, "Correlation between the acoustic and dynamic mechanical properties of natural rubber foam: Effect of foaming temperature," *Materials & Design,* vol. 32, pp. 505-511, 2011.

[5]   A. Vahidifar, S. Nouri Khorasani, C. B. Park, H. E. Naguib, and H. A. Khonakdar, "Fabrication and Characterization of Closed-Cell Rubber Foams Based on Natural Rubber/Carbon Black by One-Step Foam Processing," *Industrial & Engineering Chemistry Research,* vol. 55, pp. 2407-2416, 2016/03/02 2016.

[6]   T. Pritz, "Five-parameter fractional derivative model for polymeric damping materials," *Journal of Sound and Vibration,* vol. 265, pp. 935-952, 2003/08/28/ 2003.

[7]   N. A. Rahman, "The Certificate of Proficiency in Rubber Compounding," P. Technology, Ed., ed. Malaysia: UiTM Perlis, 2015.

[8]   "https://www.sciencemag.org/news/2015/04/tires-your-car-threaten-asian-biodiversity."

[9]   M. J. R. Loadman, "The glass transition temperature of natural rubber.," *Journal of thermal analysis,* vol. 30, pp. 929-941, July 01 1985.

[10]   "http://www.pslc.ws/macrog/exp/rubber/sepisode/pi/pi.htm."

[11]   C. M. Blow and C. Hepburn, *Rubber technology and manufacture.* London: Butterworth Scientific, 1982.

[12]   I. R. Gelling, "Modification of natural rubber latex with peracetic acid," *Rubber Chemistry and Technology,* vol. 58, pp. 86-96, 1985.

[13]   J. E. Davey and M. J. R. Loadman, "A chemical demonstration of the randomness of epoxidation of natural rubber," *British Polymer Journal,* vol. 16, pp. 134-138, 1984.

[14]   S. Cook, P. S. Brown, J. Patel, and A. Kepas-Suwara, "Ekoprena^{TM}: A polymer for high performance passenger tyre treads," in *Malaysian Rubber Board Technical Report*, ed. Hertford, United Kingdom, 2008.

[15]   N. Mohamad, J. Yaakub, J. Abd Razak, M. Y. Yaakob, M. I. Shueb, and A. Muchtar, "Effects of epoxidized natural rubber (ENR-50) and processing parameters on the properties of NR/EPDM blends using response surface methodology," *Journal of Applied Polymer Science,* vol. 131, 2014.

[16]   P. Intharapat, A. Kongnoo, and K. Kateungngan, "The potential of chicken eggshell waste as a bio-filler filled epoxidized natural rubber (ENR) composite and its properties," *Journal of Polymers and the Environment,* vol. 21, pp. 245-258, 2013.

[17]   P. K. Chattopadhyay, S. Praveen, N. Chandra Das, and S. Chattopadhyay, "Contribution of organomodified clay on hybrid microstructures and properties of epoxidized natural rubber-based nanocomposites," *Polymer Engineering & Science,* vol. 53, pp. 923-930, 2013.

[18]   M. R. B, "ENR - Pencabar getah tiruan," Malaysia Rubber Board, Malaysia1984.

[19]   R. R. I. M, "Epoxidised natural rubber.," Rubber Research Institute of Malaysia.

[20]   T. U. o. T. Tampere University of Technology, "Rubber - Some aspects of rubber chemical changes," in *Virtual Education in Rubber Technology*, ed, 2007.

[21]   Y. Wang, Q. Wang, Y. Luo, J. Zhong, Y. Li, C. He, *et al.*, "Role of epoxidized natural rubber in dynamic mechanical properties of NR/ENR/silica composites," *Advanced Materials Research,* vol. 415-417, pp. 415-419, 2011.

[22]   I. R. Gelling, "Epoxidised natural rubber.," ed. Malaysian Rubber Producers' Research Association, Hertford, United Kingdom, 1991, pp. 271-297.

[23]   "http://www.lgm.gov.my/."

[24]   C. Metherell, "Epoxidised natural rubber for controlled damping applications.," *Progress in Rubber and Plastics Technology,* vol. 9, pp. 237-251, 1993.

[25]   W. Pongdong, C. Nakason, C. Kummerlowe, and N. Vennemann, "Influence of Filler from a Renewable Resource and Silane Coupling Agent on the Properties of Epoxidized Natural Rubber Vulcanizates," *Journal of Chemistry,* vol. 2015, pp. 1-15, 2015.

[26]   C. Jiang, H. He, X. Yao, P. Yu, L. Zhou, and D. Jia, "In situ dispersion and compatibilization of lignin/epoxidized natural rubber composites: reactivity, morphology and property," *Journal of Applied Polymer Science,* vol. 132, pp. n/a-n/a, 2015.

[27]   P. Manoharan, T. Chatterjee, S. Pal, N. C. Das, and K. Naskar, "Studies on Interfacial Characteristics of Highly Dispersible Silica Reinforced Epoxidized Natural Rubber Compounds," *Polymer-Plastics Technology and Engineering,* pp. 1-11, 2017.

[28]   S. Matchawet, A. Kaesaman, N. Vennemann, C. Kumerlöwe, and C. Nakason, "Effects of imidazolium ionic liquid on cure characteristics, electrical conductivity and other related properties of epoxidized natural rubber vulcanizates," *European Polymer Journal,* vol. 87, pp. 344-359, 2017/02/01/ 2017.

[29]   S. Ahmadi Shooli and M. Tavakoli, "Styrene Butadiene Rubber/Epoxidized Natural Rubber (SBR/ENR50) Nanocomposites Containing Nanoclay and Carbon Black as Fillers for Application in Tire-Tread Compounds," *Journal of Macromolecular Science, Part B,* vol. 55, pp. 969-983, 2016/10/02 2016.

[30]   R. A. Al-Mansob, A. Ismail, N. I. M. Yusoff, S. I. Albrka, C. H. Azhari, and M. R. Karim, "Rheological characteristics of unaged and aged epoxidised natural rubber modified asphalt," *Construction and Building Materials,* vol. 102, pp. 190-199, 2016/01/15/ 2016.

[31]   W. Pongdong, C. Kummerlöwe, N. Vennemann, A. Thitithammawong, and C. Nakason, "Property correlations for dynamically cured rice husk ash filled epoxidized natural rubber/thermoplastic polyurethane blends: Influences of RHA loading," *Polymer Testing,* vol. 53, pp. 245-256, 2016/08/01/ 2016.

[32]   W. Pongdong, C. Kummerlöwe, N. Vennemann, A. Thitithammawong, and C. Nakason, "A Comparative Investigation of Rice Husk Ash and Siliceous Earth as Reinforcing Fillers in Dynamically Cured Blends of Epoxidized Natural Rubber (ENR) and Thermoplastic Polyurethane (TPU)," *Journal of Polymers and the Environment,* vol. 26, pp. 1145-1159, March 01 2018.

[33]   J. Chen, S. Li, J. Zhong, B. Wang, R. Pan, Z. Wang, *et al.*, "The effect of epoxidized natural rubber on mechanical properties of siliceous earth/natural rubber composites," *Polymer Bulletin,* vol. 74, pp. 3955-3975, October 01 2017.

[34]   S. Utara, P. Jantachum, and B. Sukkaneewat, "Effect of surface modification of silicon carbide nanoparticles on the properties of nanocomposites based on epoxidized natural rubber/natural rubber blends," *Journal of Applied Polymer Science,* vol. 134, 2017.

[35]   S. Rooj, V. Thakur, U. Gohs, U. Wagenknecht, A. K. Bhowmick, and G. Heinrich, "In situ reactive compatibilization of polypropylene/epoxidized natural rubber

blends by electron induced reactive processing: novel in-line mixing technology," *Polymers for Advanced Technologies,* vol. 22, pp. 2257-2263, 2011.

[36]   Y. Wang, L. Liao, J. Zhong, D. He, K. Xu, C. Yang, *et al.*, "The behavior of natural rubber–epoxidized natural rubber–silica composites based on wet masterbatch technique," *Journal of Applied Polymer Science,* vol. 133, pp. n/a-n/a, 2016.

[37]   X. Lu and X. Li, "Broad temperature and frequency range damping materials based on epoxidized natural rubber," *Journal of Elastomers & Plastics,* vol. 46 (1), pp. 84-95, 2014.

[38]   H. R. Ahmadi, C. Metherell, and A. H. Muhr, "Noise reduction with rubber," in *Euro.Noise 92*, Imperial College London, 1992.

[39]   T. Pritz, "Frequency power law of material damping," *Applied Acoustics,* vol. 65, pp. 1027-1036, 11// 2004.

[40]   D. I. G. Jones, *Handbook of viscoelastic vibration damping*. United States of America: John Wiley & Sons, Ltd, 2001.

[41]   L. H. Sperling, "Sound and vibration damping with polymers," in *Sound and vibration damping with polymers* vol. 424, R. D. Corsaro and L. H. Sperling, Eds., ed. Washington DC: American Chemical Society, 1990, pp. 5-22.

[42]   "Dynamic Mechanical Analysis (DMA): A beginner's guide," I. PerkinElmer, Ed., ed. United States of America, 2013.

[43]   R. J. Young and P. A. Lovell, *Introduction to Polymers*. Great Britain: Chapman & Hall, 1991.

[44]   N. Ahmad, "A methodology for developing high damping materials with application to noise reduction of railway track," Doctoral Thesis, Faculty of Engineering, Science and Mathematics, Institute of Sound and Vibration Research, University of Southampton, Southampton, 2009.

[45]   M. I. Seth A Rahim, "Postgraduate six month progress report.," The University of Sheffield, United Kingdom2016.

[46]   M. Sjoberg, "On dynamic properties of rubber isolators," Doctoral Thesis, Department of Vehicle Engineering, Royal Institute of Technology, Stockholm, 2002.

[47]   D. I. G. Jones, "Temperature-frequency dependence of dynamic properties of damping materials," *Journal of Sound and Vibration,* vol. 33, pp. 451-470, 1974/04/22 1974.

[48]   H. R. Ahmadi and A. H. Muhr, "Characterization of dynamic properties of rubber appropriate to noise and vibration control," ed. Plastics and Rubber Institute, Rubber in Engineering Group, London, 1991.

[49]   S. A. Hambric, A. W. Jarrett, G. F. Lee, and J. J. Fedderly, "Inferring Viscoelastic Dynamic Material Properties From Finite Element and Experimental Studies of Beams With Constrained Layer Damping," *Journal of Vibration and Acoustics,* vol. 129, pp. 158-168, 2006.

[50]   L. Rouleau, J. F. Deü, A. Legay, and F. Le Lay, "Application of Kramers–Kronig relations to time–temperature superposition for viscoelastic materials," *Mechanics of Materials,* vol. 65, pp. 66-75, 10// 2013.

[51]   D. Young, *Latex foam handbook*. England: British Latex Foam Manufacturers' Association, 1966.

[52]   T. D. Pendle, "A review of the moulded latex foam industry.," *Cellular Polymers,* vol. 8, pp. 1-14, 1989.

[53]   D. Klempner and V. Sendijarevic, *Handbook of polymeric foams and foam technology*. Munich: Hanser Publishers, 2004.

[54]   Z. M. Ariff, Z. Zakaria, L. H. Tay, and S. Y. Lee, "Effect of foaming temperature and rubber grades on properties of natural rubber foams," *Journal of Applied Polymer Science,* vol. 107, pp. 2531-2538, 2008.

[55]   P. J. Veale, "Investigation of the behaviour of open cell aluminum foam," Master Thesis Master Thesis, Civil and Environmental Engineering, University of Massachusetts Amherst, United States of America, 2010.

[56]   C. Hepburn. (1997). *Rubber Compounding Ingredients - Need, Theory and Innovation*.

[57]   L. Oliveira-Salmazo, A. Lopez-Gil, F. Silva-Bellucci, A. E. Job, and M. A. Rodriguez-Perez, "Natural rubber foams with anisotropic cellular structures: Mechanical properties and modeling," *Industrial Crops and Products,* vol. 80, pp. 26-35, 2// 2016.

[58]   C. Metherell, "Expanded rubber using ENR and blends with PVC.," *Rubber Developments,* vol. 45, pp. 85-90, 1992.

[59]   J. H. Kim, K. C. Choi, and J. M. Yoon, "The Foaming Characteristics and Physical Properties of Natural Rubber Foams: Effects of Carbon Black Content and Foaming Pressure," *Journal of Industrial and Engineering Chemistry,* vol. 12, pp. 795-801, 2006.

[60]   J. H. Kim, J. S. Koh, K. C. Choi, J. M. Yoon, and S. Y. Kim, "Effects of Foaming Temperature and Carbon Black Content on the Cure Characteristics and Mechanical Properties of Natural Rubber Foams," *Journal of Industrial and Engineering Chemistry,* vol. 13, pp. 198-205, 2007.

[61]   A. Khan, "Vibro-acoustic products from re-cycled raw materials using a cold extrusion process," PhD PhD, School of Engineering, Design and Technology, University of Bradford, United Kingdom, 2008.

[62]   L. J. Gibson and M. F. Ashby, *Cellular solids: structure and properties*. United Kingdom: Cambridge University Press, 1997.

[63]   K. V. Horoshenkov, A. Khan, F.-X. Bécot, L. Jaouen, F. Sgard, A. Renault*, et al.*, "Reproducibility experiments on measuring acoustical properties of rigid-frame porous media (round-robin tests)," *The Journal of the Acoustical Society of America,* vol. 122, pp. 345-353, 2007.

[64]   J. D. Ferry, *Viscoelastic properties of polymers*, 3rd ed. New York: John Wiley & Sons 1980.

[65]   L. Jaouen, A. Renault, and M. Deverge, "Elastic and damping characterizations of acoustical porous materials: Available experimental methods and applications to a melamine foam," *Applied Acoustics,* vol. 69, pp. 1129-1140, 2008/12/01/ 2008.

[66]   P. Bonfiglio, F. Pompoli, K. V. Horoshenkov, M. I. B. S. A. Rahim, L. Jaouen, J. Rodenas*, et al.*, "How reproducible are methods to measure the dynamic viscoelastic properties of poroelastic media?," *Journal of Sound and Vibration,* vol. 428, pp. 26-43, 2018/08/18/ 2018.

[67]   F. Pompoli, P. Bonfiglio, K. V. Horoshenkov, A. Khan, L. Jaouen, F.-X. Bécot*, et al.*, "How reproducible is the acoustical characterization of porous media?," *The Journal of the Acoustical Society of America,* vol. 141, pp. 945-955, 2017.

[68]   D. L. Johnson, J. Koplik, and R. Dashen, "Theory of dynamic permeability and tortuosity in fluid-saturated porous media," *Journal of Fluid Mechanics,* vol. 176, pp. 379-402, 1987.

[69]   Y. Champoux, J. F. Allard, and B. M. A., "Dynamic tortuosity and bulk modulus in air-saturated porous media," *Journal of Applied Physics,* vol. 70, pp. 1975-1979, 1991.

[70] M. E. Delany and E. N. Bazley, "Acoustical properties of fibrous absorbent materials," *Applied Acoustics,* vol. 3, pp. 105-116, 1970/04/01/ 1970.

[71] Y. Miki, "Acoustical properties of porous materials-Generalizations of empirical models," *Journal of the Acoustical Society of Japan (E),* vol. 11, pp. 25-28, 1990.

[72] N. N. Voronina and K. V. Horoshenkov, "A new empirical model for the acoustic properties of loose granular media," *Applied Acoustics,* vol. 64, pp. 415-432, 2003/04/01/ 2003.

[73] D. K. Wilson, "Relaxation-matched modeling of propagation through porous media, including fractal pore structure," *The Journal of the Acoustical Society of America,* vol. 94, pp. 1136-1145, 1993.

[74] K. V. Horoshenkov, K. Attenborough, and S. N. Chandler-Wilde, "Padé approximants for the acoustical properties of rigid frame porous media with pore size distributions," *The Journal of the Acoustical Society of America,* vol. 104, pp. 1198-1209, 1998.

[75] K. Horoshenkov, J. P. Groby, and O. Dazel, "Asymptotic limits of some models for sound propagation in porous media and the assignment of the pore characteristic lengths," *Journal of the Acoustical Society of America,* vol. 139, pp. 2436-2474, 05/06 2016.

[76] K. V. Horoshenkov, "A review of acoustical methods for porous material characterisation," *International Journal of Acoustics and Vibration,* vol. 22, pp. 92-103, 2017.

[77] K. V. Horoshenkov and M. J. Swift, "The effect of consolidation on the acoustic properties of loose rubber granulates," *Applied Acoustics,* vol. 62, pp. 665-690, 2001/06/01/ 2001.

[78] R. M. B. Fernandes, L. L. Y. Visconte, and R. C. R. Nunes, "Curing characteristics and aging properties of natural rubber/epoxidized natural rubber and cellulose II," *International Journal of Polymeric Materials and Polymeric Biomaterials,* vol. 60, pp. 351-364, 2011/03/07 2011.

[79] M. Etchessahar, S. Sahraoui, L. Benyahia, and J. F. Tassin, "Frequency dependence of elastic properties of acoustic foams," *The Journal of the Acoustical Society of America,* vol. 117, pp. 1114-1121, 2005.

[80] M. L. Williams, R. F. Landel, and J. D. Ferry, "The temperature dependence of relaxation mechanisms in amorphous polymers and other glass-forming liquids," *Journal of the American Chemical Society,* vol. 77, pp. 3701-3707, 1955/07/01 1955.

[81] K. S. Cole and R. H. Cole, "Dispersion and absorption in dielectrics I. Alternating current characteristics," *The Journal of Chemical Physics,* vol. 9, pp. 341-351, 1941.

[82] T. Pritz, "Analysis of four-parameter fractional derivative model of real solid materials," *Journal of Sound and Vibration,* vol. 195, pp. 103-115, 1996/08/08/ 1996.

[83] "ISO 6916-1:1995. Flexible cellular polymeric materials. Sponge and expanded cellular rubber products. Specification. Sheeting."

[84] N. N. Najib, Z. M. Ariff, N. A. Manan, A. A. Bakar, and C. S. Sipaut, "Effect of blowing agent concentration on cell morphology and impact properties of natural rubber foam.," *Journal of Physical Science,* vol. 20, pp. 13-25, 2009.

[85] "The natural rubber formulary and property index," ed. Kuala Lumpur, Malaysia: Malaysian Rubber Producers' Research Association, 1984.

[86] Z. M. Ariff, N. A. A. Rahim, and L. C. Low, "Effect of compound formulation on the production and properties of epoxidised natural rubber (ENR-25) foams.," in *Proceedings of the Polymer Processing Society 24th Annual Meeting*, Salerno, Italy, 2008.

[87] "https://corporate.armacell.com/en/."

[88]   "http://www.cmsdanskin.co.uk/."

[89]   P. Leclaire, O. Umnova, K. V. Horoshenkov, and L. Maillet, "Porosity measurement by comparison of air volumes," *Review of Scientific Instruments,* vol. 74, pp. 1366-1370, 2003.

[90]   L. L. Beranek, "Acoustic Impedance of Porous Materials," *The Journal of the Acoustical Society of America,* vol. 13, pp. 248-260, 1942.

[91]   Y. Champoux, M. R. Stinson, and G. A. Daigle, "Air-based system for the measurement of porosity," *The Journal of the Acoustical Society of America,* vol. 89, pp. 910-916, 1991.

[92]   "ISO 9053:1991. Acoustics. Materials for acoustical applications. Determination of airflow resistance."

[93]   "https://www.akustikforschung.de."

[94]   "http://metravib.acoemgroup.com/dma."

[95]   "ISO 10534-2:2001. Acoustics. Determination of sound absorption coefficient and impedance in impedance tubes. Transfer-function method."

[96]   Materiacustica, "Measurement of acoustical surface properties of porous media: 2mics_MAA user manual," ed. Italy, 2014.

[97]   *http://www.materiacustica.it/*.

[98]   F. Briatico-Vangosa, M. Benanti, L. Andena, C. Marano, R. Frassine, M. Rink*, et al.*, "Dynamic mechanical response of foams for noise control," *AIP Conference Proceedings,* vol. 1779, p. 090007, 2016.

[99]   D. Pilon and R. Panneton, "Behavioral criterion quantifying the effects of circumferential air gaps on porous materials in the standing wave tube.," *The Journal of the Acoustical Society of America,* vol. 116, pp. 344-356, 2004.

[100]   http://alphacell.matelys.com/.

[101]   Y. Miki, "Acoustical properties of porous materials-Modifications of Delany-Bazley models," *Journal of the Acoustical Society of Japan (E),* vol. 11, pp. 19-24, 1990.